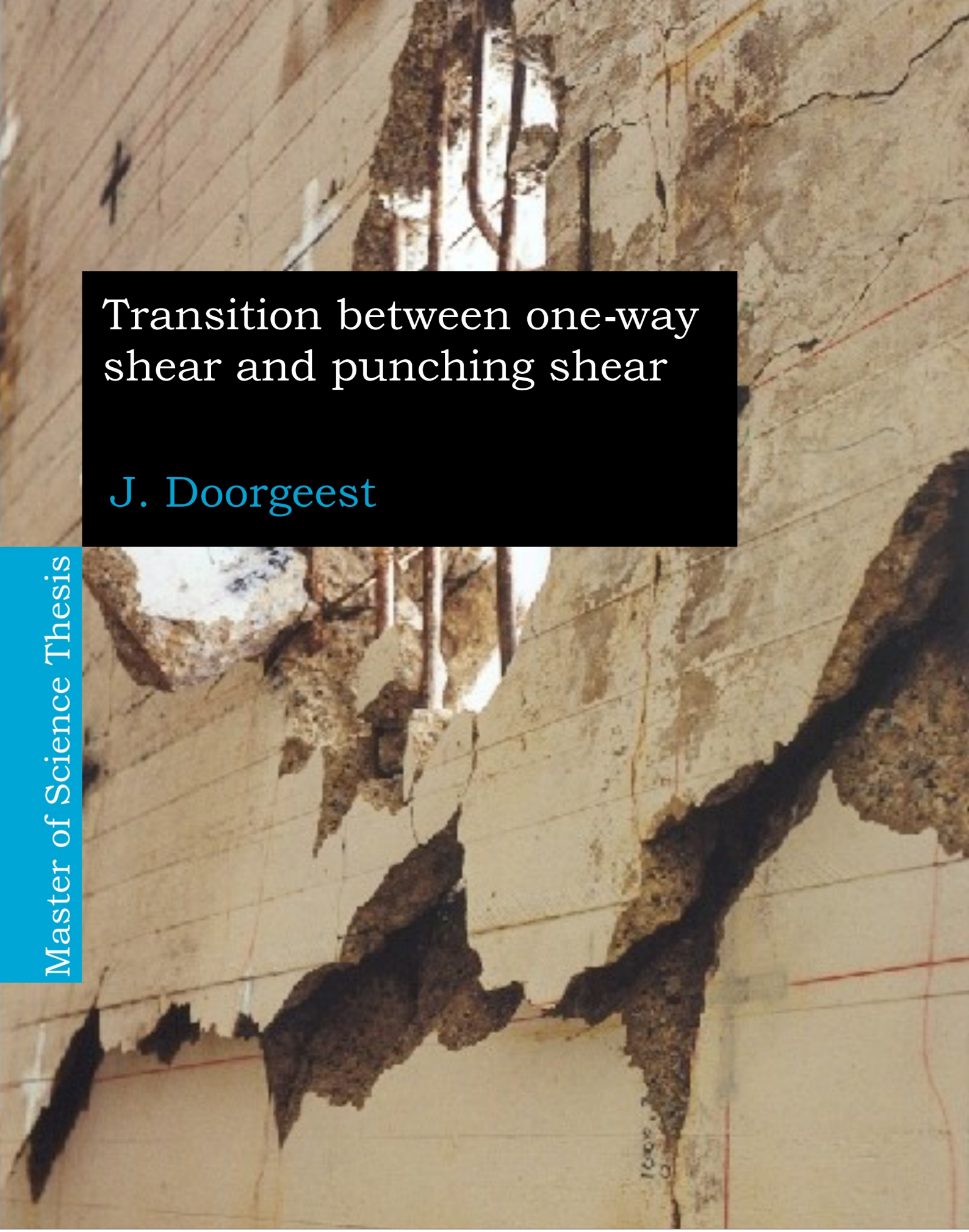

Transition between one-way shear and punching shear

J. Doorgeest

Master of Science Thesis

TU Delft Delft University of Technology

Challenge the future

Transition between one way shear and punching shear

Master of Science Thesis

For the degree of Master of Science at Delft University of Technology

Jasper Doorgeest

June 8, 2012

Faculty of Civil Engineering and Geosciences
Delft University of Technology

Thesis committee members:

Prof. dr. ir. J. C. Walraven
Delft University of Technology, Department of Concrete Structures

Dr. ir. C. van der Veen
Delft University of Technology, Department of Concrete Structures

Dr. ir. M. A. N. Hendriks
Delft University of Technology, Department of Structural Mechanics

ir. E. O. L. Lantsoght
Delft University of Technology, Department of Concrete Structures

ir. L. J. M. Houben
Delft University of Technology

Preface

In this Master Thesis the results of my study on the transition between one-way shear and punching shear are presented. The study has been conducted at the faculty of Civil Engineering and Geosciences at Delft University of Technology from August 2011 until June 2012. The master thesis project was done in cooperation with the concrete structures department.

The main objective of the thesis project was to investigate the behaviour of shear failure in reinforced concrete slabs subjected to a concentrated load close to the support. The transition between one-way shear failure and punching shear failure in this area is investigated. The aim was to provide a classification system that could be used to predict the occurring failure mechanism.

The report starts with a literature study in which information is gathered on one-way shear, punching shear, building codes and various models on shear and the parameters that are involved. The building codes are compared and analysed on their shear prediction capabilities. Later on the building codes are applied to various series of experiments in order to investigate how well the they can predict the failure mechanism and the failure load. Most attention is dedicated to the finite element models that represent two experimental tests, one that failed in one-way shear and one that failed in punching shear. These models are used to verify the two boundary situations: one-way shear and punching shear. Afterwards it was possible to investigate the area in between the two boundary situations, by using the same model. During the investigation of the transitions zone, the element width and the shear span were varied. Performing the analysis provided valuable information.

The research topic offered a challenge and the various parts of the study kept it interesting. The study brought me very valuable new knowledge about shear failure in concrete structures, about new building codes and models and about computational modelling. Hence, I would like to thank all members of my graduation committee for their guidance, support and time spent with me during the meetings.

Finally, I would like to thank my family, friends and my girlfriend for their support, help and understanding.

Jasper Doorgeest

Delft, June 2012

Contents

Chapter 1

Introduction

In the past century a lot of research has been done on concrete elements and how they fail under loading. All this research has provided some, but incomplete, insight in the mechanics behind the load carrying mechanisms and failure mechanisms. A clear physical model for shear is still not found. The current code provisions are often based on (semi)empirical models. Experience shows that this provides us with safe designs for general design cases. Due to the lack of a physical model it is often hard to use the codes for designs that are not general. It is also unknown what the exact difference is between the design capacity and the actual capacity of a structure.

It is found that in some cases the design shear capacity of slab bridges in the Netherlands is, now or in the near future, not high enough to withstand the increasing traffic load. Replacing or improving these bridges will cost a lot of work, time, traffic congestions and money. Currently the need for replacement or improvement is under discussion.

Often the lower bound based design formulas are rather conservative. They do not take into account favourable effects like increased concrete strength due to progressing hydration after 28 days, higher concrete strength for long term loading and higher shear resistance for slabs loaded near the supports.

Currently, new extensive research is being done at Delft University of Technology to analyse this additional shear capacity for slabs under concentrated loading near to the support.

When shear in reinforced concrete is studied, the focus is usually on one-way shear in beams or on punching shear in slabs. A one-way slab subjected to a concentrated load is generally designed as a wide beam, using an effective width to carry the load. How this effective width is determined and which parameters are of influence is currently under investigation. Design formulas for wide beams assume one-way shear failure while in some cases punching

shear will occur. For wide beams and slabs subjected to concentrated loads in the vicinity of the support it is not clear if and when one-way (beam) shear or two-way (punching) shear is governing.

The question arises if there is a way to predict the governing shear failure mechanism in wide beams and in one-way slabs loaded close to supports? Will there be one-way shear, will there be punching shear, or will there be a combination of these two?

Better insight will be provided by analysing test results of one-way slabs under concentrated loading in the vicinity of the support and comparing these results with the predictions from the various codes, models and FEM models. The aim is to provide better insight on the transition between one-way shear and punching shear for slabs loaded close to the support and to provide a way to predict the governing failure mechanism more consistently.

The first step in the process of answering this question is a literature review. This is done in chapter two. Various failure mechanisms are explained, existing models for one-way shear and punching shear are dealt with, the main parameters involving shear are analysed and the design formulas from various building codes are treated.

In the third chapter models to calculate one-way shear and punching shear are examined by applying them to various slabs. The focus lays on the transition from one-way shear being governing to two-way shear being governing. These results are then related to the results from the experiments recently done at Delft University of Technology.

Two finite element method models are made and analysed in chapter four. One model represents a performed test that failed in one-way shear and the other model will represent a performed test that failed in punching shear. When these two models successfully mimic the behaviour and failure mechanisms of their experimental counter parts more FEM analysis will be performed in chapter five.

The FEM models in chapter five will vary two parameters namely the shear span and the slab width. The failure mechanism will be monitored in the analyses while the parameters are being varied. In this way the transition from one-way shear failure to punching shear failure can be investigated. The aim is to be able to predict the occurring failure mechanism and to provide recommendations to the building codes in order to predict the governing failure mechanism more consistently.

The last chapter contains the overall conclusion that can be drawn from the preceding chapters.

Chapter 2

Literature review

This chapter contains a short review of related studies done in the past. Various models to describe shear in concrete beams and slabs are treated for both one-way shear as well as punching shear. The important parameters that influence the shear capacity of concrete elements are reviewed. The chapter also contains design formulas on shear capacity in concrete from the Eurocode, the ACI building code, the Model Code 2010 and the NEN6720. The information contained in this chapter will be used as a basis for the subsequent chapters.

2.1 Failure mechanisms

Failure in concrete elements can occur in many ways. The behaviour of the concrete during loading and at failure is a complex three dimensional problem influenced by numerous different parameters. In this thesis shear failure in concrete slabs subjected to a concentrated load close to the support is investigated. Kani (1964) [16] explained the origin of the term "shear failure" in this way:

When testing reinforced concrete beams, simply supported at both ends and loaded at two locations, the beams failed due to severe (diagonal) cracking outside the central part of the beam (figure 2.1). In this case the failure could not be caused by the bending moment, because the maximum bending moment was in the middle of the span. However, at the failure locations of the beam there is a shear force present. It was concluded that shear force or shear stress caused this type of failure. Hence the name "shear failure".

When considering shear in concrete elements, generally two types are considered; one-way shear and punching shear. Sometimes punching shear is also referred to as two-way shear. The term "two-way" refers to a situation

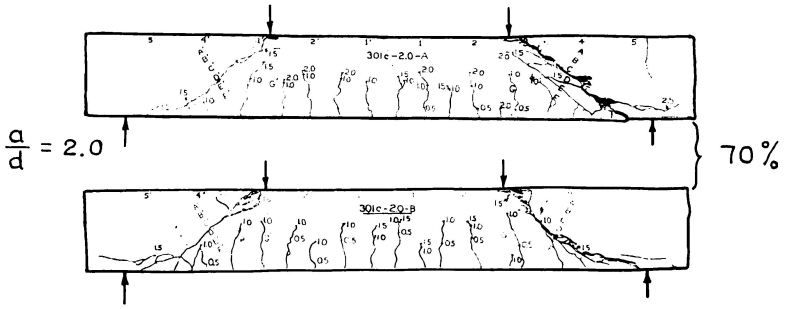

Figure 2.1: Beam failure induced by cracks outside the central section of the beam [16].

in which the principal shear lines do not run in one direction parallel to each other (figure 2.2). One-way shear can be seen in beams, or for instance in a slab between a load and a fixed end. In this case the principal shear lines run parallel to each other from the load to the support. Two-way shear is often seen in slabs around the subjection point of a concentrated load located at some distance from the support.

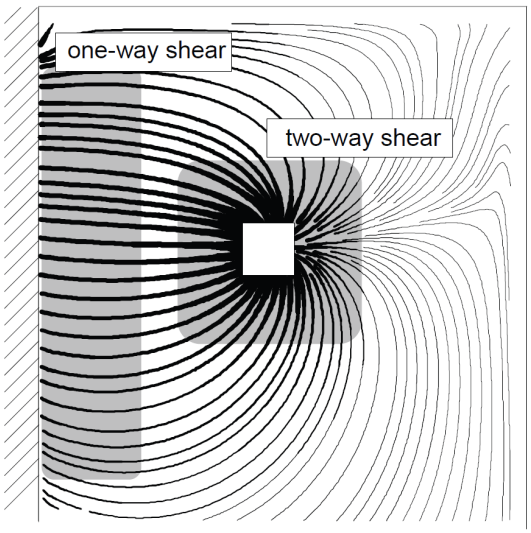

Figure 2.2: Shear flow in a slab indicating the difference between one-way shear and two-way shear [40].

2.1.1 One-way shear

The occurrence of one-way shear failure or punching shear failure in a slab depends on the dimensions of the element, the conditions at the support, reinforcement and the position and shape of the load. If the conditions are such that the shear forces flow from the load to the support in a parallel manner, it can be said the behaviour is "beam like" and the slab should be checked for one-way shear. An example is a short cantilever slab with a line load running along the tip (figure 2.3 (a)), which can be the case in a cantilever bridge slab. Another clear example typical of one-way shear failure is given in figure 2.3 (b).

There are several models available to check for one-way shear in slabs and beams without shear reinforcement. These models are for example: the tooth model (2.2.1), the strut and tie model (2.2.2) which is also available for punching shear and the critical shear crack theory (2.2.3).

Figure 2.3: One-way shear failure...

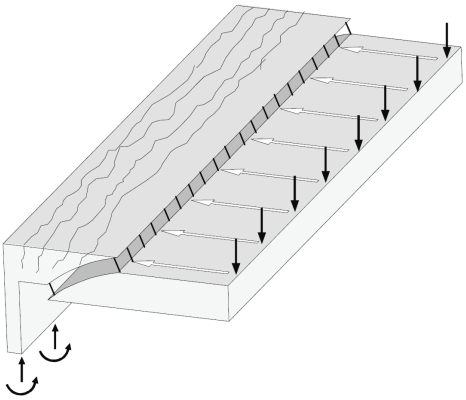

(a) ...and flow of forces in a cantilever slab subjected to a line load [40].

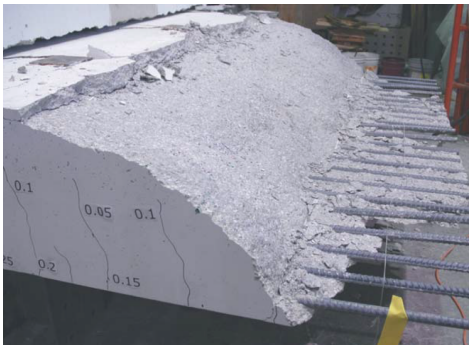

(b) ...surface in a slab [37].

2.1.2 Punching shear

Punching shear is generally associated with concentrated loads on slabs. The concentrated loads are introduced into the slab by radially developing shear forces. An example of this is a slab-column connection. The column may punch through the slab. The diagonal crack involved with this type of failure extends from the compression zone of the concrete, where the slab and column meet, to the tension zone in the slab at a certain distance away from the column. The result is a truncated conical shaped failure surface (figure 2.4).

According to Alexander and Simmonds (1987) [3] the angle of the diagonal crack is usually between 25 and 30 degrees.

When designing concrete slabs in the ultimate limit state, punching failure around concentrated loads or columns can be the governing failure mode. One-way shear can be seen as a two dimensional problem, while for punching shear three dimensions have to be considered. The three dimensional problem and the many parameters involved make the development of rational mechanical models difficult. Therefore in practice several simplifications are generally applied. Numerous models have been developed to determine the punching shear capacity. The critical shear crack theory (2.2.3) is an example of a punching shear model.

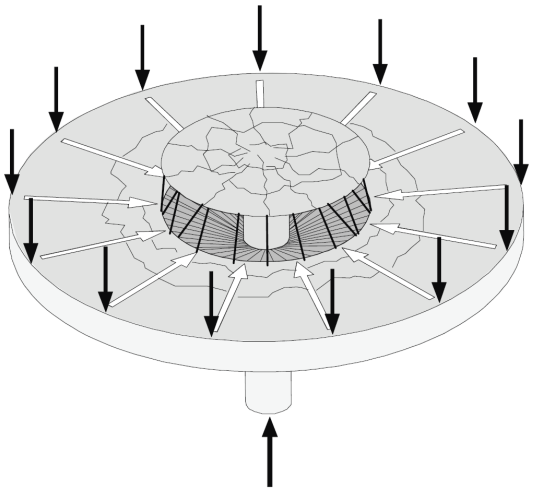

Figure 2.4: Punching shear failure and flow of forces in a flat concrete slab to column connection [40].

Axis-symmetrical conditions

One of the simplifications that is often applied for punching is the assumption of axis-symmetrical conditions. The simplification means that for both orthogonal directions of the slab the loading, slab and column geometry and reinforcement layout are considered to be the same. When a floor is carried by columns with all equal center-to-center distances this pure punching shear failure (figure 2.7 (a)) can occur at the interior column-slab connections (figure 2.5).

For an interior column four different stages in punching failure can be described (Masterson and Long 1974 [26]):

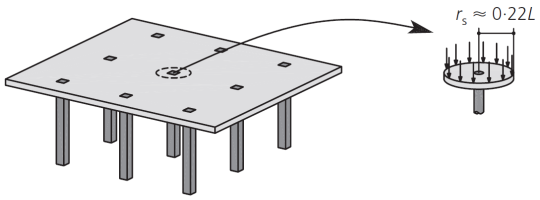

Figure 2.5: An example of axis-symmetrical conditions for an internal slab-column connection [36].

1. Flexural and shear cracks form in the tension zone of the slab near the face of the column.
2. The steel in the concrete tension zone of the slab, close to the column, yields.
3. Flexural cracks and shear cracks extend into what was the compression zone of the concrete.
4. Failure occurs before yielding in the steel extends beyond the vicinity of the column.

Diagonal punching cracks appear at load levels around 50% to 70% of the ultimate load. The cracked state is stable since unloading and reloading doesn't affect the ultimate load capacity [3].

Non-axis-symmetrical conditions

Since concrete slab bridges are generally supported only at two opposite sides, the conditions for punching are often non-axis-symmetrical (figure 2.6). Also at edge- or corner columns the conditions are non-axis-symmetrical so the assumption of axis-symmetrical conditions is not always justified. When the loading, slab and column geometry or reinforcement ratios are different for the two orthogonal directions, the behaviour of the slab might be asymmetrical. When one side of the column is subjected to a heavier load, the punching region is confined to the area on that side of the column. The opposite side may show a considerable lower stress (figure 2.7 (b)). The crack pattern for an edge column is similar (figure 2.7 (c)).

2.1.3 Between one-way shear and punching shear

For one-way slabs, like bridge deck slabs, subjected to a concentrated load very close to the support the shear failure mechanism is one-way shear. When

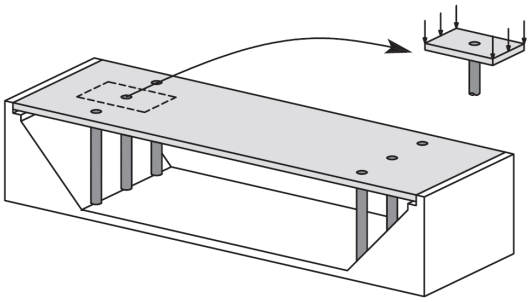

Figure 2.6: An example of non-axis-symmetrical conditions for a slab-column connection in a bridge deck slab [36].

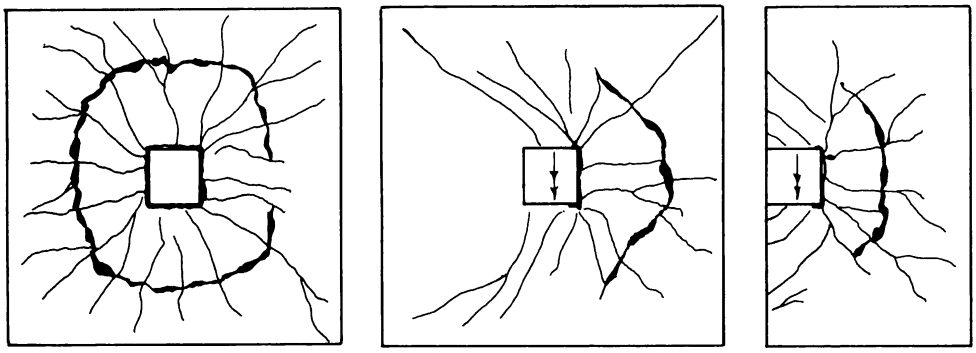

(a) Balanced (b) Unbalanced (c) Edge column

Figure 2.7: Punching failure under different load conditions [3].

the concentrated load is far away from the support, the shear failure mechanism can be described with punching shear. So as the distance from the concentrated load to the support increases, the shear failure mechanism changes from one-way shear failure to punching shear failure. The transition in failure mechanism is not sudden. Vaz Rodrigues et al. (2008) [41] stated that intermediate cases between one-way shear and two-way shear in a slab, where the shear forces develop neither parallel nor radially, can be found in practice. According to Gardner (1990) [11] punching failure will occur only if the distance between the support and the load is at least three times the slab thickness, because when the load is closer to the support the support itself interferes with the failure surface.

For wide beams and one-way spanning slabs loaded close to the support models are developed to predict the shear capacity. These models are mostly based on one-way shear using an effective width. According to the building codes, when the concentrated load is not close to the support it is customary to calculate both the one-way shear capacity and the punching shear capacity to see which failure mode is governing. So at increasing distance from the concentrated load to the support either a model for one-way shear is governing or a model for punching-shear is governing. A transition between one-way shear and punching shear is not considered.

Regan (1982) [32] developed a model for slabs subjected to a concentrated load near the support, based on a model for punching shear as used in the former British Standard. The model assumes that the failure mechanism is not fully one-way shear, but not fully punching shear either.

Experiments on slabs loaded close to support are compared to one-way shear provisions and punching shear provisions from the Eurocode (NEN-EN1992-1-1:2005) [8], the NEN (NEN 6720) [13], the ACI (ACI 318-08) [5] and Regan's method [32] in Lantsoght et al. (2010a/b) [20] [21]. The predictions from Regan's method [32] turned out to be the most accurate, suggesting that failure in one-way slabs subjected to concentrated loads near the support is neither solely one-way shear failure nor is it solely punching shear failure. The intermediate behaviour is further investigated in this thesis.

2.2 Models for shear

There are several models concerning shear. Most models focus on either one-way shear or on punching (two-way) shear. Some of them can be applied for both cases.

2.2.1 Tooth model

In an attempt from Kani (1964) [16] to provide a rational theory for the effects of shear and diagonal tension on the behaviour of reinforced concrete members, he developed a model called "tooth model". Kani classifies two main types of failure in beams; flexural failure and diagonal failure. Diagonal failure is the visible failure of all failures which are not considered flexural failures. A beam subjected to an increasing load can be represented as a comb-like structure. In the tensile zone of the beam, more or less vertical cracks appear due to insufficient concrete tensile strength. The concrete between the vertical cracks shows a resemblance with teeth. The tensile forces are carried by the (flexural) reinforcement. The concrete compressive zone of the beam can be seen as the backbone of the comb (figure 2.8).

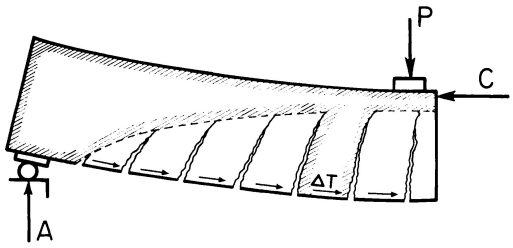

Figure 2.8: The function of teeth in the tooth model developed by Kani [16].

The tooth model makes a distinction between two types of reinforcement in beams; reinforcement with bond and reinforcement without bond. When there is no bond between reinforcement and concrete, diagonal failure will not occur. The beam will fail in flexure.

In the case of reinforcement with bond however, the tensile force from the reinforcement is gradually introduced by bond. The result is a thrust line starting at the bottom of the beam going almost vertically upward but ending at the top of the beam in horizontal direction when the steel is fully bonded (figure 2.9).

The vertical concrete teeth can be seen as cantilevers clamped at the top (backbone). A load ΔT from the reinforcement acts on the end of the teeth. The beam can be seen as a beam with a compression zone at the top with the highest compression in the top fibre for as long as the teeth can carry the load ΔT. The moment corresponding to the moment of failure of the concrete teeth can be derived as:

$$M_{CR} = M_0 \frac{\Delta x}{s} \frac{a}{d} \tag{2.1}$$

where:

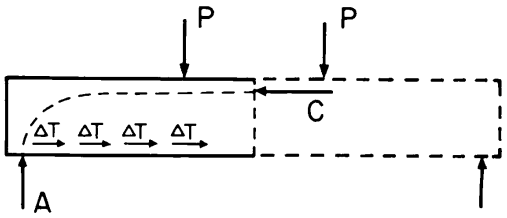

Figure 2.9: A free body diagram for Kani's Tooth model with bonded reinforcement [16].

M_{CR} is the critical moment at which the tooth can no longer carry ΔT.

M_0 is the part of the moment depending only on the cross-sectional properties.

a is the shear span: the distance from the edge of the support to the point of application of the load.

d is the effective depth of the beam.

Δx is the (average) width of a tooth.

s is average length of the teeth.

When the cross-section of the concrete and the layout of the reinforcement do not change over the length of the beam, the critical moment is a linear function of the shear span to effective depth ratio a/d. When the ratio a/d increases, the critical moment M_{CR} will increase as well. The increase is limited to the point at which the full flexural capacity of the cross section is reached (figure 2.10).

After failure of the teeth the tensile force in the reinforcement is constant over the whole length, also for a beam with reinforcement without bond. A new equilibrium of forces can be formed in the shape of a tied compressive arch (figure 2.11). A big difference between the tied arch and the beam with bonded reinforcement is that in the former case the highest compressive force is in the top fibre and in the latter case the highest compressive force is near the bottom fibre of the arch.

It was found that for beams with an a/d ratio up to 2.5 the transformation from beam action into tied compressive arch action took place gradually so there is no failure upon the formation of a diagonal crack. After transformation the beam can still have load carrying capacity. If a tied compressive arch

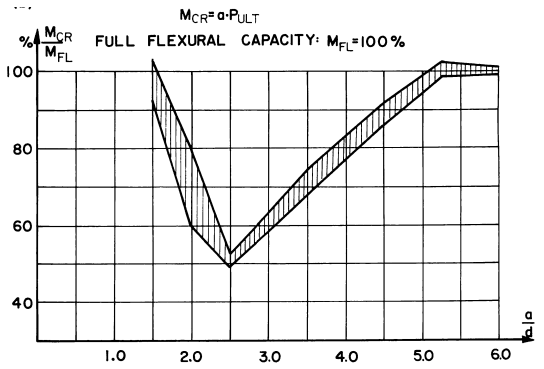

Figure 2.10: The effect of the shear-span to depth ratio on the ratio of maximum moment to theoretical flexural failure moment M_{CR}/M_{FL} [16].

is formed, the load carrying capacity can be estimated with the expression:

$$M_{CR} = \frac{M_0}{0.9}\frac{d}{a} \tag{2.2}$$

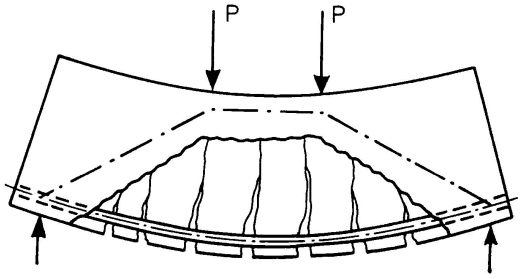

Figure 2.11: The remaining concrete arch is formulated in the tooth model [16].

Kani found three characteristic stages in the behaviour for different a/d values in his experiments. These values are influenced by various parameters: reinforcement ratio, the concrete strength, element width and loading plate width (section 2.3). In the experiments from Kani three stages where found. For a/d values smaller than 2.5 the concrete teeth will fail before the tied compressive arch fails, so the load carrying capacity of the beam is limited by the load carrying capacity of the arch. For a/d between 2.5 and 5.2 the capacity of the concrete teeth is higher than the capacity of the tied compressive arch, resulting in sudden collapse of the structure after the teeth fail or at the formation of a diagonal crack. For a/d values above 5.2 the

load carrying capacity is limited by the flexural strength of the beam. These stages can be clearly distinguished in figure 2.10.

Olonisakin and Alexander (1999) [29] conducted research on reinforced concrete beams. Taking into account the tooth model for one-way shear, they analysed the contribution of the beam action and arching action under increased loading until failure.

$$V = \frac{dM}{dx} = \frac{d\,(Tjd)}{dx} = jd\frac{dT}{dx} + T\frac{jd}{dx} \tag{2.3}$$

where:

V is the one-way shear (gradient of bending moment along the length of the member).

M is the bending moment in the beam.

T is the tensile steel force.

jd is the effective moment arm.

$jd\frac{dT}{dx}$ is the shear carried by beam action.

$T\frac{jd}{dx}$ is the shear carried by arching action.

Both beam action and arching action take place and their contribution to the shear capacity changes as the load increases. In the tests they performed beam action only accounted for one third to two thirds of the total shear force at failure. Olonisakin and Alexander conclude that beam action shear did not account for all or even a consistent fraction of the total shear at failure. It was also concluded that yielding of the reinforcement within the shear span forces a shift from beam action to arching action. As a consequence, the formulation of a plastic hinge may precipitate a shear failure. In the design codes, the formulas are based on beam action only. The predictions from the design codes are mostly reasonable, but they often are based on empirical relations.

2.2.2 Strut and tie model

Strut and tie models (sometimes called truss models) are models to describe the flow of forces in concrete. The system consists of compressive struts and tension ties. The compressive struts form in the concrete and the tension ties can be tensile reinforcement bars, prestress tendons or tensile stress

fields. Traditionally the strut and tie model assumes that the compressive strut runs parallel to the direction of cracking and that stresses can not be transferred across cracks. Newer models based on the strut and tie principle assume tensile stresses that exist in transverse direction to the struts and/or shear stresses that are transferred across the inclined crack by aggregate interlock or friction. The assumptions implicate that the angle of the principal compression stress is less than the crack angle and that there is a vertical force component along the crack that contributes to the shear strength of the concrete element (ACI 445-99 [2]). An example of a basic strut and tie model can be found in figure 2.12

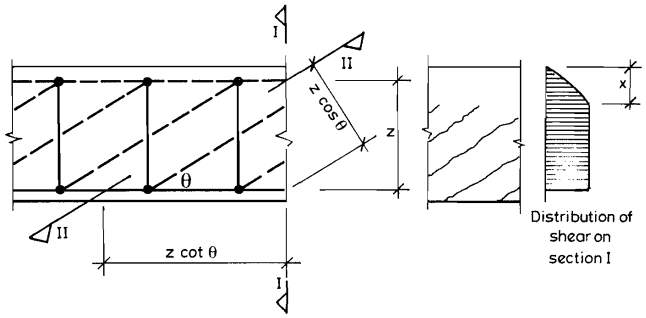

Figure 2.12: An example of a strut and tie model [33].

In slabs or wide beams subjected to concentrated loads three dimensional models are required to describe the flow of forces in the concrete. Alexander and Simmonds (1987) [3] created a strut and tie model for slabs. Their model predicts the ultimate capacities of the slab. Punching is defined as failure of the slab to confine concrete compression forces out of the plane of the slab. In their proposed model the reinforcing steel and the concrete compression fields are broken down into individual bar-strut units. Two types of compression struts are distinguished: compression struts which run parallel to the plane of the slab (anchoring struts, figure 2.13 (a)) and compression struts running at some angle α to the plane of the slab (shear struts, figure 2.13 (b)). The compression struts are equilibrated by two perpendicular reinforcing bars. One bar has to pass through the loading area, parallel to the axis about which the unbalanced moment is acting, and the other is some distance from the column. The bars at some distance from the column are able to exert moment on the connection by flexure.

Slabs are subjected to distributed loading so the load application point does not coincide with the junction of the tensile and compressive force. As result, α is not predefined at the position of the load. The vertical (shear)

component is not equilibrated at the bar-strut junction by the applied load. There exists a force component out of the plane of the slab that must be balanced by some form of tension field within the concrete. The result is a three dimensional strut and tie system as shown in figure 2.14. The proposed model assumes however that the compression failure of the concrete strut will not be governing. The out-of-plane component can be described with three parameters: tributary width of each reinforcing bar s, the cover of the reinforcement d' and the strength of the concrete.

Failure can occur in three ways. Failure of the slab to confine concrete compression forces out of the plane of the slab, failure of the compression strut, or failure of the tension tie. The failure types require the reinforcement anchorage not to be governing. The accuracy of the model depends on the right prediction of the angle of inclination of the compression strut α.

$$K = \frac{s_{eff} d' \sqrt{f'_c}}{A_{\text{bar}} f_y \sqrt[4]{c/d_s}} \tag{2.4}$$

$$\tan \alpha = \frac{P_{\text{failure}}}{A_{\text{st}^T} f_y} K \tag{2.5}$$

where:

s_{eff} is the tributary width of each reinforcing bar.

d' is the concrete cover depth of the reinforcement.

f'_c is the concrete cylinder compression strength.

A_{bar} is the cross-sectional area of a single reinforcement bar.

f_y is the yield stress value of the steel.

c is the dimension of the column face perpendicular to the considered bar.

d_s is the effective depth of the reinforcing mat measured from the center of the mat to the compression surface of the slab.

P_{failure} is the failure load.

A_{st^T} is the cross-sectional area of the top mat strut steel.

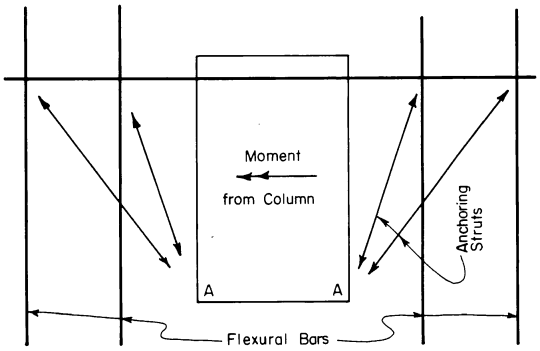

(a) Anchoring struts

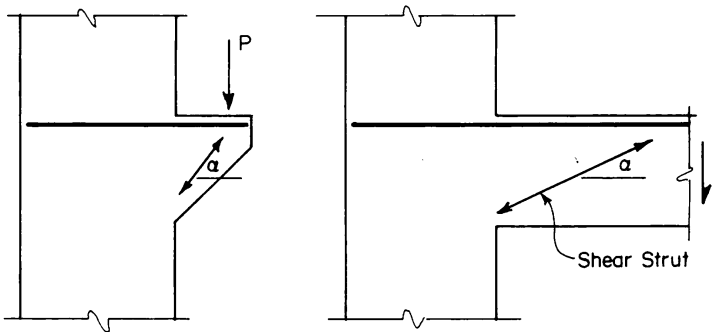

(b) Shear struts

Figure 2.13: Types of compression struts in the 3D truss model from Alexander and Simmonds (1987) [3].

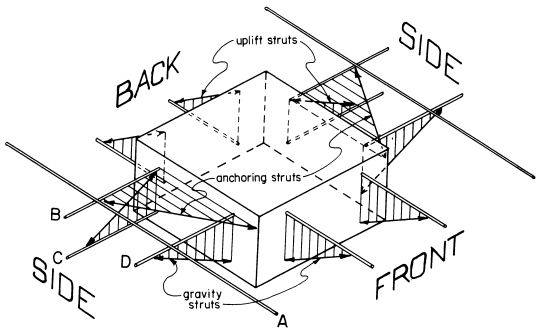

Figure 2.14: A three dimensional strut and tie system [3].

2.2.3 Critical shear crack theory

The critical shear crack theory (CSCT) [28] is a failure criterion for shear proposed by Muttoni (2008) [27]. The CSCT assumes that the width of the critical shear crack is proportional to the slab rotation, multiplied by the effective depth of the member, and corrected by a factor to account for the maximum diameter of the aggregate and the concrete strength. The CSCT is based on a mechanical model. It allows for both one-way shear failure mechanisms and punching shear mechanisms.

The CSCT is based on the assumption that shear strength of members without transverse reinforcement is governed by the width and roughness of a shear crack. The shear crack develops through the inclined compression strut carrying shear. When the critical shear crack opens, the strength of the inclined concrete compression strut which carries the shear reduces, ultimately leading to shear failure.

Originally, the CSCT was developed for slabs without transverse reinforcement and for axis-symmetrical conditions. Through further research the CSCT was extended for use in shear reinforced slabs and columns with non-axis-symmetrical conditions (Sagaseta et al. 2011 [36]).

CSCT for beams and one-way slabs

The following formula has been derived for beams and one-way slabs without shear reinforcement:

$$V_R = \frac{1}{3} \cdot \frac{bd\sqrt{f_c}}{1 + 120\dfrac{\epsilon d}{d_{g,0} + d_g}} \tag{2.6}$$

where:

V_R is the one-way shear resistance.

b is the (effective) width.

d_g is the maximum aggregate size.

d is the average flexural depth of the concrete slab.

ϵ the strain in a control depth at $0.6d$.

$d_{g,0}$ is the reference aggregate size (16 mm).

When a depth of the compression zone $c = 0.35d$ is assumed, the value for ϵ can be estimated with this equation:

$$\epsilon = \epsilon_s \frac{0.6d - c}{d - c} \approxeq 0.41\epsilon_s \tag{2.7}$$

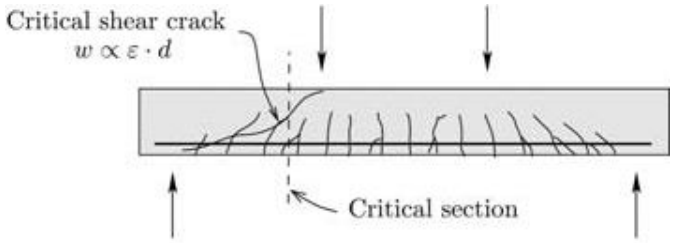

Figure 2.15: CSCT for beams and one-way slabs [28].

where:

ϵ_s is the reinforcement strain ($\epsilon_s = f_{yd}/E_s$ at yielding).

c is an estimation of the height of the concrete compression zone $c = 0.35d$.

d is the effective depth of the concrete.

E_s is the modulus of elasticity for the steel.

f_{yd} is the design yield strength of the steel.

Figure 2.16 compares the result from equation 2.6 with 272 tests on beam shear. It can be seen that there is a good agreement between the derived equation and the test results.

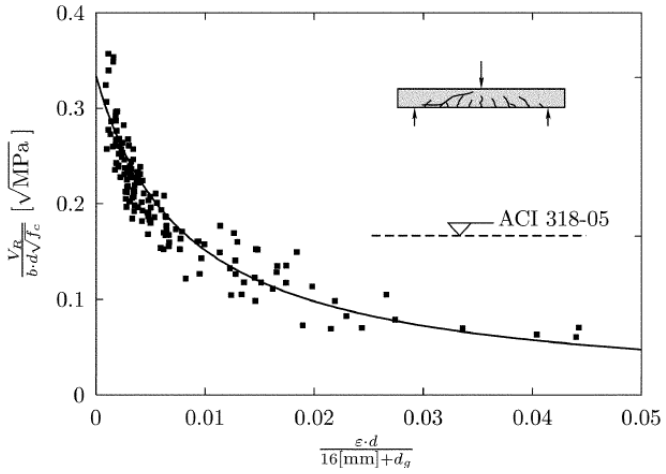

Figure 2.16: CSCT one-way shear strength compared with 272 experimental results [1].

CSCT for slabs

The formula has been derived for slabs without shear reinforcement:

$$V_R = \frac{3}{4} \cdot \frac{b_0 d \sqrt{f_c}}{1 + 15 \dfrac{\psi d}{d_{g,0} + d_g}} \tag{2.8}$$

where:

V_R is the shear resistance.

b_0 is the control perimeter at a distance from the face of the column equal to λd ($\lambda = 0.5$ in the CSCT).

d_g is the maximum aggregate size.

d is the average flexural depth of the concrete slab.

ψ is the slab rotation for axis-symmetrical cases. The slab rotation is assumed to be constant outside the perimeter separated by the critical shear crack.

$d_{g,0}$ is the reference aggregate size (16 mm)

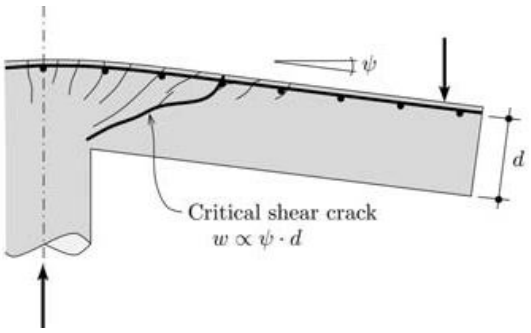

Figure 2.17: CSCT for slabs [28].

The deformation capacity can be predicted by using a non-linear finite-element analysis or by using a simplified formula (formula 2.9) for axis-symmetrical cases proposed by Muttoni (2008) [27]. A more complex formula is necessary in case of thick slabs with low reinforcement ratios to accurately take into account the effects of concrete tensile strength and tension stiffening.

$$\psi = 1.5 \frac{r_s}{d} \frac{f_y}{E_s} \left(\frac{V}{V_{flex}} \right)^{3/2} \tag{2.9}$$

where:

r_s is the radius of the isolated slab considered.

V_{flex} is the flexural strength.

E_s is the modulus of elasticity for the steel.

f_{yd} is the design yield strength of the steel.

The failure criterion can provide both the punching load at failure and the rotation capacity of the slab. When combined, this gives the ductility of the slab.

The critical shear crack theory takes into account the following aspects [27]: the effect of an increase in the bending reinforcement, the effect of column size relative to the slab thickness, the effect of effective slab thickness, effect of concrete strength, effect of steel type and steel yield stress, span to depth ratio of the slab.

Figure 2.18 compares the result from equation 2.8 with 99 punching tests. It can be seen that there is a good agreement between the derived equation and the test results.

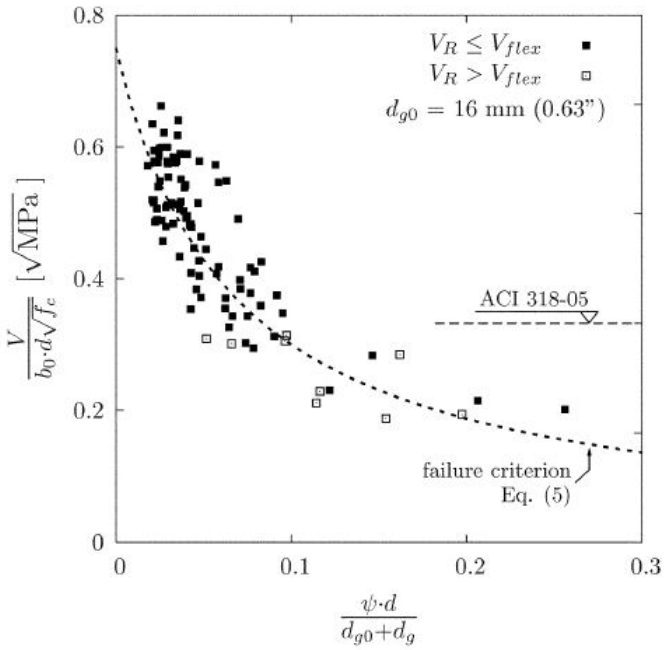

Figure 2.18: CSCT punching shear strength compared with 99 experimental results [27].

Size effect

Muttoni (2008) [27] states that the size effect in the CSCT is introduced by multiplying the slab rotation with the effective slab thickness (ψd). In the simplified formula for the deformation capacity (formula 2.9) a slenderness factor is present (r_s/d). When equation 2.9 is substituted into the formula for shear capacity (formula 2.8), the factor for the reduction of strength for the size effect becomes a function of the span (r_s).

Aggregate interlock

For the critical shear crack theory (Muttoni and Fernandez Ruiz 2008) [1], the value representing the aggregate interlock d_g is set to zero when the compressive strength of the concrete becomes above 60 MPa or when the concrete is lightweight. The limitation is required is because in those cases the concrete matrix might be stronger than the aggregates, causing the cracks to go through the aggregate material.

Concrete strength

In the critical shear crack theory (Muttoni and Fernandez Ruiz 2008) [1], the relation between the square root of the concrete compressive strength and the shear strength is linear (formula 2.6). For larger concrete compressive strengths, the shear failure load increases. The strains developed by the reinforcement become larger as well, resulting in a larger width of the critical shear crack. The above suggest a less than linear relationship between the square root of concrete strength and the shear strength.

Critical section

The control perimeter that is considered in the critical shear crack theory is positioned at a distance $0.5d$ from the face of the column. The control perimeter has curved corners.

(Non-)axis-symmetrical conditions

According to Sagaseta et al. (2010) [36] theoretical and empirical approaches for punching in non-axis-symmetrical conditions are adapted versions of approaches for axis-symmetrical conditions. These adoptions are often done by using a series of factors. The theoretical background is considered the same, but this is not true. Non-axis-symmetrical conditions can occur due to loading, slab and column geometry or due to reinforcement layout. A relevant

example is the concentrated loads from heavy trucks in slab bridges near the supports.

Sagaseta et al. (2011) [36] tested the punching shear strength of concrete slabs with non-axis-symmetrical conditions ($\rho_x \neq \rho_y$). It was observed that the crack pattern was non-axis-symmetrical in these slabs (figure 2.19). The shear failure cone turned out to be the steepest in the direction of the lowest reinforcement ratio. Based on these results it was proposed to treat punching shear in slabs with $\rho_x \neq \rho_y$ by considering the orthogonal directions individually.

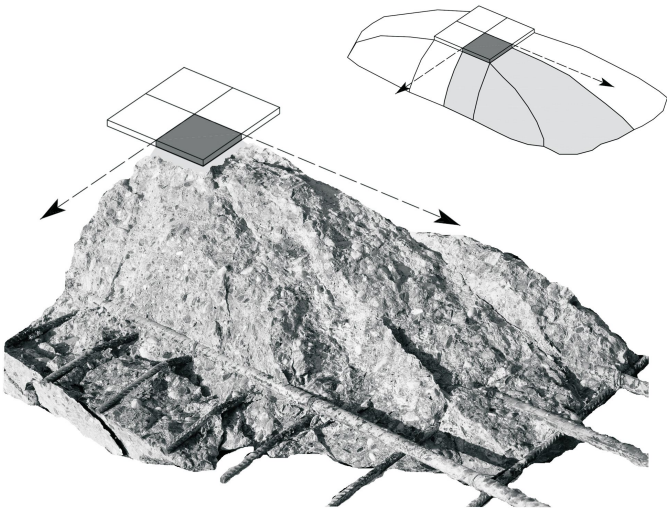

Figure 2.19: Non-axis-symmetrical punching shear failure cone for $\rho_x \neq \rho_y$ [36].

Because in non-axis-symmetrical slabs the slab rotations ($\psi_x \neq \psi_y$, figure 2.20a) are different for both orthogonal directions, it can be said that the nominal punching strength $v_R(s)$ along the control perimeter is non-uniform (figure 2.20b). So during increased loading, the ultimate strength is not reached along the whole perimeter at the same amount of loading. Some parts of the perimeter will still have additional strength capacity. There is shear softening at the segments with the largest rotation and increasing shear at segments with the lower rotations. The redistribution of shear stresses causes a higher punching shear resistance (figure 2.21). In practice a constant nominal shear stress v_{Rmax} around the perimeter is assumed, not taking into account this additional strength capacity.

When the punching strength needs to be calculated, the nominal strength can be integrated along the control perimeter. For square columns the punching shear can be calculated in the following manner: Along the straight seg-

Figure 2.20: [36] For a non axis symmetrical slab, along the control perimeter the non-uniform...

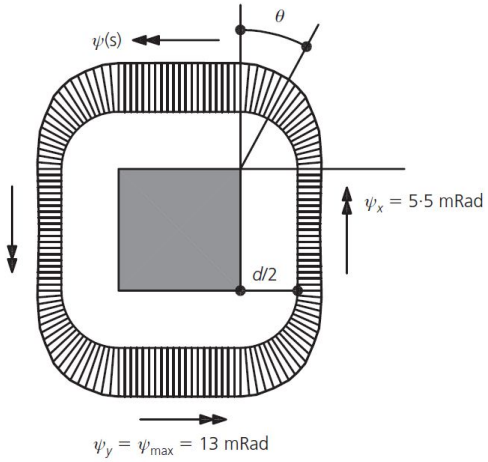

(a) ...slab rotations

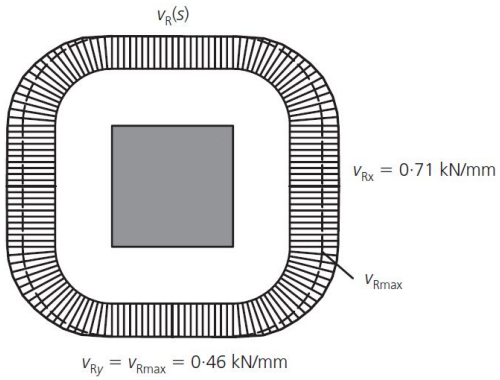

(b) ...nominal strength corresponding to the slab rotations

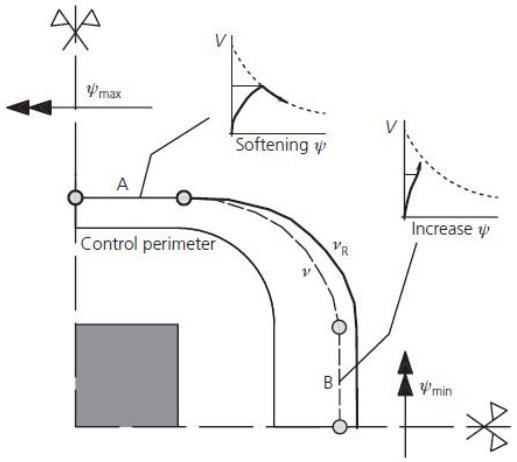

Figure 2.21: Redistribution of nominal shear stress in CSCT [36].

ments of the control perimeter, the rotations $\psi(s)$ of the slab are assumed to be constant. At the corners, the transition from $\psi_(x)$ to ψ_y takes place in an approximately parabolic fashion. Taking this into account results in the following equation:

$$V_R = \int_{cp} v_R(s)ds = 2c\,(v_{Rx} + v_{Ry}) + V_{R,\text{corners}} \tag{2.10}$$

$$v_{Rx} = \frac{3}{4} \cdot \frac{d\sqrt{f_c}}{1 + 15\dfrac{\psi_x d}{d_{g,0} + d_g}} \tag{2.11}$$

$$v_{Ry} = \frac{3}{4} \cdot \frac{d\sqrt{f_c}}{1 + 15\dfrac{\psi_y d}{d_{g,0} + d_g}} \tag{2.12}$$

$$V_{R,\text{corners}} = 4\int_0^{\pi/2} v_R(\theta)\frac{d}{2}d\theta \tag{2.13}$$

where:

V_R is the punching strength.

cp stands for control perimeter.

v_R is the punching shear stress per unit length (nominal strength).

c is the side length of the column

s is the position along the control perimeter.

$V_{R,\text{corners}}$ is the total punching strength of the four control perimeter corners.

θ is the angle of the corner (varying between 0 and $\pi/2$).

b_x, b_y are the segments of the control perimeter corresponding to the x and y directions.

A simplified method to determine the punching shear strength for square rectangular columns using the CSCT is to divide the control perimeter into only four sections.

$$V_R = v_{Rx}b_x + v_{Ry}b_y = \frac{V_{Rx}}{b_0}b_x + \frac{V_{Ry}}{b_0}b_y \tag{2.14}$$

where:

$b_0 = b_x + b_y$

2.2.4 The (modified) compression field theory

The compression field theory is a model that can predict the load-deformation response of reinforced concrete elements subjected to in-plane shear stresses and normal stresses. The model distinguishes itself by treating cracked concrete and undamaged concrete as separate materials. The theory uses the average stresses and average strains. Local stress conditions at crack locations are also considered. The model is considered important because it is used as a basis in the FEM analysis that is performed in the next chapters.

In concrete reinforced slabs under loading the stresses in the reinforcing bars will vary along the lengths of the bars. The highest stresses will be at the crack locations. It is assumed that the concrete can transfer shear and compression across the cracks, but not tension. Tension forces will exist in the reinforcement and in the concrete between the cracks. The original compression field theory ignored tension in the cracked concrete, but the modified compressive field theory however, does not (Vecchio and Collins 1986 [43]). In both the CFT and MCFT a stress-strain curve incorporating a softening coefficient is used as proposed by Vecchio and Collins (figure 2.22). They discovered that the principle compressive stress in a reinforced concrete panel was softened by principal tension.

Membrane elements represent a portion of the concrete structure. The individual elements are assumed to be relatively small and uniform in thickness. It is also assumed that the loads (axial and shear) acting on the element edges are uniform and that the edges of a deformed element remain straight and parallel. The in-plane stresses f_x, f_y and v_{xy} are related to the in-plane strains ϵ_x, ϵ_y and γ_{xy}. When the three strain components are known, the strain in any other direction can be derived by using Mohr's circle. A summary of the MCFT is given in figure 2.23.

The inclination θ of the diagonal compressive stresses is determined using the strain conditions. The factor to account for tensile stresses in the cracked concrete is β. Simplified methods to determine these unknowns are provided by Bentz et al. 2006 [6].

$$\beta = \frac{0.4}{1 + 1500\epsilon_x} \frac{1300}{1000 + s_{xe}} \tag{2.15}$$

$$\theta = (29 \text{ deg} + 7000\epsilon_x)\left(0.88 + \frac{s_{xe}}{2500}\right) \leq 75 \text{ deg} \tag{2.16}$$

$$\text{where: } s_{xe} = \frac{35 s_x}{a_g + 16} \tag{2.17}$$

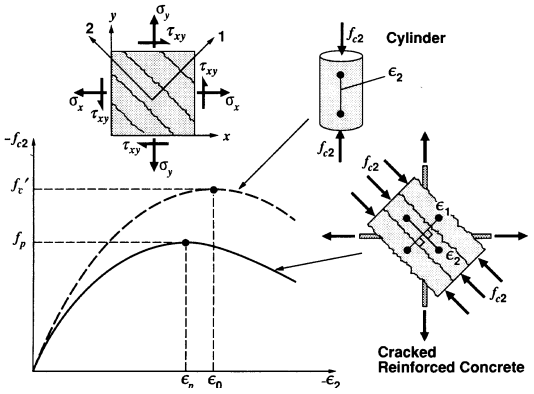

Figure 2.22: Deteriorated compression response in cracked reinforced concrete [42].

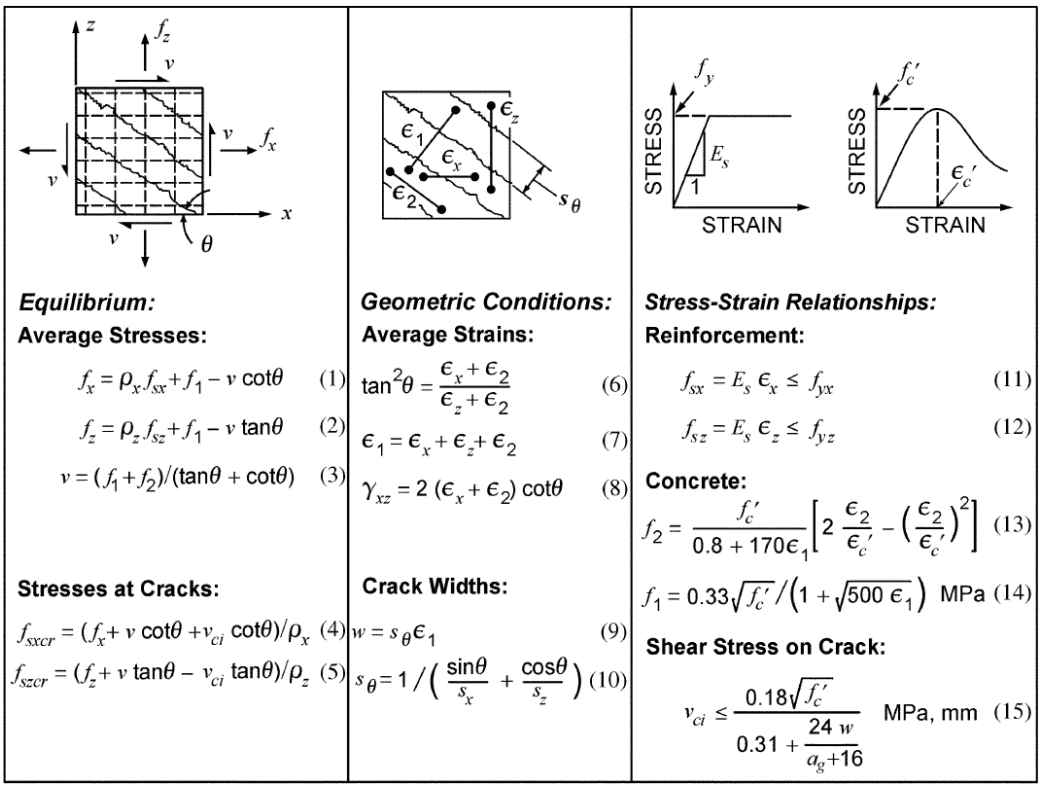

Figure 2.23: Modified Compressive Field Theory [6].

2.3 Parameters influencing shear

There are many parameters influencing the shear capacity of reinforced concrete elements. The parameters listed below are considered of significant importance and are briefly described.

Geometry
- Element width and effective width
- Shear span to depth ratio a/d
- Size effect

Material
- Concrete strength
- Maximum aggregate size
- Type of reinforcement
- Reinforcement ratio and layout

Loading and support
- Size and shape of the load
- Type of support
- Support conditions

2.3.1 Geometry

Element width and effective width

The behaviour of a slab subjected to concentrated loads is different for slabs spanning in one direction and for slabs spanning in two directions. The shear resistance of one-way slabs under concentrated load is researched by Regan and Rezai-Jorabi (1988) [34]. For slabs subjected to a concentrated load, axis-symmetrical conditions are often assumed. However when the slab is spanning in only one direction, the conditions are different. The shear force is neither distributed more or less uniformly across the width of the element like in beams, nor is it uniform around the load like in axis-symmetrical slabs. The shear force in the one-way slab subjected to a concentrated load is non-uniform across the width of the element. The non-uniformity is shown by measuring steel strains in transverse reinforcement bars across the width of the plate (figure 2.24).

Regan and Rezai-Jorabi (1988) [34] suggest that, in case of one-way slabs or wide beams under concentrated loads, the load is transferred in two ways. The first is primary action, where the concentrated load is spread symmetrically to a square area. The secondary action is the transfer of the load only

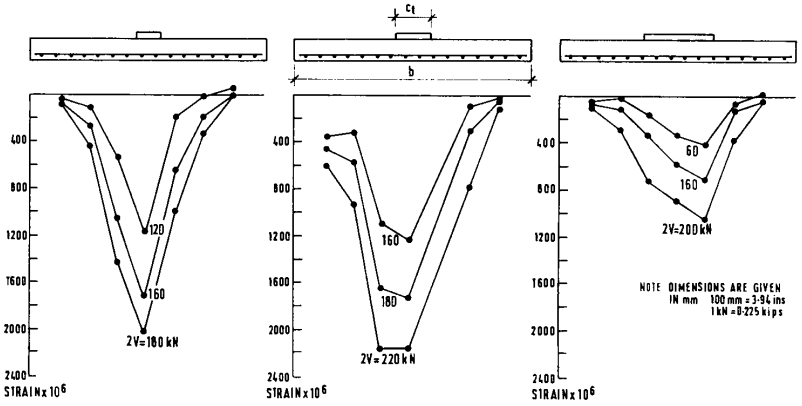

Figure 2.24: Steel strains in the transverse reinforcement bars of one-way slabs subjected to concentrated loads [34]. ($b = 1000mm$)

in the longitudinal direction towards the supports. This suggest that the effective width can not be larger than the square area and it is only affected by the load plate area (and limiting slab width) and not by the shear span.

In the case of one-way spanning slabs subjected to a uniform line load across the width it turns out that the width of the element is not of significant influence (figure 2.25) according to Sherwood et al. (2006) [37].

For slabs spanning in only one direction subjected to a concentrated load, building codes usually assess the shear capacity by assuming that the shear is carried by only a portion of the slab: the effective width. Within this strip the shear distribution is assumed constant over the width. The principle is applied for loads close to the support (figure 2.26). The minimum effective width for loads applied in the middle of the width of the element is $2d$ and when the load is applied at the side edge a minimum effective width of d is commonly used in Dutch practice.

As the load is applied closer to the support, the effective width gets smaller in the method in figure 2.26. The method is simple but not always accurate. Regan (1982) [32] developed a method for the shear capacity in one-way slabs based on a punching shear formula, which uses a perimeter around the load. In the case of Regan's method the part of the perimeter that is within $0.5d$ and runs parallel to the support is treated differently than the other parts of the perimeter. Comparisons of experimental results with predictions from the Eurocode and Regan's method (Lantsoght et al. (2011b) [23]) indicate that Regan's method provides the better predictions. The comparisons indicate that using an effective width may not be the best solution in determining the shear capacity of slabs.

A method of load spreading used in France is illustrated in figure 2.27.

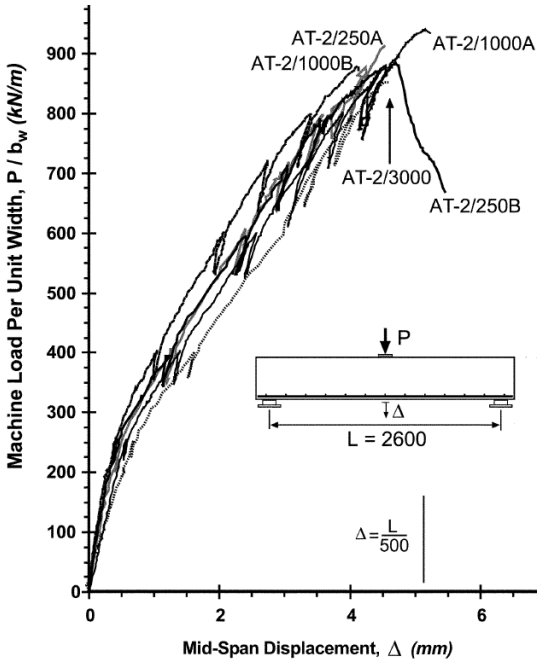

Figure 2.25: Element width influence on one-way shear capacity under tire load [37]. The element widths are indicated in the graph names (250mm, 1000mm, 3000mm). The element height, length, concrete strength and longitudinal reinforcement ratio are constant.

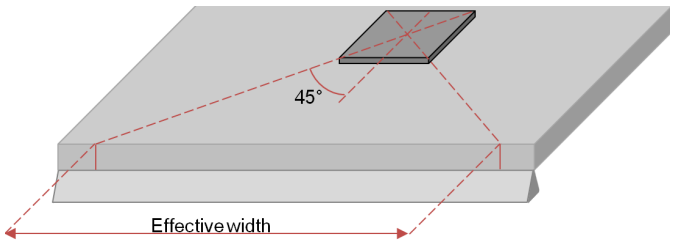

Figure 2.26: Determination of the effective width in a one-way slab subjected to a concentrated load in proximity of the support.

The load spreading is assumed under an angle of 45 degrees from the far corners of the loading plate. The approach incorporates the effect of the size of the loading on the effective width (section 2.3.3). Comparing the two methods to determine the effective width (figure 2.26, 2.27) with experimental results (Lantsoght et al. 2011c [24]) indicates that the method used in France is a better approximation.

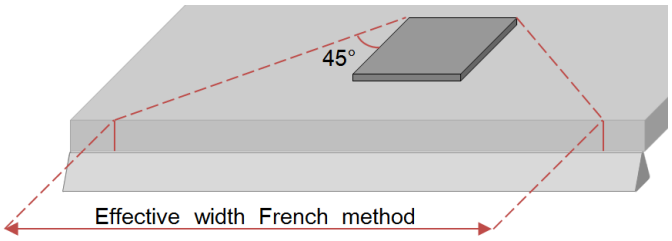

Figure 2.27: French method of determining the effective width in a one-way slab subjected to a concentrated load in proximity of the support.

Shear span to depth ratio

Around 1908 Talbot [38] indicated that the shear capacity is mainly influenced by the longitudinal reinforcement ratio, the concrete compressive strength and the span to effective depth ratio. Later it was found that the shear span to effective depth ratio was of influence and in 1964 Kani [16] provided a sound theoretical explanation for the effect of the shear span to effective depth ratio (a/d) on the ratio of maximum moment to theoretical flexural failure moment (M_{CR}/M_{FL}). The results are based on tests on beams. The effect is known as "the valley of shear" or "Kani's valley" (figure 2.10). The effect can be explained by a strut-and-tie model. Close to the support a direct compression strut can develop between the support and the load. The capacity of the compression strut increases when the angle increases. When the load moves closer to the support, the load carrying capacity increases. This form of direct load transfer is included in the Eurocode (chapter 2.4.2).

Another explanation is the reduced aggregate interlock for high a/d ratio values. When the value of the a/d ratio increases, the moments occurring in the elements increase in magnitude as well. Since the flexural cracks and their widths are dependant on the flexural moment, the crack widths increase. In it's turn, the increased crack width reduces the aggregate interlock or crack friction, this leads to less shear force transfer across the cracks so the shear capacity reduces.

The application of the strut-and-tie model applied to slabs with a concentrated load (figure 2.28 (b)) is different than for beams (figure 2.28 (a)). The shear span a is the smallest horizontal distance between the load and the support. The distance can be seen as the horizontal length of the compressive strut. Now let us call the average horizontal length of all the compressive struts in the fan of struts between the loading plate and the support a^*. For elements with a relative small width the compressive struts in the fan of compressive struts from the load to the support all have approximately the same length (so $a^*/a \approx 1$). When the element width is relatively big like in wide beams or slabs, the compressive struts in the fan of compressive struts do not have approximately the same length (so $a^*/a > 1$). If we now use distance a^* instead of distance a to determine the shear span to depth ratio, its value will increase ($a/d < a^*/d$), this might suggest a horizontal shift to the left in the valley of shear (figure 2.10) when applied to slabs instead of beams.

Figure 2.28: Compression strut between load and support.

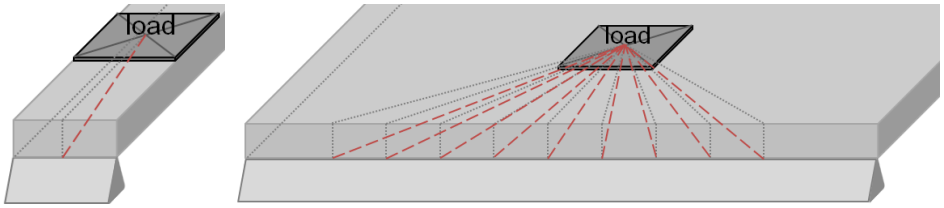

(a) Direct compression strut in a beam.

(b) Fan of compression struts in a slab.

The influence of the a/d ratio on the shear capacity for slabs subjected to concentrated loads was investigated by Lantsoght et al. (2011b) [23]. Test results indicate that the increase in loading capacity when the load is applied closer to the support is less for slabs than it is for beams. The increase can be explained by redistribution of forces after cracking, this is possible due to the large width of the slab compared to beams. The crack widths remain small and therefore the loss of aggregate interlock is limited.

The influence of the element width on the load capacity for decreasing a/d ratios is further investigated by Lantsogth et al. (2011c) [24]. It is clear that the increase in capacity, when the a/d ratio is lowered from 2.26 to 1.51, is much higher for small element widths than it is for elements with a bigger width (figure 2.29).

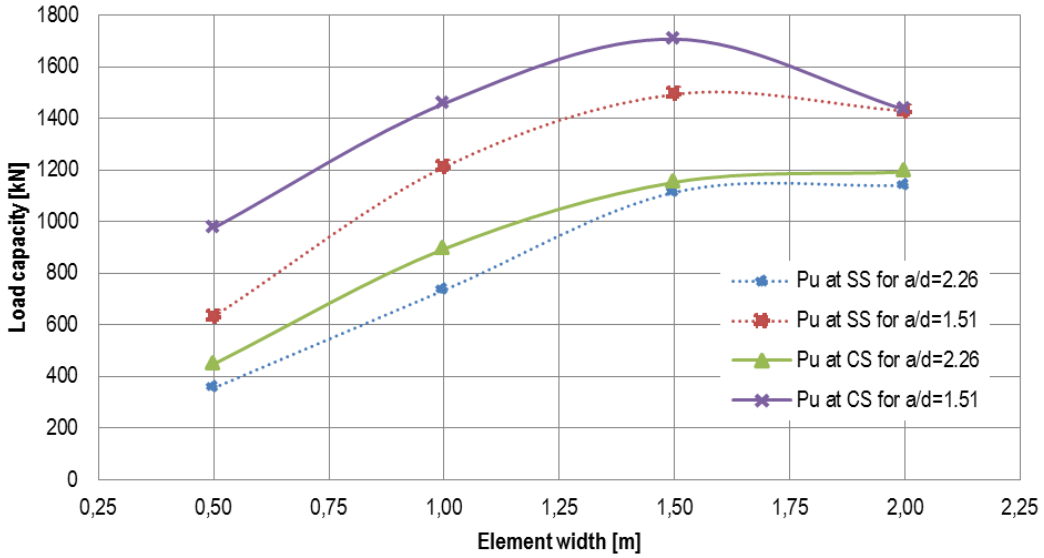

Figure 2.29: Influence element width on load capacity increase for decreasing a/d ratio. (Data obtained from Lantsoght et al. 2011c [24])

Size effect and aggregate size

Related to the slab geometry and the shear span to depth (a/d) ratio is the size effect. The size effect is the decrease in shear stress at failure when the member depth increases. Uzel et al. (2011) [39] show the size effect in shear (figure 2.30). One of the explanations for the size effect is the following: Compared to small members, in large members, the crack widths that occur during loading are large as well. The aggregate interlock capacity lowers as the crack width increases, this causes failure at lower stresses. The size effect is thus closely related to aggregate interlock and therefore the aggregate size.

Uzel et al. (2011) [39] also compared several tests on size effect with different a/d ratios. It was found that for large shear span to depth ratios ($a/d = 6$) the size effect was substantial. For moderate shear span to depth ratios ($a/d = 3$) the size effect was less pronounced and for $a/d = 2$ there was no size effect found. The above is shown in figure 2.31.

2.3.2 Material properties

Concrete strength

To describe the effects of concrete strength on the shear capacity, some shear transfer mechanisms need to be introduced first.

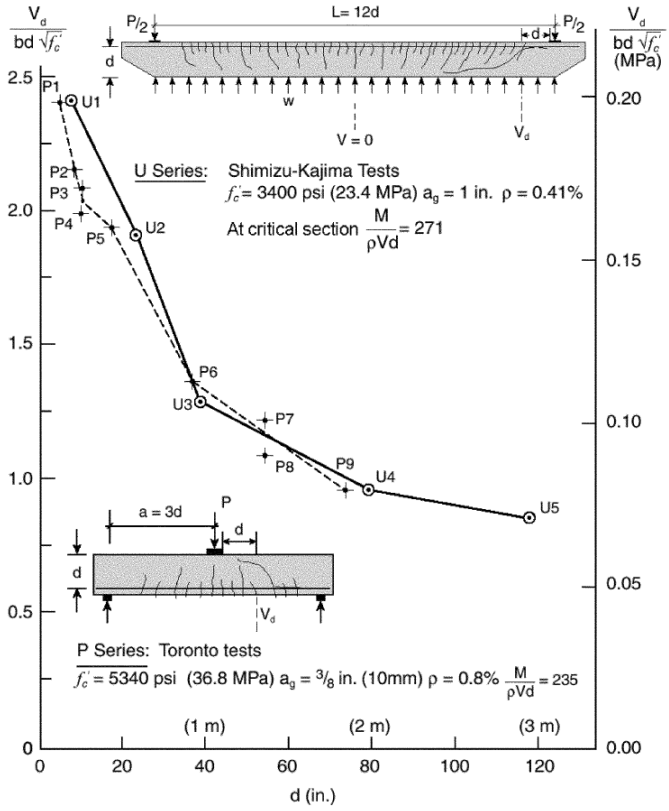

Figure 2.30: The size effect in shear for uniformly loaded members (U series) and for concentrated loaded members (P series) [39]

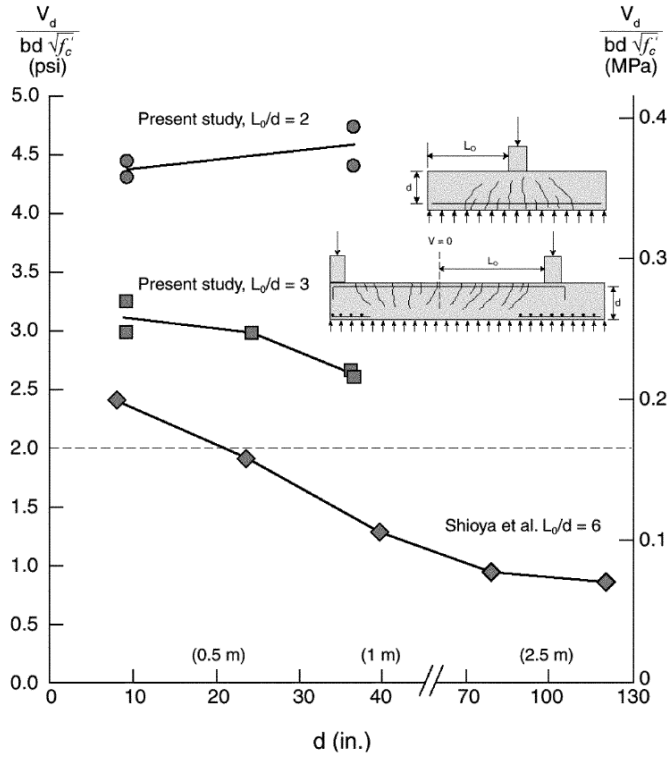

Figure 2.31: The effect of the a/d ratio on the size effect [39] (where: $L_0/d = a/d$).

Aggregate interlock When concrete is cracked, forces can still be transferred across the crack through a mechanism called aggregate interlock. Cracks in concrete are never completely smooth. For normal strength concrete, the aggregates in the concrete are stronger than the cement matrix. The cracks go around the aggregates creating a rough crack surface. The two opposite faces can still interlock and therefore resist shear forces. The interlock capacity depends on the aggregate size, the aggregate type, the aggregate strength, the concrete strength and the width of the crack. Aggregate interlock is illustrated in figure 2.32 (a).

Dowel action denotes the resistance of a reinforcing bar, crossing a crack, to shear displacement. Dowel action is illustrated in figure 2.32 (b) (Walraven 1980 [44]). The concrete deforms a little as does the steel over the free length, causing the bar deflection. The maximum shear stress that can be carried by the dowel action is limited by the tensile strength of the concrete cover supporting the dowel. The dowel action contribution to shear resistance increases for larger amounts of reinforcements (ACI 445-99 [2]). The parameters that influence the dowel action are the shear deformation, the level of steel-concrete bond, the amount of tensile steel and the concrete tensile strength.

Arching action is considered as the load transfer between a load and a support through a compressive strut. Arching action is important for a/d values smaller than 2.5 as is explained in section 2.2.1. There may be two possibilities for developing arching action. The first one is the development of an elbow-shaped strut that deviates the compression strut to avoid the cracks. The possibility depends on the crack pattern and the limited tensile strength of the member. The second possibility is the load transfer via the direct strut that is possible due to crack friction (aggregate interlock). At failure both mechanisms are active according to Muttoni and Fernández Ruiz (2008) [28]. These mechanisms are illustrated in figure 2.33

All codes and models with regard to shear strength take the concrete strength into account. This can be the concrete tensile strength (for design purposes derived from the concrete compressive strength), or the concrete compressive strength. The concrete tensile strength influences the dowel capacity, the compressive strength influences the strength of the concrete compressive zone. The aggregate interlock capacity is also related to the concrete strength. These parameters all influence the shear capacity, indicating a considerable effect of the concrete strength on the shear capacity.

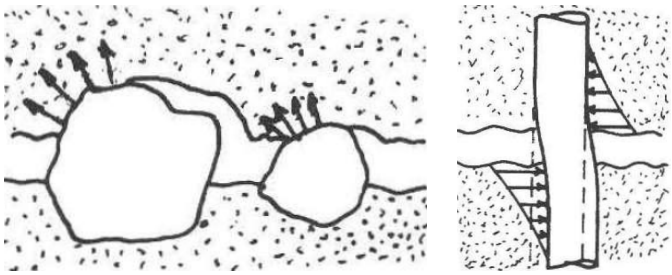

(a) (b)

Figure 2.32: Aggregate interlock (a) and dowel action (b) [44].

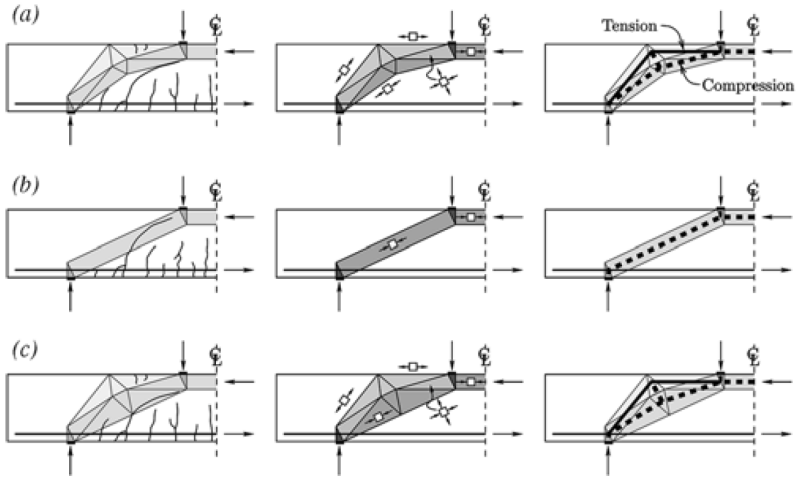

Figure 2.33: Load-carrying mechanisms after development of a diagonal shear crack: (a) elbow-shaped strut, (b) straight strut, (c) combined action. [28]

Reinforcement ratio and layout

Research performed on punching in concrete slabs without shear reinforcement by Kinnunen and Nylander (1960) [17] indicated different failure behaviour for different reinforcement ratios (figure 2.34).

When the reinforcement ratios are low $\rho = 0.5\%$, the slab behaves ductile. The strength of the slab is limited by the flexural capacity. Large plastic deformations occur before brittle punching failure.

In case of intermediate reinforcement ratios $\rho = 1.0\%$ the behaviour tends to be more brittle. Limited yielding of the reinforcement occurs before punching. The behaviour indicates that the flexural capacity is higher than the capacity of the slab.

For large reinforcement ratios $\rho = 2.0\%$ the flexural capacity is much higher than the slab capacity. Before the occurrence of yielding in the reinforcement, punching will occur, causing sudden brittle failure.

Increasing the reinforcement ratio results in a higher punching capacity, but it limits the deformation capacity of the element.

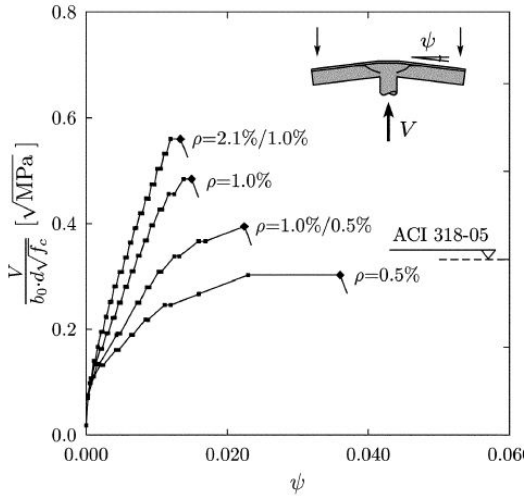

Figure 2.34: Plots of load-rotation curves for tests by Kinnunen and Nylander [17] [27]

Sagaseta et. al. [36] conducted experiments on punching shear ($V_R < V_{\text{flex}}$) in plates with symmetrical and asymmetrical loading and different reinforcement ratios ($\rho_x \neq \rho_y$). It was concluded that flexural reinforcement has a significant influence on the punching strength of the slab and the symmetry of the reaction (when $\rho_x \neq \rho_y$). When the reinforcement ratio in one direction is low (0.3%) and the ratio in the other direction is about twice as

high, a plastic hinge forms and punching failure occurs in an asymmetrical way. However when the reinforcement ratio in the one direction is about 0.75% and in the other 1.5% failure occurs in a symmetric way.

2.3.3 Loading and support

Size and shape of the load

When using an effective width to address the shear capacity in the design of a one-way slab, the size of the load plate is not of influence on the effective width according to the method described in figure 2.26 (for square loading areas). However, experiments on one-way slabs (Furuuchi et al. 1998 [10], Regan 1982 [32]) show that this assumption is not true. As the width of the loading plate increases, the shear capacity increases. As can be seen in figure 2.24 the distribution of forces across the width is not only influenced by the element width, but also by the geometry of the loading plate. The influence from the size of the load on the maximum load capacity for concrete slabs is investigated as part of a large scale test program at TU Delft University. Lantsoght et al. (2010a/2011c) [20] [24]) reported a 40% load capacity increase in undamaged slabs (2.5m in width) when the loading plate was increased from 200 mm x 200 mm to 300 mm x 300 mm. For initially damaged slabs, the increase in capacity was 20%. With decreasing element width the effect of a bigger loading plate diminishes. For elements with a width of 2.0 meters the average increase in capacity was 24.2% when applying a bigger loading plate. For elements of 1.0 m or 1.5 m in width the average increase was under 1%.

When the effective width is considered related to the loading plate, the above results can be explained by the limited element width. For small elements shear is spread between the load and the support over a theoretical effective width. When the load plate is wider, the effective width increases, but this increase is limited by the actual width of the element. When the element width is not limiting (in the case of 2.5 m wide slabs), the effective width can increase further. The increasing width causes a larger capacity increase for wider loading plates when the element width is not the limiting factor, this is illustrated in figure 2.35.

Type of support and support conditions

Beams and slabs can be supported in various ways. For slabs supported by columns punching shear must be checked. For beams one-way shear is checked. There are some situations that are in between. Wide beams or

Figure 2.35: Limited effect of load capacity increase for increased load plate size due to small element widths limiting the effective width.

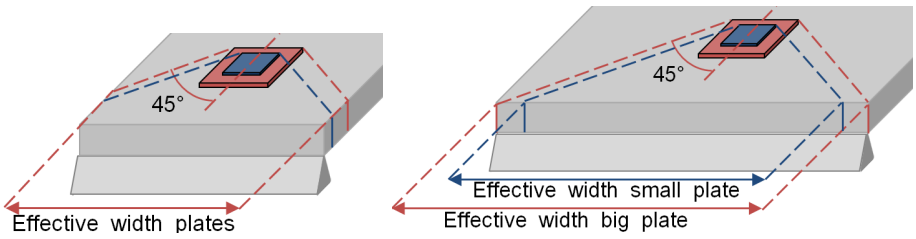

(a) Effective widths in strip limited by element width.

(b) Effective widths in slab not limited by element width.

slabs, for example, can be supported along the full width or only along a part of the width. Lubell et al. (2008) [25] investigated the effect of the "element width to support width" ratio on the one-way shear capacity. The element not being supported along the whole width will cause a disturbance in the flow of forces. A disturbance in the flow of forces is also the case for elements that are supported along the whole length, but loaded only along a part of the width. They concluded that the one-way shear capacity of a member decreases when the loaded width or supported width is narrower than the width of the member.

The type of support also influences the behaviour of the concrete slab. When simple supports and continuous supports were compared by Lantsoght et al. (2011c) [24] it was observed that the effective widths of the plate that are used to transfer the shear force are smaller at the continuous supports.

The degree of rotational restraint of the slab is also an important factor. When a loaded concrete slab is unable to expand freely at its supports compressive membrane forces can develop. The effect is generally qualified as secondary and it is assumed that it only occurs after cracking of the concrete or yielding of the reinforcement. The effect of this compressive membrane action, arching action or dome effect, caused by restraints on punching shear resistance is investigated by Kuang and Morley (1992) [18]. They tested square slabs subjected to a concentrated load, connected to an edge beam at all four sides. The size of the edge beam, the reinforcement ratio and the thickness of the slab were varied. It was found that as the width of the edge beam (and thus the restraining level) increased, the compressive membrane action increased resulting in a higher punching shear resistance (figure 2.36).

It was also found that the amount of flexural reinforcement on the punching shear capacity for restrained slabs is significant for low reinforcement ratios but the effect reduces as the reinforcement ratio increases. The thickness

of the restrained slab also influences the punching strength. For thicker slabs the punching strength for restrained slabs is higher (figure 2.37).

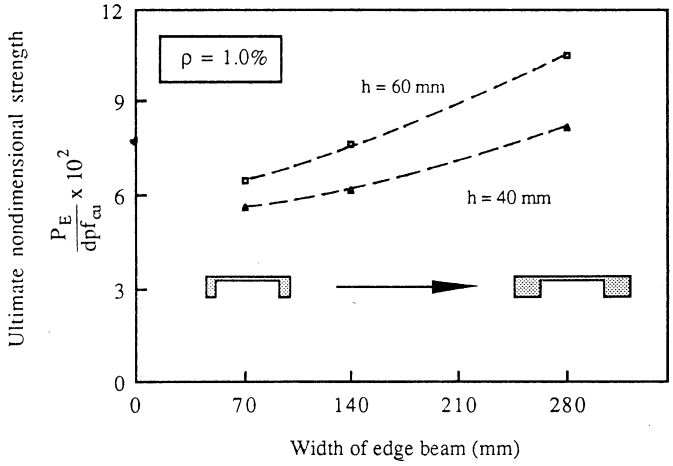

Figure 2.36: The effect of edge restraint on punching shear capacity for different slab thickness [18].

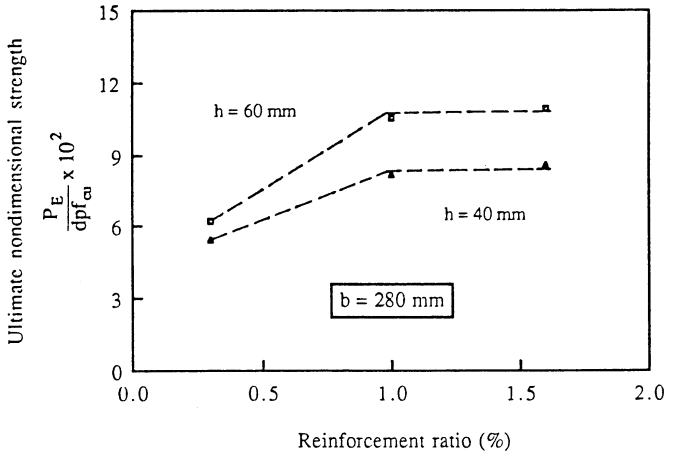

Figure 2.37: The effect of edge reinforcement ratio on punching shear capacity for constrained slabs [18].

The deflections of the slab were found to decrease as the amount of restraint increased, this suggests that compressive membrane forces influence the amount of slab deflection. The amount of reinforcement also plays an important role in the deflection of the slab because it controls cracking. There was also an influence on the cracking pattern by the compressive membrane forces. The cracks were wide and small in number for slabs with a low level

of restraint while the cracks where fine and large in number for slabs with higher levels of restraint.

Loading history

A concrete slab previously subjected to an increasing concentrated load that causes cracks and local failure is still able to carry loads at other points on the slab. Lantsoght et al. (2011a) [22] reported an average remaining loading capacity of 84% when the locally failed slab was loaded at a location in the vicinity of the previous load location.

2.4 Codes on shear

This chapter will deal with several different building codes with respect to shear. The formulas used in the codes to predict the shear capacity of the concrete are briefly stated. A distinction is made between one-way shear and punching shear. The former Dutch building code (NEN 6720), the European code (NEN-EN 1992 (2005)), the American code (ACI 318 (2008)), the Model Code 2010, and Regans formula (based on the former British Standard) will be considered.

2.4.1 NEN 6720

The NEN 6720 [13] is the building code used in the Netherlands before the Eurocode.

One-way shear

The requirements for one-way shear according to the NEN 6720 article 8.2 are briefly described in this section. Influence of shear reinforcement is not taken into account.

$$\tau_1 = 0.4 f_b k_\lambda k_h \sqrt[3]{\omega_o} \geq 0.4 f_b \tag{2.18}$$

$$\tau_1 \leq \tau_2 = 0.2(f_b')k_n k_\theta \tag{2.19}$$

$$k_n = \frac{5}{3}\left(1 - \frac{\sigma'_{\text{bmd}}}{f_b'}\right) \leq 1.0$$

$k_\theta = 1$ (no shear reinforcement is applied)

For corbels and members at end supports where a compression strut can be formed between the load and the support:

$$k_\lambda = \frac{12}{g_\lambda}\sqrt[3]{\frac{A_o}{bd}} \geq 1$$

$$g_\lambda = \begin{cases} 1+\lambda_v^2 & \text{if } \lambda_v \geq 0.6 \\ 2.5 - 3\lambda_v & \text{if } \lambda_v < 0.6 \end{cases}$$

For other cases

$$k_\lambda = 1$$

$$\lambda_v = \frac{M_{d\max}}{dV_{d\max}}$$

$$\omega_o = \frac{100\,(A_s + A_p)}{bd}$$

$$0.7 - 0.5\lambda_v \leq w_o \leq 2.0$$

$$k_h = 1.6 - h \geq 1$$

where:

τ_1 is the beam shear capacity of the concrete.

σ'_{bmd} is the average concrete compression stress caused by normal force, including the prestress.

f'_{ck} is the characteristic concrete cube compressive strength.

f_b is the concrete design tensile strength. $f_b = \dfrac{f_{\text{brep}}}{\gamma_m}$

f_{brep} is the representative value of the concrete tensile strength $f_{\text{brep}} = 0.7(1.05 + 0.05f'_{ck})$

γ_m is a material factor ($\gamma_m = 1.4$ for concrete tensile strength).

f'_b is design value of the concrete compressive strength. $f'_b = \dfrac{f'_{\text{brep}}}{\gamma_m}$

f'_{brep} is the representative value of the concrete compressive strength $f'_{\text{brep}} = 0.72f'_{ck}$

γ_m is a material factor ($\gamma_m = 1.2$ for concrete compressive strength).

ω_o is the flexural reinforcement ratio in the considered cross section.

A_s is the cross sectional area of the reinforcement steel.

A_p is the cross sectional area of the prestress steel.

A_o is the smallest value of the load- or support area. The value may not exceed bd.

b is the effective width of the element for a 45° angle from the edges of the loading area side facing the support.

d is the effective depth of the element.

λ_v is the shear slenderness factor.

$M_{d\max}$ is the maximum absolute moment in the member.

$V_{d\max}$ is the maximum absolute shear force in the member.

h is the total height of the concrete cross section considered in meters.

The factor k_λ is used for members at end support. The influence on continuous supports might be different but the NEN does not take this into account.

Punching shear

Section 8.3 of the NEN 6720 describes punching in concrete. For slabs subjected to punching without shear reinforcement the requirement is:

$$\tau_1 = 0.8 f_b k_d \sqrt[3]{\omega_o} k_1 k_2 \geq 0.8 f_b k_1 k_2 \tag{2.20}$$

When both k_1 and k_2 are unequal to 0, $\tau_1 \geq 0.4 f_b$

$$\tau_1 \leq \tau_2 = 0.15(f_b') \leq 5.0\text{N/mm}^2 \tag{2.21}$$

$$k_1 = \begin{cases} \left(2 - \dfrac{a_l}{2a_b}\right) \geq 0.5 & \text{if } a_l > 2a_b \\ 0 & \text{if } a_l \leq 2a_b \end{cases}$$

$$k_2 = \begin{cases} \left(\dfrac{4}{2 + a/d}\right) \geq 0.5 & \text{if } a > 2d \\ 0 & \text{if } a \leq 2d \end{cases}$$

where:

τ_1 is the shear capacity of the concrete.

f_b is the concrete design tensile strength. $f_b = \dfrac{f_{\text{brep}}}{\gamma_m}$

f_{brep} is the representative value of the concrete tensile strength $f_{\text{brep}} = 0.7(1.05 + 0.05 f'_{ck})$

γ_m is a material factor ($\gamma_m = 1.4$ for concrete tensile strength).

d is the effective height of the plate around the concentrated load.

k_d is a scale factor. $k_d = 1.5 - 0.6d \geq 1.0$ where d is in meters.

a_l is the length (not height) of the rectangular column.

a_b is the width of the rectangular column.

a is the diameter of the circular shaped loading area. When the loading area is rectangular, an equivalent circular area is calculated with: $a = 2/\pi(a_l + a_b)$.

ω_o is the flexural reinforcement ratio. $\omega_o = \sqrt{\omega_{ox}\omega_{oy}} \leq 2.0$.

ω_{ox}, ω_{oy} are the fully anchored flexural reinforcement ratios in the x and y direction within the considered perimeter.

The perimeter distance is $0.5d$ from the edge of the load area.

$$p = \begin{cases} \pi\,(d + a) & \text{for a middle load/column} \\ 0.5\pi\,(d + a) + 2a_r & \text{for an edge load/column} \\ 0.25\pi\,(d + a) + 2a_r & \text{for a corner load/column} \end{cases}$$

where:

p is the perimeter length.

a_r is the distance from the centre of gravity of the loading area to the edge of the plate. a_r is limited to:

$a_r = 0.25\pi(d + a)$ for an edge load/column.

$a_r = 0.375\pi(d + a)$ for a corner load/column.

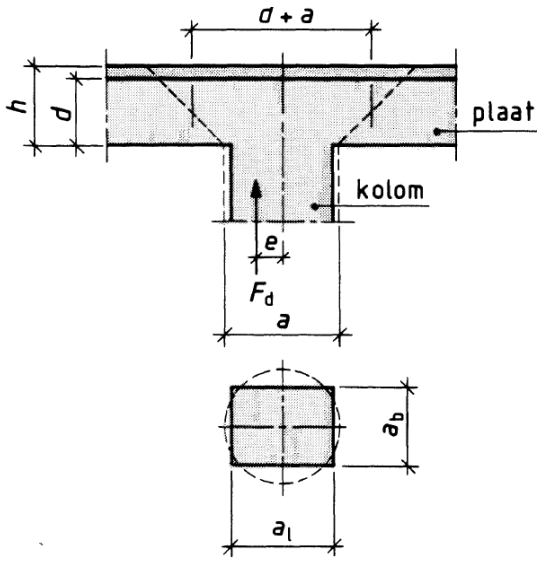

Figure 2.38: The first control perimeter as defined in NEN 6720 [13]

2.4.2 Eurocode

The Eurocode [8] NEN-EN 1992-1-1:2005 is based on CEB-FIP MC90. The provisions found in the Eurocode are similar to those found in CEB-FIP MC90. However, in the Eurocode the size effect and the reinforcement terms are limited. In-plane stresses can be taken into account and a minimum shear strength is given.

One-way shear

In NEN-EN1992-1-1:2005 article 6.2.2 a formula can be found for checking the shear resistance of the concrete. The value is limited by a minimum.

$$V_{Rd,c} = \left[\frac{C_{R,c}}{\gamma_c} \left(1 + \sqrt{\frac{200}{d}} \right) (100 \rho_l f_{ck})^{1/3} + k_1 \sigma_{cp} \right] b_w d \geq (v_{\min} + k_1 \sigma_{cp})\, b_w d \tag{2.22}$$

$$v_{\min} = 0.035 \left(1 + \sqrt{\frac{200}{d}} \right)^{3/2} \sqrt{f_{ck}} \tag{2.23}$$

where:

$V_{Rd,c}$ is the design value of the concrete contribution to the resistance to shear.

$C_{Rd,c}$ is a factor for shear resistance of the concrete $C_{R.c} = 0.18$.

k_1 is a factor with value 0.15.

ρ_l is the tensile reinforcement ratio $\rho_l = \frac{A_{sl}}{b_w d} \leq 0.02$.

A_{sl} is the cross sectional area of the tensile reinforcement that passes $\geq (l_{bd} + d)$ beyond the considered cross section.

b_w is the smallest width of the cross section in the tension zone.

σ_{cp} is compression stress in the concrete caused by normal force or prestress. $\sigma_{cp} = N_{Ed}/A_c < 0.2 f_{cd}$

N_{Ed} is the normal force in the cross section due to loading or prestressing.

A_c is the area concrete in the considered cross-section.

For elements with loads on the upper side of the member within a distance $0.5d \leq a_v \leq 2.0d$ to the edge of the support, the contribution of the load to the shear force V_{Ed} may be multiplied with a factor $\beta = a_v/2.0d$. In order to be able to apply this factor it is required that the flexural reinforcement is fully anchored at the support. For $a_v \leq 0.5d$ a value of $a_v = 0.5d$ must be used. The shear force V_{Ed}, calculated without the reduction by β, should always fulfil the following requirement:

$$V_{Ed} \leq 0.5 b_w d f_{cd} \nu \tag{2.24}$$

$$\nu = 0.6 \left[1 - \frac{f_{ck}}{250}\right] \tag{2.25}$$

where:

ν is a strength reduction factor for concrete cracked in shear.

f_{cd} is the design value for the concrete cylinder compressive strength .

The method to account for increase in shear capacity with decreasing distance to the support provided by the Eurocode (section 2.4.2) is derived from experiments on beams. When applied to full scale slabs, as done by Lantsoght et al. (2011b) [23], this method provides only conservative results. Better but less conservative predictions are obtained for the Eurocode when the French national annex is applied:

For slabs benefiting from a transverse redistribution effect under the load case considered:

$$v_{\min} = 0.34 \sqrt{f_{ck}} \tag{2.26}$$

For beams and slabs not benefiting from a transverse redistribution effect:

$$v_{\min} = 0.053 \left(1 + \sqrt{\frac{200}{d}}\right)^{3/2} \sqrt{f_{ck}} \tag{2.27}$$

The effective width is determined according to figure 2.27.

Punching shear

The formula for punching shear is based on the formula for one-way shear, only in this case a perimeter is used. There are some minor differences.

NEN-EN 1992-1-1 article 6.4 describes punching shear. It states that punching should be checked at the edge of the column and at the first control perimeter u_1. When punching reinforcement is required another perimeter should be found where the reinforcement is no longer required. The first control perimeter may be set at a distance $2.0d$ from the loaded area. It's length should be as small as possible. For the effective depth of the plate a constant value is assumed $d_{\text{eff}} = (d_y + d_z)/2$. The punching resistance of slabs and column plates without punching reinforcement at the first control perimeter is given by:

$$V_{Rd,c} = \left[\frac{C_{R,c}}{\gamma_c}\left(1 + \sqrt{\frac{200}{d_{\text{eff}}}}\right)(100\rho_l f_{ck})^{1/3} + k_1\sigma_{cp}\right] u_1 d_{\text{eff}} \geq (v_{min} + k_1\sigma_{cp})\, u_1 d_{eff} \tag{2.28}$$

where:

$V_{Rd,c}$ is the design value of the concrete contribution to the resistance to shear at the control perimeter considered.

u_1 is the first control perimeter at a distance from the face of the column equal to λd.

d_{eff} is the slab effective depth in mm $d_{\text{eff}} = (d_y + d_z)/2$.

ρ_l is the geometric average between the percentage of reinforcement ρ_x and ρ_z. $\rho_l = \sqrt{\rho_x \rho_z} < 0.02$

f_{ck} is the characteristic concrete compressive strength.

σ_{cp} is compression stress in the concrete caused by normal force or prestress: $\sigma_{cp} = \dfrac{\sigma_{cx} + \sigma_{cz}}{2}$. Where σ_{cx}, σ_{cz} are the normal concrete stresses in the critical section (compression positive).

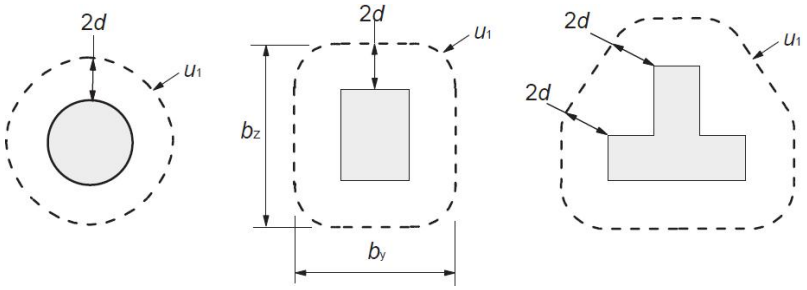

Figure 2.39: The first control perimeter defined in NEN-EN 1992-1-1 [8]

k_1 is a factor with value 0.1 for compression and 0.5 for tension.

Punching reinforcement is not required when acting shear is not higher than the design shear capacity of the concrete:

$$v_{Ed} = \beta \frac{V_{Ed}}{u_i d_{\text{eff}}} < v_{Rd,c} = \frac{V_{Rd,c}}{u_i d_{\text{eff}}} \tag{2.29}$$

where:

β is the position factor for the column (1,5 for a corner column, 1,4 for an edge column and 1,15 for an internal column).

2.4.3 ACI Code

The ACI 318-08 design code [5] is mainly based on semiempirical approaches. There are a lot of rules for special design cases, but applying the code to unique design cases is not always possible. The limitation is caused by the fact that the code is not based on a clear physical model according to ACI445-99 [2].

One-way shear

ACI 318-08 [5] section 11.1 states that the shear strength is based on an average shear stress on the full effective cross section $b_w d$. In a member without shear reinforcement, shear is assumed to be carried by the concrete web. In a member with shear reinforcement, a portion of the shear strength is assumed to be provided by the concrete and the remainder by the shear reinforcement. ACI 318-08 article 11.2.1.1 and article 11.2.2.1 (alternative) provide

the concrete shear strength for members subjected to shear and flexure only:

$$V_c = \frac{2}{12}\lambda\sqrt{f'_c}b_w d \tag{2.30}$$

$$V_c = \frac{1}{12}\left(1.9\lambda\sqrt{f'_c} + 2500\rho_w\frac{V_u d}{M_u}\right)\varphi b_w d \leq \frac{3.5}{12}\lambda\varphi\sqrt{f'_c}b_w d \tag{2.31}$$

$$\tag{2.32}$$

$$\frac{V_u}{d} \leq 1.0$$

$$\rho_w = \frac{A_s}{b_w d}$$

where:

SI units are used.

λ is a factor for lightweight concrete. In case of normal weight concrete $\lambda = 1.0$.

f'_c is the concrete cylinder compressive strength.

b_w is the width of the web.

d is the distance from extreme compression fibre to centroid of longitudinal tension reinforcement.

A_s is the longitudinal tension reinforcement.

V_u is the factored shear force at the considered section.

M_u is the factored moment at the considered section.

φ is a partial safety factor for shear. In design $\varphi = 0.75$.

According to Sherwood et al. (2006) [37] the size effect can be implemented into the ACI318 formula for shear capacity (equation 2.30) by multiplying with:

$$\frac{1248}{1000 + s_e} \tag{2.33}$$

$$s_e = \frac{31.5d}{a_g + 16} \tag{2.34}$$

where:

s_e is the effective crack spacing.

a_g is the maximum aggregate size.

f'_c in equation 2.30 is limited to 70 MPa.

The limitation on the concrete strength takes into account the aggregate strength. For concrete strengths above 70 MPa the cracks may not pass around the aggregate but through it, reduces the crack roughness. When taking a_g = 0mm into account for concrete strengths above 70 MPa the adapted formula can still be used. The size effect is illustrated in figure 2.40 where the adapted ACI formula for shear strength is compared to experimental results.

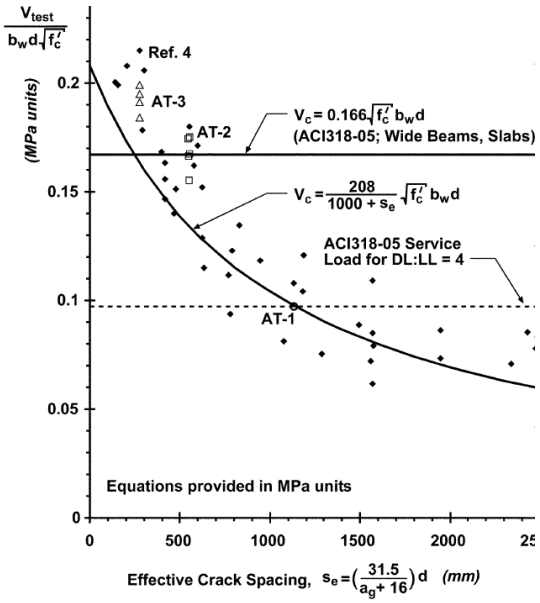

Figure 2.40: The effect of effective crack spacing on the shear stress [37].

Punching shear

ACI 318-08 11.11.1 indicates that the shear strength of slabs and footings in the vicinity of columns, concentrated loads, or reactions is governed by the more severe of two conditions:

a) Beam action where each critical section to be investigated extends in a plane across the entire width. For beam action, the slab or footing shall be designed in accordance with the method for one-way shear.

b) For two-way action, each of the critical sections to be investigated shall be located so that its perimeter b_o is a minimum but need not approach closer than $d/2$ to: Edges or corners of columns, concentrated loads, or reaction areas; and changes in slab thickness.

For two-way action, the concrete shear resistance for non-prestressed slabs and footings with two-way actions is calculated using article 11.11.2.1 of the ACI 318-08:

$$V_c = \alpha\varphi\lambda\sqrt{f'_c}b_0 d \tag{2.35}$$

$$\alpha = \min \begin{cases} \dfrac{1}{12}\left(2 + \dfrac{4}{\beta_c}\right) \\ \dfrac{1}{12}\left(\alpha_s \dfrac{d}{u} + 2\right) \\ \dfrac{4}{12} \end{cases} \tag{2.36}$$

where:

SI units are used.

λ is a factor for lightweight concrete. In case of normal weight concrete $\lambda = 1.0$.

f'_c is the concrete cylinder compressive strength.

b_o is the perimeter of critical section for shear in slabs and footings at a distance $d/2$ from the edge of the loaded area.

d is the distance from extreme compression fibre to centroid of longitudinal tension reinforcement.

α_s is a factor depending on the column location. $\alpha_s = 40$ for interior columns, $\alpha_s = 30$ for edge columns and $\alpha_s = 20$ for corner columns.

β is the ratio of long side to short side of the column or loaded area.

φ is a partial safety factor for shear. In design $\varphi = 0.75$.

2.4.4 Model Code 2010

The CEB-FIP Model Code 2010 (MC2010) is a new code [15] on the design of concrete structures. The intention of the MC 2010 is to serve as a basis for building codes in the future. The design approach used in the MC2010 is somewhat different from other codes in terms of determining the resistance

of an element to shear and punching. Several levels of approximation can be used. The difference between these levels is the precision. Each level has is different in terms of complexity and obtained precision. The three levels can be used for different design stages or requirements:

Level I: for the conception or the design of a new structure.

Level II: for the design of a new structure as well as for a general or brief assessment of an existing member.

Level III: for the design of a member in a complex loading state or a more elaborate assessment of a structure.

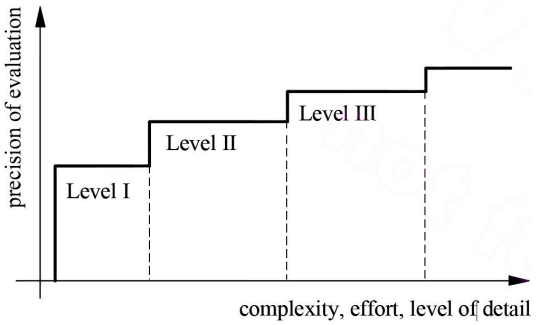

Figure 2.41: Different levels of approximation as found in the Model Code 2010 [15].

The theoretical framework used in the MC2010 is based on the mechanical model of the Critical Shear Crack Theory for punching (Sagaseta et al. 2011 [36]) found in section 2.2.3. For one-way shear the MC2010 is based on the modified compressive field theory (section 2.2.4).

Effective width and loads close to the support

Recommendations for an effective width, and a contribution factor for point loads applied within a small distance from the face of the support where added to the Model Code 2010 in the final draft.

When a load is applied within a distance of $d < a_v \leq 2d$ from the face of the support, the design shear force may be reduced with a factor $\beta = a_v/(2d)$. When the load is applied closer to the support, the reduction factor will remain $\beta = 0.5$.

The effective width that is used to check the one-way shear capacity in slabs is defined in figure 2.42. The control section is taken as the lesser of a distance equal to d and $a_v/2$ from the face of the support. The angle at which the load distributes from the simple support is taken as $\alpha = 60^o$.

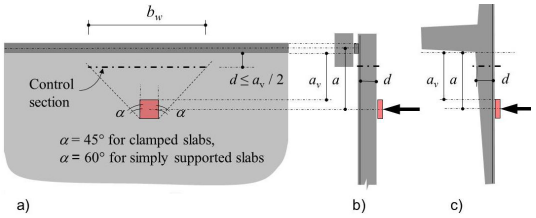

Figure 2.42: The effective width as defined in the Model Code 2010.

One-way shear

The concrete contribution to the shear resistance is given by:

$$V_{Rd,c} = k_v \frac{\sqrt{f_{ck}}}{\gamma_c} z b_w \tag{2.37}$$

In which in case of approximation level II for members without shear reinforcement:

$$k_v = \frac{0.4}{1 + 1500\epsilon_x} \frac{1300}{1000 + k_{dg} z}$$

$$\epsilon_x = 0 \geq \frac{\frac{M_{Ed}}{z} + V_{Ed}}{2 E_s A_s} \geq 0.003$$

where:

$V_{Rd,c}$ is the design value of the concrete resistance to shear.

f_{ck} is the characteristic concrete cylinder compression strength. $\sqrt{f_{ck}}$ is limited to 8 MPa.

γ_c is the partial material concrete for concrete.

z is the shear depth in mm.

b_w is the effective width in mm.

ϵ_x is the strain in the compressive zone of the concrete.

$$k_{dg} = \frac{32}{16 + d_g} \geq 0.75$$

d_g is the aggregate diameter. When the concrete strength exceeds 70 MPa, then $d_g = 0$.

M_{Ed} is the load effect bending moment at the control section, taken as a positive quantity.

V_{Ed} is the load effect shear force at the control section, taken as a positive quantity.

E_s is the reinforcement steel modulus of elasticity.

A_s is the longitudinal bending reinforcement cross-sectional area.

Punching shear

Punching shear is given by Model Code 2010 [15] article 7.3.5. The formula provided is based on the formula for one-way shear. The contribution of the concrete to the shear resistance is given by the formula:

$$V_{Rd,c} = k_\psi \frac{\sqrt{f_{ck}}}{\gamma_c} b_0 d_v \tag{2.38}$$

$$k_\psi = \frac{1}{1.5 + 0.9\psi d k_{dg}} \leq 0.6 \tag{2.39}$$

$$\psi_{\text{level II}} = 1.5 \frac{r_s}{d} \frac{f_{yd}}{E_s} \left(\frac{m_{sd}}{m_{Rd}} \right)^{1.5} \tag{2.40}$$

$$\tag{2.41}$$

where:

$V_{Rd,c}$ is the design value of the concrete contribution to the shear resistance of the member.

f_{ck} is the characteristic concrete cylinder compressive strength.

γ_c is the partial safety factor for concrete.

b_0 is the shear-resisting control perimeter.

d_v is the effective depth of the slab.

k_ψ is a parameter depending on the deformations of the slab around the support region.

d is the mean value of the effective depth in the x and y directions.

r_s is the distance between the column axis and the position where the radial bending moment is 0.

f_{yd} is the design yield strength of the steel.

E_s is the modulus of elasticity of the steel.

m_{sd} is the average moment per unit length for calculation of the flexural reinforcement in the support strip (for the considered direction).

m_{Rd} is the design average flexural strength per unit length in the support strip (for the considered direction).

b_s is the width of the support strip used to calculate m_{sd}. $b_s = 1.5\sqrt{r_{s,x}r_{s,y}} \leq L_{\min}$

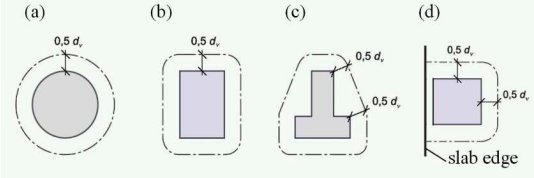

Figure 2.43: The control perimeter as defined in the Model Code 2010.

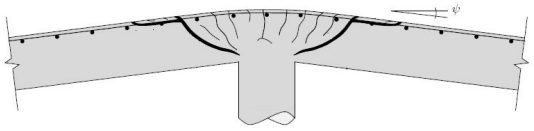

Figure 2.44: Model Code 2010 rotation of a slab around the support region [15].

2.4.5 Regan's model

P. E. Regan performed research to shear resistances of concrete slabs at concentrated loads close to supports (1982) [32]. In his research he developed a formula to predict the punching shear resistance at concentrated loads near supports:

$$P_R = P_{R1} + P_{R2} \tag{2.42}$$

$$P_{R1} = \Sigma\xi_s v_c u d \tag{2.43}$$

$$P_{R2} = \left(\frac{2d}{a_v}\right)\xi_s v_c u_2 d < \frac{\sqrt{f_{cu}}}{\gamma_m} u_2 d \tag{2.44}$$

where:

P_R is the total resistance to punching shear.

P_{R2} is the shear resistance for a part of the perimeter that runs parallel to the support and either extends beyond the face of the support or lies within a distance $0.5d$ of it.

P_{R1} is the shear resistance for the remaining parts u of the perimeter. $\Sigma u = u_1$.

a_v is the clear distance between the load and the support.

ξ_s is a size effect factor $\sqrt[4]{500/d}$.

v_c is a shear stress (resistance) $v_c = \dfrac{0.27}{\gamma_m}\sqrt[3]{100\rho_1 f_{cu}}$, $\rho_1 = \dfrac{\rho_x + \rho_y}{2}$.

u_2 is the length of the part of the perimeter considered.

γ_m is the partial material safety factor.

f_{cu} is the concrete cube compressive strength.

d is the effective depth of the concrete slab.

d_t, d_l or ρ_t, ρ_l are used depending on which part of the perimeter is considered.

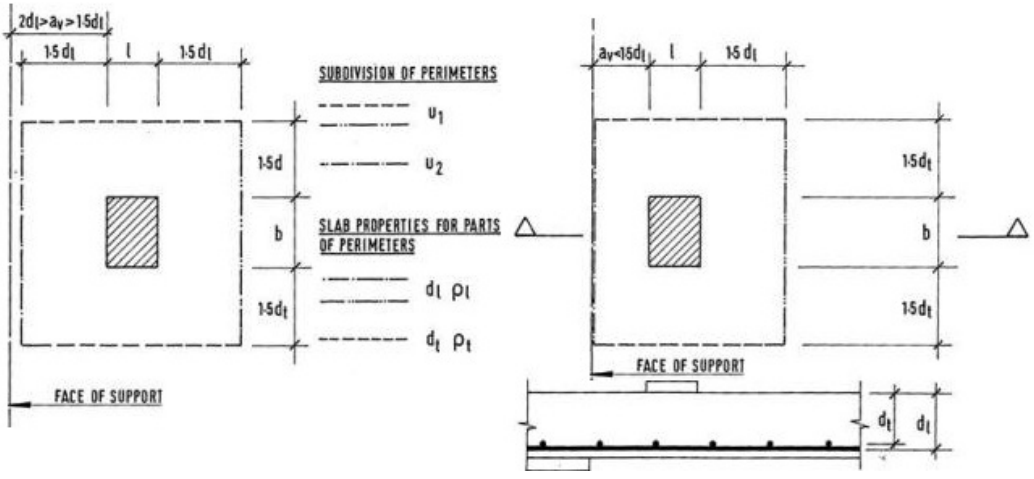

Figure 2.45: Punching shear design method as proposed by Regan.

In case of a continuous support the shear resistance is higher than in case of a simple support. To take this effect into account, the calculated shear

resistance P_R is multiplied with a factor $\alpha = \sqrt{(M_1 + M_2)/M_1}$ where M_1 and M_2 are respectively the larger and smaller moments at the ends of the shear span.

The research on the a/d ratio done by Regan was on small scale specimens loaded in the middle of the element width. Experiments concerning the influence of the a/d ratio on full scale slabs and for loads varying in location along the width was done by Lantsoght et al. (2010b) [21]. Experiments suggest that the method developed by Regan (section 2.4.5) is also valid for large scale slabs and, when the perimeter is modified, also for loads close to the side edge.

2.4.6 Comparing the codes

In this chapter the codes will be briefly compared on the effects that are taken into account. Comparing is done for the one-way (beam) shear formulas and for the punching provisions.

Comparing one-way shear formulas

The one-way shear provisions are briefly compared. A table can be found on page 59. Contrary to the ACI, the Eurocode and the Model Code 2010 take into account the flexural reinforcement ratio in span direction and the size effect. In the design formulas found in the Eurocode can be seen that the influence of $\rho_l \leq 0.02$ on the shear strength is proportional to $(100\rho_1)^{1/3}$. In the Model Code 2010 the flexural reinforcement ratio is incorporated in the variable ϵ_x. The Model code 2010 also takes into account the aggregate size. It is clear that the ACI code is the most simplified. The most effects are taken into account by the Model Code (level II approximation or higher).

Comparing punching shear formulas

The formulas for punching shear are briefly compared in the table on page 59. The way the reinforcement ratio is incorporated is different for all codes. The Eurocode uses $\rho_{\text{ave}} = \sqrt{\rho_l \rho_t}$ and Regan's method, based on the former British Standard, uses $\rho_{\text{ave}} = (\rho_l + \rho_t)/2$. The ACI code for punching ignores the reinforcement ratio completely. For the Model Code 2010, the reinforcement is ignored in a level I approximation. For higher approximation levels the design average flexural strength per unit length in the support strip is required to determine the slab rotation. The strength is influenced by the flexural reinforcement in the considered direction. The slab rotation should be checked in two directions individually. The ACI code is the only code

that does not take into account the size effect. The way the size effect is taken into account is different for the three other methods. The influence of the slab-thickness to load dimensions ratio is considered in the Eurocode and the ACI code. The simplest is again the ACI code and the most factors are taken into account by the Model Code 2010.

Comparing multiple building codes on one-way shear in members without shear reinforcement			
Influence factors on shear strength	**EN 1992-1-1**	**ACI 318-08**	**MC2010**
Concrete strength	$\sqrt[3]{f_{ck}}$	$\lambda\sqrt[2]{f'_c}$	$\sqrt[2]{f_{ck}} < 8$ MPa
Flexural reinforcement ratio	$\sqrt[3]{100\rho_l}$	Optional	Yes, incorporated into ϵ_x
Slab thickness (size effect)	$k = 1 + \sqrt{\frac{200}{d_l}} < 2.0$	No	$\epsilon_x z$
Safety factor	$\gamma_c = 1.5$, $\gamma_s = 1.15$	$\varphi = 0.75$	$\gamma_c = 1.5$, $\gamma_s = 1.15$
Shear-span to depth	$\beta = \frac{a_v}{2.0d_l}$ if $0.5d_l \leq a_v \leq 2.0d_l$	No	$\beta = \frac{a_v}{2d_l}$
Aggregate size	No	No	$k_{dg} = \frac{48}{d_{g0} + d_g} \geq 1.0$
Element continuity	No	through $\frac{V_u d}{M_u}$	Yes, through ϵ_x
$f_{ck} = f'_c$ is the characteristic cylinder compressive strength. λ is a reduction factor for lightweight concrete. $\rho_{l,\text{Eurocode}} = \frac{A_{sl}}{b_w d} < 0.02$			

Comparing multiple building codes on punching shear in members without shear reinforcement				
Influence factors on shear strength	**EN 1992-1-1**	**ACI 318-08**	**MC2010**	**Regan**
Concrete strength	$\sqrt[3]{f_{ck}}$	$\lambda\sqrt[2]{f'_c}$	$\sqrt[2]{f_{ck}} < 8$ MPa	$\sqrt[2]{f_{cu}}$
Flexural reinforcement ratio	$\sqrt[3]{100\rho_{ave}}$	No	Yes, through ψ.	$\sqrt[3]{100\rho_{ave}}$
Slab thickness (size effect)	$k = 1 + \sqrt{\frac{200}{d_{ave}}} < 2.0$	No	Yes through ψd	$\epsilon = \sqrt[4]{\frac{500}{d_{ave}}}$
Load shape (rectangularity)	Yes, through k.	Yes, through β_c	No	Limited.
Slab thickness to load dimension ratio	Yes, through β	Yes, through $\frac{d}{b_o}$	No	No
Perimeter distance	$2.0d_{ave}$	$0.5d_{ave}$	$0.5d_{ave}$	$1.5d_{ave}$
Safety factor	$\gamma_c = 1.5$, $\gamma_s = 1.15$	$\varphi = 0.75$	$\gamma_c = 1.5$, $\gamma_s = 1.15$	$\gamma_c = 1.25$
Span to depth ratio	No	No	r_s/d	No
shear-span to depth ratio	No	No	No	Yes, $\frac{2d}{a_v}$
Aggregate size	No	No	$k_{dg} = \frac{48}{d_{g0} + d_g} \geq 1.0$	No
Steel type and yield stress	No	No	f_y/E_s	No
Slab continuity	No	limited, through α_s	Yes, through ψ	$\sqrt{(M_1 + M_2)/M_1}$
f_{ck} and f'_c are the characteristic cylinder compressive strength. f_{cu} is the characteristic cube compressive strength. $\rho_{ave,\text{Eurocode}} = \sqrt{\rho_l \rho_t} < 0.02$, and $\rho_{ave,\text{Regan}} = (\rho_l + \rho_t)\,0.5$ k is the fraction of the unbalanced moment M_f resisted by shear stresses M_1 and M_1 are the largest and smallest moments at the end of the shear span at the continuous support.				

2.5 Conclusion

The literature study provided a lot of information on one-way shear and punching shear. Both failure mechanisms depend on a lot of different parameters. The important parameters and their known effects have been described. During the literature study various important observations are made:

- In the literature study several theories, models and building codes that consider one-way shear and punching are described. These models focus on either one-way shear failure or on punching shear failure. Most models do not take into account the possibility of a combined mechanism.

- There are many factors that influence the shear capacity of a concrete element. It is very difficult to take all these factors into account and therefore simplifications are made. Despite these simplifications, the building codes mostly provide safe approximations in terms of design capacity. These simplifications however are also limitations. An example is the assumption of axis symmetrical conditions for punching, which is often applied, but not often true. When this assumption is disregarded, it is possible to have redistribution of forces and an additional shear capacity.

- The available research also shows that there is not much known about concentrated loads near supports, especially in slabs. In beams, where one-way shear is the acting mechanism, an increase in shear strength can be found. The increase depends on the shear span and the depth of the beam. As the beam width increases, until the beam can be seen as a slab, this increase in capacity changes as well.

- When the shear span for slabs subjected to a concentrated load increases, the shear capacity changes and the failure mechanism changes as well. The amount of change in shear capacity is also related to the element width.

- The shear force from the concentrated load on a slab is transferred to the support. When one-way shear is considered the shear force is transferred only by a portion of the slab width. The determination of this width is not fixed in the currently used building codes. In the Eurocode there is a recommendation in the French national annex. In the new Model Code 2010 (final draft) another method is given. Both methods will be described in the next chapter.

- Different building codes are compared for one way-shear and punching shear. The amount and type of parameters they take into account differ. A transition from one way shear to punching shear is not considered. The (governing) failure mechanism in this transition remains a grey area.

The literature study is made to obtain an overview of the research that has been done on the subject. It will be used as a basis for the next chapters in this MSc thesis report.

Chapter 3

Calculation methods

3.1 Introduction

In this chapter the EN 1992-1-1:2005 [8] is analysed and compared with the ACI 318-08 [5], the NEN6720 [13] and the Model Code 2010 [15]. The model from Regan [32], which is based on the former British Standard, is also considered. In the previous chapter the calculation methods in these codes for shear and punching are briefly described. In this chapter the codes will be applied to various concrete elements that are tested at Delft University of Technology (Lantsoght et al. 2010a,b [20], [21]). The calculation methods for shear and punching provided by the building codes are also applied to a fictitious plate. This plate has properties that resemble the actual tested elements, but only the parameter a_v/d_l is varied. This is done to gain a better insight in when a code provision is governing (shear or punching). By using a fictitious plate and varying only one parameter at a time it is also easier to visualize the differences in shear and punching provisions for the various codes.

The parameters that are investigated are (1) the shear span, (2) the element width and (3) the longitudinal reinforcement ratios in the span direction and in the direction parallel to the support.

3.2 Fictional Model

The fictional model that will be used has strong similarities to the tested concrete elements. Not all properties are used by all building codes. All partial safety factors are set to one.

Fictitious concrete element properties		
Category	**Property**	**Value**
Element size	Height	$h = 300$ mm
	Span length	$l_s = 3600$ mm
	Element width	$b = 2500$ mm
Reinforcement	Longitudinal bars	ϕ 20 mm
	Longitudinal bar distance	s_l 125 mm
	Transverse bars	ϕ 10 mm
	Transverse bar distance	s_t 125 mm
	Shear reinf. ratio	$\rho_w = 0$ %
	Steel modulus of elasticity	$E_s = 200000$ N/mm^2
	Char. yield strength	$f_{yk} = 540$ N/mm^2
Concrete	Strength	$f_{ck} = 40$ N/mm^2
	Aggregate size	$d_g = 16$ mm
	Cover	$c = 25$ mm
Support	Support length (span dir.)	$l_{\text{sup}} = 100$ mm
Load	Load plate length	$c_l = 200$ mm
	Load plate width	$c_t = 200$ mm
ACI	Lightweight concrete	$\lambda = 1.00$
	Safety factor	$\varphi = 1.00$
	Length/width ratio load	$\beta_c = 1.00$
	Column position	$\alpha_s = 40$
EC	Safety factor	$\gamma_c = 1.00$
	Factor	$C_{R,c} = 0.18$
MC2010	Safety factor	$\gamma_c = 1.00$
	Aggregate size factor	$k_{dg} = 1.5$
Regan 1982	Safety factor	$\gamma_m = 1.0$
	Cube compressive strength	$f_{cu} = 48$ N/mm^2
NEN6720	Safety factor tension	$\gamma_m = 1.0$
	Concrete tension strength	$f_b = 2.14$ N/mm^2
	Safety factor compression	$\gamma_m = 1.0$
	Concrete compr. strength	$f'_b = 48.8$ N/mm^2
	Concrete depth factor	$k_h = 1.3$

$$
\begin{aligned}
d_l &= h - c - 0.5\phi_l = 265 \text{ mm} \\
d_t &= h - c - \phi_l - 0.5\phi_t = 250 \text{ mm} \\
d_{\text{ave}} &= 0.5\,(d_l + d_t) = 257.5 \text{ mm} \\
z_l &= 0.9 d_l = 238.5 \text{ mm} \\
\rho_l &= \frac{0.25\pi\phi_l^2}{s_l d_l} = 0.948\ \% \\
\rho_t &= \frac{0.25\pi\phi_t^2}{s_t d_t} = 0.126\ \%
\end{aligned}
$$

3.3 Effective width and Perimeter

3.3.1 Effective width

The effective width is determined using the French method. Various tests indicate that this approach provides better results than when the traditional Dutch approach is used. (Lantsoght et al. 2011c [24], Falbr, J. 2011 [9]).

To determine the effective width a line is drawn from the far side corner of the load to the support. The line makes an angle of 45 degrees with the support and the load plate. When this line is drawn from both far corners of the load area, the enclosed space at the support is the effective width. The determination of the effective width is already illustrated in chapter 2. The width can be expressed with the following formula:

$$b_{\text{eff}} = 2\,(a_v + c_l) + c_t \tag{3.1}$$

The loading area, the support width and the effective depth are constant so the only variable in the equation for the effective width is the (clear) shear span.

In the new version (final draft) of the Model Code 2010, a method to determine the effective width is given. This method is described in chapter 2. The effective width at simple supports can be determined with the following formula:

$$b_{\text{eff}} = 2\,(a_v + c_l - \min\{d; a_v/2\})\tan(60^o) + c_t \tag{3.2}$$

The width is taken at the control section, which is located at a distance of $\min\{d; a_v/2\}$ from the edge of the support. Nevertheless the resulting effective width is substantially larger than the effective width according to the French method.

The effective width is, for both the French method and the MC2010 method, limited by the element width.

3.3.2 Perimeter

A factor that greatly varies among the various building codes is the perimeter. The distance between the perimeter and the edge of the load and the shape can be different. For the Model Code 2010 and the Eurocode 2 the perimeter has four straight sides with rounded corners. For the ACI code it is allowed to use straight corners, but rounded corners may also be applied. In this thesis rounded corners are used. The distances between the edge of the load and the perimeter (a_p) is $a_p = 0.5d_{\text{ave}}$ for the ACI code and the Model Code 2010. For the Eurocode this is $a_p = 2.0d_{\text{ave}}$ and for Regan's model the distance is $a_p = 1.5d_{\text{ave}}$. The shape of the perimeter for Regan is rectangular and divided into sections. The NEN6720 uses a rounded perimeter shape. A rectangular load shape is represented as a circular load. The distance between the edge of the load and the perimeter is $a_p = 1.0d$. When the distance between the perimeter and the support is larger than the clear shear span (a_v), the length of the perimeter is reduced:

$$b_{o,\textbf{ACI, EC, MC2010}} = \begin{cases} 2(c_1 + c_2) + 2\pi a_p & \text{if } a_v \geq a_p \\ 2(c_1 + c_2) + 2\pi a_p - 2(a_p - a_v) & \text{if } a_v < a_p \end{cases}$$

In case of Regan's formula:

$$u_{1,\textbf{Regan}} = u_{1a} + u_{1b}$$

$$u_{2,\textbf{Regan}} = \begin{cases} 1(c_2 + 2a_p) & \text{if } (a_v - a_p) \leq 0.5d_{\text{ave}} \\ 0 & \text{if } (a_v - a_p) > 0.5d_{\text{ave}} \end{cases}$$

Where:

$$u_{1a} = \begin{cases} 2(c_1 + 2a_p) & \text{if } a_v \geq a_p \\ 2(c_1 + 2a_p) - 2(a_p - a_v) & \text{if } a_v < a_p \end{cases}$$

$$u_{1b} = \begin{cases} 1(c_2 + 2a_p) & \text{if } (a_v - a_p) \leq 0.5d_{\text{ave}} \\ 2(c_2 + 2a_p) & \text{if } (a_v - a_p) > 0.5d_{\text{ave}} \end{cases}$$

For the NEN7620

$$b_{o,\textbf{NEN6720}} = \begin{cases} \pi\left(\dfrac{2c_l + 2c_t}{\pi} + a_p\right) & \text{if } a_v \geq a_p \\ \pi\left(\dfrac{2c_l + 2c_t}{\pi} + a_p\right) - 2(a_p - a_v) & \text{if } a_v < a_p \end{cases}$$

In figure 3.1 the great differences in perimeter lengths can be observed. The graph is computed using the properties of the fictional model. All codes show an increasing perimeter length before remaining constant. This represents

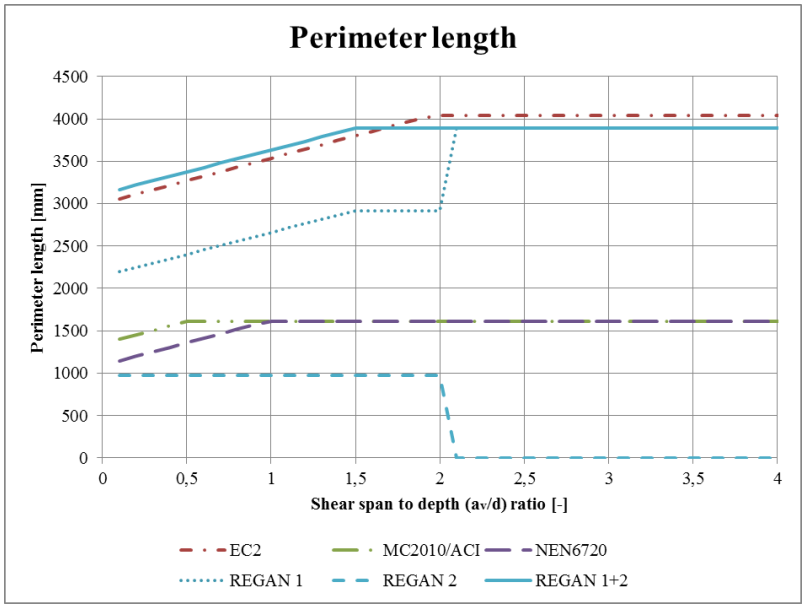

Figure 3.1: Perimeter length for the various building codes.

the reduction in perimeter length when the perimeter shifts over the edge of the support. The perimeter used in Regan's method consists of two parts when near to a support.

As described in the previous chapter, the Eurocode, Model Code 2010 final draft and the NEN6720 take into account the increased load carrying capacity for loads close to the support. The ACI building code officially does not take the increase into account. In the next section where the various codes will be compared however, the factor β that incorporates this capacity increase is also applied to the ACI code.

3.4 Comparing code provisions

When test results are compared to predicted results from a building code, the prediction will almost always be on the conservative side. When an empirical design code is developed based on a number of tests, a certain factor is applied to ensure safe results. It is therefore not valid to make a statement based on the average tested-to-predicted ratio. However, the standard deviation and the coefficient of variation can be used to tell if a design code provides a good approximation. A good approximation of the tests by the building code provisions is characterised by a small value of the standard deviation and the coefficient of variation.

Equation safety index

Gardner (2011) [12] stated that the code equations cannot be compared directly due to their different philosophies used in their derivations. The ACI 318-08 for example uses the 5% probability value to determine the equation coefficients, whereas the EN 1992-1-1 uses the mean value coefficients. The only valid comparisons are to compare the equation safety indexes or to adjust the various methods to the same philosophy. In this thesis the equation safety indices are determined and compared. The method is explained in the next section.

Method of comparing

In fib bulletin 12 [30] comparisons are made between code rules and tests for flat slabs without shear reinforcement. The method of comparing the codes is briefly described here. This is the method that is applied in this chapter. Additionally, an equation safety index (Allen, 1975 [4]) is determined. This enables the possibility of a fair comparison of the different building codes [12]. Method description:

Mean values of material strength are used.

Individual safety ratio: $\mu = \dfrac{V_{test}}{V_c}$.

Mean safety ratio: $\overline{\mu} = \dfrac{1}{n}\sum \mu$.

Standard deviation: $\sigma = \sqrt{\dfrac{1}{n-1}\sum \left(\mu - \overline{\mu}\right)^2}$

Coefficient of variation: $c_v = \dfrac{\sigma}{\overline{\mu}}$

Equation safety index: $\mathrm{ESI} = \dfrac{\ln\left[\mathrm{SF}\overline{\mu}\sqrt{\dfrac{1+c_{v,S}^2}{1+c_{v,R}^2}}\right]}{\sqrt{\ln\left[\left(1+c_{v,S}^2\right)\left(1+c_{v,R}^2\right)\right]}}$

The ESI assumes normal distributions. The experimentally determined maximum load capacities are denoted with an R. The code predictions are denoted with an S.

The equation safety index or ESI is commonly denoted with β. In this report β is also used in this chapter as a factor to take into account an increase is shear capacity for one-way shear when an element is loaded close to the support. In chapter four and five β represents the shear retention factor. Therefore it is chosen to denote the equation safety index with ESI.

SF is the design equation overall design safety factor. The SF includes the code partial safety factor.

Failure of a structure occurs when the tested element strength (R) is smaller than the load effect or predicted resistance (S), so when failure occurs when $R < S$. R and S are random variables and they are considered statistically independent so the failure criteria can be written as: $\ln R - \ln S = u < 0$. The probability of failure corresponds to the area underneath the probability distribution curve of u in the tail $u < 0$. The mean value for u is $\overline{u} = \overline{\ln R} - \overline{\ln S}$. The number of standard distributions between the mean value $\overline{u}$ and 0 is the equation safety index. This is illustrated in figure 3.2.

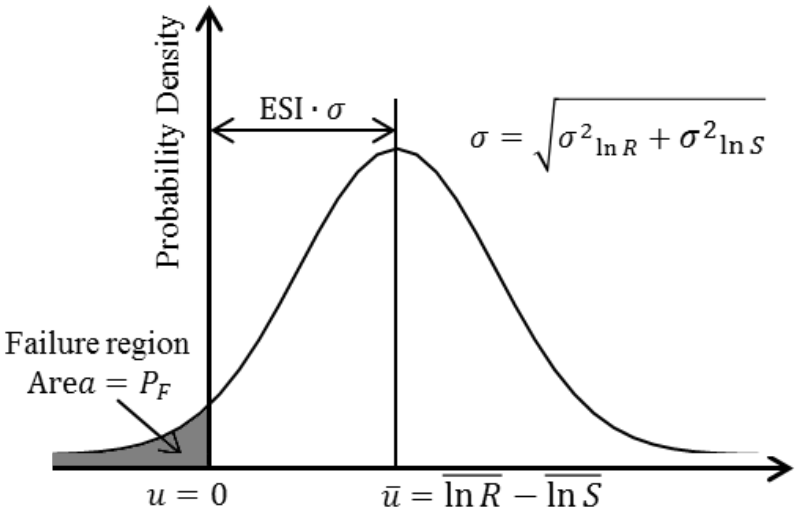

Figure 3.2: Equation safety index definition.

3.4.1 Failure mode

The experiments used in this thesis are all loaded with a concentrated load close to the simple support. The observed failure mode is either (wide) beam shear failure, punching shear failure, or a combination of (wide) beam shear failure and punching shear failure. At this moment it is not precisely known if

and when the code provisions for punching and one-way shear are applicable. By applying the various building codes to the test results, comparing the predicted and observed failure modes and comparing the equation safety indices, an attempt is made to determine if and when the building codes are applicable.

The following steps will be taken to compare the building codes to the experimental results.

1. For each experimentally tested element the building code provisions for one-way shear and punching shear will be applied when possible. In some instances the element width is smaller than the width of the punching control perimeter, resulting in an impossibility to apply the punching shear provision. The predicted shear force will be compared to the experimental shear force. This will result in the individual safety ratio.

2. For each experimentally tested element the observed failure mode is compared to the predicted (limiting) failure mode.

3. For each series of tests (BS (width = 500 mm), BM (1000 mm), BL (1500 mm), BX (2000 mm), S (2500 mm), Regan, Reissen and Hegger) the mean safety ratios and standard deviations will be determined for one-way shear and punching shear. This enables the possibility to determine the coefficient of variation, the safety ratio and the ESI. Based on this information it is possible to determine if it is reasonable to apply the one-way shear provision or punching shear provision on the type of element in combination with the location of the concentrated load.

The reliability index is linked to the probability of failure. $P_f = \Phi(-ESI)$ (Gardner 2011 [12]). In the table below, some probabilities of failure are given with their equation safety index.

P_f	10^{-1}	10^{-2}	10^{-3}	10^{-4}	10^{-5}	10^{-6}	10^{-7}	10^{-8}	10^{-9}
ESI	1.28	2.33	3.09	3.71	4.26	4.75	5.19	5.62	5.99

Concrete strength

The concrete strengths from the element tested in the experiments are determined from concrete cubes tested on the day of the experiment. The average concrete cube compressive strengths are given ($f_{cm,cube}$). The different building codes use different compressive strengths. The ACI 318-08 uses the specified cylinder compressive strength (f'_c). The EN1992-1-1:2005 and

the MC2010 use the characteristic cylinder compressive strength (f_{ck}) and Regan (1982) uses the characteristic cube compressive strength ($f_{ck,cube}$).

To be able to compare the results from the different building codes as fair as possible, the mean measured concrete strengths should be used and not the characteristic or the specified compressive strength (Gardner, 2011 [12]).

3.5 Building codes applied to the fictional concrete element

3.5.1 The ACI code

The ACI 318-08 code provisions for shear and punching are applied to the fictional slab described in section 3.2. The only parameter that is being varied is the clear shear span a_v. The effective width and the perimeter described in section 3.3 are used. The calculation for $a = 600$ mm is given as an example. The self weight of the concrete is not included in the calculation below. The minimum value for $b_{\text{eff}} = 600$ mm.
One-way shear and maximum concentrated load

$$a_v = a - 0.5\,(l_{\text{sup}} + c_{\text{l}}) = 450 \text{ mm}$$

$$\frac{a_v}{d_l} = 1.7$$

$$b_{\text{eff,French}} = 2\,(a_v + c_l) + c_t = 1500 \text{ mm}$$

$$V_c = \frac{2}{12}\lambda\varphi\sqrt{f'_c}\,b_{\text{eff}}d_l = 419 \text{ kN}$$

$$\beta = \max\left\{\begin{array}{l} \min\left\{\begin{array}{l} \dfrac{a_v}{2d_l} \\ 1.00 \end{array}\right. \\ 0.25 \end{array}\right. = 0.849$$

$$F_c = \frac{V_c}{1 - \dfrac{a}{l_{\text{span}}}} = 503 \text{ kN}$$

$$F_{\text{c,max}} = \frac{F_c}{\beta} = 592 \text{ kN}$$

Punching shear

$$\beta_c = \max\left\{\frac{c_l}{c_t}; \frac{c_t}{c_l}\right\} = 1.00$$

$$b_o = 2\left(c_l + c_t\right) + 2\pi 0.5 d_{\text{ave}} = 1633 \text{ mm}$$

$$F_{c,\text{pun}} = \varphi\lambda\frac{1}{12}\sqrt{40}b_o d_{\text{ave}} \min\left\{\begin{array}{l}\left(2 + \dfrac{4}{\beta_c}\right) \\ \left(\alpha_s \dfrac{d_{\text{ave}}}{b_o} + 2\right) \\ 4\end{array}\right. = 886 \text{ kN}$$

Figure 3.3 shows a graph in which the ACI code shear provision is compared to the punching provision for the fictional concrete element. The only variable is the clear shear span a_v. The dashed line is the maximum concentrated load determined with the one-way shear strength with the factor β incorporated. As can be seen the punching load capacity is constant except for $0 < a_v < 0.5d_{\text{ave}}$. For these shear span ratios the perimeter is reduced. The one way shear capacity increases with a constant rate up to a value of $a_v/d_{\text{ave}} = 3.6$. After that the maximum concentrated load is increasing constantly at a lower rate. This is caused by the limited element width. The effective width can not increase beyond the width of the element. The load that can be applied on the element still increases because as the load approaches the middle of the span ($a_v/d_l = 6.8$), more load will be transferred to the other support. The maximum shear force in the element between the load and the first support will remain constant. It can be observed that for this concrete element one way shear is governing when $a_v/d_{\text{ave}} \leq 3.2$.

3.5.2 The Eurocode

The same fictional slab the ACI318-08 code is applied to above, is now subjected to the Eurocode provisions for shear and punching. As example, a calculation for the one-way shear provision and the punching shear provision is provided for $a = 600$ mm. The self weight of the concrete has been left out of the equations.

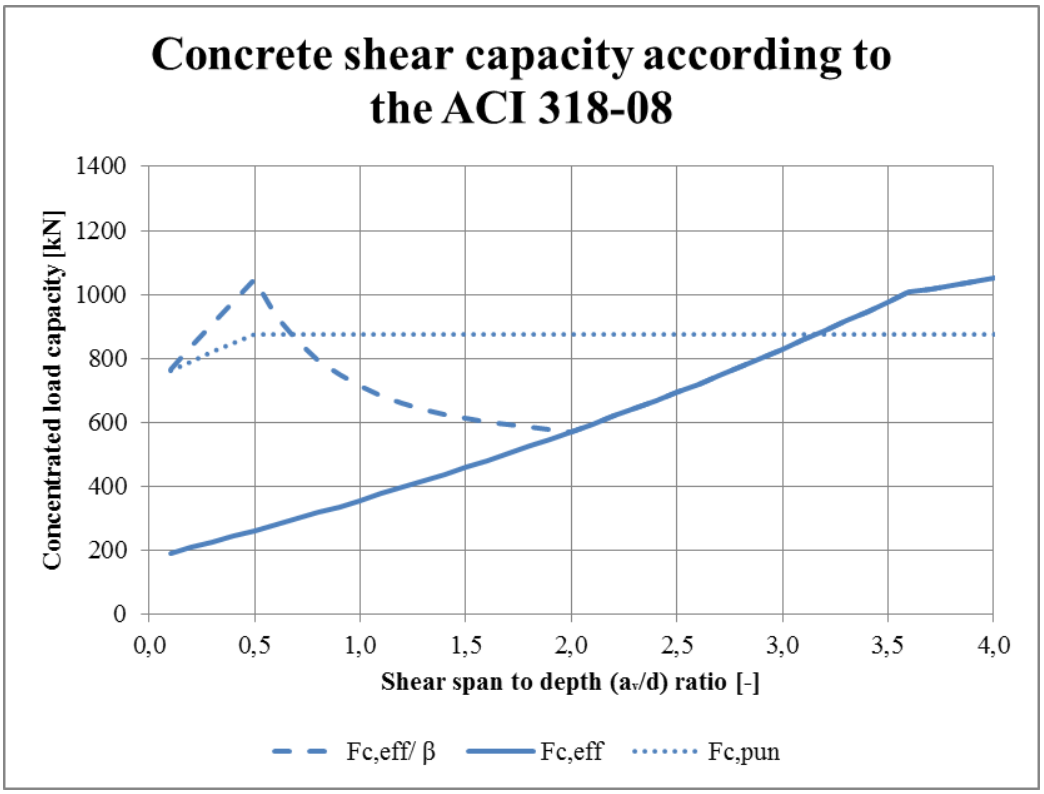

Figure 3.3: Maximum concentrated load according to the ACI318-08 when applied to the concrete element described in section 3.2.

One-way shear and maximum concentrated load:

$$C_{R,c} = 0.18$$
$$\gamma_c = 1.00$$
$$k = 1 + \sqrt{\frac{200}{d_l}} = 1.869$$
$$v_{\min} = 0.035 k^{3/2} \sqrt{f_{ck}} = 0.565 \text{ MPa}$$
$$V_{R,c} = \frac{1}{\beta} \frac{C_{R,c}}{\gamma_c} k \left(100 \rho_l f_{ck}\right)^{1/3} b_{\text{eff}} d_l \geq v_{\min} b_{\text{eff}} d_l = 529 \text{ kN}$$
$$F_{c,\max} = \frac{V_{R,c}}{\left(1 - \frac{a}{l_{\text{span}}}\right)} = 635 \text{ kN}$$

Punching

$$u_o = 2\left(c_l + c_t\right) + 2\pi 2.0 d_{\text{ave}} = 3906 \text{ mm}$$
$$\rho_{\text{ave}} = \sqrt{\rho_l \rho_t} \leq 2 \text{ \%} = 0.345 \text{ \%}$$
$$k_{\text{pun}} = 1 + \sqrt{\frac{200}{d_{\text{ave}}}} = 1.881$$
$$v_{\min,\text{pun}} = 0.035 k_{\text{pun}}^{3/2} \sqrt{f_{ck}} = 0.571$$
$$V_{R,c} = \frac{C_{R,c}}{\gamma_c} k_{\text{pun}} \left(100 \rho_{\text{ave}} f_{ck}\right)^{1/3} u_o d_{\text{ave}} \geq v_{\min,\text{pun}} u_o d_{\text{ave}} = 817 \text{ kN}$$

As can be seen in the graph from figure 3.4, the value for punching shear strength is constant when $a_v > 2.0 d_{\text{ave}}$. Before this value the perimeter is reduced. When $a_v / d_l > 2.8$, punching shear is governing. The effective width in the one-way shear provision is limited by the element width when the shear span to depth ratio exceeds 3.6. This can be seen in the graph as a slower increasing concentrated load capacity.

3.5.3 The Model Code 2010

In this section the Model Code 2010 draft is applied to the fictional model described in section 3.2. Example calculations are provided for a shear span of $a = 600$ mm. First the shear arm in span direction z_l and the distance from the center of the support to the control section in the concrete a_c are

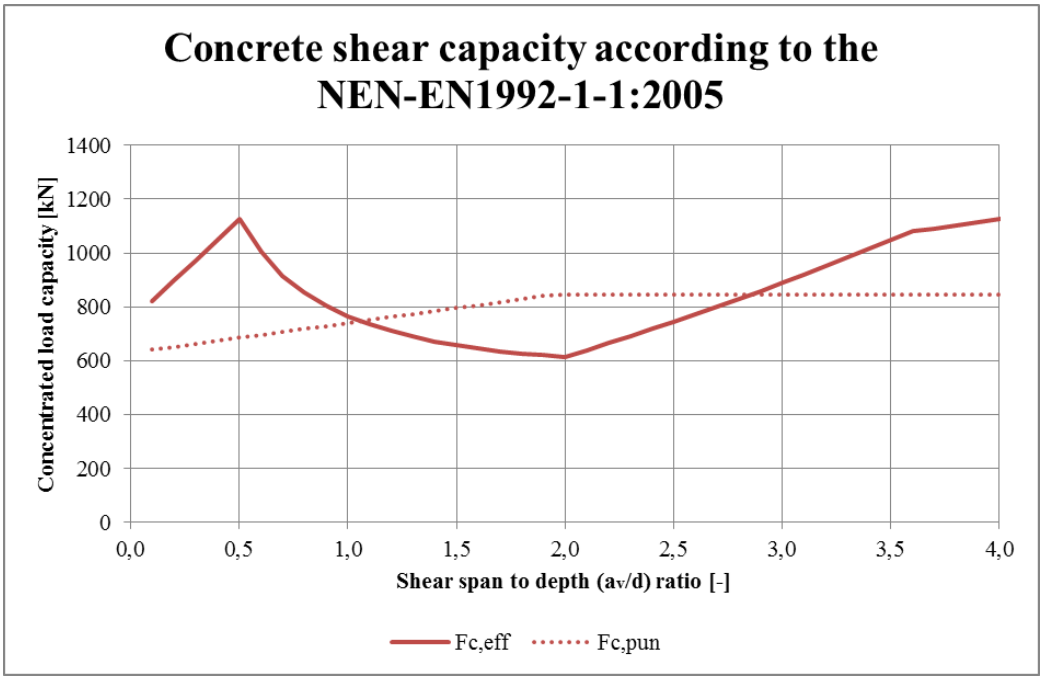

Figure 3.4: Concrete shear capacity according to the NEN-EN1992-1-1 when applied to the concrete element described in section 3.2.

determined. These are then used to calculate the effective width $b_{\text{eff,MC2010FD}}$.

$$z_l = 0.9d_l = 238.5 \text{ mm}$$

$$a_c = 0.5l_{\text{sup}} + \min \begin{cases} a_v/2 \\ d_l \end{cases} = 275 \text{ mm}$$

$$b_{\text{eff,MC2010FD}} = \min \begin{cases} c_t + 2 \cdot (c_l + a_v - \min\{a_v/2; d_l\}) \cdot \tan\left(\dfrac{60\pi}{180}\right) \\ b \end{cases}$$

$$= 1672 \text{ mm}$$

The factor to take the aggregate size into account k_{dg} and the reinforcement steel area in span direction A_s are determined.

$$k_{dg} = \frac{32}{16 + d_g} = 1.00$$

$$A_s = \frac{b_{\text{eff,MC2010FD}}}{s_l} 0.25\pi\phi_l^2 = 4775 \text{ N/mm}^2$$

Now a value for the load is assumed. This value is used to determine the support reaction at the simple support V_{ss}. Since the self weight is not taken into account, this shear force is the same as the shear force at the control section of the element $V(a_c)$. The bending moment at the control section can also be determined $M_E(a_c)$.

$$\begin{aligned} F &= 684 \text{ kN} \\ V_{ss} = F\left(1 - \frac{a}{l_{\text{span}}}\right) &= 598 \text{ kN} \\ V(a_c) &= V_{ss} \\ M_E(a_c) = V_{ss} a_c &= 165 \text{ kNm} \end{aligned}$$

The above information is required to determine the longitudinal strain at mid-depth of the member ϵ_x. Now the factor for shear k_v and the one-way shear resistance $V_{R,c}$ can be calculated. A unity check is performed to determine if the calculated capacity does not exceed the shear force caused by the applied load. If this is the case, the load is reduced until the unity check is equal to zero.

$$\begin{aligned} \epsilon_x &= \frac{M_E(a_c)/z + V_E(a_c)}{2E_s A_s} = 0.00067 \\ k_v = \frac{0.4}{1 + 1500\epsilon_x} \frac{1300}{1000 + k_{dg} z} &= 0.209 \\ V_{R,c} = k_v \frac{\sqrt{f_{ck}}}{\gamma_c} z b_{\text{eff}} &= 598 \text{ kN} \\ \text{u.c.} = \frac{V_{R,c}}{V(a_c)} &= 1.00 \end{aligned}$$

Now the factor β for loads loaded close to the support is applied. First the factor is determined. In the Model Code 2010, the factor is used to reduce the applied load. In this case it is used to increase the calculated capacity. To obtain a maximum concentrated load instead of a shear force, the maximum

shear is divided by $\left(1 - \frac{a}{l_{\text{span}}}\right)$.

$$\beta = \max \left\{ \begin{array}{l} \min \left\{ \begin{array}{ll} \frac{a_v}{2d_l} \\ 1.00 \end{array} \right. \quad = 0.489 \\ 0.50 \end{array} \right.$$

$$F_{R,c} = \frac{V_{R,c}}{\left(1 - \frac{a}{l_{\text{span}}}\right)} = 718 \text{ kN}$$

$$F_{R,c,\max} = \frac{F_{R,c}}{\beta} = 846 \text{ kN}$$

For punching first the length of the shear perimeter is calculated. To calculate the rotation ψ of the element, the distance r_s between the load axis and the position where the bending moment is zero is required. In this case this distance r_s is the same as the shear span a because the bending moment above the simple support is zero. The calculation provided is a level I approximation. This makes the calculation a very rough conservative estimate.

$$b_o = 2\left(c_l + c_t\right) + 2\pi 0.5 d_{\text{ave}} = 1609 \text{ mm}$$

$$r_s = a = 600 \text{ mm}$$

$$\psi = 1.5 \frac{r_s}{d_{\text{ave}}} \frac{f_y}{E_s} = 0.00944$$

$$k_\psi = \frac{1}{1.5 + 0.9\psi d_{\text{ave}} k_{dg}} \leq 0.6 = 0.305$$

$$F_{\text{R,c,pun}} = k_\psi \frac{\sqrt{f_{ck}}}{\gamma_c} d_{\text{ave}} b_o = 799 \text{ kN}$$

In figure 3.5, three capacities are plotted. One is calculated using the French effective width in the one-way shear provision (solid line). The second (dashed line) shows the capacity using the effective width as provided by the Model Code 2010 Final draft. The third (dotted line) is the capacity calculated using the punching shear provision.

The calculated punching shear capacity is decreasing with an increasing shear span. Only in the first part ($0.0 < a_v/d_{\text{ave}} < 0.5$) the capacity is increasing. This is caused by the reduced perimeter length. The perimeter length is constant for $a_v/d_{\text{ave}} \geq 0.5$. The reduction in punching shear capacity is caused by the increasing distance between the load and the point where the bending moment is zero r_s.

Compared to the one-way shear capacity that is calculated using the effective width from the MC2010, the punching shear provision is governing for $a_v/d_{\text{ave}} > 2.0$. For values of $1.0 < a_v/d_{\text{ave}} < 2.0$ the calculated capacity is about the same. Compared to the one-way shear capacity that is calculated using the French method, punching is governing for $a_v/d_{\text{ave}} > 2.2$. As expected, the one-way shear capacity is higher for the effective width from the Model Code than from the Eurocode French national annex.

The graphs for one-way shear can be divided into four parts. In the first part the capacity is increasing. This is because the effective width is increasing and the distance from the support to the load is increasing. The factor β for an additional capacity for loads close to the support is constant. When $1.0 < a_v/d_l < 2.0$ the value for β decreases, causing a decrease in shear capacity. For $a_v/d_l > 2.0$ the shear capacity increases again due to the increasing shear span and effective width. When the effective width is limited by the element width only a slight capacity increase remains due to the increasing shear span.

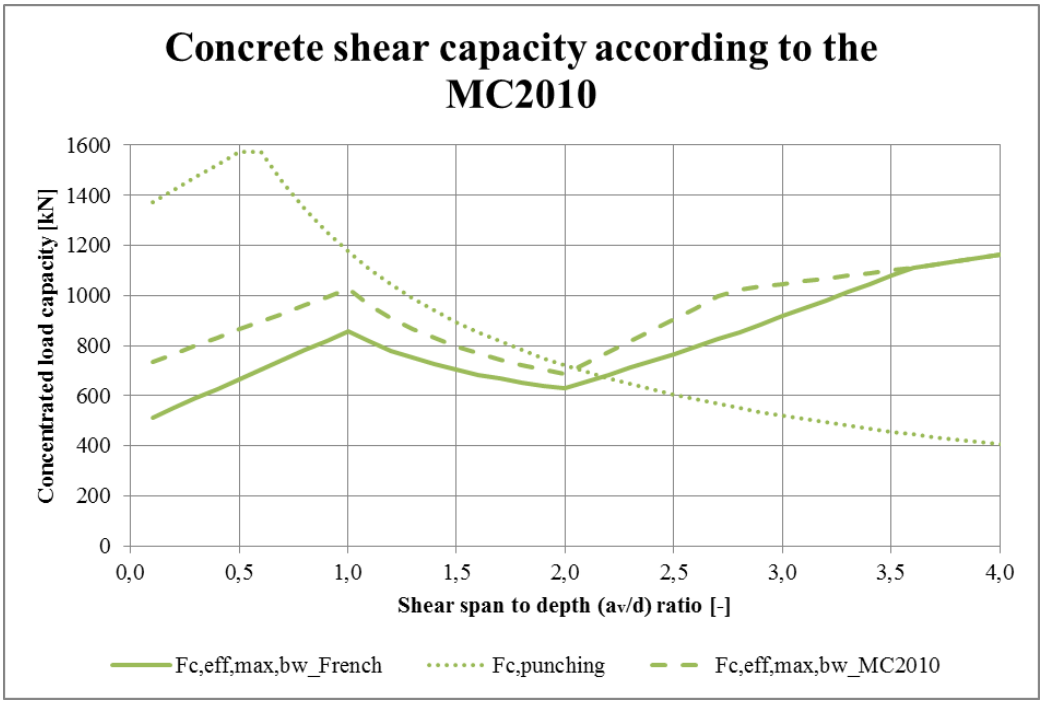

Figure 3.5: Concrete shear capacity according to the Model Code 2010 when applied to the concrete element described in section 3.2.

3.5.4 The NEN 6720

The NEN 6720 [13] is also applied to the fictional slab. One-way shear and punching are compared in figure 3.6. An example calculation for $a = 600$ mm is worked out here:
First the concrete compressive strength and the concrete tension strength is calculated.

$$\begin{aligned}
\gamma_{\text{m,tension}} &= 1.00 \\
\gamma_{\text{m,compression}} &= 1.00 \\
f_{\text{b,rep}} = 0.7\,(1.05 + 0.05 f'_c) &= 2.135 \text{ N/mm}^2 \\
f_b = \frac{f_{\text{b,rep}}}{\gamma_{\text{m,tension}}} &= 2.135 \text{ N/mm}^2 \\
f'_{\text{b,rep}} = 0.72 f'_c &= 28.8 \text{ N/mm}^2 \\
f'_b = \frac{f'_{\text{b,rep}}}{\gamma_{\text{m,compression}}} &= 28.8 \text{ N/mm}^2
\end{aligned}$$

Then a value for the concentrated load is assumed. With static equilibrium, the shear force and support reaction V_{ss} can be calculated. The self weight of the concrete is not taken into account. The maximum bending moment $M_{\max}$ will occur at the location of the concentrated load. The shear slenderness λ_v is also determined.

$$\begin{aligned}
F &= 520 \text{ kN} \\
V_{ss} = F\left(1 - \frac{a}{l_{\text{span}}}\right) &= 434 \text{ kN} \\
M_{\max} = aV_{ss} &= 260 \text{ kNm} \\
\lambda_v = \frac{M_{\max}}{d_l V_{ss}} &= 2.26
\end{aligned}$$

When the concentrated load is applied in close proximity of a support, a direct compression strut can be formed. This is calculated with g_λ and k_λ.

A factor for the element height k_h and the load area A_o are also calculated.

$$g_\lambda = \begin{cases} 1+\lambda_v^2 & \text{if } \lambda_v \geq 0.6 \\ 2.5-3\lambda_v & \text{if } \lambda_v < 0.6 \end{cases} = 6.13$$

$$k_\lambda = \max \begin{cases} 1 \\ \dfrac{12}{g_\lambda}\left(\dfrac{c_l c_t}{d_l b_{\text{eff}}}\right)^{1/3} \end{cases} = 1.00$$

$$k_h = \max \begin{cases} 1 \\ 1.6 - h[\text{m}] \end{cases} = 1.3$$

$$A_o = c_l \cdot c_t = 0.040 \text{ m}^2$$

Now all factors to determine the one-way shear capacity are known. The shear capacity is calculated as τ_1. To prevent crushing of the concrete the calculated shear stress may not exceed a value of τ_2. Eventually the used shear stress is called τ_u.

$$\tau_1 = \max \begin{cases} 0.4 f_b k_\lambda k_h \left(100\rho_l\right)^{1/3} \\ 0.4 f_b \end{cases} = 1.091\text{N/mm}^2$$

$$\tau_2 = 0.2 f_b' = 5.760\text{N/mm}^2$$

$$\tau_u = \min \begin{cases} \tau_1 \\ \tau_2 \end{cases} = 1.091\text{N/mm}^2$$

From the maximum shear stress, the maximum shear capacity V_c for the given cross-section is determined. This value is translated into a concentrated load $F_{c,\max}$. A unity check is done to prevent the shear caused by the assumed load to exceed the calculated maximum shear. The assumed concentrated load is changed until the unity check reads 1.00.

$$V_c = \tau_u b_{\text{eff}} d_l = 434 \text{ kN}$$

$$\text{u.c.} = \frac{V_c}{V_{ss}} = 1.00$$

$$F_{c,\max} = \frac{V_c}{\left(1 - \dfrac{a}{l_{\text{span}}}\right)} = 520 \text{ kN}$$

Now an example calculation using the NEN6720 provision for punching:
A factor to take into account the size and shape of the load k_1 and an equivalent load diameter a_{load} is calculated first. Then a factor to account

for the effect of load size-to effective width is determined. k_d takes into account the element thickness.

$$k_1 = \begin{cases} max \begin{cases} 0.5 \\ 2 - \dfrac{c_l}{2c_t} & \text{if } c_l > 2c_t \\ 1.0 & \text{if } c_l < 2c_t \end{cases} \end{cases} = 1.00$$

$$a_{\text{load}} = \frac{2\left(c_l + c_t\right)}{\pi} = 0.255 \text{ m}$$

$$k_2 = \begin{cases} max \begin{cases} 0.5 \\ \dfrac{4}{2 + \dfrac{a_{\text{load}}}{d_{\text{ave}}}} & \text{if } a_{\text{load}} \geq 2d_{\text{ave}} \\ 1.0 & \text{if } a_{\text{load}} < 2d_{\text{ave}} \end{cases} \end{cases} = 1.00$$

$$k_d = \max \begin{cases} 1.00 \\ 1.5 - 0.6d_{\text{ave}} \text{ [m]} \end{cases} = 1.35$$

With the average bending reinforcement ratio ρ_{ave} and the factors calculated above, the maximum shear stress can be calculated. Multiplying the stress with the effective depth d_{ave} and the perimeter length u_o gives the punching capacity $F_{\text{c,pun}}$.

$$\rho_{\text{ave}} = \sqrt{\rho_l \rho_t} \leq 2\ \% = 0.345\ \%$$

$$\tau_1 = \max \begin{cases} 0.8 f_b k_1 k_2 \\ 0.8 f_b k_1 k_2 k_d \left(100 \rho_{\text{ave}}\right)^{1/3} \end{cases} = 1.708 \text{N/mm}^2$$

$$\tau_2 = \min \begin{cases} 5.00 \\ 0.15 f_b' \end{cases} = 4.320 \text{N/mm}^2$$

$$\tau_u = \min \begin{cases} \tau_1 \\ \tau_2 \end{cases} = 1.708 \text{N/mm}^2$$

$$u_o = \pi \left(a_{\text{load}} + d_{\text{ave}}\right) = 1609 \text{ mm}$$

$$F_{c,\text{pun}} = \tau_u u_o d_{\text{ave}} = 708 \text{ kN}$$

The graph shown in figure 3.6 is clear. Up to a clear shear-span to depth ratio of about $a_v/d = 1.6$, a direct compression strut is assumed in the one-way shear capacity. This direct strut effect is more prominent if the load is closer to the support. An increasing effective width causes the increasing maximum load capacity for $a_v/d > 1.6$. The slower increase in shear capacity after $a_v/d = 3.6$ is caused by the limited element width. The continuing increase is caused by shifting static equilibrium. The shear capacity of the concrete remains constant, but the maximum load that can be applied still increases.

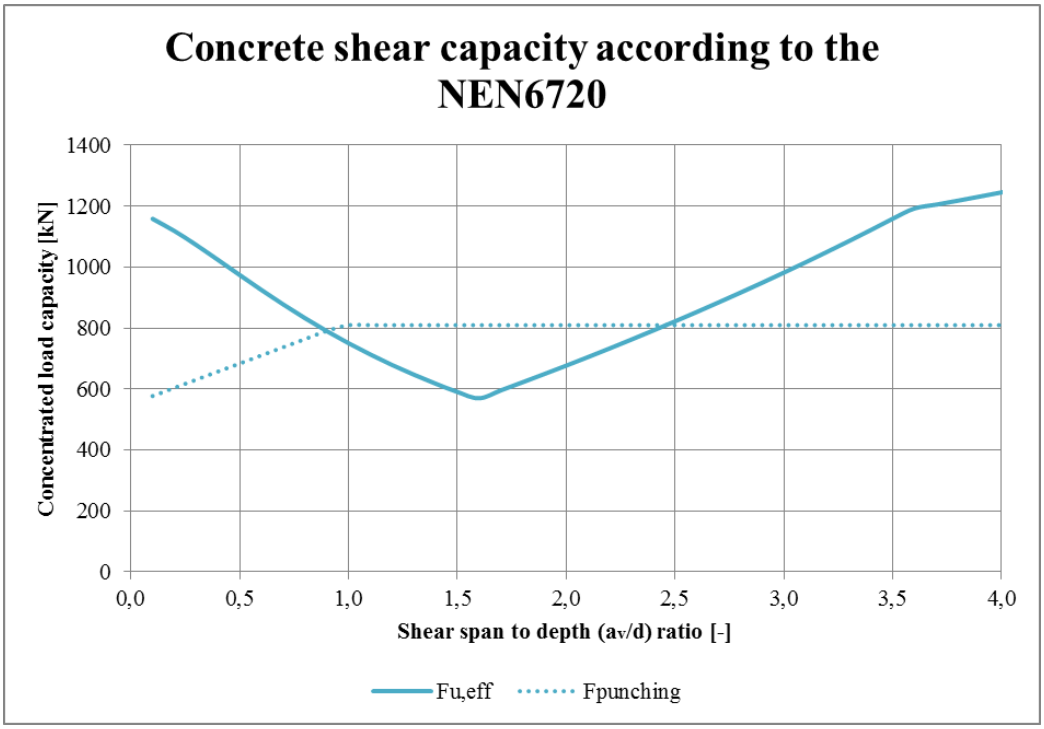

Figure 3.6: Concrete shear capacity according to the NEN6720 when applied to the concrete element described in section 3.2.

The punching shear strength increases until $a_v/d = 1.0$. This is due to limited perimeter length. After this value, the punching strength remains constant.

3.5.5 Regan's model (1982)

The method developed by P. E. Regan to determine the shear strength for elements loaded close to the support is applied to the fictional element. An example calculation ($a = 600$ mm) is given here:
First the average bending reinforcement ratio is calculated. This method uses the concrete cube compressive strength. This is calculated from the concrete cylinder compressive strength.

$$\rho_{\text{ave}} = \frac{\rho_l + \rho_t}{2} = 0.537\ \%$$
$$f_{\text{c,cube}} = f_c/0.82 = 48.8\ \text{N/mm}^2$$

The average reinforcement ratio and effective depth are applied as a simplification. The simplification is also applied by P.E. Regan himself in his report describing the model [32].

The control perimeter consists of two parts. Part two is the part located between the load and the support, and running parallel to the support. In close proximity of the support this part is considered to have a higher capacity. When the concentrated load is applied at a distance $a_v/d_{\text{ave}} > 2.0$ the length of part two of the perimeter is zero (figure 3.7) and the whole perimeter is considered as the first part of the perimeter. Part one is calculated first.

$$u_{1a} = \begin{cases} 0 & \text{if } b < 2 \cdot 1.5 \cdot d_{\text{ave}} + c_t \\ 2 \cdot 1.5 \cdot d_{\text{ave}} + c_t & \text{if } a_v - 1.5d_{\text{ave}} \leq 2 \cdot 0.5d_{\text{ave}} \\ 2\left(2 \cdot 1.5 \cdot d_{\text{ave}} + c_t\right) & \text{if } a_v - 1.5d_{\text{ave}} > 2 \cdot 0.5d_{\text{ave}} \end{cases} = 973\ \text{mm}$$

$$u_{1b} = \begin{cases} 0 & \text{if } b < 2 \cdot 1.5 \cdot d_{\text{ave}} + c_t \\ 2\left(2 \cdot 1.5 \cdot d_{\text{ave}} + c_l\right) & \text{if } a_v \geq 1.5d_{\text{ave}} \\ 2\left(2 \cdot 1.5 \cdot d_{\text{ave}} + c_l\right) - 2\left(1.5d_{\text{ave}} - a_v\right) & \text{if } a_v < 1.5d_{\text{ave}} \end{cases}$$
$$u_{1b} = 1946\ \text{mm}$$

Part two is calculated here. As explained before, part two is only considered

when $a_v/d_{\text{ave}} < 2.0$.

$$u_2 = \begin{cases} 0 & \text{if } b < 2 \cdot 1.5 \cdot d_{\text{ave}} + c_t \\ c_t + 2 \cdot 0.5 \cdot d_{\text{ave}} & \text{if } a_v - 1.5d_{\text{ave}} \leq 0.5d_{\text{ave}} \\ 0 & \text{if } a_v - 1.5d_{\text{ave}} > 0.5d_{\text{ave}} \end{cases} = 973 \text{ mm}$$

For each perimeter part the punching capacity is calculated. For the second perimeter part an additional factor of $\frac{2d_{\text{ave}}}{a_v}$ is applied. The total punching shear capacity P_R is the sum of the two capacities.

$$P_{R1} = \sqrt[4]{\frac{500}{d_{\text{ave}}}} \frac{0.27}{\gamma_c} \sqrt[3]{100\rho_{\text{ave}} f_{\text{c,cube}}} (u_{1a} + u_{1b}) d_{\text{ave}} = 711 \text{ kN}$$

$$P_{R2} = \frac{2d_{\text{ave}}}{a_v} \sqrt[4]{\frac{500}{d_{\text{ave}}}} \frac{0.27}{\gamma_c} \sqrt[3]{100\rho_{\text{ave}} f_{\text{c,cube}}} (u_{1a} + u_{1b}) d_{\text{ave}} = 271 \text{ kN}$$

$$P_R = P_{R1} + P_{R2} = 982 \text{ kN}$$

Using these equations, varying the shear span results in the graph shown in figure 3.7. In the graph a distinction is made between the total shear capacity and the shear capacity provided by the two different parts of the perimeter. At a distance of $a_v/d_{ave} > 2.0d_{\text{eff}}$ from the support the model considers the shear to be constant along the perimeter. The shear capacity remains constant after this point. Before $a_v/d_{ave} = 2.0d_{\text{eff}}$ the shear strength increases when the load is closer to the support.

3.6 Comparing one-way shear provisions

In figure 3.8 the one-way shear code provisions from the previous sections are combined in one graph. Generally it can be said that the shapes are similar. In the first branch of the graphs there is a strength increase (except for the NEN6720). The capacity increase in this branch is due to the increasing effective width. In the first branch, before the peak, the β factor is limited by a lower bound and has a constant value. In the second branch, after the peak, the factor β decreases rapidly, causing the shear capacity to decrease as well despite the increasing effective width. When the factor β may not be applied any more the maximum concentrated load increases again due to the increasing effective width. After the maximum effective width has been reached, the maximum concentrated load capacity still increases. This is due to the fact that the force required to obtain the same shear stress increases

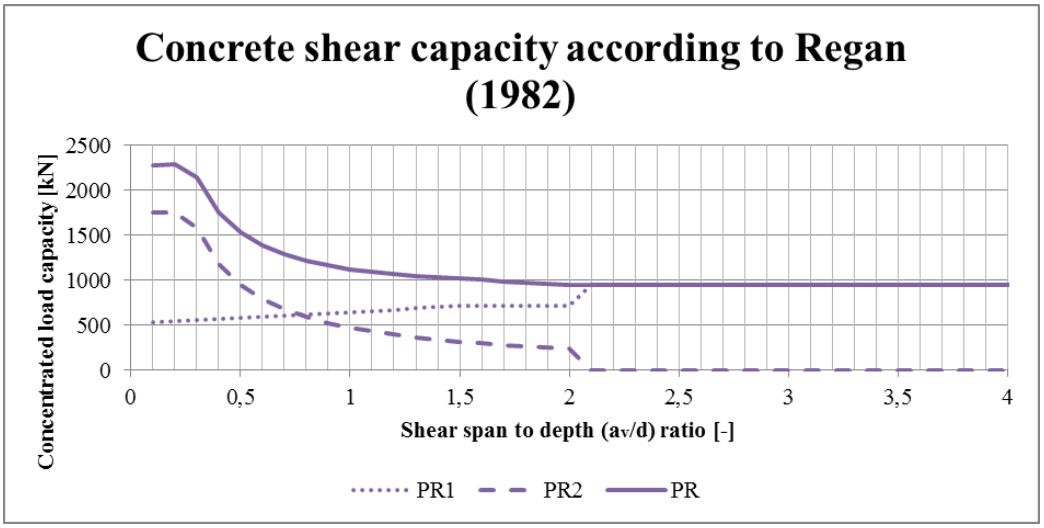

Figure 3.7: Concrete shear capacity according to the Regan's model (1982) when applied to the concrete element described in section 3.7.

as the distance between the load and the nearest support increases. The maximum concentrated load capacity will increase until the shear span is larger than half the span length (which corresponds to an $a_v/d_l = 6.8$).

When all provisions use the same effective width, the calculated capacity is similar. Especially for $a_v/d > 2.0$. The solid green line represents the one-way shear capacity for the Model Code 2010, using its own effective width. This effective width is proposed in the Final draft of the Model Code 2010.

The most conservative code provisions seem to be the ACI and the NEN6720. The least conservative predictions are done using the Eurocode 2 and the Model Code 2010, especially with the new effective width.

3.7 Comparing Punching shear provisions

The provisions for punching shear given in the codes and the model developed by Regan are compared in figure 3.9. The difference in capacity between the NEN6720 and Regan's method for $a_v/d > 2.0$ is about 250 kN. All capacities, except for the MC2010 (level I prediction) are constant for $a_v/d > 2.0$. When the load is close to the support, the MC2010 and Regan predict a capacity increase. The capacity increase in Regan's method is not limited. The lower capacities for low a_v/d values can be explained by reduced perimeter lengths.

The Model Code 2010 punching shear provision is calculated according to a level I approximation. This level of approximation implies that the pre-

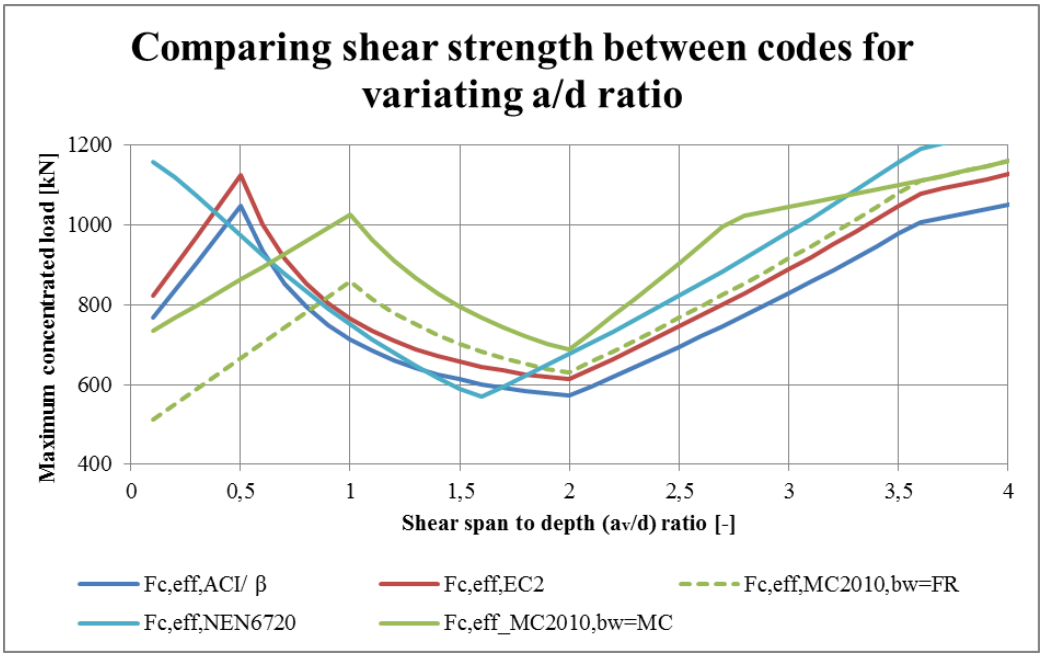

Figure 3.8: Comparing the one-way shear capacity provisions for increasing a_v/d_l ratio.

dicted capacity is very conservative. A more detailed level of approximation and therefore a better prediction can be obtained by using a (non)linear finite element calculation as input for the MC2010.

3.8 Effect of reinforcement ratios on shear strength

In this section the influence of increased reinforcement ratios is shown. Since the ACI code does not take reinforcement into account this can only be done for the Model Code 2010, the NEN6720, the Eurocode and Regan's Model.

3.8.1 Eurocode

In the NEN-EN-1992-1-1:2005 the influence of reinforcement ratio is taken into account. For one way shear the reinforcement ratio in span direction is considered and for punching the reinforcement ratio in longitudinal and transverse direction is taken into account by means of the average: $\rho_{\text{ave}} = \sqrt{\rho_l \rho_t}$.

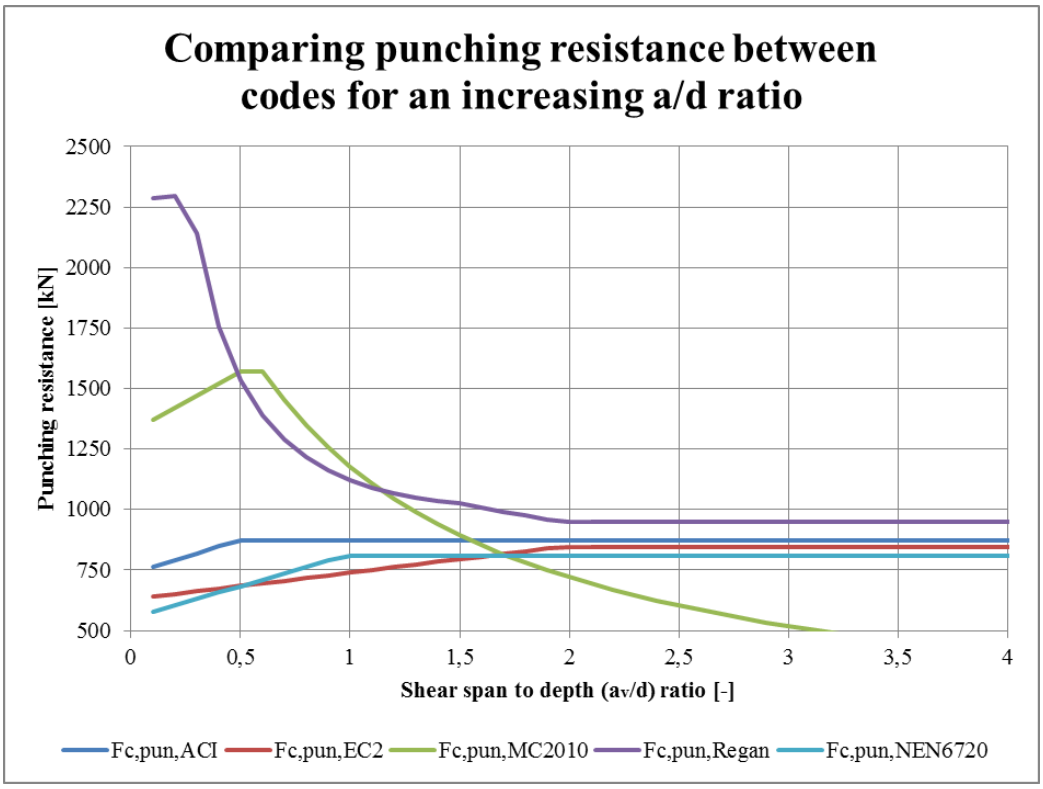

Figure 3.9: Comparing the punching shear capacity provisions for increasing a_v/d_l ratio.

The effect on one-way shear capacity of increasing or decreasing the bending reinforcement in span direction by a factor $(x \cdot \rho_l)$, can easily be derived from the code formula. Since the reinforcement ratio is positioned under the cube root of the formula, multiplying the bending reinforcement ratio in span direction with a factor x, the shear capacity will be multiplied by $\sqrt[3]{x}$.

The effect of increasing the reinforcement ratios on the punching shear strength is a little different since an average value is taken. When the bending reinforcement in span direction ratio is changed by a factor x, and the ratio in transverse direction is changed by a factor y, the capacity changes with a factor $\sqrt[3]{\sqrt{x} \cdot \sqrt{y}}$.

3.8.2 Model Code 2010

For the MC2010 one-way shear formulas the reinforcement area is used to determine the longitudinal strain ϵ_x in the element. This strain is used to determine a shear factor k_v. The relationship between reinforcement ratio and shear capacity is less direct than in the Eurocode or Regan's method. The example calculation performed for the MC2010 is done again. Only the reinforcement ratio is multiplied by 2 and by 0.5. When using half the amount of bending reinforcement in span direction, the shear capacity decreases by a factor 0.78. When the reinforcement ratio is doubled, the capacity increases by a factor of about 1.24. Note that factors are not general and therefore only apply to the fictitious element.

In the Model Code 2010 the Level of approximation that is used for punching shear capacity does not take into account the reinforcement ratios for punching shear.

3.8.3 Regan's method

The effect of the reinforcement ratios in the model developed by P. E. Regan (1982) is a different than for example in the Eurocode. The average reinforcement ratio is considered to be $\rho_{\text{ave}} = (\rho_l \rho_t)/2$. If the bending reinforcement ratio in span direction is changed by a factor x and the ratio in the transverse direction by a factor y, the shear capacity changes with a factor $\sqrt[3]{\frac{x \cdot \rho_x + y \cdot \rho_y}{2}}$. Contrary to the Eurocode, it does matter if either the longitudinal or the transverse reinforcement ratio is increased with a factor. Doubling the amount of reinforcement in the transverse direction (which has a low reinforcement ratio for the considered fictitious slab) has less effect than doubling the reinforcement ratio in the longitudinal direction.

3.8.4 NEN6720

The effect of reinforcement ratio on the one way-shear and punching shear capacity is the same as for the EN1992-1-1:2005.

3.9 Description of the tested concrete elements

3.9.1 Test setup

In the Stevin 2 Laboratory at Delft University of technology a series of test is performed on large reinforced concrete elements. The elements are subjected to a concentrated load at a relatively small distance from the support. The test set-up is shown in figure 3.10.

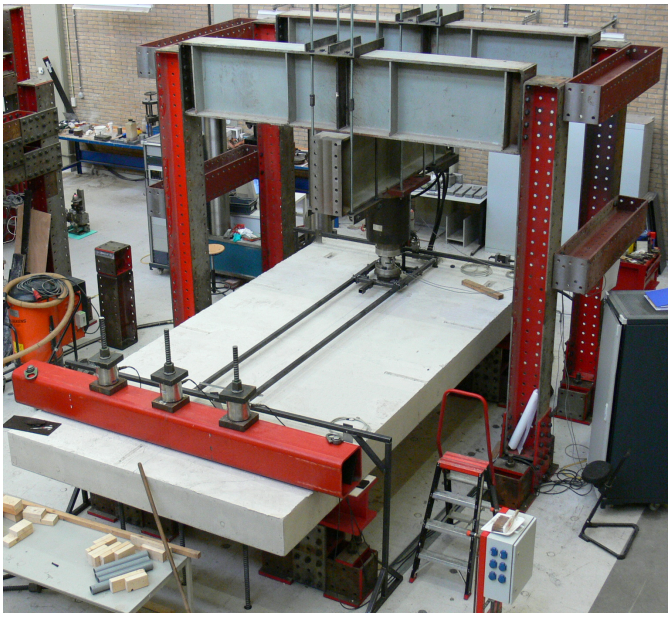

Figure 3.10: The test setup for experiments performed in the Stevin II Laboratory 2009-2011 [20].

The elements are all 300 mm thick and 5000 mm in length. The width is varied between 500 mm and 2500 mm. One side of the element is placed on a simple support. On the other side of the element a continuous support is simulated. The continuous support is located 1100 mm from the edge of the element. This cantilever part of the element was connected with prestressed bars to the laboratory floor. This situation created a negative bending moment at the support.

The concentrated load is applied at various distances from the two supports and at various positions over the width. Also multiple tests are performed on the same element. This means that some tests are carried out on damaged elements. In this thesis, only the tests performed on uncracked elements, loaded at the simple support in the middle of the element width are used.

The sizes of the load plate are either 200 mm x 200 mm or 300 mm x 300 mm. The load plate can represent a (scaled) truck wheel load. The maximum load that could be applied as concentrated load was 2000 kN. Between the concrete element and the supports, a layer of 10 or 15 mm felt and 8 mm plywood is placed.

The amount and layout of the reinforcement and concrete strength are also varied in the tests. The elements are cast in the laboratory. For each concrete cast session, a series of cubes are produced to monitor the hydration process during the hardening period of the concrete.

3.9.2 Element properties

The tested elements that are used in this thesis are described in the tables below. A distinction is made between slabs (S-series), and beams (B-series). Within the beam series small beam widths (S), medium beam widths (M), large beam widths (L) and very large widths (X) are tested. A lot of characteristics are the same for the beams and slabs.

Element properties **Lantsoght 2009-2011**						
All	b_{BS}	500	mm			
	b_{BM}	1000	mm			
	b_{BL}	1500	mm			
	b_{BX}	2000	mm			
	b_{S}	2500	mm			
	h	300	mm			
	l	5000	mm			
	l_s	3600	mm			
	l_c	1100	mm			
	l_{sup}	100	mm			
	d_l	265	mm			
	d_t	250	mm			

	$f'_{\mathrm{cm,cube}}$	$f'_{\mathrm{cm,cube}}$	c_l, c_t	ρ_l	ρ_t	a_v
	[N/mm^2]	[N/mm^2]	[mm]	[%]	[%]	[mm]
S1T1	35.8	29.4	200	0.996	0.132	450
S2T1	34.5	28.3	300	0.996	0.132	400
S3T1	51.6	42.3	300	0.996	0.258	400
S5T4	48.2	39.5	300	0.996	0.258	200
S8T1	77.0	63.1	300	0.996	0.258	400
S9T1	81.7	67.0	200	0.996	0.258	250
BS1T1	81.5	66.8	300	0.948	0.258	400
BS2T1	88.6	72.7	200	0.948	0.258	250
BS3T1	91.0	74.6	200	0.948	0.258	450
BM1T2	81.5	66.8	300	0.948	0.258	400
BM2T1	88.6	72.7	200	0.948	0.258	250
BM3T1	91.0	74.6	200	0.948	0.258	450
BL1T1	81.5	66.8	300	0.948	0.258	400
BL2T1	94.8	77.7	200	0.948	0.258	250
BL3T1	81.4	66.7	200	0.948	0.258	450
BX1T1	81.4	66.7	300	0.948	0.258	400
BX2T1	70.4	57.7	200	0.948	0.258	250
BX3T1	78.8	64.6	200	0.948	0.258	450

3.9.3 Experimental results from literature

In literature only few tests can be found on plates loaded close to one of its two supports. However, there are some experiments performed that are similar to the experiment described above. Two experiments are used in this

chapter. One series of experiments dates from 1982 and is carried out by P. E. Regan [32]. Regan based his failure model for loads loaded close to support on these tests. The element dimensions however, are much smaller than the dimensions used in practice. Another experiment, recently performed by K. Reissen and J. Hegger [35] is similar to the experiments carried out in Delft. The element dimensions, reinforcement ratios and concrete strengths are comparable. The distance between the load and support on the other hand is larger. The experimental results for the other two test series are provided here:

Regan 1982

Regan 1982 [32]					
All	b	1200	mm		
	h	100	mm		
	l	1600	mm		
	l_s	1150	mm		
	l_c	400	mm		
	l_{sup}	100	mm		
	ρ_l	0.602	%		
	ρ_t	0.208	%		
	d_l	84	mm		
	d_t	77	mm		

	$f'_{\text{cm,cube}}$	$f'_{\text{cm,cube}}$	c_l	c_t	a_v
	[N/mm^2]	[N/mm^2]	[mm]	[mm]	[mm]
1SS	29.3	24.0	100	100	120
2SS	27.1	22.2	100	100	80
3SS	35.4	29.0	100	100	40
4SS	41.3	33.9	100	100	20
5SS	35.7	29.3	200	100	80
6SS	32.4	26.6	100	200	80
7SS	43.2	35.4	200	100	40

In Regan's experiment, the slabs were placed on roller and rocker bearings along the full width. A plaster layer was applied to obtain even bearings. On the 7 plates that have been tested for this experiment, two tests were carried out. First the concentrated load was applied at the simple support and in the second scenario the load was placed at the continuous support. This is illustrated in figure 3.11. Only the results for the tests at the simple support are used in this thesis. In the experiments the shear span and the loading plate dimensions were varied.

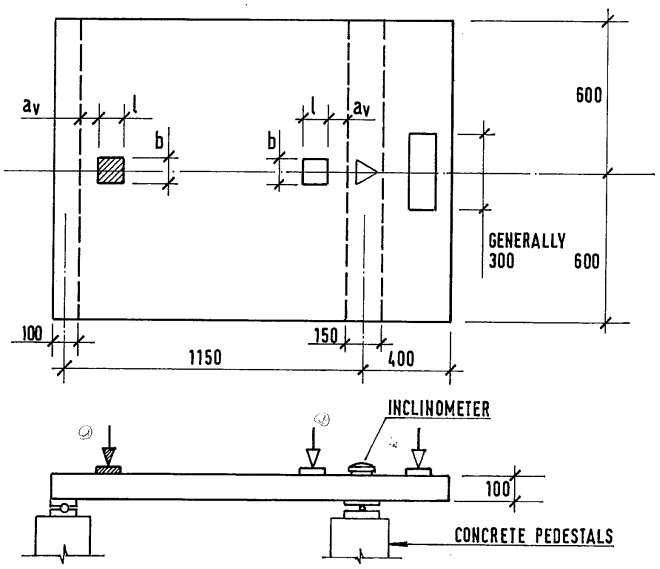

Figure 3.11: The test setup for experiments performed by Regan in 1982 [32].

Reissen and Hegger 2010

Reissen and Hegger 2010 [35]				
All	h	280	mm	
	l	4400	mm	
	c_l	400	mm	
	c_t	400	mm	
	a_v	750	mm	
	l_{sup}	100	mm	
	ρ_l	0.982	%	
	ρ_t	0.466	%	
	d_l	240	mm	
	d_t	226	mm	

	$f'_{\text{cm,cube}}$	$f'_{\text{cm,cyl}}$	b_s	l_s
	[N/mm^2]	[N/mm^2]	[mm]	[mm]
50-2T	40.1	33.7	500	3000
50W-1TV	43.7	39.2	500	4000
50W-2TV	46.1	40.5	500	3000
150-1TV	43.4	37.7	1500	4000
150-2TV	45.0	38.2	1500	3000
250-1TV	23.7	27.9	2500	4000
250-2TV	33.4	29.5	2500	3000
350-1TV	45.3	35.9	3500	4000
350-2TV	47.8	38.2	3500	3000

Each element was used in an experiment twice. In the first test the concentrated load was applied until failure of the plate. Then the support located at the damaged side of the slab was moved inward and the concentrated load was applied at the undamaged side of the slab in the second test. This is illustrated in figure 3.12. In figure 3.13 a more detailed view of the load and support is given. It can be seen that a layer of felt is applied between the load and the elements. Between the supports and the elements a layer of plasterboard is placed. The parameter that has been varied in this series of test is the element width.

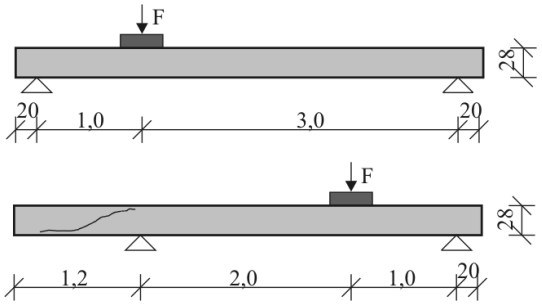

Figure 3.12: Reissen and Hegger experiments loading scheme [35].

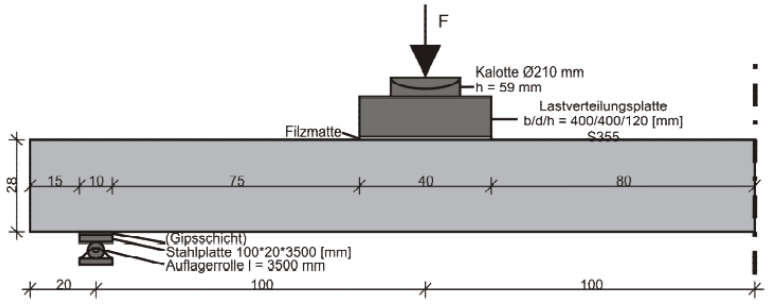

Figure 3.13: Reissen and Hegger experiments load and support detail [35].

3.10 Building codes applied to the tested concrete elements

The various building codes are described and analysed in the previous sections. In this section the building codes and model will be applied to a series of slabs, beams and wide beams that have been tested at Delft University of

Technology. The analysis will also be applied to the test series from Regan (1982) and Reissen and Hegger (2010).

The ACI 318-08, EC1992-1-1, Model Code 2010, NEN6720 and Regan's model, both for one-way shear and punching, are applied to the slabs. The effective width and perimeters are determined as described in section 3.3. A worked out calculation is provided for slab S3T1 only. The data required to perform the calculations are provided in the table below. The other slabs are calculated in the same way, but a detailed calculation is not provided. Instead the result of the calculations is displayed in a table.

Properties of element S3T1			
Symbol	**Value**	**Unit**	**Explanation**
c	25	mm	Concrete cover
ϕ_l	20	mm	Diameter longitudinal reinforcement
n_l	21	mm	Number of longitudinal bars
ϕ_t	10	mm	Diameter transverse reinforcement
n_t	41	mm	Number of transverse bars
l	5000	mm	Total length of the element
l_s	3600	mm	Free span length
l_c	1100	mm	Cantilever length at continuous supp.
b	2500	mm	Width of the concrete
h	300	mm	Height of the concrete
$f_{\mathrm{cm,cube}}$	51.6	$\mathrm{N/mm^2}$	Mean concrete cube compr. strength
$f_{\mathrm{cm,cyl}}$	42.3	$\mathrm{N/mm^2}$	Mean concrete cylinder compr. strength
a	600	mm	Shear span
l_sup	100	mm	Size of the support in span direction
c_l	300	mm	Size of the load in span direction
c_t	300	mm	Size of the load in other direction
α_s	40	-	Internal/edge/corner column
k_g	16	mm	Maximum aggregate diameter
E_s	200000	$\mathrm{N/mm^2}$	Steel modulus of elasticity
n_p	3	-	Number of pre-stress cables at continuous support.
F_p	18	kN	Initial pre-stress force in the cable
l_p	600	mm	Distance between continuous support and pre-stress cable
F_u	1371	kN	Ultimate concentrated load
V_u	1154	kN	Maximum shear force in the concrete
g_c	25	$\mathrm{kN/m^3}$	Weight of the reinforced concrete
F.M.	WB	-	Failure mode: wide beam shear failure

First the effective depths d_l, d_t and d_ave of the element is calculated. The clear shear span a_v, effective width (French method) b_eff and the bending reinforcement ratios in span direction ρ_l and transverse direction ρ_t are de-

termined.

$$
\begin{aligned}
d_l &= h - c - 0.5\phi_l = 265 \text{ mm} \\
d_t &= h - c - \phi_l - 0.5\phi_t = 250 \text{ mm} \\
d_{\text{ave}} &= 0.5\,(d_l + d_t) = 257.5 \text{ mm} \\
a_v &= a - 0.5\,(l_{\text{sup}} + c_{\text{l}}) = 400 \text{ mm} \\
b_{\text{eff}} &= 2\,(a_v + c_l) + c_t = 1700 \text{ mm} \\
\rho_l &= \frac{n_l \cdot 0.25 \cdot \pi \cdot \phi_l^2}{b \cdot d_l} = 0.996 \ \% \\
\rho_t &= \frac{n_t \cdot 0.25 \cdot \pi \cdot \phi_t^2}{l \cdot d_t} = 0.258 \ \%
\end{aligned}
$$

From geometry, pre-stress forces $n_p \cdot F_p$ and ultimate applied load P_u, the support reactions at the simple support V_{SS} and the continuous support V_{CS} are calculated below. Self weight is included. The shear force just left of the load $V_{\text{left}}(a)$, between the load and the support, is also calculated.

$$
\begin{aligned}
V_{SS} &= P_u \left(1 - \frac{a}{l_s}\right) + \frac{bhl_s g_c}{2} - \frac{n_p F_p l_p}{l_s} - \frac{bhg_c \dfrac{l_c^2}{2}}{l_s} \\
V_{SS} &= 1166 \text{ kN} \\
V_{CS} &= P_u \left(1 - \frac{a}{l_s}\right) + \frac{bhl_s g_c}{2} + \frac{n_p F_p l_p}{l_s} + \frac{bhg_c \dfrac{l_c^2}{2}}{l_s} + n_p F_p + bhg_c \\
V_{CS} &= 339 \text{ kN} \\
V_{\text{left}}(a) &= V_{SS} - a \cdot \frac{V_{SS} + V_{CS} - P_u - n_p F_p - bhl_c g_c}{l_s} = 1154 \text{ kN}
\end{aligned}
$$

3.10.1 The Eurocode

Experimental element S3T1 calculated with the EN1992-1-1:2005

Example calculation

One-way shear capacity and maximum concentrated load:

$$C_{R,c} = 0.18$$
$$\gamma_c = 1.00$$
$$k = 1 + \sqrt{\frac{200}{d_l}} = 1.869$$
$$v_{\min} = 0.035 k^{3/2} \sqrt{f_{ck}} = 0.582$$
$$V_{\mathrm{c,EC}} = \frac{C_{R,c}}{\gamma_c} k \left(100 \rho_l f_{ck}\right)^{1/3} b_{\mathrm{eff}} d_l \geq v_{\min} b_{\mathrm{eff}} d_l = 527 \text{ kN}$$
$$\beta = \max \left\{ \begin{array}{l} \min \left\{ \begin{array}{l} \frac{a_v}{2d_l} \\ 1.00 \end{array} \right. \\ 0.25 \end{array} \right. = 0.755$$
$$V_{\mathrm{c,EC,max}} = \frac{V_{\mathrm{c,EC}}}{\beta} = 699 \text{ kN}$$
$$\frac{V_u}{V_{\mathrm{c,EC,max}}} = 1.65$$

$V_{\mathrm{c,EC,max}}$ is the maximum calculated shear force that can be resisted by the concrete. The concentrated load $F_{c,EC}$ at the given shear span that is required to create this shear force is calculated here:

$$F_{c,EC} = \frac{V_c - \left(\frac{bhl_s g_c}{2} - \frac{n_p F_p l_p}{l_s} - \frac{bhl_c^2 g_c}{2l_s} \right)}{\beta \left(1 - \frac{a}{l_{\mathrm{s}}} \right)} = 802 \text{ kN}$$

For punching the calculation is given:

$$u_{o,\mathrm{EC}} = \left\{ \begin{array}{ll} 2(c_1 + c_2) + 2\pi 2.0 d_{\mathrm{ave}} & \text{if } a_v \geq 2.0 d_{\mathrm{ave}} \\ 2(c_1 + c_2) + 2\pi 2.0 d_{\mathrm{ave}} - 2(2.0 d_{\mathrm{ave}} - a_v) & \text{if } a_v < 2.0 d_{\mathrm{ave}} \end{array} \right.$$
$$u_{o,\mathrm{EC}} = 4206 \text{ mm}$$
$$\rho_{\mathrm{ave}} = \sqrt{\rho_l \rho_t} \leq 2\ \% = 0.506\ \%$$
$$k_{\mathrm{pun}} = 1 + \sqrt{\frac{200}{d_{\mathrm{ave}}}} = 1.881$$
$$v_{\mathrm{min,pun}} = 0.035 k_{\mathrm{pun}}^{3/2} \sqrt{f_{ck}} = 0.587$$
$$F_{R,c} = \frac{C_{R,c}}{\gamma_c} k_{\mathrm{pun}} \left(100 \rho_{\mathrm{ave}} f_{ck}\right)^{1/3} u_o d_{\mathrm{ave}} \geq v_{\mathrm{min,pun}} u_o d_{\mathrm{ave}} = 1019 \text{ kN}$$
$$\frac{F_u}{F_{\mathrm{c,EC,pun}}} = 1.35$$

The table below consists of 8 columns. In the third column, the observed failure modes from the experiments are provided. The observed failure mode was determined by analysing crack patterns. In the last column, the limiting failure criterion from the building code is provided. When the maximum calculated concentrated load for one way shear $F_{\mathrm{c,EC}}$ is lower than the calculated punching shear $F_{\mathrm{c,EC,pun}}$, then one-way shear failure is governing (denoted with "B"), otherwise, punching shear is governing (denoted with "P"). In the case of S3T1 $802 < 1019$ so the governing failure mode is one-way shear "B".

Calculated results

Experimental results and EN1992-1-1 predictions							
Test	F_u	FM	F_c	$F_{\mathrm{c,pun}}$	$\frac{F_u}{F_c}$	$\frac{F_u}{F_{\mathrm{c,pun}}}$	FM
	[kN]	[-]	[kN]	[kN]	[-]	[-]	[-]
S1T1	954	WB	549	749	1.73	1.27	B
S2T1	1374	WB+P	696	797	1.97	1.72	B
S3T1	1371	WB	802	1019	1.71	1.35	B
S5T4	1755	WB	1106	901	1.59	1.95	P
S8T1	1481	WB	921	1164	1.61	1.27	B
S9T1	1523	WB+P	893	990	1.71	1.54	B
BS1T1	290	B	274	-	1.06	-	B
BS2T1	633	B	425	-	1.49	-	B
BS3T1	356	WB	254	-	1.40	-	B
BM1T2	720	WB	548	-	1.19	-	B
BM2T1	1212	WB	850	-	1.43	-	B
BM3T1	735	WB	508	-	1.45	-	B
BL1T1	1034	WB	826	1177	1.25	0.88	B
BL2T1	1494	WB	949	1032	1.58	1.45	B
BL3T1	1114	WB	734	1092	1.52	1.02	B
BX1T1	1331	WB + P	931	1176	1.22	1.13	B
BX2T1	1429	WB + P	844	934	1.69	1.53	B
BX3T1	1141	WB + P	719	1081	1.59	1.06	B
1SS	120	P	65	78	1.85	1.54	B
2SS	130	P	77	71	1.68	1.82	P
3SS	195	P	128	73	1.52	2.67	P
4SS	230	P	118	74	1.95	3.10	P
5SS	190	P	105	91	1.81	2.09	P
6SS	160	WB	126	88	1.27	1.82	P
7SS	200	P	175	91	1.14	2.19	P
50-2T	204	B	191	-	1.07	-	B
50W-1TV	183	B	176	-	1.04	-	B
50W-2TV	215	B	204	-	1.06	-	B
150-1TV	543	WB	522	1076	1.04	0.50	B
150-2TV	638	WB	602	1080	1.06	0.59	B
250-1TV	664	WB	782	973	0.85	0.68	B
250-2TV	780	WB	917	991	0.85	0.79	B
350-1TV	985	P	908	1058	1.08	0.93	B
350-2TV	1024	P	1072	1080	0.96	0.95	B/P

The above table contains the experimentally determined maximum concentrated load capacity for each tested concrete element. The maximum shear

stress is calculated using this maximum load. These values are compared to the calculated values from the EN1992-1-1:2005 by means of a tested-to-predicted ratio. A ratio ≥ 1.00 means a safe approximation by the code.

For one-way shear, the predictions are all on the safe side except for the series of tests performed by Reissen and Hegger. A possible explanation for this an overestimated effective width. The shear span used in the series is $a = 1000$ mm. There is no limit provided for the effective width. This results indicate that the effective width should be limited for shear spans greater than at least $a = 600$ mm in plates with similar dimensions.

When punching shear failure is considered, it can be observed that the predictions are all on the unsafe side for the test series from Reissen and Hegger, especially for the elements smaller in width. This suggests that, although the perimeter fits within the element width, the perimeter cannot fully develop. For the S-series and the Regan series the punching shear predictions are all on the safe side. For the B series the results are on the safe side for elements with $b \geq 2000$ mm. It can also be seen that in the B-series, when the shear span is $a = 600$ mm, the predictions are just on the safe side.

The predicted failure modes do not always match the observed failure modes, but generally the predictions are good. In 5 out of 34 cases the prediction is wrong. In two cases, 350-1TV and 350-2TV the EN1992-1-1:2005 provides unsafe predictions.

EN1992-1-1:2005								
	One-way shear				Punching shear			
Series	μ	σ	c_v	ESI	μ	σ	c_v	ESI
S	1.64	0.13	0.08	2.89	1.40	0.33	0.24	2.98
BS	1.29	0.22	0.17	1.12	-	-	-	-
BM	1.37	0.07	0.05	1.51	-	-	-	-
BL	1.42	0.16	0.12	2.53	1.12	0.30	0.27	2.35
BX	1.52	0.12	0.08	4.18	1.24	0.25	0.21	3.87
Regan	1.54	0.29	0.19	2.41	2.18	0.54	0.25	4.66

In the table above, the average tested-to-predicted strength ratios μ , the standard deviation σ, the coefficient of variation c_v and the equation safety index ESI for the given series are provided for the one-way shear predictions and the punching shear predictions. The calculation method is explained in chapter 3.4. The values for the series from Reissen and Hegger are not calculated. This is because of the varying element dimensions, which makes a fair comparison impossible. It has to be kept in mind that each B series,

only consists of three tests. The Regan series (seven tests) and the S series (six tests) are considered more important in this case.

A good approximation of the tests by the building code provisions is characterised by a small value of the standard deviation and the coefficient of variation. When applying this to the table above, the S series, BM series and the BX series are all approximated well by the one-way shear provision from the Eurocode. Using the Eurocodes one way shear provision will provide safe results, based on the S series and the Regan series. The equation safety index values for the S and Regan series are 2.89 and 2.41. In the equation safety index the punching strength determined by tests is used as value for the resistance R and the predicted strength by the code is used as the value for S. The ESI values are lower than expected (ESI $>$ 4.26 is desired (unsafe in only 1 in 10000 cases). The concrete strengths used in the calculations are experimentally determined mean values and not the characteristic concrete compressive strengths this results in lower ESI values. Other partial safety factors are taken into account through the variable FC in the ESI formula.

For punching shear the approximations provided by the Eurocode are not as good as the one-way shear approximations. The standard deviations and coefficients of variation are rather high. Nevertheless the predictions are still on the safe side.

In figure 3.14 experimental results, using elements varying in width with a load plate of 200 mm x 200 mm and a shear span of either 400 mm or 600 mm, are compared to the one-way shear capacity and punching shear capacity as predicted by the EN1992-1-1:2005. The solid lines represent the experimental results, the dotted lines the punching shear predictions and the dashed lines give the one-way shear predictions. The red lines are assigned to the elements having a shear span of $a = 600$ mm and the blue lines are assigned to the elements having a shear span of $a = 400$ mm. It is clear that the predictions for both one-way shear and punching shear are safe. There is no margin in punching shear for the shear span $a = 600$ mm. When the shear span increases further, the punching shear predictions will become more unsafe. The predictions for one-way shear are well on the safe side for the S series. The margin for $a = 400$ mm is larger than for $a = 600$ mm. This suggest that the used factor β for concentrated loads close to the support is underestimated for the slabs.

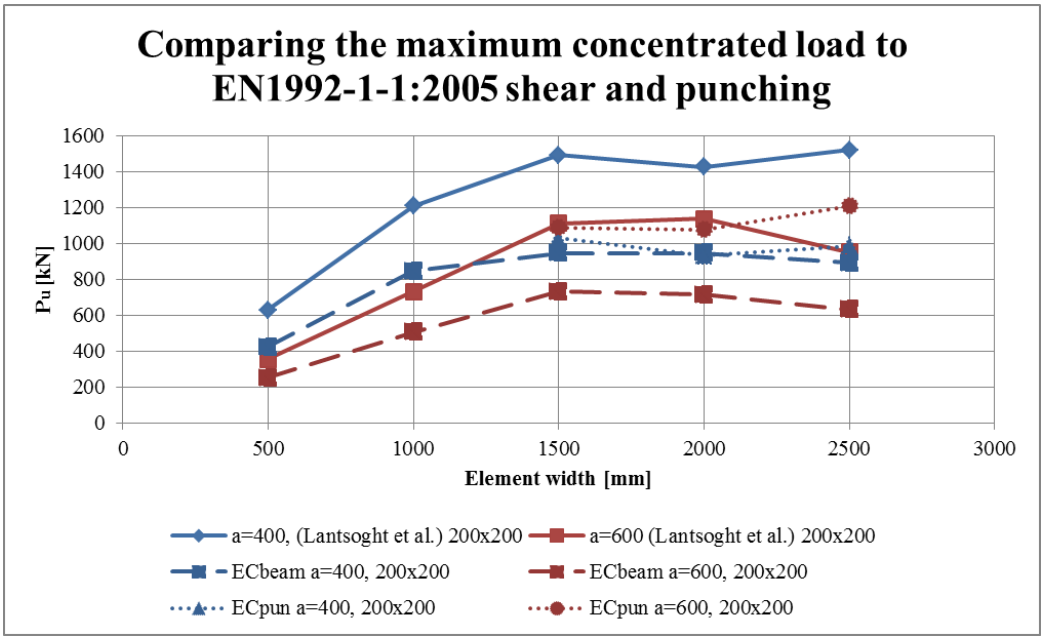

Figure 3.14: Experimental results compared to the values predicted by the Eurocode.

3.10.2 The ACI Code

Example calculation

Experimental element S3T1 calculated with the ACI 318-08*. The * is added because the increased shear capacity factor β is applied. This was done in the first place to refrain from unfair comparisons.
One-way shear and maximum concentrated load:

$$\lambda = 1.00$$

$$\varphi = 1.00$$

$$V_{c,ACI} = \frac{2}{12}\lambda\varphi\sqrt{f_{cm,cyl}}b_{eff}d_l = 488 \text{ kN}$$

$$\beta = \max\left\{\begin{array}{l}\min\left\{\begin{array}{l}\dfrac{a_v}{2d_l}\\ 1.00\end{array}\right. \\ 0.25\end{array}\right. = 0.755$$

$$V_{c,ACI,max} = \frac{V_{c,ACI}}{\beta} = 647 \text{ kN}$$

$$\frac{V_u}{V_{c,ACI,max}} = 1.78$$

$V_{\mathrm{c,ACI,max}}$ is the maximum shear force that can be resisted by the concrete. The concentrated load $F_{c,ACI}$ at the given shear span that is required to create this shear force is calculated here:

$$F_{\mathrm{c,ACI}} = \frac{V_c - \left(\frac{bhl_s g_c}{2} - \frac{n_p F_p l_p}{l_s} - \frac{bhl_c^2 g_c}{2l_s}\right)}{\beta\left(1 - \frac{a}{l_s}\right)} = 740 \text{ kN}$$

Punching shear:

$$\beta_c = \max\left\{\frac{c_l}{c_t}; \frac{c_t}{c_l}\right\} = 1.00$$

$$b_{o,\mathrm{ACI}} = \begin{cases} 2(c_1 + c_2) + 2\pi 0.5 d_{\mathrm{ave}} & \text{if } a_v \geq 0.5 d_{\mathrm{ave}} \\ 2(c_1 + c_2) + 2\pi 0.5 d_{\mathrm{ave}} - 2(0.5 d_{\mathrm{ave}} - a_v) & \text{if } a_v < 0.5 d_{\mathrm{ave}} \end{cases}$$

$$b_{o,\mathrm{ACI}} = 2009 \text{ mm}$$

$$F_{\mathrm{c,ACI,pun}} = \varphi\lambda\frac{1}{12}\sqrt{f_{\mathrm{cm,cyl}}} b_o d_{\mathrm{ave}} \min\left\{\begin{array}{l} \left(2 + \frac{4}{\beta_c}\right) \\ \left(\alpha_s \frac{d_{\mathrm{ave}}}{b_o} + 2\right) \\ 4 \end{array}\right. = 1122 \text{ kN}$$

$$\frac{F_u}{F_{\mathrm{c,ACI,pun}}} = 1.22$$

The governing calculated failure mode is one-way shear failure "B" ($740 < 1122$).

Calculated results

Experimental results and ACI318-08 predictions*							
Test	F_u	FM	F_c	$F_{\mathrm{c,pun}}$	$\frac{F_u}{F_c}$	$\frac{F_u}{F_{\mathrm{c,pun}}}$	FM
	[kN]	[-]	[kN]	[kN]	[-]	[-]	[-]
S1T1	954	WB	475	748	2.01	1.27	S
S2T1	1374	WB+P	598	917	2.30	1.50	S
S3T1	1371	WB	740	1122	1.85	1.22	S
S5T4	1755	WB	1007	1084	1.74	1.62	P
S8T1	1481	WB	912	1370	1.62	1.08	S
S9T1	1523	WB+P	893	1130	1.70	1.35	P
BS1T1	290	B	279	-	1.04	-	S
BS2T1	633	B	438	1177	1.45	0.54	S
BS3T1	356	WB	263	1193	1.35	0.30	S
BM1T2	720	WB	557	1410	1.29	0.51	S
BM2T1	1212	WB	876	1177	1.38	1.03	P
BM3T1	735	WB	526	1193	1.40	0.62	S
BL1T1	1034	WB	840	1410	1.23	0.73	S
BL2T1	1494	WB	990	1218	1.51	1.23	P
BL3T1	1114	WB	746	1128	1.49	0.99	S
BX1T1	1331	WB + P	946	1409	1.41	0.94	S
BX2T1	1429	WB + P	836	1049	1.71	1.36	P
BX3T1	1141	WB + P	727	1110	1.57	1.03	S
1SS	120	P	61	85	1.97	1.41	S
2SS	130	P	71	82	1.83	1.59	P
3SS	195	P	123	94	1.59	2.08	P
4SS	230	P	116	95	1.98	2.42	P
5SS	190	P	101	123	1.89	1.55	P
6SS	160	WB	120	117	1.89	1.37	P
7SS	200	P	174	135	1.34	1.48	P
50-2T	204	B	167	-	1.22	-	S
50W-1TV	183	B	157	-	1.16	-	S
50W-2TV	215	B	184	-	1.17	-	S
150-1TV	543	WB	462	1111	1.17	0.49	S
150-2TV	638	WB	535	1118	1.19	0.57	S
250-1TV	664	WB	656	955	1.01	0.70	S
250-2TV	780	WB	780	982	1.00	0.79	S
350-1TV	985	P	796	1084	1.24	0.91	S
350-2TV	1024	P	953	1118	1.07	0.92	S
* β was included in the ACI building code one-way shear calculations.							

When the ACI 318-08 one-way shear formula is applied and compared to the tested values, the results turn out to be safe. When the shear span is $a = 1000$ mm the tested-to-predicted ratio is around 1.00. Just as with the Eurocode, the effective width that is applied is the cause of this. The effective width is overestimated and should be limited.

For punching shear the results are unsafe for elements with a small width (B series). The perimeter fits within the width of the element, however in practice the perimeter can not fully develop. This also seems to be the case for the Reissen and Hegger series, except for the 350-1TV and 350-2TV elements. Limiting the perimeter length as the element width approaches the control perimeter width, might be a solution.

In 8 out of the 34 cases the wrong failure mechanism is predicted.

ACI 318-08								
	One-way shear				Punching shear			
Series	μ	σ	c_v	ESI	μ	σ	c_v	ESI
S	1.78	0.20	0.11	2.64	1.33	0.17	0.13	2.20
BS	1.26	0.21	0.17	0.86	0.42	0.17	0.40	-
BM	1.33	0.06	0.04	1.20	0.72	0.27	0.38	-
BL	1.38	0.15	0.11	2.00	0.98	0.25	0.25	1.11
BX	1.52	0.13	0.09	3.58	1.11	0.22	0.20	2.04
Regan	1.62	0.31	0.19	2.11	1.70	0.40	0.23	2.73
* β was included in the ACI building code one-way shear calculations.								

For one-way shear, based on the standard deviation σ and the coefficient of variation c_v, the ACI predictions are good. The equation safety indexes for the S and Regan test series are just a little lower than for the Eurocode.

For punching shear the results are unsafe for the B-series smaller in width than 2000 mm. In figure 3.15 can be seen that the results are also unsafe for $a \geq 600$ mm. The one way shear predictions are safe and have sufficient margin. The margin is bigger when the shear span is small. As concluded before, the factor β is underestimated.

3.10.3 The NEN 6720

Example calculation

Experimental element S3T1 calculated with the NEN6720.
One way shear capacity and the maximum concentrated load:

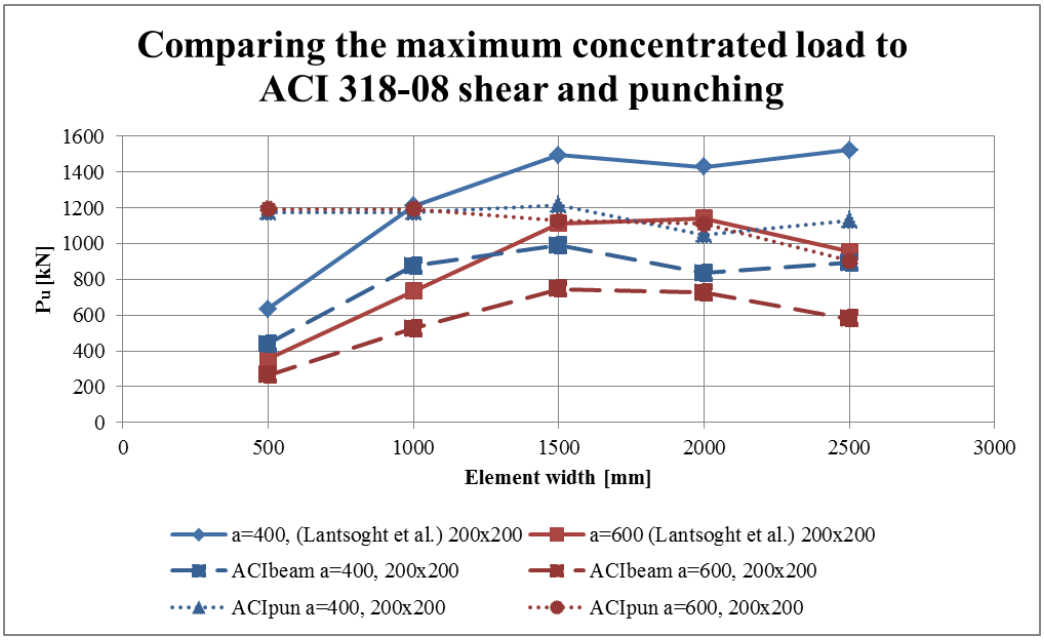

Figure 3.15: Experimental results compared to the values predicted by the ACI 318-08.

First the required concrete tension and compression strength are calculated.

$$\gamma_{\text{m,tension}} = 1.00$$
$$\gamma_{\text{m,compression}} = 1.00$$
$$f_{\text{b,rep}} = 0.7\,(1.05 + 0.05 f_c') = 2.22 \text{ N/mm}^2$$
$$f_b = \frac{f_{\text{b,rep}}}{\gamma_{\text{m,tension}}} = 2.22 \text{ N/mm}^2$$
$$f'_{\text{b,rep}} = 0.72 f_c' = 30.46 \text{ N/mm}^2$$
$$f'_b = \frac{f'_{\text{b,rep}}}{\gamma_{\text{m,compression}}} = 30.46 \text{ N/mm}^2$$

A concentrated load F is assumed and used to calculate the support reaction at the simple support V_{SS}. The maximum bending moment M_{max}, located at the concentrated load, is determined . The shear force at the simple support will also be the maximum shear force between the load and the support. These are required to calculate the effect of the direct compression strut k_λ. This strut can occur when the shear span is small. A factor for the element

height and the loading area are also computed.

$$
\begin{aligned}
F &= 633 \text{ kN} \\
V_{\text{SS}} = F\left(1 - \frac{a}{l_s}\right) + \frac{bhl_s g_c}{2} - \frac{n_p F_p l_p}{l_s} - \frac{0.5 \cdot bhl_c^2 g_c}{l_s} &= 551 \text{ kN} \\
M_{\max} \approx aV_{ss} &= 345 \text{ kNm} \\
\lambda_v = \frac{M_{\max}}{d_l V_{ss}} &= 2.37 \\
g_\lambda = \begin{cases} 1 + \lambda_v^2 & \text{if } \lambda_v \geq 0.6 \\ 2.5 - 3\lambda_v & \text{if } \lambda_v < 0.6 \end{cases} &= 6.60 \\
k_h = \max \begin{cases} 1 \\ 1.6 - h[\text{m}] \end{cases} &= 1.3 \\
k_\lambda = \max \begin{cases} 1 \\ \dfrac{12}{g_\lambda}\left(\dfrac{c_l c_t}{d_l b_{\text{eff}}}\right)^{1/3} \end{cases} &= 1.06 \\
A_o = c_l \cdot c_t &= 0.090 \text{ m}^2
\end{aligned}
$$

The maximum shear stress that can be resisted by the concrete is calculated below. Also some limitations are calculated. A unity check is performed to determine if the earlier assumed concentrated load is correct.

$$
\begin{aligned}
\tau_1 = \max \begin{cases} 0.4 f_b k_\lambda k_h \left(100\rho_l\right)^{1/3} \\ 0.4 f_b \end{cases} &= 1.22\text{N/mm}^2 \\
\tau_2 = 0.2 f_b' &= 6.09\text{N/mm}^2 \\
\tau_u = \min \begin{cases} \tau_1 \\ \tau_2 \end{cases} &= 1.22\text{N/mm}^2 \\
V_c = \tau_u b_{\text{eff}} d_l &= 551 \text{ kN} \\
\text{u.c.} = \frac{V_c}{V_{ss}} &= 1.00 \\
\frac{V_u}{V_{\text{c,NEN}}} &= 2.10
\end{aligned}
$$

The maximum (one-way) shear force is now known. The corresponding concentrated load at the given location is calculated here:

$$
F_{c,NEN} = \frac{V_c - \left(\dfrac{bhl_s g_c}{2} - \dfrac{n_p F_p l_p}{l_s} - \dfrac{bhl_c^2 g_c}{2l_s}\right)}{1 - \dfrac{a}{l_s}} = 633 \text{ kN}
$$

Punching:
First the factor for the load shape k_1, load size to thickness factor k_2 and a factor for the element thickness k_d are required.

$$k_1 = \begin{cases} max \begin{cases} 0.5 \\ 2 - \dfrac{c_l}{2c_t} & \text{if } c_l > 2c_t \\ 1.0 & \text{if } c_l < 2c_t \end{cases} \end{cases} = 1.00$$

$$a_{\text{load}} = \frac{2\left(c_l + c_t\right)}{\pi} = 0.382 \text{ m}$$

$$k_2 = \begin{cases} max \begin{cases} 0.5 \\ \dfrac{4}{2 + \dfrac{a_{\text{load}}}{d_{\text{ave}}}} & \text{if } a_{\text{load}} \geq 2d_{\text{ave}} \\ 1.0 & \text{if } a_{\text{load}} < 2d_{\text{ave}} \end{cases} \end{cases} = 1.00$$

$$k_d = \max \begin{cases} 1.00 \\ 1.5 - 0.6 d_{\text{ave}} \text{ [m]} \end{cases} = 1.35$$

With the above factors and the average flexural reinforcement ratio in longitudinal and transverse directing the maximum shear stresses that the concrete can carry are calculated.

$$\rho_{\text{ave}} = \sqrt{\rho_l \rho_t} \leq 2 \text{ \%} = 0.506 \text{ \%}$$

$$\tau_1 = \max \begin{cases} 0.8 f_b k_1 k_2 \\ 0.8 f_b k_1 k_2 k_d \left(100 \rho_{\text{ave}}\right)^{1/3} \end{cases} = 1.90 \text{N/mm}^2$$

$$\tau_2 = \min \begin{cases} 5.00 \\ 0.15 f_b' \end{cases} = 4.57 \text{N/mm}^2$$

$$\tau_u = \min \begin{cases} \tau_1 \\ \tau_2 \end{cases} = 1.90 \text{N/mm}^2$$

The shear stress capacity multiplied with the length of the control perimeter u_o and the effective depth d_{ave} provide the maximum shear force $F_{\text{c,NEN,pun}}$.

$$u_o = \pi \left(a_{\text{load}} + d_{\text{ave}}\right) = 2009 \text{ mm}$$

$$F_{\text{c,NEN,pun}} = \tau_u u_o = 984 \text{ kN}$$

$$\frac{F_u}{F_{\text{c,NEN,pun}}} = 1.39$$

Calculated results

Experimental results and NEN6720 predictions							
Test	F_u	FM	V_c	$F_{\text{c,pun}}$	$\frac{F_u}{F_c}$	$\frac{F_u}{F_{\text{c,pun}}}$	FM
	[kN]	[-]	[kN]	[kN]	[-]	[-]	[-]
S1T1	954	WB	409	584	2.23	1.63	B
S2T1	1374	WB+P	475	714	2.89	1.92	B
S3T1	1371	WB	633	984	2.16	1.39	B
S5T4	1755	WB	929	886	1.89	1.98	P
S8T1	1481	WB	868	1307	1.71	1.13	B
S9T1	1523	WB+P	922	1085	1.65	1.40	B
BS1T1	290	B	414	-	0.70	-	B
BS2T1	633	B	599	-	1.06	-	B
BS3T1	356	WB	342	-	1.04	-	B
BM1T2	720	WB	650	1353	1.11	0.53	B
BM2T1	1212	WB	946	1145	1.28	1.06	B
BM3T1	735	WB	536	1180	1.37	0.62	B
BL1T1	1034	WB	848	1353	1.22	0.76	B
BL2T1	1494	WB	1053	1207	1.42	1.24	B
BL3T1	1114	WB	732	1083	1.52	1.03	B
BX1T1	1331	WB + P	908	1352	1.47	0.98	B
BX2T1	1429	WB + P	817	963	1.75	1.48	B
BX3T1	1141	WB + P	708	1057	1.61	1.08	B
1SS	120	P	43	67	2.81	1.78	B
2SS	130	P	43	65	3.02	2.01	B
3SS	195	P	65	66	3.01	2.97	B
4SS	230	P	82	67	2.82	3.43	P
5SS	190	P	75	90	2.54	2.12	B
6SS	160	WB	56	85	2.85	1.88	B
7SS	200	P	110	91	1.82	2.19	P
50-2T	204	B	173	-	1.18	-	B
50W-1TV	183	B	166	-	1.10	-	B
50W-2TV	215	B	195	-	1.10	-	B
150-1TV	543	WB	489	1018	1.11	0.53	B
150-2TV	638	WB	566	1026	1.13	0.62	B
250-1TV	664	WB	670	847	0.99	0.78	B
250-2TV	780	WB	800	875	0.97	0.89	B
350-1TV	985	P	836	986	1.18	1.00	B
350-2TV	1024	P	1008	1026	1.02	1.00	B/P

For one-way shear the predictions match the experimental values quite well. Some tested to predicted ratios are only a bit on the unsafe side. When

safety factors would be applied, all predictions would be on the safe side. Once more it can be concluded that the used effective width in the Reissen and Hegger test series is overestimated.

The predictions for punching shear are only safe in the S and Regan series and the 350-1TV and 350-2TV elements. The other elements are too small in width. For the S elements with a small shear span (a = 400 mm) the punching predictions are on the safe side. This is shown in figure 3.16.In this figure experimental results, using elements varying in width with a load plate of 200 mm x 200 mm and a shear span of either 400 mm or 600 mm, are compared to the one-way shear capacity and punching shear capacity as predicted by the NEN6720. When the shear span increases beyond 600 mm, the punching shear strength predictions will become even more unsafe.

The failure mechanism was predicted wrong by the NEN6720 in 8 out of the 34 considered elements.

NEN7620								
	One-way shear				Punching shear			
Series	μ	σ	c_v	ESI	μ	σ	c_v	ESI
S	2.01	0.37	0.18	2.91	1.48	0.34	0.23	2.49
BS	0.93	0.20	0.21	0.40	-	-	-	-
BM	1.24	0.13	0.11	1.16	0.80	0.37	0.47	-
BL	1.37	0.15	0.11	2.01	1.01	0.24	0.23	1.45
BX	1.58	0.14	0.09	4.17	1.18	0.27	0.22	2.43
Regan	2.63	0.40	0.15	3.46	2.34	0.62	0.26	4.26

The standard deviations are rather high for one-way shear and punching shear, especially for the Regan test series and S series. The coefficients of variation and the equation safety indexes on the other hand are quite favourable. Compared to the ACI 318-08 and the EN1992-1-1:2005 the NEN6720 has a high ESI for the S series and the Regan series, for both failure mechanisms.

3.10.4 The Model Code 2010

Example calculation

Experimental element S3T1 calculated with the Model Code 2010 Final Draft.
The one-way shear capacity in the MC2010 uses the shear arm z_l. The effective width that is used differs as well. The used angle is 60 degrees for simple supports instead of 45 degrees as used in the French method. The cross-section that is being checked is positioned at a distance a_c from the

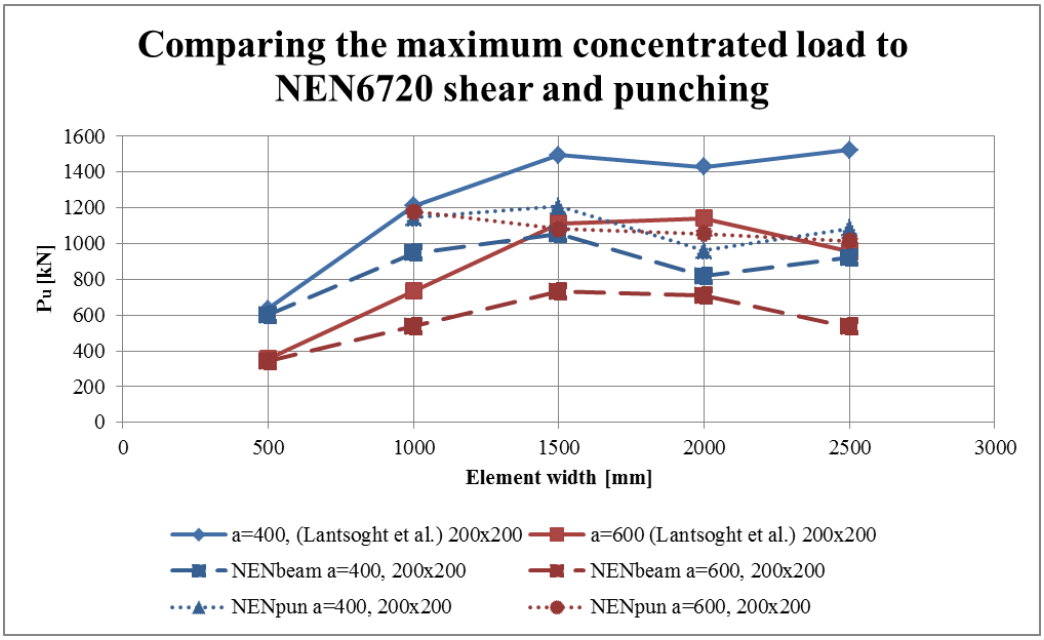

Figure 3.16: Experimental results compared to the values predicted by the NEN6720.

support. The factor k_{dg} is used to take into account the effect of aggregate size.

$$z_l = 0.9 d_l = 239 \text{ mm}$$

$$a_c = 0.5 l_{\text{sup}} + \min \left\{ \begin{array}{l} a_v/2 \\ d_l \end{array} \right. = 250 \text{ mm}$$

$$b_{\text{eff,MC2010FD}} = \min \left\{ \begin{array}{l} c_t + 2\left(c_l + a_v - \min\{a_v/2; d_l\}\right) \tan\left(\dfrac{60\pi}{180}\right) \\ b \end{array} \right. = 2032 \text{ mm}$$

$$k_{dg} = \frac{32}{16 + d_g} = 1.00$$

In this method a concentrated load is assumed. It is used to determine the shear force at the simple support V_{SS}, the shear force at the control section is $V(a_c)$. The bending moment at the control section is denoted as $M_E(a_c)$. These values are required to compute the longitudinal strain ϵ_x at mid depth

of the section.

$$F = 781 \text{ kN}$$

$$V_{\text{SS}} = F\left(1 - \frac{a}{l_s}\right) + \frac{bhl_s g_c}{2} - \frac{n_p F_p l_p}{l_s} - \frac{0.5 \cdot bhl_c^2 g_c}{l_s} = 674 \text{ kN}$$

$$V(a_c) \approx V_{ss}$$

$$M_E(a_c) = -0.5bhg_c\left(a_c^2 + \frac{l_c^2 - l_s^2}{l_s}a_c\right) + a_c\left(F\left(1 - \frac{a}{l_s}\right) - \frac{n_p F_p s_p}{l_s}\right)$$

$$M_E(a_c) = 168 \text{ kNm}$$

$$\epsilon_x = \frac{M_E(a_c)/z + V_E(a_c)}{2E_s\rho_l b_{\text{eff,MC2010FD}} d_l} = 0.00064$$

Now the shear factor k_v and the concrete shear capacity V_c can be determined. The unity check is done to check if the assumed concentrated load was correct. Then a correction factor β is applied.

$$k_v = \frac{0.4}{1 + 1500\epsilon_x}\frac{1300}{1000 + k_{dg}z} = 0.214$$

$$V_c = k_v\frac{\sqrt{f_{ck}}}{\gamma_c}zb_{\text{eff}} = 674 \text{ kN}$$

$$\text{u.c.} = \frac{V_{R,c}}{V(a_c)} = 1.00$$

$$\beta = \max\left\{\begin{array}{l} \min\left\{\begin{array}{l} \frac{a_v}{2d_l} \\ 1.00 \end{array}\right. \\ 0.50 \end{array}\right. = 0.755$$

$$V_{\text{R,c,max}} = \frac{V_{\text{R,c}}}{\beta} = 893 \text{ kN}$$

$$\frac{V_u}{V_{\text{R,c,max}}} = 1.29$$

The maximum shear force is created by the concentrated force. This force is determined here:

$$F_{c,MC} = \frac{V_{R,c} - \left(\frac{bhl_s g_c}{2} - \frac{n_p F_p l_p}{l_s} - \frac{bhl_c^2 g_c}{2l_s}\right)}{\beta\left(1 - \frac{a}{l_{\text{span}}}\right)} = 1035 \text{ kN}$$

Punching

To check the plate in terms of punching, the perimeter length b_o is calculated.

The distance from the load to the location where the bending moment is zero r_s is also required to calculate the rotation ψ of the element.

$$b_o = \begin{cases} 2(c_1 + c_2) + 2\pi 0.5 d_{\text{ave}} & \text{if } a_v \geq 0.5 d_{\text{ave}} \\ 2(c_1 + c_2) + 2\pi 0.5 d_{\text{ave}} - 2(0.5 d_{\text{ave}} - a_v) & \text{if } a_v < 0.5 d_{\text{ave}} \end{cases}$$

$$b_o = 2009 \text{ mm}$$

$$r_s = a = 600 \text{ mm}$$

$$\psi = 1.5 \frac{r_s}{d_{\text{ave}}} \frac{f_y}{E_s} = 0.00947$$

$$k_\psi = \frac{1}{1.5 + 0.9 \psi d_{\text{ave}} k_{dg}} \leq 0.6 = 0.271$$

$$F_{\text{c,MC,pun}} = k_\psi \frac{\sqrt{f_{ck}}}{\gamma_c} d_{\text{ave}} b_o = 911 \text{ kN}$$

$$\frac{F_u}{F_{\text{c,MC,pun}}} = 1.51$$

Calculated results

Experimental results and Model Code 2010 predictions							
Test	F_u	FM	F_c	$F_{\mathrm{c,pun}}$	$\frac{F_u}{F_c}$	$\frac{F_u}{F_{\mathrm{c,pun}}}$	FM
	[kN]	[-]	[kN]	[kN]	[-]	[-]	[-]
S1T1	954	WB	649	607	1.47	1.57	P
S2T1	1374	WB+P	898	745	1.53	1.85	P
S3T1	1371	WB	1035	911	1.32	1.51	P
S5T4	1755	WB	1270	1097	1.38	1.60	P
S8T1	1481	WB	1187	1112	1.25	1.33	P
S9T1	1523	WB+P	1118	983	1.36	1.55	P
BS1T1	290	B	282	-	1.03	-	B
BS2T1	633	B	403	798	1.57	0.79	B
BS3T1	356	WB	237	608	1.50	0.59	B
BM1T2	720	WB	564	967	1.28	0.74	B
BM2T1	1212	WB	805	798	1.50	1.52	P
BM3T1	735	WB	474	608	1.55	1.21	B
BL1T1	1034	WB	850	967	1.22	1.07	B
BL2T1	1494	WB	1090	825	1.37	1.81	P
BL3T1	1114	WB	743	779	1.50	1.43	B
BX1T1	1331	WB + P	1134	972	1.17	1.37	P
BX2T1	1429	WB + P	1100	1062	1.30	1.35	P
BX3T1	1141	WB + P	840	873	1.36	1.31	B
1SS	120	P	82	111	1.47	1.08	B
2SS	130	P	102	114	1.27	1.14	B
3SS	195	P	99	140	1.98	1.40	B
4SS	230	P	97	147	2.36	1.57	B
5SS	190	P	132	171	1.44	1.11	B
6SS	160	WB	184	150	0.87	1.07	P
7SS	200	P	126	201	1.58	0.99	B
50-2T	204	B	193	-	1.05	-	B
50W-1TV	183	B	178	-	1.03	-	B
50W-2TV	215	B	206	-	1.04	-	B
150-1TV	543	WB	528	646	1.03	0.84	B
150-2TV	638	WB	609	650	1.05	0.98	B
250-1TV	664	WB	791	556	0.84	1.20	P
250-2TV	780	WB	928	571	0.84	1.37	P
350-1TV	985	P	1211	630	0.81	1.56	P
350-2TV	1024	P	1420	650	0.72	1.58	P

The MC2010 beam shear calculations approach the tested results well. The effective width used for the Model Code 2010 is larger than the effective

width used in the one-way shear calculations from the other building codes. Since no limit is given on the effective width, the width used in the Reissen and Hegger series where $a = 1000$ mm is too large. This is also the case for test 6SS (Regan).

As noted before, the Model Code 2010 final draft punching shear provisions are only a level I approximation. This should result in very conservative results. This is represented in the table in the tested-to-predicted ratios. Only for elements with a small width, the results are unsafe. The control perimeter fits within the element width, but the perimeter can not be fully developed.

In figure 3.17 experimental results, using elements varying in width with a load plate of 200 mm x 200 mm and a shear span of either 400 mm or 600 mm, are compared to the one-way shear capacity and punching shear capacity as predicted by the Model Code 2010 Final Draft. The punching shear predictions are on the safe side when $a = 600$ mm and when $a = 400$ mm provided that the B element has sufficient width ($b \geq 1500$ mm, $l_s/b \leq 2.40$).

Model Code 2010 final draft								
	One-way shear				Punching shear			
Series	μ	σ	c_v	ESI	μ	σ	c_v	ESI
S	1.34	0.11	0.08	2.31	1.54	0.16	0.10	3.09
BS	1.34	0.29	0.21	1.20	0.69	0.15	0.21	-
BM	1.42	0.14	0.10	1.60	1.16	0.39	0.34	1.39
BL	1.34	0.14	0.10	2.07	1.44	0.37	0.26	3.27
BX	1.25	0.09	0.07	2.82	1.34	0.03	0.02	4.69
Regan	1.53	0.47	0.30	2.85	1.19	0.21	0.17	1.88

The above table confirms that the one-way shear provision from the MC2010FD provides safe results. Except for the Regan series, the standard deviations σ and the coefficients of variation c_v are low. For the Regan series this is not the case, but due to the high average tested-to-predicted ratio the results are still on the safe side.

For punching shear, the MC2010 level I approximation can provide unsafe results. This is indicated by the low equation safety indices (1.39 and 1.88). An ESI of 1.88 means that the chance of the predicted capacity being smaller than the actual capacity is about 0.5.

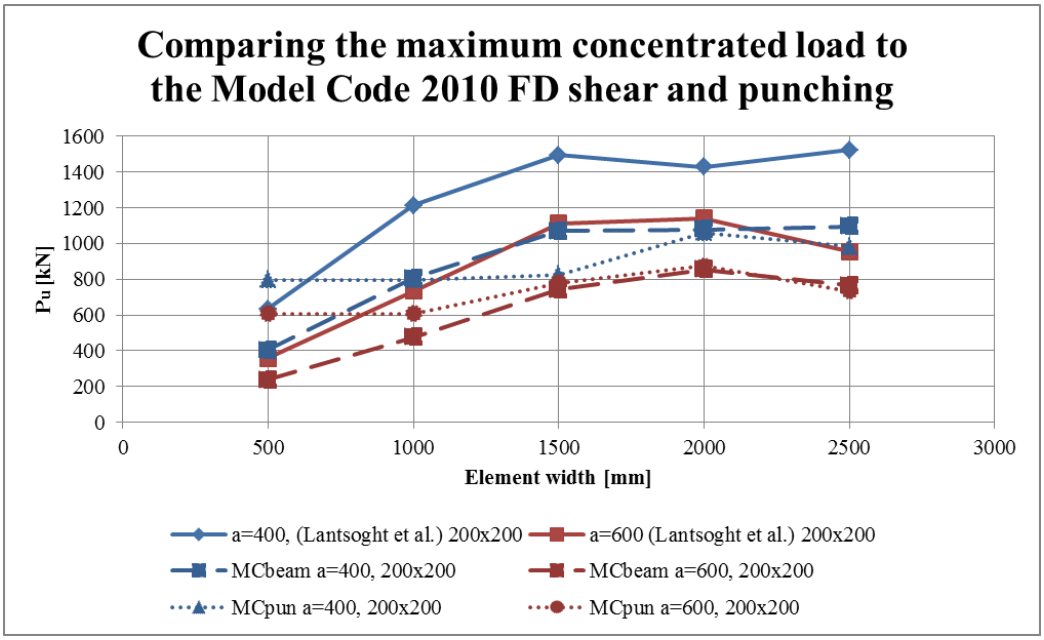

Figure 3.17: Experimental results compared to the values predicted by the MC2010FD.

3.10.5 Regan's model (1982)

Example calculation

Experimental element S3T1 calculated with Regan's method 1982.
As explained before, the perimeter used in Regan's method consists of two parts, the shear resistance is different for each part. The summation of the individual perimeter strengths is the total shear resistance.

$$\rho_{\text{ave}} = \frac{\rho_l + \rho_t}{2} = 0.627\ \%$$

$$u_{1a} = \begin{cases} 0 & \text{if } b < 2 \cdot 1.5 \cdot d_{\text{ave}} + c_t \\ 2 \cdot 1.5 \cdot d_{\text{ave}} + c_t & \text{if } a_v - 1.5d_{\text{ave}} \leq 2 \cdot 0.5d_{\text{ave}} \\ 2\left(2 \cdot 1.5 \cdot d_{\text{ave}} + c_t\right) & \text{if } a_v - 1.5d_{\text{ave}} > 2 \cdot 0.5d_{\text{ave}} \end{cases} = 1073 \text{ mm}$$

$$u_{1b} = \begin{cases} 0 & \text{if } b < 2 \cdot 1.5 \cdot d_{\text{ave}} + c_t \\ 2\left(2 \cdot 1.5 \cdot d_{\text{ave}} + c_l\right) & \text{if } a_v \geq 1.5d_{\text{ave}} \\ 2\left(2 \cdot 1.5 \cdot d_{\text{ave}} + c_l\right) - 2\left(1.5d_{\text{ave}} - a_v\right) & \text{if } a_v < 1.5d_{\text{ave}} \end{cases}$$

$$u_{1b} = 2145 \text{ mm}$$

$$u_2 = \begin{cases} 0 & \text{if } b < 2 \cdot 1.5 \cdot d_{\text{ave}} + c_t \\ c_t + 2 \cdot 0.5 \cdot d_{\text{ave}} & \text{if } a_v - 1.5d_{\text{ave}} \leq 0.5d_{\text{ave}} \\ 0 & \text{if } a_v - 1.5d_{\text{ave}} > 0.5d_{\text{ave}} \end{cases} = 1073 \text{ mm}$$

$$P_{R1} = \sqrt[4]{\frac{500}{d_{\text{ave}}}} \frac{0.27}{\gamma_c} \sqrt[3]{100\rho_{\text{ave}} f_{\text{c,cube}}} (u_{1a} + u_{1b}) d_{\text{ave}} = 841 \text{ kN}$$

$$P_{R2} = \frac{2d_{\text{ave}}}{a_v} \sqrt[4]{\frac{500}{d_{\text{ave}}}} \frac{0.27}{\gamma_c} \sqrt[3]{100\rho_{\text{ave}} f_{\text{c,cube}}} (u_{1a} + u_{1b}) d_{\text{ave}} = 361 \text{ kN}$$

$$P_R = P_{R1} + P_{R2} = 1202 \text{ kN}$$

$$\frac{F_u}{F_{\text{c,Regan}}} = 1.14$$

Calculated results

Experimental results and Regan 1982 predictions				
Test	F_u	FM	F_c	$\frac{F_u}{F_c}$
	[kN]	[-]	[kN]	[-]
S1T1	954	WB	901	1.06
S2T1	1374	WB+P	1015	1.35
S3T1	1371	WB	1202	1.14
S5T4	1755	WB	1433	1.22
S8T1	1481	WB	1374	1.08
S9T1	1523	WB+P	1417	1.08
BS1T1	290	B	-	-
BS2T1	633	B	-	-
BS3T1	356	WB	-	-
BM1T2	720	WB	-	-
BM2T1	1212	WB	1437	0.84
BM3T1	735	WB	1257	0.58
BL1T1	1034	WB	1382	0.75
BL2T1	1494	WB	1470	1.02
BL3T1	1114	WB	1211	0.92
BX1T1	1331	WB + P	1382	0.96
BX2T1	1429	WB + P	1331	1.07
BX3T1	1141	WB + P	1198	0.95
1SS	120	P	115	1.05
2SS	130	P	123	1.06
3SS	195	P	184	1.06
4SS	230	P	246	0.93
5SS	190	P	160	1.19
6SS	160	WB	147	1.09
7SS	200	P	241	0.83
50-2T	204	B	-	-
50W-1TV	183	B	-	-
50W-2TV	215	B	-	-
150-1TV	543	WB	1055	0.51
150-2TV	638	WB	1068	0.60
250-1TV	664	WB	862	0.77
250-2TV	780	WB	967	0.81
350-1TV	985	P	1070	0.92
350-2TV	1024	P	1089	0.94

The calculation method provided by Regan (1982) is applied on the tested slabs. The calculation method was based on a series of tests, part of which

is also used in this chapter (SS series). The tested-to-predicted ratios are all very close to 1.00. For the B series, the predictions are really unsafe for the small element widths. The predicted ratios for the Reissen and Hegger elemements are also on the unsafe side, especially for the elements with a width $n \leq 2500$ mm. This is also visualized in figure 3.18. The predictions (dotted lines) are on the safe side for a shear span of $a = 400$ mm, but not for $a = 600$ mm. For increasing shear spans the results will become even more unsafe.

Regan's method				
Series	μ	σ	c_v	ESI
S	1.08	0.16	0.15	1.98
BS	-	-	-	-
BM	0.71	0.18	0.26	-
BL	0.89	0.14	0.15	1.25
BX	1.00	0.07	0.07	2.98
Regan	1.03	0.12	0.11	1.21

The equation safety index values are low meaning that the predictions are not on the safe side. The standard deviations and the coefficient of variations are all small which means that the predicted maximum concentrated loads are close to the tested maximum concentrated loads, especially for slabs. To obtain predictions that are on the conservative side, a higher safety factor is required.

3.11 Analysis of experimental results

The various building codes are compared to each other and to the experimental results. In this section the experimental results will be analysed. The influence of the element width on the shear force is investigated. In figure 3.19 the maximum shear force in the elements (between the load and the simple support) is plotted for various test series. The individual elements vary greatly in concrete strength. Therefore a normalisation is applied in figure 3.20. The shear capacity is divided by the square root of the measured concrete strength $\sqrt{f_{\mathrm{cm,cyl}}}$ and multiplied by square root of the overall average mean concrete strength $\sqrt{40}$.

A few things can be noted from figure 3.20. As the element width increases, the increase in shear capacity slows down. This is clear for the series "a=400/a=600 (Lantshoght et al) 200x200", "a=1000, 2TV Reissen and Hegger 400x400". For the series "a=600 (Lantsoght et al) 300x300" and "a=1000 (Reissen and Hegger) 400x400" the increase in shear strength as

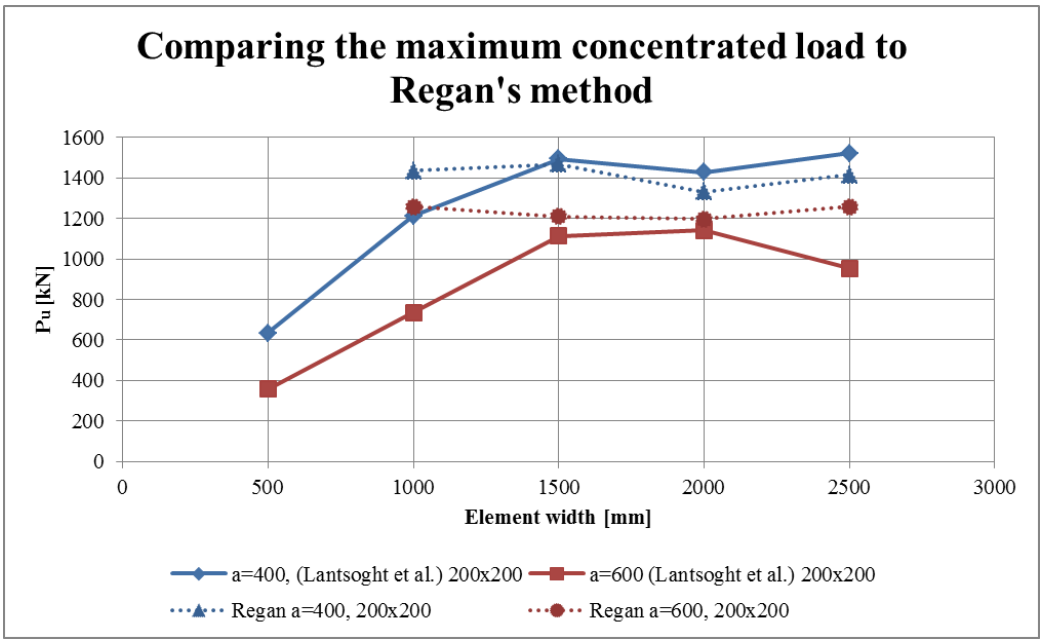

Figure 3.18: Experimental results compared to the values predicted by Regan's method.

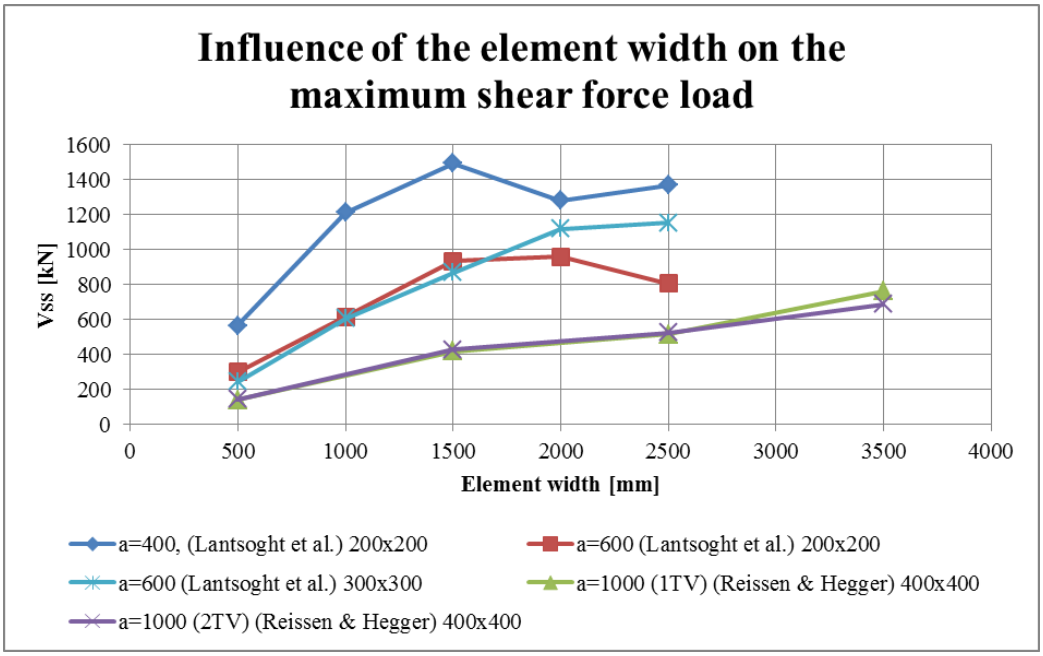

Figure 3.19: Experimental results. Influence of element width on the shear capacity.

the element width increases seems not to change. This suggests that small load plates limit the shear capacity increase as the element width increases. For smaller shear spans $a = 400$ mm this effect is stronger than for larger shear spans $a = 600$ mm, $a = 1000$ mm.

The difference between the two series from Reissen and Hegger is the span length. For the 1TV series the span is 4000 mm and for the 2TV series the span is 3000 mm. It appears that there is no influence of the span length on the shear strength, at least not for $a = 1000$ mm and for plate widths up to 2500 mm.

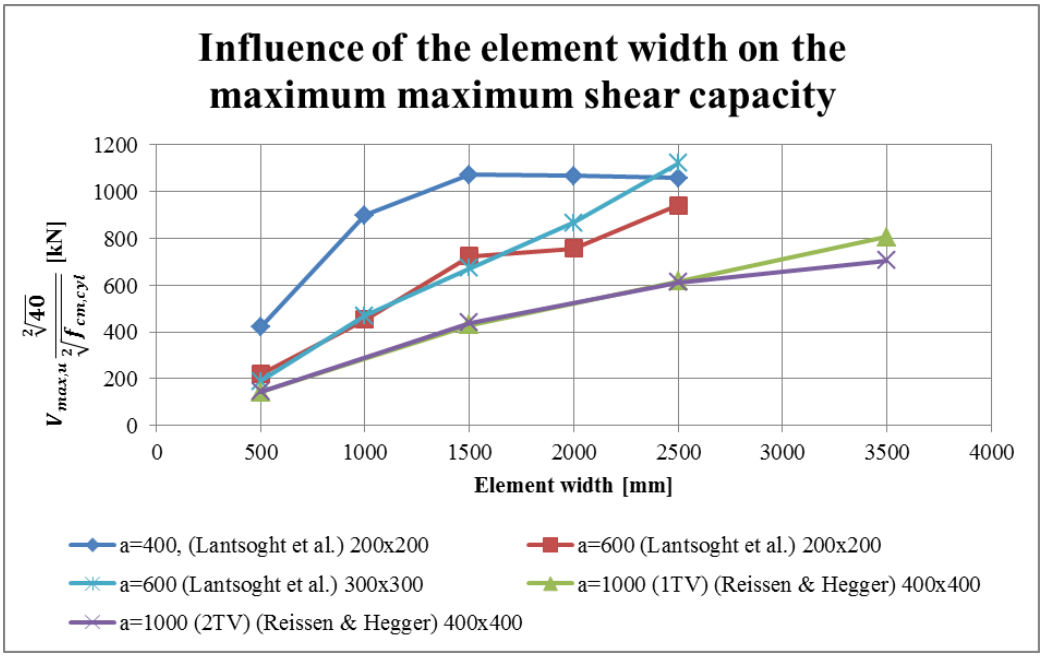

Figure 3.20: Experimental results. Influence of element width on the shear capacity. Normalized for concrete strength.

In figure 3.21 an attempt is made to remove the effect of the shear span. By multiplying the shear strength with the shear span a and dividing it by 1000 mm the shear span is normalized to 1 m. This is possible due to the similarities in plate dimensions, span lengths and reinforcement ratios. Unfortunately the load plate dimensions are not similar. By normalizing the shear span it can be seen that the shear capacity is the same for elements up to a width of $b = 1500$ mm. For the larger elements, the difference in shear strength increases. The increase in shear strength is low (or non-existent) for the element tested with a small load plate (200 x 200).For the elements tested with the larger load plates (300 x 300 and 400 x 400), the shear capacity is

substantially higher.

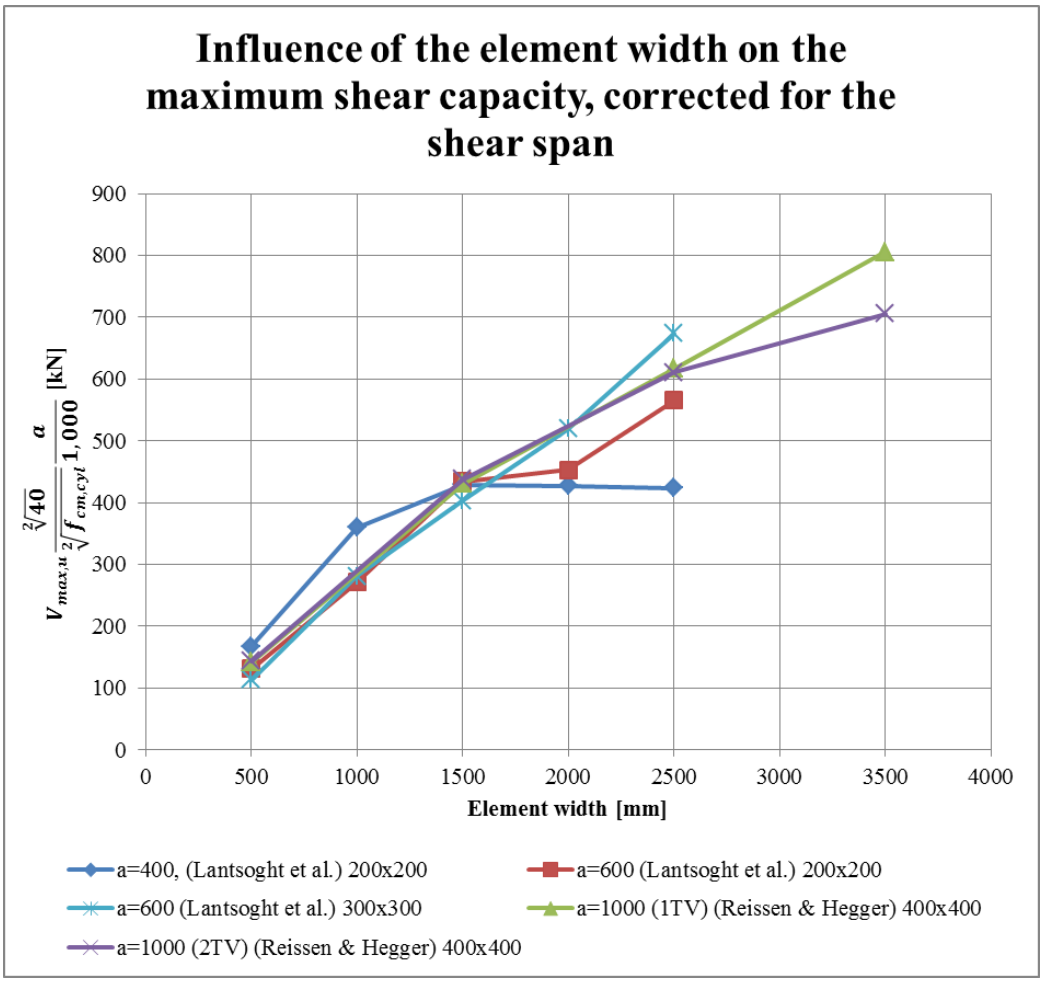

Figure 3.21: Experimental results. Influence of element width on the shear capacity.

3.12 Two boundary situations

In chapter four finite element calculations will be used to model the transition between one-way shear and punching shear. The parameters that will be varied in the first place are the shear span a and the element width b. In order to do this, two boundary situations are required. One in which the element failed only in punching and one in which the element failed in solely one-way shear. Finding an element for the one-way shear situation turned out

to be a problem, however in two tests performed by aforementioned Reissen and Hegger the element failed in punching.

For one way shear failure there are more examples. The example that will be used as a boundary condition will be slab S8T1. The failure crack pattern for S8T1 can be viewed in figures 3.22 and 3.23.

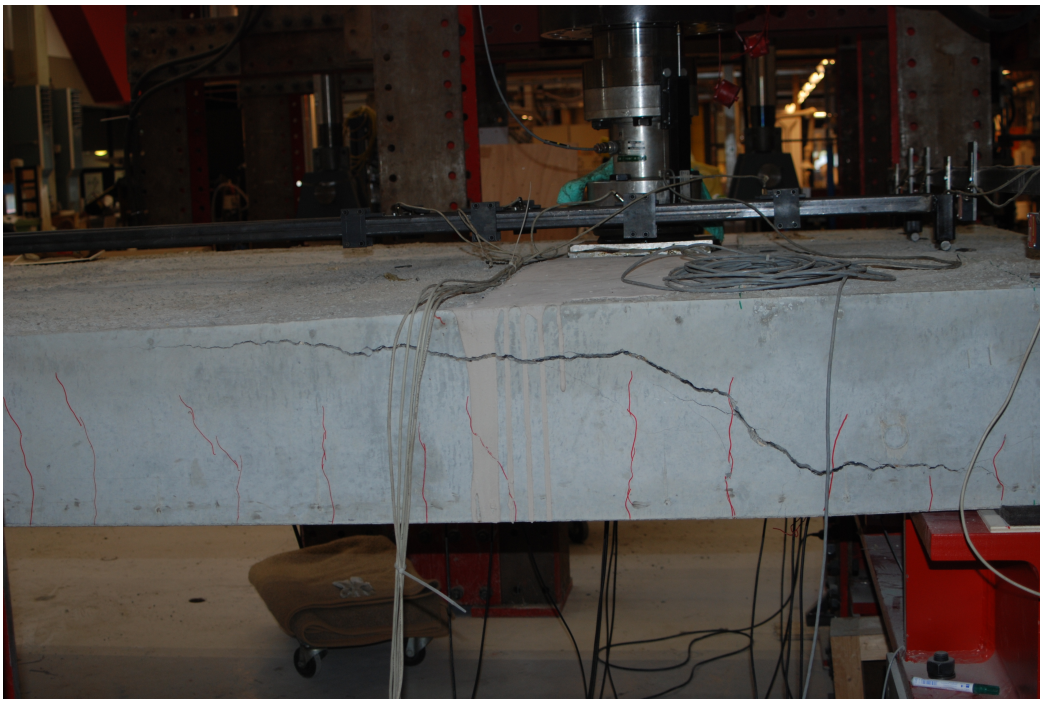

Figure 3.22: Crack pattern at failure S8T1 side view.

There are some clear cases of punching shear failure found in literature. An example of a slab failed in punching comes from the test series from Regan (1982) (figure 3.24). In the more recent experiment from Reissen and Hegger, two clear examples for punching are provided (figures 3.25 and 3.26).

Figure 3.23: Crack pattern at failure S8T1 bottom view.

The two tests from Reissen and Hegger will be used in chapter four as boundary condition. This is because they closely resemble the elements tested by Lantsoght et al., as opposed to the small-scale tests performed by Regan.

A finite element model will be made for the two boundary conditions in order to check if the model represents the test results. When this is the case, the models will be adapted, varying the width and the shear spans. The aim is to obtain a better view of the transition between the one-way shear behaviour and the punching shear behaviour.

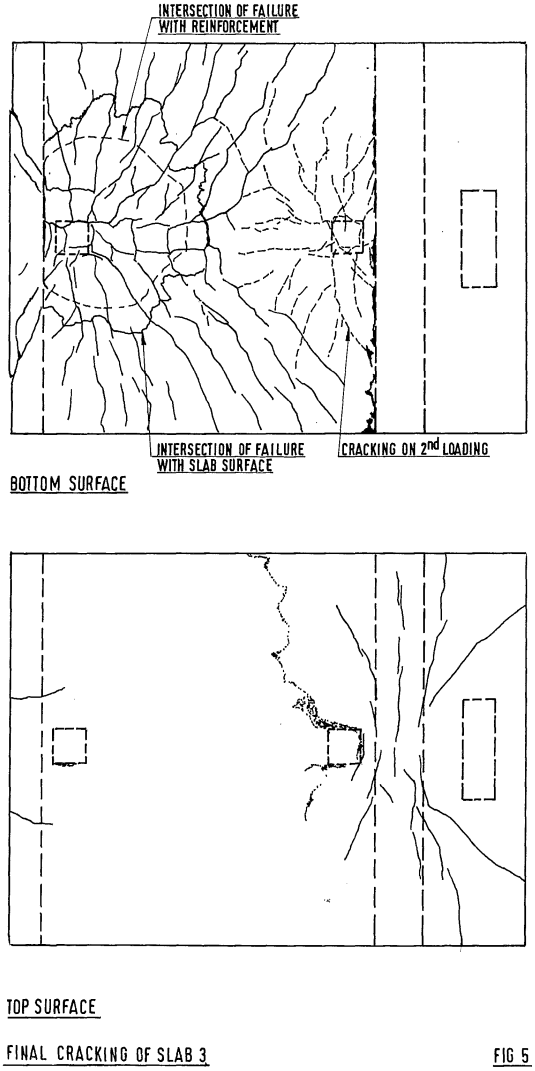

Figure 3.24: Punching shear failure crack pattern in Regan test series (1982) [32].

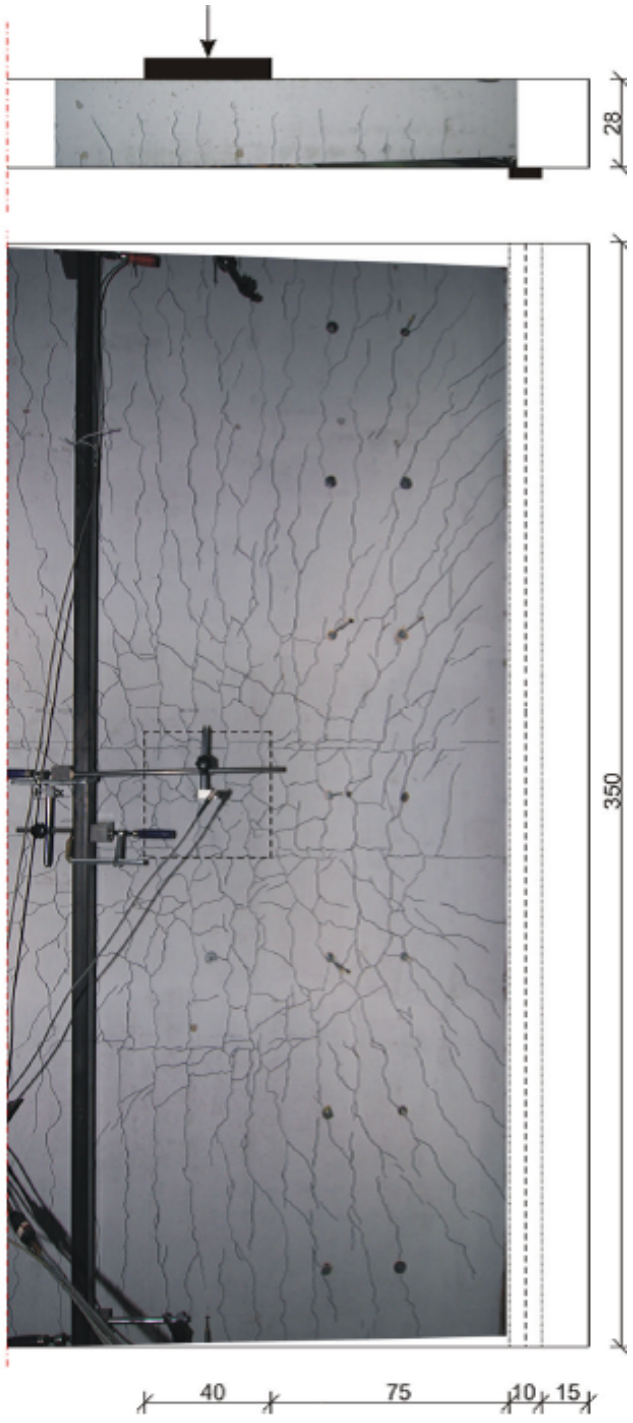

Figure 3.25: Punching shear failure crack pattern in element 350-1TV from Reissen and Hegger (2010) [35].

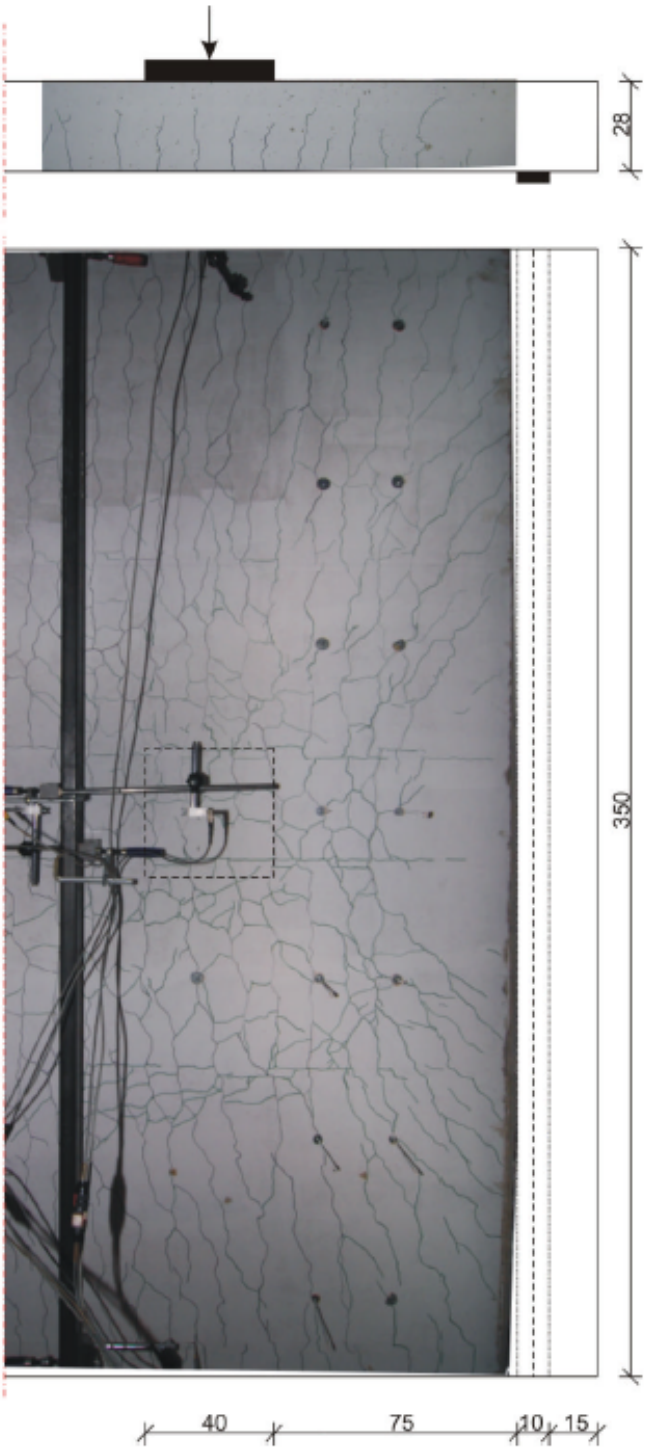

Figure 3.26: Punching shear failure crack pattern in element 350-2TV from Reissen and Hegger (2010) [35].

3.13 Conclusion and recommendations

In this chapter the building codes were compared to each other and to various series of experiments. During the comparisons various conclusions were drawn:

- **One-way shear code provisions:**
  - The code provisions were compared to eachother by using a fictitious plate. Upon comparing the one-way shear behaviour, it turned out that when the same effective width is used, all codes provide similar results for $a_v/d \geq 2.0$. The ACI 318-08 and the NEN6720 provided the more conservative predictions while the Model Code 2010 and the NEN-EN1992-1-1:2005 gave the least conservative predictions.
  - For $a_v/d < 2.0$ the code predictions are substantially different. The Eurocode, NEN6720 and Model Code 2010 final draft incorporate an increase in shear strength for concentrated loads near a simple support. The ACI does not include this effect, but in this thesis the same measure of strength increase as for the Eurocode was applied. It can be concluded that the resulting predictions are safe. The most conservative results for $a_v/d < 2.0$ come from the NEN6720.
  - It is recommended for the ACI 318-08 building code to incorporate the factor β to take into account the effect of an increased shear capacity for concentrated loads close to the support in beams.
- **Punching shear code provisions:**
  - The punching shear formulas from the different building codes were also compared by using the fictitious element. The Model Code 2010 and Regan's method show an increase in shear capacity for concentrated loads close to the support. The ACI 318-08, NEN6720 and the NEN-EN1992-1-1:2005 do not.
  - The NEN6720 and NEN-EN1992-1-1:2005 punching shear provisions are the most conservative for the fictitious plate. Regan's method is overall the least conservative, especially at low a_v/d ratios.
  - The Model Code 2010 level I approximation punching shear provision is the most conservative for $a_v/d > 2$.

- **The Eurocode:**
  - The punching shear provision for the Eurocode provides unsafe predictions in the S series when $a \geq 600$ mm ($a/d_{\text{ave}} \geq 2.30$).
  - The one way shear provision for the Eurocode provides safe results. The margin between tested and predicted slab shear capacities increases as the shear span decreases. This suggest an underestimation of the used factor for concentrated loads close to the support β.
  - In terms of predicting the right failure mechanism, the Eurocode had the least incorrect predictions.
- **The ACI code:**
  - The ACI318-08 punching shear provisions provide unsafe predictions for the B-series when the element width is below 2000 mm ($l_s/b \leq 1.80$) and when $a \geq 600$ mm ($a/d_{\text{ave}} \geq 2.30$).
  - The ACI 318-08 one-way shear calculations give safe results for small shear spans. For the used element dimensions, in the tests from Lantsoght et al. and Reissen and Hegger, the predictions can become unsafe for shear spans $a \geq 1000$ mm ($a/d_l \geq 4.18$).
- **The NEN:**
  - The NEN6720 punching capacity prediction is on the safe side for the tests with the smaller shear span ($a = 400$ mm / $a/d_{\text{ave}} = 1.51$), for the series of tests using $a = 600$ mm / $a/d_{\text{ave}} = 2.26$ the results are less safe, when the shear span increases the predictions will become even more unsafe.
  - The NEN6720 one way shear predictions are safe for the tested elements. However when the shear span increases further, the used effective width must be limited to maintain the safe predictions.
- **The Model Code 2010 final draft:**
  - The Model Code 2010 one way shear formulas predict conservative - and thus safe - capacities. There is no limit provided for the effective width. For large shear spans ($a \geq 1000$ mm / $a/d_l \geq 4.18$, in combination with the used plate dimensions) this might result in unsafe situations.

  - The punching shear capacity level I approximation from the Model Code 2010 provides conservative predictions. However for elements with a small width, the control perimeter length should be reduced, even if the perimeter fits within the element width. In this way safe predictions are given.

- **Regan's method:**

  - The method proposed by Regan returns safe results provided that the elements are wide enough. When the control perimeter width and element width are about the same size, a reduction should be applied to the perimeter length. For an increasing shear span the predictions become less safe or even unsafe. For the tested series the shear span $a = 400$ mm ($a/d = 1.51$)) was safely predicted but for $a = 600$ mm ($a/d = 2.26$)) the predictions were just on the unsafe side.

- **General:**

  - The Model Code 2010 and French effective width used in the one way shear provisions should be limited. Unsafe results are provided for large shear spans $a/d_l \approx 4.1$. It is recommended to limit the French effective width to the width obtained for $a/d_l = 3.5$ and for the Model code 2010 the limit value should be obtained for $a/d_l = 3.0$.
  - In all punching shear provisions (except for the Model Code 2010) the capacity predictions are unsafe for large shear spans ($a/d \geq 4.1$). This can be explained by the fact that the plates only span in one direction, while the punching shear provisions are based on slabs spanning in two directions. When punching shear provisions are applied to one-way spanning slabs with a large shear spans ($a/d \geq 4.1$) the predicted capacity can be unsafe.
  - In the experiments performed at Delft University of Technology by Lantsoght et al., the observed failure modes were either one-way shear or a combination of one-way shear and punching. The shear span and plate properties used in the experiments did not provide the conditions for punching shear to be the only failure mechanism. The tests performed by Reissen and Hegger however, had larger shear spans and element widths and punching shear failure was observed.

Chapter 4

Finite element models

In this chapter two experiments are modelled in a finite element analysis. The first experiment that will be described in chapter 4.1 is performed at Delft University of Technology. The considered slab failed in one-way shear. The second experiment that is described in chapter 4.2 is performed at the RWTH Aachen University. The considered slab failed due to punching shear. The last part of this chapter 4.3 provides the conclusions drawn from the comparisons.

4.1 One-way shear failure: S8T1

This section describes the experiment and the FEM model of S8T1, which is boundary situation 1: An element failed in one-way shear.

The slab is 5000 mm long, 2500 mm in width and 300 mm in height. At one end the slab is supported by a simple support. At the other end a continuous support is simulated by using pre-stress cables on a cantilever part of the slab that connect the slab to the laboratory floor. Between the load and the support a felt and plywood layer of 100 mm width is applied. The load plate of 300 x 300 mm is applied at a distance of 600 mm away from the simple support. The center to center distance of the supports is 3600 mm. The cantilever part has a length of 1100 mm. The pre-stress cables are connected at 600 mm from the continuous support.

In the paragraphs below first the experiments and their characteristics are described. Then the FEM model is described, followed by a comparison of the experiment and the modelled results.

4.1.1 Experimental test

The important properties of the experiment are described in the paragraphs below.

Concrete mixture and strength

The concrete used in slab S8 was cast on Tuesday the 23rd of February 2010. Portland cement, fly ash, blast furnace B cement and gravel aggregates (4-16 mm) were used.

Mix composition			
Materials	**Wet**	**Dry**	**Fine**
CEM I 52.5 R	280 kg	280 kg	88.9 l
CEM III/B 42.5 N LH/HS NA	145 kg	145 kg	49.2 l
Concrete sand 0-4 Grensmaas	296 kg	285 kg	17.6 l
Concrete sand 0-4	550 kg	529 kg	20.0 l
Gravel 4-16	915 kg	898 kg	1.1 l
Fly ash	60 kg	60 kg	27.3 l
PL BV-IM	1698 kg	1698 kg	0.0 l
SPL VC 1550	3153 kg	3153 kg	0.0 l
Cold water	160 kg	157 kg	0.0 l
Air	15 l	15 l	0.0 l

The air content of the mix was measured at 1.5%. The slump of the mix was 170 mm. The slab was cast in five layers. Poker vibrators were used to compact the concrete. After one week the slab was removed from the form work and stored in the laboratory (65% RH and $15 - 20^o$ C). For testing purposes, 102 cubes were cast and stored in a fog room (99% RH and 20^o C). Test 1 on slab S8 was carried out 47 days after casting. Three cubes of the same age were tested on compression strength and three were tested on splitting tensile strength. The results can be found in the table below:

Concrete cube strengths					
Cube nr.	**age [days]**	f_{cc} **[MPa]**	**Cube**	**age [days]**	$f_{\mathbf{c,spl}}$ **[MPa]**
25	47	77.99	28	47	6.03
26	47	76.12	29	47	5.98
27	47	76.94	30	47	6.00

The mean values of the concrete compressive strength and the concrete tensile strength are calculated:

$$f_{\text{cm,cube}} = \frac{77.99 + 76.12 + 76.94}{3} = 77.0 \text{ MPa}$$
$$f_{\text{cm,cyl}} = 0.82 \cdot f_{\text{cm,cube}} = 63.14 \text{ MPa}$$
$$f_{\text{c,ctm,sp}} = \frac{6.03 + 5.98 + 6.00}{3} = 6.0 \text{ MPa}$$
$$f_{\text{ctm}} = \alpha_{\text{sp}} \cdot f_{\text{ctm,sp}} = 6.0 \text{ MPa}$$

The mean concrete tensile strength is calculated according to the Model Code 2010 final draft.

Concrete modulus of elasticity

The Young's Modulus can be calculated according to several models. For example, a formula suggested for high strength concrete by Gutierrez and Canovas, 1995 [14], the method from the Model Code 2010 and according to the NEN-EN1992-1-1:2005.

$$E_{\text{GandC}} = 8330 \cdot \sqrt[3]{f_{\text{cm}}} = 35438 \text{ MPa}$$
$$E_{\text{MC2010}} = 21.5 \cdot 10^3 \cdot \alpha_E \cdot \left(\frac{f_{cm}}{10}\right)^{1/3} = 42456 \text{ MPa}$$
$$E_{\text{EC2}} = 22 \left(\frac{f_{cm}}{10}\right)^{0.3} = 40590 \text{ MPa}$$

In the equations above it can be seen that the difference between the calculation methods is substantial. There is no general consensus on how to calculate the Modulus of elasticity in concrete. In this case the modulus of elasticity calculated according to the Model Code 2010 will be used. The above calculated values are static moduli. This means that the modulus is determined using the secant line in a stated point of the stress - strain curve. The modulus of elasticity for concrete is influenced by the moduli of the cement paste, the aggregates and by the relative proportions of components.

Concrete fracture energy

According to the Model Code 2010, the tensile fracture energy of concrete G_f is the energy required to propagate a tensile crack of unit area. When there is no experimental data available on the fracture energy its value can be estimated with the formula:

$$G_f = 73 \cdot f_{cm}^{0.18} = 0.160 \text{ N/m} \tag{4.1}$$

The fracture energy depends on the water-cement ratio, the maximum aggregate size, the age of the concrete, the curing conditions, structural member size and the member depth above a crack or a notch. For high strength concrete the aggregate type and content affect the fracture energy more, while the aggregate size has less influence when compared to normal strength concrete. The fracture energy can be experimentally determined directly with a uni-axial tension test or indirect with a three-point bending test on a notched beam.

The compressive fracture energy is calculated here:

$$G_c = 250 \cdot G_f = 40 \text{ N/m}$$

Reinforcement properties

The concrete plate is reinforced with ribbed reinforcement. Two diameter sizes are used. The bottom reinforcement consists of $41\phi10 - 125$ in transverse direction and $21\phi20 - 125$ in span direction. The top reinforcement in the transverse direction is also $41\phi10 - 125$. The top reinforcement in longitudinal direction above the continuous support is $21\phi20 - 125$ with a length of 3000 mm and from midspan to the simple support $11\phi10 - 250$ 2200 mm in length. No shear reinforcement is applied. The used reinforcement is tested [31]. The performed tensile strength tests are code based. The stress-strain diagram for the used ribbed bars $\phi10$ mm and $\phi20$ mm can be seen in figure 4.1(a) and 4.1(b). The concrete cover is at least 25 mm. The longitudinal bottom bending reinforcement ratio is $\rho_l = 0.996\%$ and the transverse bottom bending reinforcement ratio is $\rho_t = 0.258\%$.

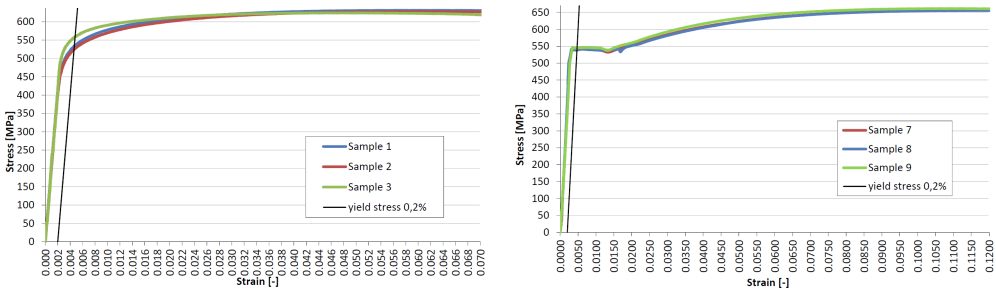

(a) 10 mm bars (b) 20 mm bars

Figure 4.1: Stress-strain diagram for the ribbed reinforcement bars.

For the ribbed reinforcement bars with a diameter of 10 mm the yield strength is $f_y = 537$ MPa and the ultimate strength is $f_u = 628$ MPa. The ribbed reinforcement bars of 20 mm have a yield strength of $f_y = 554$ MPa

and an ultimate strength of $f_u = 640$ MPa. The modulus of elasticity for the reinforcement is $E = 210000$ MPa.

Steel support beams

The plate is supported by two HEM 300 steel profiles. The two profiles are supported by two columns which are connected to the laboratory floor. In the FEM model the HEM 300 profiles are modelled. The steel stiffness of the HEM300 profile is $E = 210000$ MPa. The Poisson's ratio is $\nu = 0.3$. The moment of inertia in the strong direction of the profile is $I_y = 59201 \cdot 10^4$ mm^4. The HEM profile in the FEM model is represented by a rectangular beam of 100 mm x 340 mm. To represent the HEM profile correctly an equivalent stiffness is calculated and used:

$$E_{\text{equivalent}} = \frac{EI_y}{I_{\text{box}}} = \frac{210000 \cdot 59201 \cdot 10^4}{\frac{1}{12} \cdot 100 \cdot 340^3} \approx 380000 \text{ N/mm}^2$$

Interface layer

Between the steel support beams and the concrete plate there is an interface layer consisting of 15 mm felt and 8 mm plywood. The felt and plywood interface layer has been tested in a compression test [31]. The dynamic loading behaviour was tested for the type of felt used in the experiment S8T1. A long term (24 hours) test with a constant load was not performed for the used interface layer. The behaviour of the plywood and felt under constant loading will be stiffer than the behaviour shown by the dynamic loading test. The tested specimens (100 mm x 100 mm) were loaded up to 80 kN. The displacement during loading was measured with four linear variable differential transformers (LVDT's). The specimen was loaded three times. A stress strain diagram of the performed test can be seen in figure 4.2.

The linear normal stiffness is calculated using the average stiffness of the three tests: $K_n = \frac{E}{t} = \frac{\delta\sigma}{\delta\varepsilon} \cdot \frac{1}{t} = 1.1$ N/mm^3 and the (average) linear tangential stiffness $K_t = \frac{K_n}{10} = 0.11$ N/mm^3. In this case the layer thickness $t = 15+8 = 23$ mm is used. This test does not include the effect of long term loading. A better agreement between the experiment and the results from the model is obtained when a value of $K_n = 1.7$ N/mm^3 and $K_t = 0.17$ N/mm^3 is used. This is shown in figure 4.19. The load displacement curves from the experiment and the model have the same angle when the interface stiffness $K_n = 1.7$ N/mm^3. When the interface stiffness is $K_n = 1.1$ N/mm^3 the

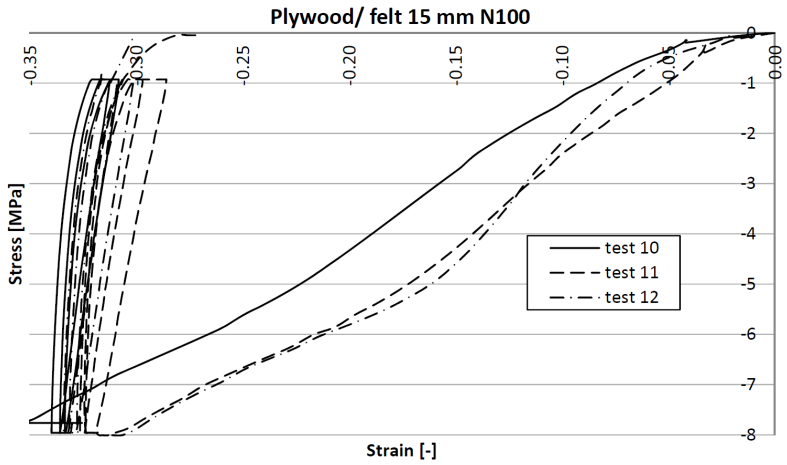

Figure 4.2: Stress-strain diagram for dynamic loading test on 8mm plywood + 15 mm N100 felt.

behaviour under loading is different. The interface layer allows for more deformation under the same load. The plate will rotate easier above the support, decreasing the slope of the load displacement curve.

Load plate

In test S8T1 a concentrated load is applied on the concrete slab by means of an hydraulic jack. Between the jack and the concrete plate a steel plate of 300 mm x 300 mm is used. The load was applied at a shear span of $a = 600$ mm from the simple support in the middle of the width. The load is deformation controlled. The steel stiffness of the loading plate is $E = 200000$ MPa. The Poisson's ratio is $\nu = 0.3$.

4.1.2 FEM model properties

In this paragraph the computer model to simulate the experiment is described. All the information that is used to build the model in the FEM program TNO Diana is provided. First the geometry of the model is described, followed by the reinforcement, applied loads and boundary conditions, the material properties, element types, mesh, analysis method and analysis parameters.

Geometry, reinforcement

The geometry of the reinforcement, the load plate and the interface layer are modelled like their real counterparts used in the experiments. The steel HEM beams that act as the support are simplified. The geometry of the model can be seen in figure 4.4. The concrete slab is 5000 mm x 2500 mm x 300 mm. The simple support (100 mm in width) has its center at 300 mm from the short edge of the plate. The center to center distance of the supports is 3600 mm. The interface layer between the concrete plate and the steel profile is (8 mm plywood + 15 mm felt) 23 mm in thickness and has a width of 100 mm. The steel profile is modelled as a rectangular beam with a height of 340 mm and a width of 100 mm. The modulus of elasticity is chosen as such that the bending stiffness is the same as an HEM 300 steel profile. The steel load plate is 300 mm x 300 mm. The distance from the center of the load plate to the center of the simple support is 600 mm. No interface layer is applied between the load plate and the concrete slab. The reinforcement bars are individually modelled. The reinforcement configuration is shown in figure 4.3.

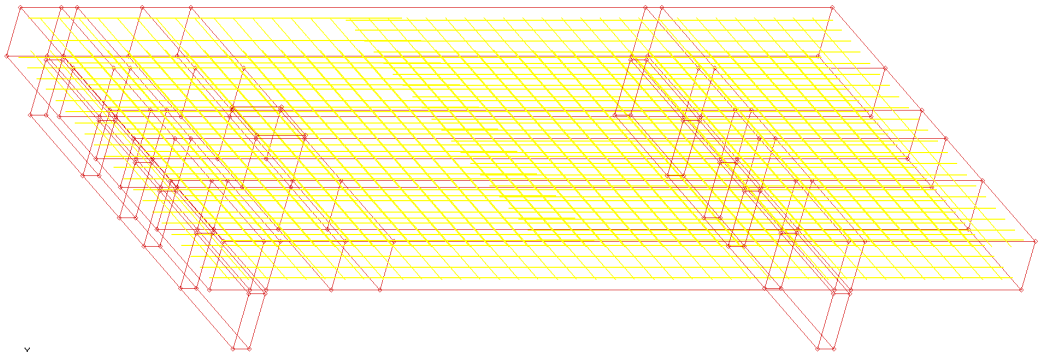

Figure 4.3: S8T1 FEM model reinforcement.

Loading and boundary conditions

The concentrated load is applied as a prescribed displacement. The load is placed on the top face of the load plate. The boundary conditions can be seen in figure 4.4. The steel beams are supported over the whole length. Analysis performed with the steel beams only supported at the ends showed no significant difference in the behaviour of the slab. The support is modelled with a restriction in vertical (global y direction) movement. The movement in z direction is also restricted.

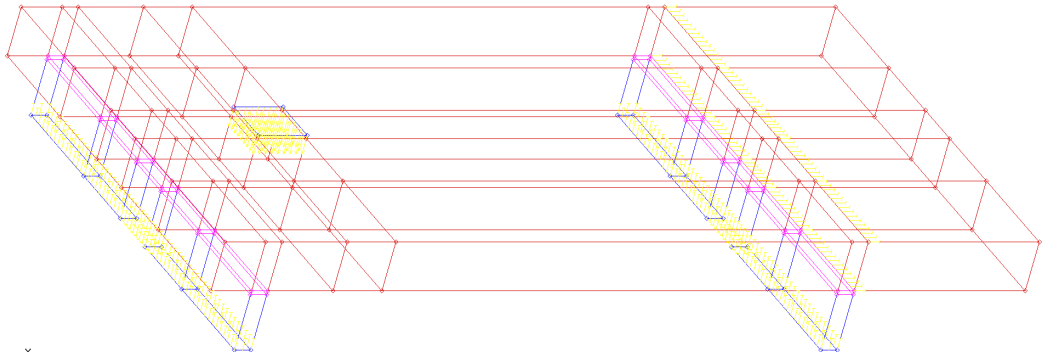

Figure 4.4: S8T1 FEM model loading and boundary conditions.

Above the support on the right hand side, the concrete plate is limited in its rotation. The limited rotation is modelled through two lines of springs running along the width on the top and bottom edge of the plate and this is done to model the continuous support. Several boundary situations are investigated: a simple support, a clamped support and a partially clamped support (figure 4.15).

The spring stiffness per unit length is calculated here. To calculate the spring stiffness it is required to calculate the rotation of the plate above the continuous support at the maximum load. The ultimate concentrated load (P_u = 1481 kN) and the deflection at the load (δ_P = 8.868 mm) are known from the experiment . The distance between the concentrated load and the continuous support is $l_{\text{span}} - a$ = 3000 mm. The rotation can now be estimated as 8.87/3000 = 0.00296 rad. The rotation causes a horizontal displacement in the top and bottom of the concrete plate. The displacement can be calculated as $0.00296 \cdot 300/2 = 0.4434$ mm.

The reaction forces in the supports and the bending moments above the continuous support and at the concentrated load just before failure of the plate can be calculated from static equilibrium (self weight of the concrete not included). The prestress force measured at the ultimate concentrated load (1481 kN) is 224 kN. The reaction force at the simple support is 1198 kN and at the continuous support it is 508 kN. The maximum bending moment at the concentrated load is 718.8 kNm and above the continuous support it is 134.4 kNm. Per meter width of the plate this is 134.4/2.5 = 53.8 kNm/m. The bending moment can be represented by a pair of forces with an arm of 0.3 m (which is the thickness of the plate). 53.8/0.3 = 179 kN.

The spring stiffness per unit length can now be calculated: $k = 179 \cdot 10^3/0.4434 = 403.7 \cdot 10^3$ N/mm.

Material properties

The material properties are already determined in the previous sections. A summary is given here:

Material properties		
Parameter	**Value**	**Unit**
Concrete		
$f_{\mathrm{cm,cyl}}$	63.14	MPa
f_{ctm}	6.00	MPa
E	42456	MPa
ν	0.2	
G_f	0.160	N/m
G_c	40	N/m
Reinforcement		
E	210000	MPa
f_y	546	MPa
Load plate		
E	200000	MPa
ν	0.3	
Supports		
$E_{\mathrm{equivalent}}$	380000	MPa
ν	0.3	
k	$403.7 \cdot 10^3$	N/mm
Interface layer		
K_n	1.7	N/mm^3
K_t	0.17	N/mm^3

Element types and mesh

To carry out the FEM analysis, discretization by means of finite elements is required. The element types used are CHX60 (figure 4.5), CQ48I (figure 4.6) and the bar reinforcement element type (figure 4.7). The first is used for the steel beams, the loading plate and the concrete slab. The second is used for the interface layer between the steel profiles and the concrete slab. The third element is used for all the reinforcement bars.

The CHX60 is a solid isoparametric element with twenty nodes. The element is based on quadratic interpolation and Gauss integration. A 3 x 3 x 3 or a 2 x 2 x 2 integration scheme can be used with this type of element.

The CQ48I interface element can be used as interface between two planes in three-dimensional models. The element is based on quadratic interpola-

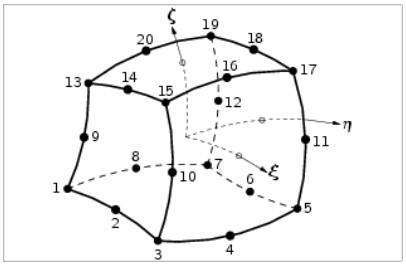

Figure 4.5: Regular solid element CHX60.

tion. Several integration schemes can be applied on this type of element. The 3 x 3 Gauss integration scheme is used because of the compatibility with the CHX60 element type; each face has 8 nodes and each side has 3 nodes. The compatibility ensures a uniform mesh.

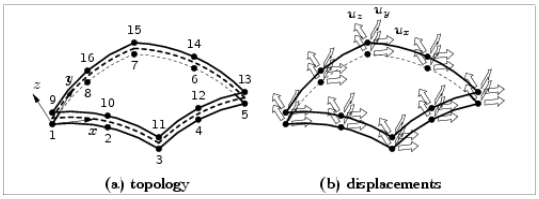

Figure 4.6: Structural interface element CQ48I.

The bar reinforcement element is an element type that can be embedded in various other element types, for example in solid elements. The bar is divided in several particles. The particle must be completely inside a structural element. The number of Gauss integration points in each particle can vary between 2 and 5. The reinforcing bars are automatically discretized according to the applied meshing of the concrete slab.

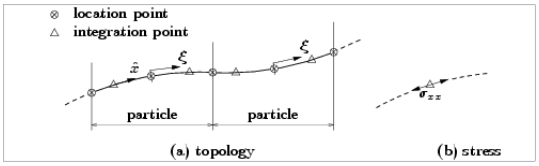

Figure 4.7: Bar reinforcement element.

Various mesh element sizes are applied in order to investigate the most suitable mesh size. A coarse mesh will shorten the computational time while a fine mesh can provide more detailed information on, for example, stress distributions.

The height of the compression zone in the concrete is estimated to determine the minimum element height. A preliminary analysis is performed to determine the stresses in the reinforcement at the occurrence of the first crack. The following calculation is done to estimate the height of the compression zone:

$$N_{s,b} = \sigma_{s,b} A_{s,b} = 54.6 \cdot 2639 = 144 \cdot 10^3 \text{ N}$$
$$N_{s,t} = \sigma_{s,t} A_{s,t} = 31.3 \cdot 346 = 108 \cdot 10^3 \text{ N}$$
$$b = 1000 \text{ mm}$$
$$c = 25 \text{ mm}$$
$$d_l = 265 \text{ mm}$$
$$x = \frac{-\left(N_{s,b} + N_{s,t}\right) + \sqrt{\left(N_{s,b} + N_{s,t}\right)^2 - 4\left(\frac{bf_{cm}}{2}\right)\left(-N_{s,b}d_l - N_{s,t}c\right)}}{2\left(\frac{bf_{cm}}{2}\right)}$$
$$x \approx 33 \text{ mm}$$

When three elements over the height of the slab are applied the first Gauss point is at $1/6 \cdot 300/3 = 16.7$ mm < 33 mm from the top of the slab, meaning that the Gauss point falls within the concrete compression zone. The second Gauss point from the top of the slab falls out of the concrete compression zone 50 mm > 33 mm. In order to have two Gauss points within the concrete compression zone at least 5 elements over the height of the slab have to be applied. To have three elements over the height about 2200 elements are required. To have five elements over the height 12500 elements are required. The computational time for one analysis would increase to more than one week. A mesh size of 99 mm x 93 mm x 100 mm (l x b x h) is applied, which results in 3 elements over the height of the slab.

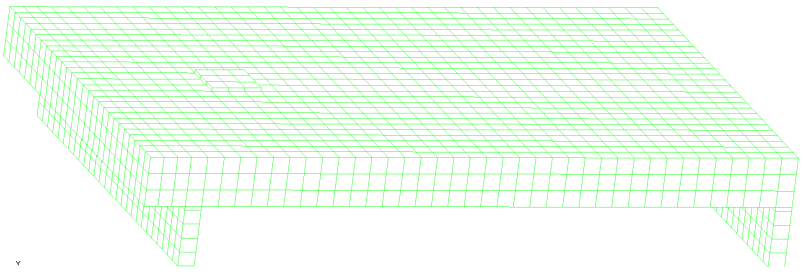

Figure 4.8: S8T1 mesh size 100 mm.

Analyses method

The materials can be modelled in various ways. For the material concrete there are multiple options to model the behaviour for cracking. Basically there are two main model categories that model cracking in reinforced concrete: "Discrete Crack models" and "Smeared Crack models" [7]. The first type tries to simulate the initiation and propagation of dominant cracks. The second model type is based on the idea that many small cracks form in the heterogeneous reinforced concrete. As the load increases, the small cracks merge to form one or more dominant cracks. The individual cracks are not numerically resolved in the smeared crack models, but the deterioration process is captured through a constitutive relation. In this way the cracks are smeared out over an element.

In the smeared crack approach, when a crack occurs in a volume allocated to an integration point, the deterioration is taken into account by reducing the stiffness and strength at that integration point. A crack is initiated when the combination of stresses satisfy a specified criterion. For example when the major principal stress reaches the tensile strength f_t and when the angle between the existing crack and the principal stress exceeds the value of a threshold angle. This is a drawback in the model because it enables the possibility of the principal stress being more than three times larger than the tensile strength.

After cracking the isotropic stress-strain relationship is replaced by an orthotropic elasticity type relation. In this relationship the *n,s*-axes are the axis of orthotrophy. The n axis points in the direction normal to the crack and the s axis is tangential to the crack. For a plane-stress situation, the orthotrophic relation can be defined as:

$$\begin{pmatrix} \sigma_{nn} \\ \sigma_{ss} \\ \sigma_{ns} \end{pmatrix} = \begin{bmatrix} 0 & 0 & 0 \\ 0 & E & 0 \\ 0 & 0 & 0 \end{bmatrix} \begin{pmatrix} \varepsilon_{nn} \\ \varepsilon_{ss} \\ \varepsilon_{ns} \end{pmatrix} \tag{4.2}$$

Where the stiffness matrix is defined as $\mathbf{D}^s$. The normal stiffness and shear stiffness are set to zero after cracking. This results in the lack of lateral contraction and expansion effects. When $\sigma_{\mathbf{ns}} = (\sigma_{nn}, \sigma_{ss}, \sigma_{ns})^T$ and $\varepsilon_{\mathbf{ns}} = (\varepsilon_{nn}, \varepsilon_{ss}, \varepsilon_{ns})^T$ then:

$$\sigma_{\mathbf{ns}} = \mathbf{D^s}\varepsilon_{\mathbf{ns}} \tag{4.3}$$

By introducing the angle ϕ as the angle between the x-axis and the y-axis and by using standard transformation matrices ($\mathbf{T}_\varepsilon(\phi)$, $\mathbf{T}_\sigma(\phi)$: $\varepsilon_{\mathbf{ns}} = \mathbf{T}_\varepsilon(\phi)\varepsilon_{\mathbf{xy}}$ and $\sigma_{\mathbf{ns}} = \mathbf{T}_\sigma(\phi)\sigma_{\mathbf{xy}}$), the components $\sigma_{\mathbf{ns}}$ and $\varepsilon_{\mathbf{ns}}$ can be related to those in the global x,y-coordinate system:

$$\sigma_{\mathbf{xy}} = \mathbf{T}_\sigma^{-\mathbf{1}}(\phi)\mathbf{D^s}\mathbf{T}_\varepsilon(\phi)\varepsilon_{\mathbf{xy}} \tag{4.4}$$

There are two subtypes for the smeared crack models. One in which the angle ϕ changes continuously such that the direction of the crack is always orthogonal to the direction of the major principal stress. The mentioned type of modelling is known as the rotating smeared crack model. The other subtype uses the angle ϕ that is found at the moment of crack initiation. The angle remains constant, this is known as the fixed smeared crack model.

The above equation can have convergence difficulties and unrealistic crack patterns can be obtained. This problem can be circumvented by inserting a reduced shear modulus βG into the stiffness matrix. Another cause for numerical troubles is the sudden drop in stiffness normal to the crack directly after crack initiation. By gradually reducing the stiffness μE, this problem can be evaded. The result is physically more realistic since the concrete within the considered volume can have multiple cracks. Between the cracks there is still concrete bonded to the reinforcement. The intact part of the concrete that remains after cracking is underestimated by a sudden drop of the tensile carrying capacity to zero. With μE the tension-stiffening effect can be taken into account and it is also possible to implement tension-softening. Concrete has still some residual load carrying capacity after reaching the tensile strength. The factor μ can be used to model the gradually diminishing tensile strength of concrete as the crack width increases.

$$\mathbf{D^s} = \begin{bmatrix} \mu E & 0 & 0 \\ 0 & E & 0 \\ 0 & 0 & \beta G \end{bmatrix} \tag{4.5}$$

Using a shear retention factor β has another advantage besides providing more realistic crack patterns and less convergence problems and it also can improve the fixed smeared crack models because the effect of aggregate interlocking and crack friction can be implemented.

The different behaviour of concrete in tension and in compression can be described using various relationships. In the FEM model, an exponential tension curve (figure 4.9(b)) and a parabolic compressive curve (figure 4.9(a)) are used because they properly model the behaviour after the peak stress has been reached.

4.1.3 Comparing FEM and experiment

Observations from S8T1

The observations made during the first test on slab 8 (S8T1) are described here [19]: At 400 kN, long cracks of less than 0.05 mm wide in the east-west direction appeared at the bottom face. The cracks were slightly inclined

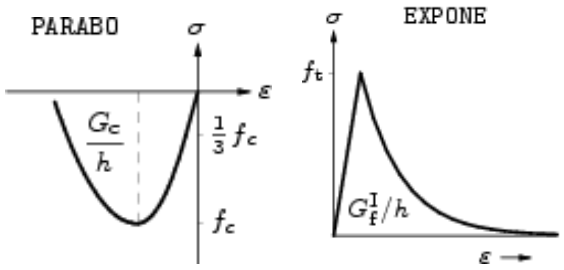

(a) Compression (b) Tension

Figure 4.9: Behaviour (stress-strain relationship) of the concrete under compression and under tension.

towards the support. On the east side face a first bending crack was observed, which did not cover the whole depth. At the west side face three bending cracks were observed. The bending cracks ran up to halfway the depth. At 600 kN the maximum width of the bending crack at the side face was 0.1 mm. The crack width at the bottom face near to the support was 0.15 mm. At the bottom face close to the load the crack was 0.2 mm wide. More long cracks running in the east-west direction appeared. Around the load cracks in the span-direction appeared. One crack was inclined towards the support. At 800 kN the maximum crack width of the flexural crack at the side face was 0.1 mm. At the bottom face the maximum crack width was 0.30 mm close to the support and 0.25 mm close to the load. At the front face a crack of 0.4 mm wide appeared. At 1000 kN the existing bending cracks at the side face had grown. The maximum crack width was 0.1 mm. At the front face the maximum crack width was 0.4 mm. The existing crack at the front face became longer and inclined. A second crack at the front face appeared. At 1200 kN the maximum crack widths were: 0.45 mm at the front face at the east side; 0.5 mm at the front face in the middle and 0.1 mm at the side face. At the east side face a bending crack appeared in the shear span along with a crack above the support starting at the top face. At 1313 kN a loud crack was heard. At 1450 kN a shear crack appeared at the west side face. Initially it had a very small width, but then grew rapidly. The observed failure was brittle. At the top face a crack ran from the load towards the west side face. The peak load was 1481 kN. After failure the maximum crack widths were 0.6 mm at the bottom face close to the load; 0.35 mm at the bottom face close to the support; 0.5 mm at the front face in the middle; 0.35 mm at the front face close to the west side face; 0.15 mm for a flexural crack at the east side face and 7 mm for the shear crack at the west side face.

(a) Bottom face

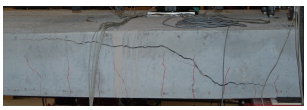

(b) West side face

(c) North side face

(d) East side face

Figure 4.10: Crack pattern S8T1.

Influence of the shear retention factor β

The shear behaviour of the concrete has to be modelled for the fixed crack models. After cracking the shear stiffness is reduced (figure 4.11). The reduction is realized through the reduction factor β which is known as the shear retention factor. $G^{\text{cr}} = \beta \cdot G$. The shear retention factor can vary between $0 \leq \beta \leq 1$.

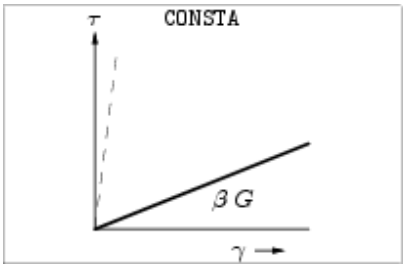

Figure 4.11: Constant shear retention for Total Strain crack models. Shear retention factor β.

The effect of the shear retention factor on the FEM model is investigated. In figure 4.12 the influence of the shear retention factor on the load displacement curve is shown. The displacement is measured directly underneath the load plate. The shear retention factor has a standard value of 0.01 in TNO Diana. When the shear retention factor is increased, the graph is stretched. The first part of the graph is the same for all factors. The similarity is due to the fact that concrete is uncracked until a displacement of about 2 mm is reached. After that the shear modulus is gradually reduced by the shear retention factor. When a factor β of 0.25 is used, the maximum concentrated load and the ultimate displacement are similar to the values found in the experiment.

For three shear retention factors that have been applied to the FEM model, the crack pattern is plotted. In figure 4.13 the crack pattern on the bottom face, north side face and west side face are shown. The (enlarged) deformations are shown as well. In figure 4.14 the crack pattern on the top face, east side face and west side face can be seen.

For an increasing shear retention factor β, the crack pattern can develop further, which is expected because the shear modulus is reduced at a slower rate for a higher factor β, increasing the redistribution of forces.

For $\beta = 0.01$ the cracks occur mainly directly underneath the load plate on the bottom face of the concrete slab. Cracks run in span direction from the simple support towards the load plate and from the load plate to both edges of the slab. The crack pattern on the bottom face seems to be slightly inclined

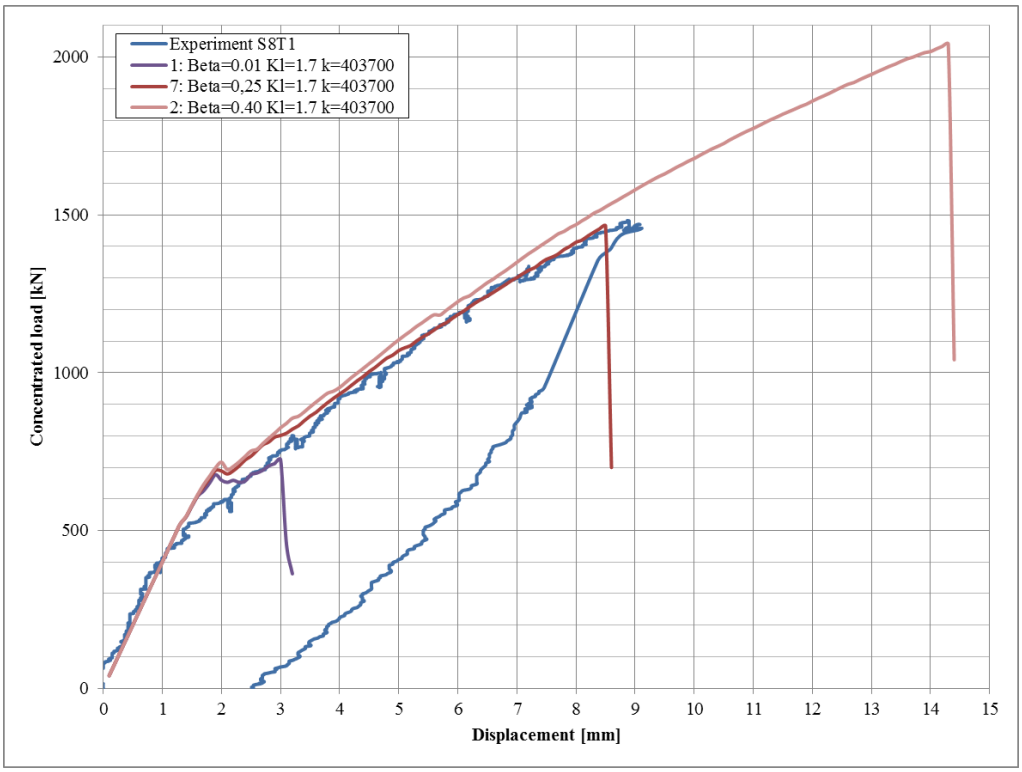

Figure 4.12: Influence of the shear retention factor β on the load displacement diagram.

towards the edges. On the top face very little cracking is observed. The modelled slab fails due to a crack over the whole height of the slab that runs from the simple support. In the middle of the width of the plate, directly to the concentrated load. Also some cracks occur above the continuous support. The cracks run over a third of the slabs height along the full width.

When $\beta = 0.25$ the general pattern of the cracks is similar as when $\beta = 0.01$, only the cracks are spread over a larger area, indicating an increased load redistribution. The amount and depth of the cracks above the continuous support are also increased. The direction of the crack from the load towards the support is solely perpendicular to the simple support for a low β factor, but as the β factor increases, more inclined cracks occur that run from the simple support to the load area.

When $\beta = 0.40$ the crack pattern becomes even more extensive. The bottom face is cracked over two thirds of the area. More inclined cracks run from the load plate outwards towards the simple support. Around the moment of failure, the top face shows cracks between the load plate and the simple support. At the continuous support extensive cracks occur in the top half of the cross section and minor cracking is observed over the full height.

During the experiment no cracking was observed above the continuous support or on the top face near the load plate.

Influence of the continuous support

The support located close to the concentrated load is a simple support. The concrete plate is not restricted in rotating. The other support is a continuous support, meaning that in the experiment the rotation above the support was limited. The effect of this limitation is investigated in the FEM model. Five cases are modelled: a fully clamped support (no rotation possible), a simple support (rotation can occur without restrictions), and three cases with limited rotation capacity at the continuous support. The effect on the load-displacement diagram is shown in figure 4.15. The fully clamped support shows a higher maximum displacement and concentrated load. The plate also reacts more stiff when compared to the experiment S8T1. When a simple support is applied, the final deformation is the same as for the fully clamped support. The maximum concentrated load however is lower. The behaviour of the plate is less stiff when compared to the experiment. For the clamped situation, rotation above the continuous support is only possible when the concrete cracks, which requires a higher load compared to the situation where there is a simple support. Therefore the curve of the load displacement is less steep when the simple support is applied.

For the FEM models with a limited rotation above the support the spring

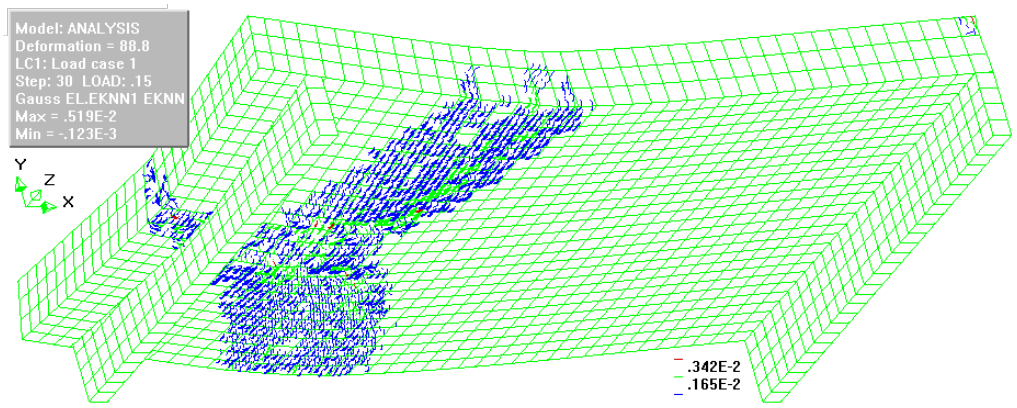

(a) $\beta = 0.01$

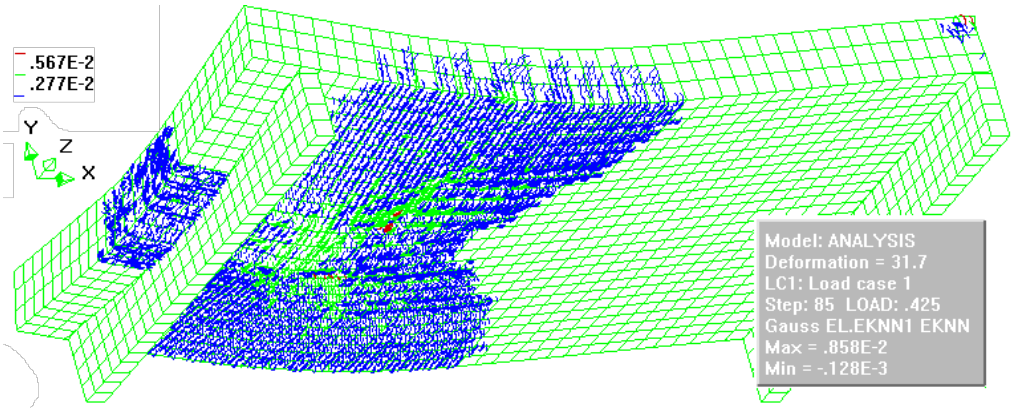

(b) $\beta = 0.25$

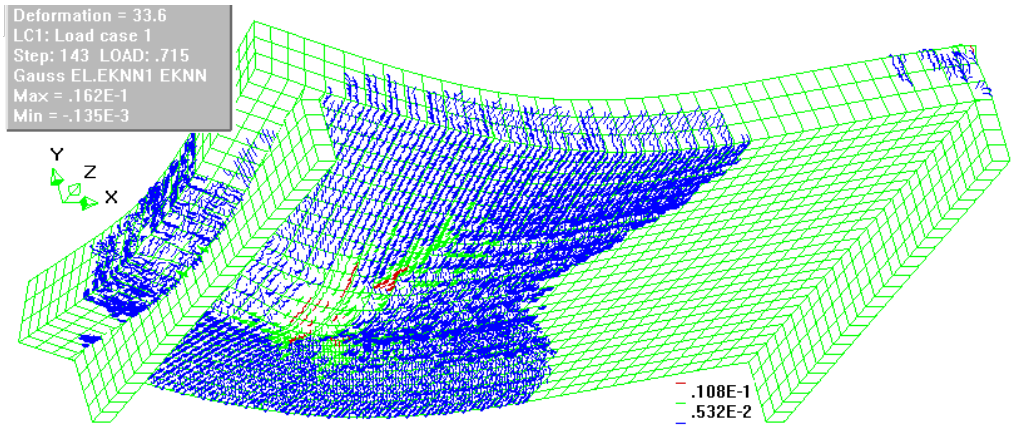

(c) $\beta = 0.4$

Figure 4.13: S8T1 FEM Analysis crack pattern, bottom view

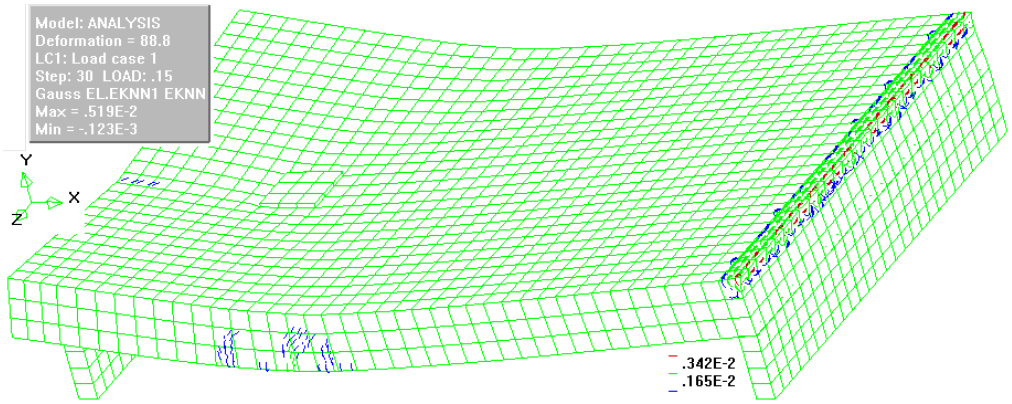

(a) $\beta = 0.01$

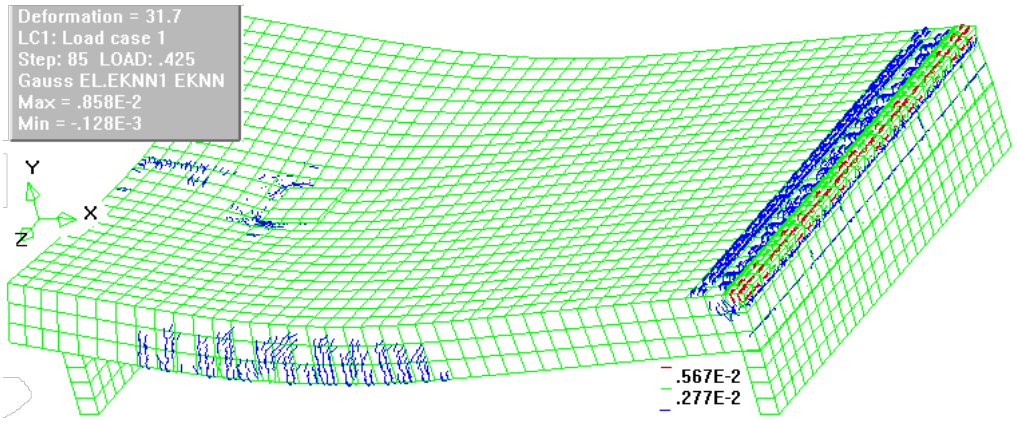

(b) $\beta = 0.25$

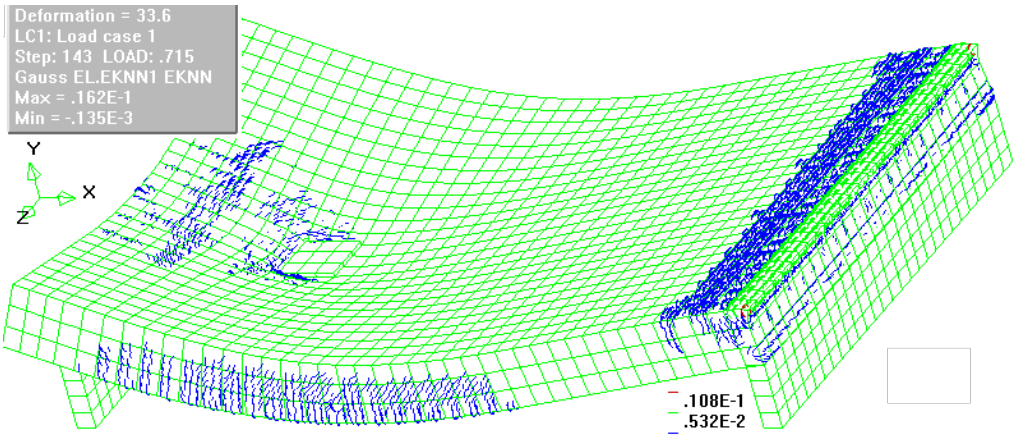

(c) $\beta = 0.4$

Figure 4.14: S8T1 FEM Analysis crack pattern, top view

stiffness was calculated earlier in chapter 4.1.2. For a spring stiffness of about 400000 N/mm, the maximum load and deflection are respectively 1464 kN and 8.5 mm. When the spring stiffness decreases to 300000 N/mm, the maximum load and deflection are 1491 kN and 9.0 mm. Thus when the stiffness is reduced from 400000 N/mm to 300000 N/mm the maximum concentrated load increases. When the stiffness is reduced to 200000 N/mm the maximum load and deflection increase even further, to 1681 kN and 10.8 mm. However, when the stiffness is even further reduced, to 100000 N/mm, the maximum load and deflection do not increase, but decrease to about 1502 kN and 9.1 mm. These values are about the same as when a spring stiffness of 300000 N/mm is applied, as is illustrated in figure 4.16. In all cases the plate appears to fail at the location of the concentrated load and not above the continuous support. The change in maximum capacity for varying spring stiffness values can be explained by distribution of moments.

When the stiffness is high (400000 N/mm), the bending moment above the continuous support is high, and the bending moment at the location of the concentrated load is relatively low. The stresses above the support increase rapidly, causing the concrete to crack at this location. The cracks allow the rotation of the plate and redistribution of the forces. The stresses in the concrete underneath the load area are increasing, eventually causing failure of the slab.

Compared to the previous situation, when the stiffness decreases (200000 N/mm), the bending moment above the continuous support decreases and the bending moment below the concentrated load increases. Apparently this is an optimal condition since a higher redistribution of forces is allowed. Cracking above the support occurs more gradually, limiting the rotation of the plate above the support and also limiting the increase in stresses at the loading area.

When the stiffness decreases even further (100000 N/mm), the bending moment above the continuous support reduces further as well. Consequently the bending moment at the concentrated load increases. The higher bending moment causes higher stresses in the concrete underneath the load, reducing the load capacity.

In figures 4.17 and 4.18 the influence of the support type on the crack pattern at maximum capacity is shown. The main differences between the crack pattern of the model with the simple support (figure 4.17(a)) and the model with the clamped support (figure 4.17(b)), are extensive cracking above the continuous support and the crack running from the load area towards the continuous support in span direction in the case of a clamped support.

In case of the continuous support where the rotations are only partially restricted, the important difference between the crack patterns (figure 4.18) is

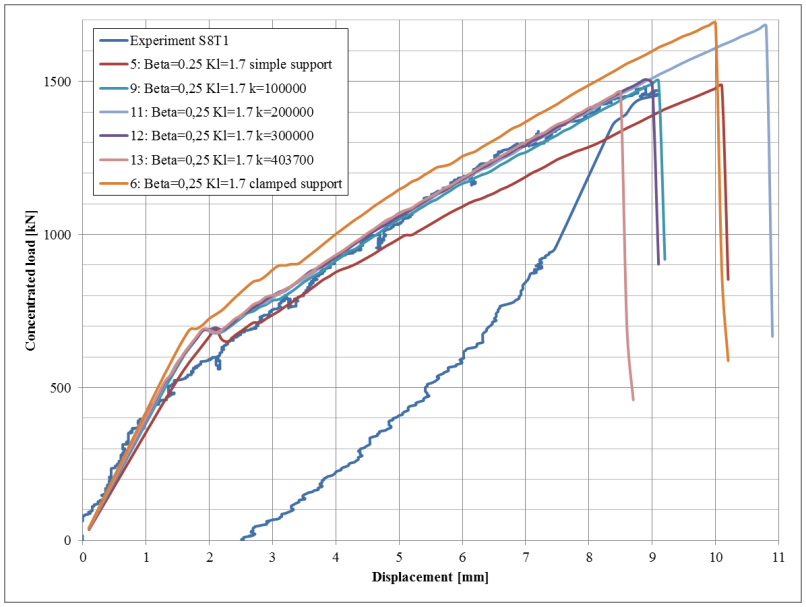

Figure 4.15: Influence of the support type on the load-displacement diagram.

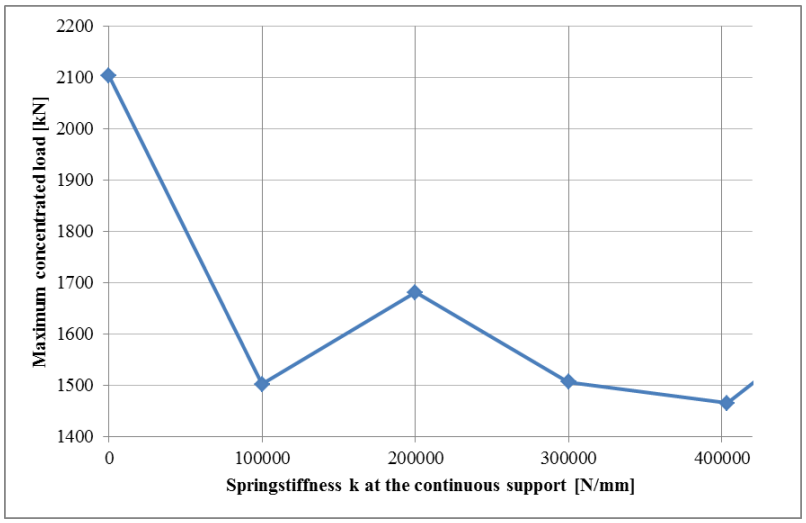

Figure 4.16: The influence of the support spring stiffness on the maximum concentrated load.

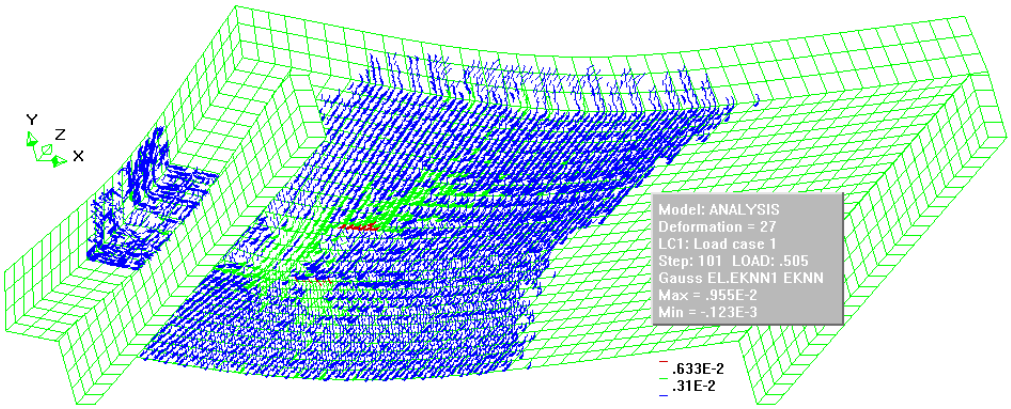

(a) $\beta = 0.25$, $K_l = 1.7$ N/mm^3, simple support

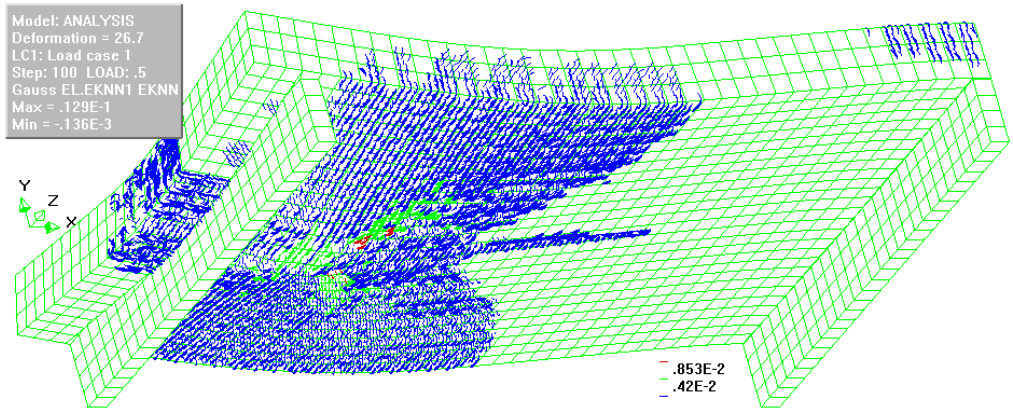

(b) $\beta = 0.25$, $K_l = 1.7$ N/mm^3, clamped support

Figure 4.17: S8T1 FEM Analysis crack pattern, bottom view

the increase in cracks above the continuous support when the spring stiffness increases. When the spring stiffness is set at $k = 200000$ N/mm (figure 4.18(b)) the crack pattern on the bottom face of the slab is more extensive.

Influence of the interface layer

The interface material (felt and plywood) has a substantial influence on the behaviour of the model. The effect of the interface material stiffness on the FEM model is investigated and illustrated in figure 4.19. The slope of the graph (before and after cracking) is lower when the interface layer stiffness is lower. The interface layer has no effect on the maximum concentrated load that can be applied, but the maximum deformation increases for a lower interface material stiffness. When the stiffness of the interface material is lowered (for example from a value of 1.7 to 1.1), the slab will deform more at a lower load level. As a result, the maximum deflection of the slab is reached at a lower load level. Thus, the interface layer stiffness influences the amount of rotation of the slab above the support. In chapter 4.1.1 it was calculated that the interface stiffness is $K_l = 1.1$ N/mm^3. However a better approximation of the experiment in terms of load-displacement behaviour S8T1 is obtained for an interface stiffness of $K_l = 1.7$ N/mm^3.

Crack pattern

In the FEM model, various parameters have been varied to obtain the best approximation of the real experiment that has been conducted. In the experiments no cracks were observed above the continuous support. The lack of cracking above the continuous support can be approached in the FEM model by a low spring stiffness at the continuous support. The interface layer stiffness of $K_l = 1.7$ N/mm^3 combined with a shear retention factor of $\beta = 0.25$ and a spring stiffness at the continuous support of $k = 100000$ N/mm provided the closest resemblance to the experiment. The failure mechanism for S8T1 was one-way shear, showing a clear diagonal shear crack over the side of the plate, running from the support to the concentrated load (figure 4.23(b)). This crack pattern was not found in any of the performed FEM analysis. A detailed comparison of the crack patterns is shown in the figures 4.20 - 4.24.

In figure 4.20 the crack pattern of the bottom face of the FEM model near the concentrated load and simple support is compared to a photo of the crack pattern of S8T1. The crack pattern generated by iDiana shows a much denser crack pattern. The cracks shown by the program include micro-cracks. The direction of these cracks resemble the direction of the cracks marked on the picture of S8T1. Inclined cracks run from the location of the

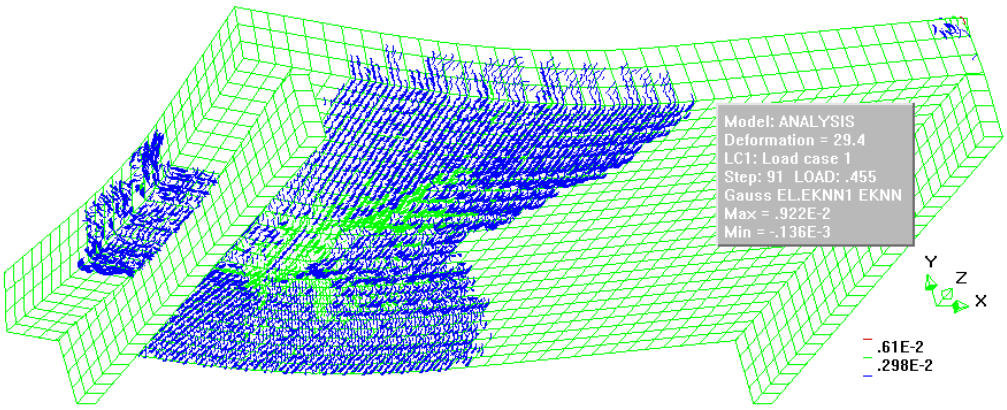

(a) $\beta = 0.25$, $K_l = 1.7$ N/mm^3, $k = 100000$ N/mm

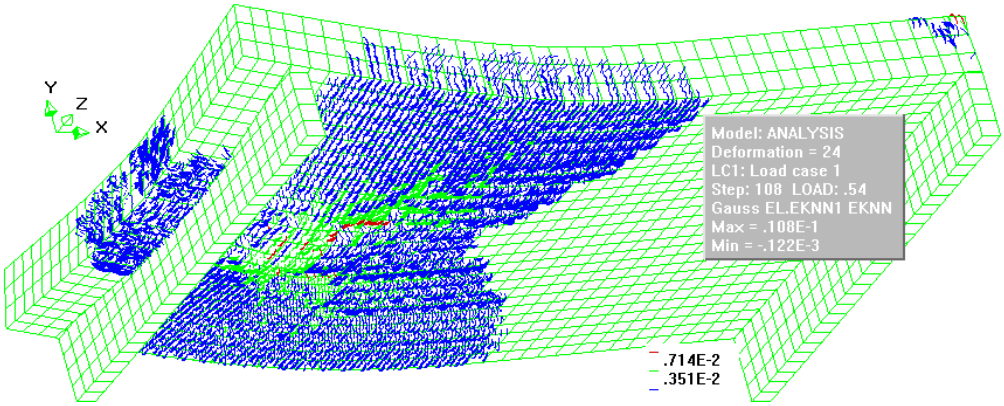

(b) $\beta = 0.25$, $K_l = 1.7$ N/mm^3, $k = 200000$ N/mm

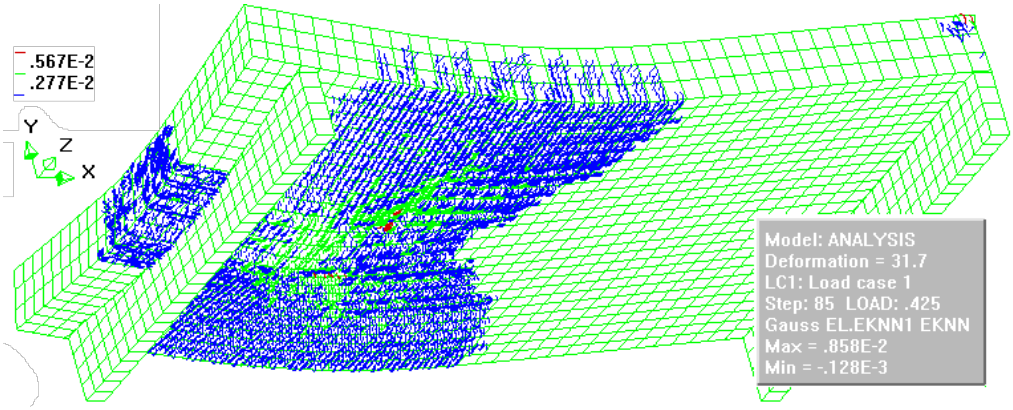

(c) $\beta = 0.25$, $K_l = 1.7$ N/mm^3, $k = 403700$ N/mm

Figure 4.18: S8T1 FEM Analysis crack pattern, bottom view

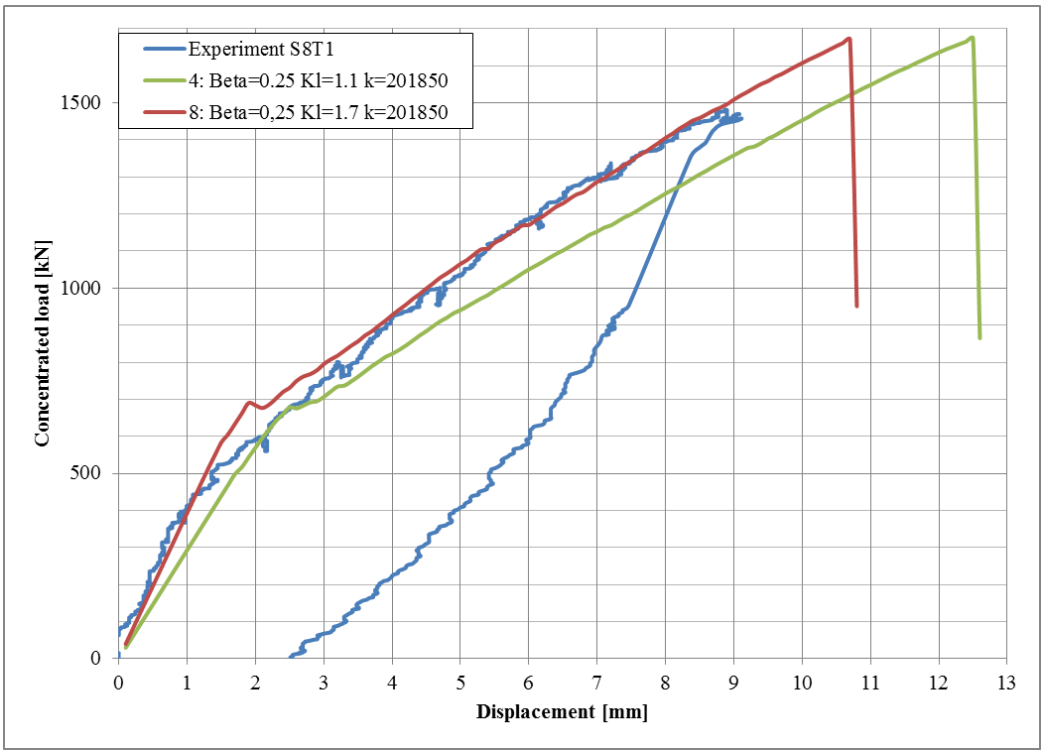

Figure 4.19: Influence of the interface layer stiffness on the load-displacement diagram.

load to the simple support. In between these inclined cracks, some cracks run in the direction parallel to the support and some cracks run perpendicular to the support. At the load area, straight cracks run parallel to the supports. Further away from the simple support and the load area, the crack pattern is somewhat inclined towards the edges of the plate.

In figure 4.21 the crack pattern of the east side face of the FEM model near the concentrated load and simple support is compared to a photo of the crack pattern of S8T1. In the photograph vertical cracks marked in red can be seen, starting just next to the interface material of the support. The spacing between the cracks is regular (about 15 cm). The cracks vary in length and some have a small inclination. A similar crack pattern can be seen in figure 4.21(a). However, the vertical cracks start to occur at a small distance from the interface layer. The cracks marked in red are the cracks that also can be seen in figure 4.21(b).

A very clear difference is the prominent shear crack running from the edge of the interface material in diagonal upward direction beyond the location of the load. The characteristic inclined crack was not seen on the outside side face in any of the FEM model analysis.

On the side face of the modelled plate, the characteristic diagonal shear crack can not be seen. In figure 4.22, various cross sections are made near the simple support. It becomes clear from figure 4.22(b) and 4.22(d) that inclined cracks run between the simple support and the load plate. These cracks indicates one-way shear failure. In the transverse direction (figures 4.22(c) and 4.22(e)) the cracks spread out towards the sides from the load plate at top to bottom of the slab. In figures 4.22(f) and 4.22(g) contour plots of the strains are given. It can be seen that there is a large area under tension between the load and the support, where the shear crack occurs. Between the load plate and the continuous support the strain levels are substantially lower. The contour plot of cross section four shows cracks on the bottom face of the slab. It also shows cracks within the concrete underneath the load plate can be seen.

The same crack pattern, but without the diagonal shear crack, as on the east side can be seen on the west side face of the beam. The crack pattern predicted by the FEM model is similar to the crack pattern in the experiment.

The north side face experimental crack pattern (figure 4.24(b)) is compared to the predicted crack pattern by the FEM analysis (figure 4.24(b)). In the middle of the width a vertical crack over the whole height of the slab can be seen in both images. Next to the vertical crack, a small inclined crack is also observed. In the photograph another crack is shown close to the side edge of the plate, but this crack is not seen in the FEM model.

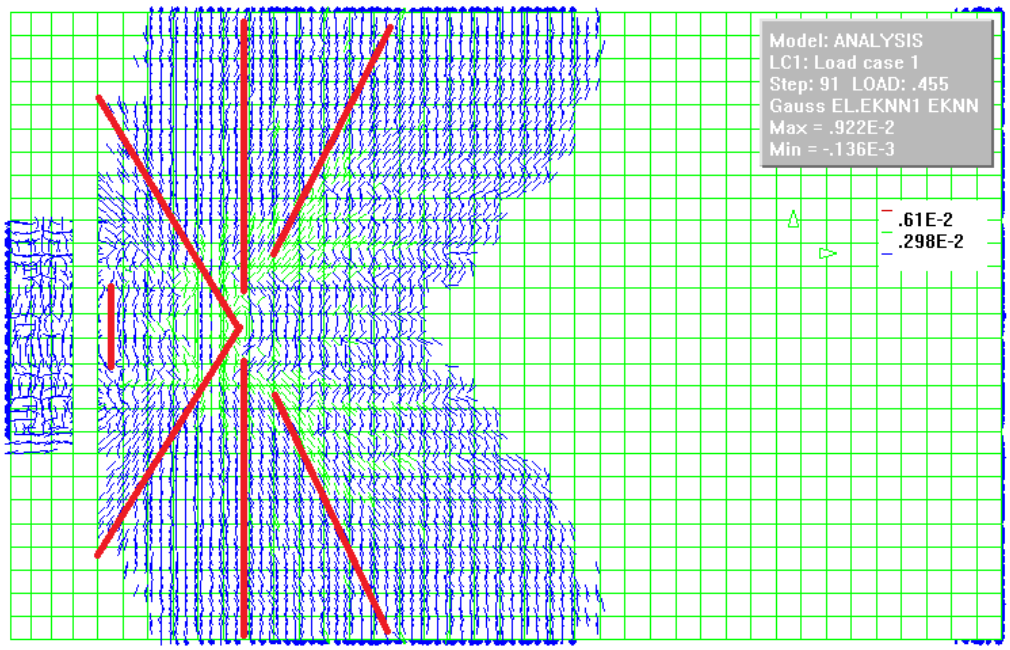

(a) $\beta = 0.25$, $K_l = 1.7$ N/mm^3, $k = 100000$ N/mm

(b) S8T1

Figure 4.20: Crack pattern S8T1 compared to FEM Analysis , bottom view.

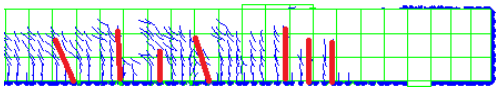

(a) $\beta = 0.25$, $K_l = 1.7$ N/mm^3, $k = 100000$ N/mm

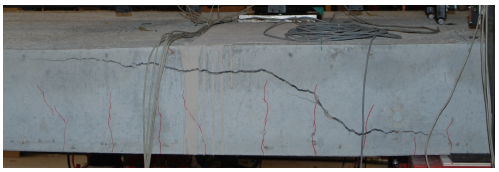

(b) S8T1

Figure 4.21: Crack pattern S8T1 compared to FEM Analysis , east side view.

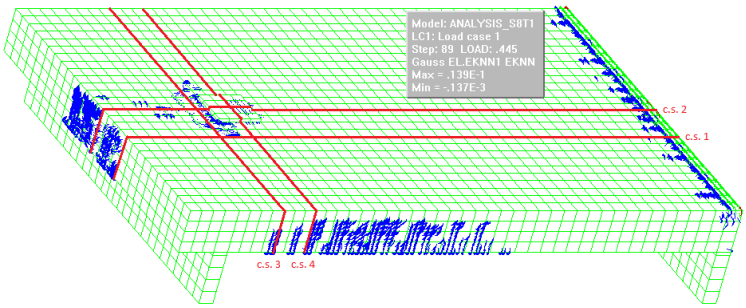

(a) Cross sections overview

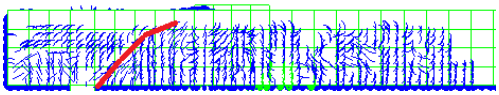

(b) Cross section 1

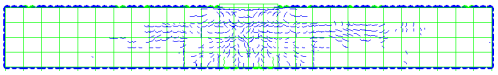

(c) Cross section 3

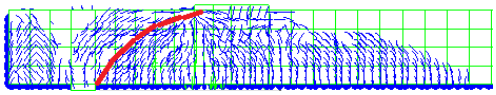

(d) Cross section 2

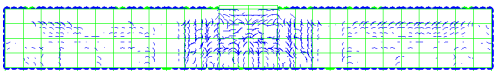

(e) Cross section 4

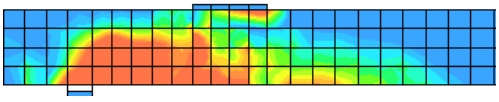

(f) Cross section 2 principal strains

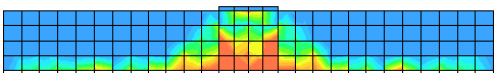

(g) Cross section 4 principal strains

Figure 4.22: S8T1 modelled crack pattern in cross sections at failure load.

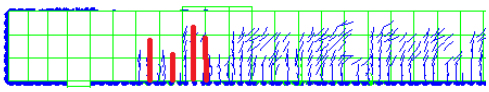

(a) $\beta = 0.25$, $K_l = 1.7$ N/mm^3, $k = 100000$ N/mm

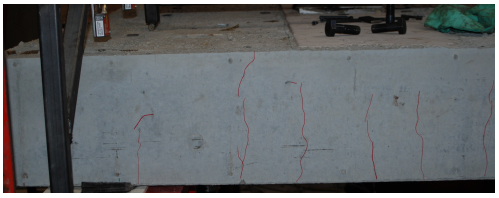

(b) S8T1

Figure 4.23: Crack pattern S8T1 compared to FEM Analysis , west side view.

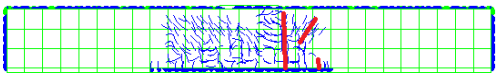

(a) $\beta = 0.25$, $K_l = 1.7$ N/mm^3, $k = 100000$ N/mm

(b) S8T1

Figure 4.24: Crack pattern S8T1 compared to FEM Analysis , north side view.

The FEM model of the plate fails in a similar manner as the experiment. Although the large diagonal crack on the side face of the plate is not observed, characteristic one-way shear cracks can be observed in cross sections of the model (figure 4.22). An explanation for the diagonal crack between the load and the support not running all the way to the side face of the plate is that the FEM analysis is unable to obtain convergence in the calculation due to the sudden occurrence of the crack and the relatively large deformations that follows. The nature of the crack model (smeared cracking) can also explain the lack of one wide diagonal shear crack. An analysis with more elements over the height might provide a solution, however this will cost a even more computational time.

The slab fails in shear between the load and the support in the middle of the width of the plate. After this moment, the model stops to work properly because the FEM analysis can not reach convergence.

Reinforcement

The yielding in the bottom reinforcement at the moment of failure is shown in figure 4.26(a). At the moment before failure very little yielding of the reinforcement is observed in the longitudinal reinforcement underneath the

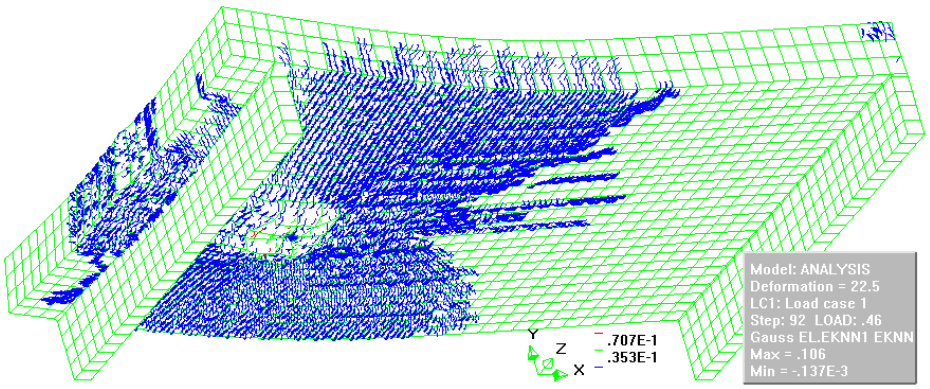

Figure 4.25: Modelled crack pattern and deformations at failure of S8T1.

load plate. In the load step directly after failure of the load plate (figure 4.26(b)) failure in the longitudinal bottom reinforcement can be seen over the whole width of the slab.

Effective width

In figure 4.27 a vector plot of the stress distribution in the interface layer at the simple support is shown. Just before failure of the slab the load is distributed along the full width of the plate. In the figure the effective width is determined. The area enclosed by the black rectangle is the same area as underneath the red arrows. The width of the rectangle (1592 mm) is the effective width. The measured effective width in the experiment is 1680 mm. The effective width calculated according to the French method is 1700 mm and with the Model Code 2010 final draft it has a calculated effective width of 2032 mm. The French estimates the effective width very well (+1%). The Model Code 2010 final draft overestimates the width (+21%) and the FEM model slightly underestimates it (-5%).

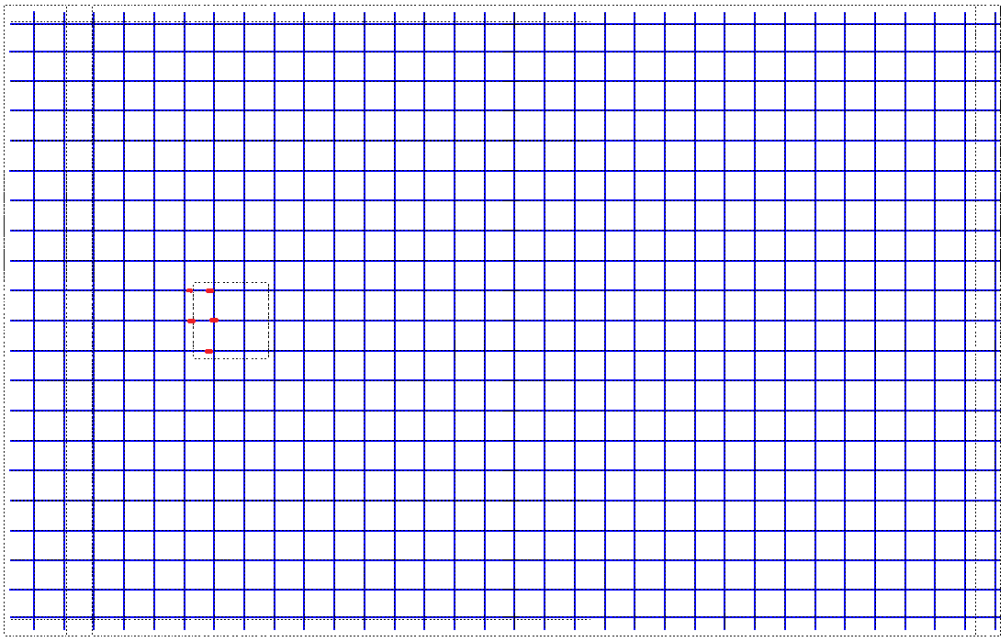

(a) Before failure

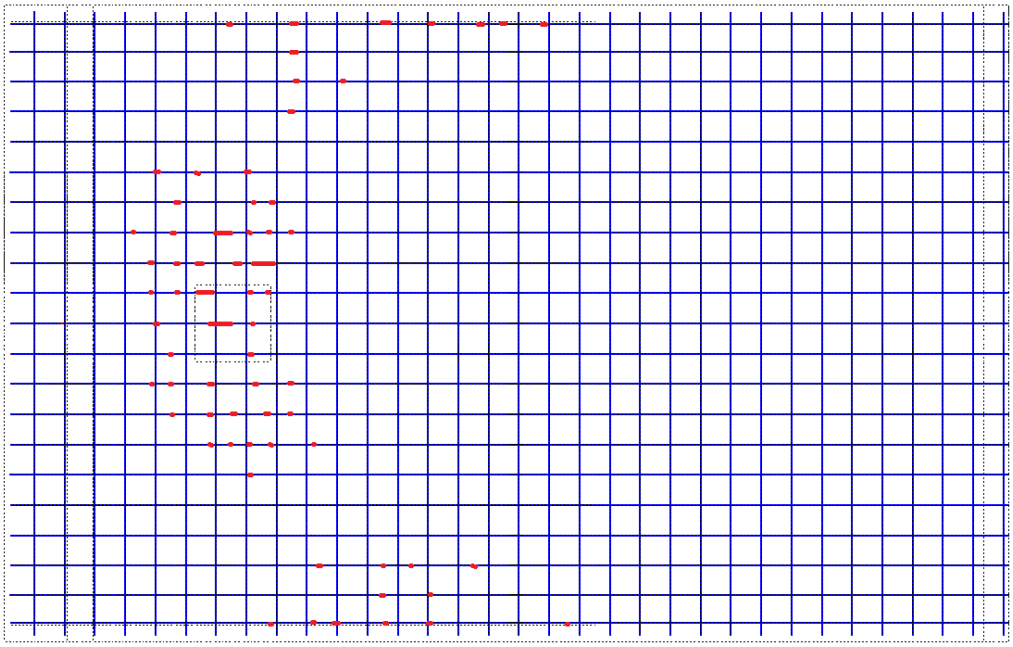

(b) After failure

Figure 4.26: S8T1 FEM Model yielding of the bottom reinforcement.

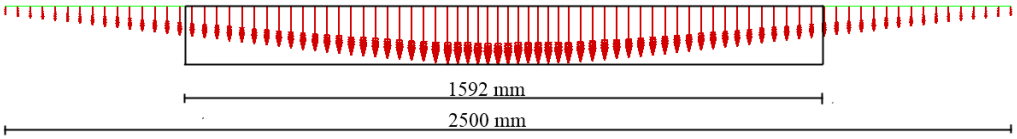

Figure 4.27: Stress distribution and effective width measured in the interface layer above the support closest to the concentrated load just before failure.

4.2 Punching shear failure: RH-350-1TV

The current section describes the experiment and the FEM model of RH-350-1TV, which is boundary situation 2: an element failed in punching shear.

In the paragraphs below, first the experiments and their characteristics are described. Then the FEM model is described, followed by a comparison of the experiment and the modelled results.

4.2.1 Experimental test

Experiments performed at Aachen University performed by J. Hegger and K. Reissen [35] on concrete slabs subjected to a concentrated load, are similar to the plates tested at Delft University of Technology. Some of the tests resulted in punching failure. An experiment failed in punching is denoted as RH-350-1TV. The tested slabs are have similar dimensions as the tests in Delft, Ranging from 500 mm width to 3500 mm width. The length of the slabs is 4400 mm and the applied height is 280 mm. The reinforcement ratios are in the same order of magnitude. The differences between the experiments in Delft and Aachen are the support types , concrete strength, shear span, interface material, load plate dimensions and reinforcement layout. The concentrated load was applied on the slab through a steel plate of 400 mm x 400 mm. The shear span was 1000 mm.

Geometry

The plate dimensions are summarized in the table below. A side view of the experiment set-up is given in figure 4.28.

Dimensions	
Parameter	**Value [mm]**
Length	4400
Width	3500
Height	280
Span	4000
Shear span	1000

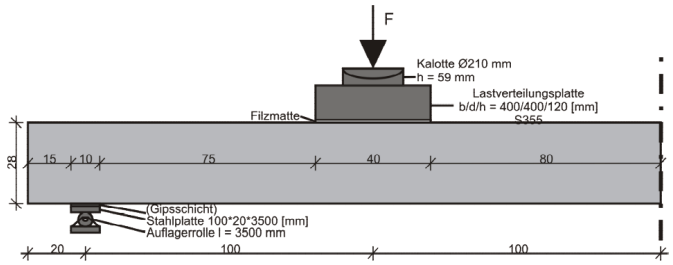

Figure 4.28: Load plate and support of the concrete slab tested in Aachen (plate dimensions are given in cm) [35].

Concrete

The concrete class that was used in this experiment was C30/37. The concrete mixture that was used is given in the table below:

Concrete mixture	
Parameter	**Value [kg/m^3]**
Cement type	CEM II/A-LL 42.5 R
addition 0-2 mm	769
addition 2-8 mm	403
addition 8-16 mm	659
Water	170
Superplasticizer	< 1.5
Retarder	< 1.0
Water/cement ratio	0.5 [-]

The fresh concrete properties were tested. A slump of 47 cm was seen, the consistency class was determined as F3 and the density was 2.353 kg/dm^3.

The concrete properties are determined by performing standard tests on cubes (150 mm x 150 mm x 150 mm), cylinders (ϕ150 mm x 300 mm) and small beams (700 mm x 150 mm x 100 mm). The beams are used to drill

cores. On the day of the experiment, the concrete compressive strength, tensile strength and E modulus are determined by performing standardized experiments on the cubes, cylinders and drilled cores. The average concrete properties are given in the table below:

Concrete strength parameters	
Parameter	**Value [MPa]**
$f_{\mathrm{cm,cyl}}$	35.9
$f_{\mathrm{cm,cube}}$	45.3
f_{ctm}	2.8
$f_{\mathrm{cm,spl}}$	3.1
E	28200

Fracture energy

The tensile fracture energy of the concrete G_f is calculated according to the Model Code 2010 final draft recommendations. The compressive fracture energy is also calculated.

$$G_f = 73 \cdot f_{cm}^{0.18} \approx 0.14 \text{ N/m}$$
$$G_c = 250 \cdot G_f = 40 \text{ N/m}$$

Reinforcement

In the concrete slab three bar diameters and two strength classes are used (10 mm (S500), 12 mm (S500), 15 mm (S900)). The yield strength and modulus of elasticity are experimentally determined.

Reinforcement properties			
Location	**Amount**	**Yield strength**	**E-modulus**
	[mm]	f_y [MPa]	E [MPa]
Bottom reinforcement			
Span direction	$46\phi 15 - 75$	885	199481
Transverse direction	$\phi 12 - 100$	573	200387
Top reinforcement			
Span direction	$25\phi 10$	573	200387
Transverse direction	$\phi 12 - 100$	573	200387

Supports and interface layer

The supports used in this experiments are roller supports at both ends of the plate. Between the support and the concrete plate only a layer of gypsum

is applied. Unfortunately no material properties were available. The layer of gypsum has a width of 100 mm. The steel beams that carry the concrete slab are welded beams with a height of 940 mm. The moment of inertia is calculated as $I_{yy} = 657000$ cm^4.

Load plate

The load plate dimensions (in mm) are 400 x 400 x 120. The steel quality used is S355.

4.2.2 FEM model properties

The FEM model build to model experiment S8T1 was adapted to model RH-350-1TV. The concrete plate dimensions were changed, the reinforcement layout was replaced. In the experiment, some vertical reinforcement was applied at the ends of the slab and in the middle. The FEM model is simplified by only applying the horizontal reinforcement. Both supports were simple supports. Also the load plate dimensions and the interface layer thickness was changed.

Geometry, load, and boundary conditions

In figure 4.29 the FEM model used to model experiment RH-350-1TV is shown. The reinforcement layout can be seen in figure 4.30. The steel welded

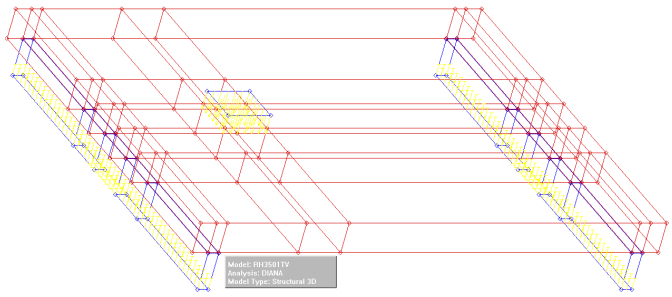

Figure 4.29: RH-350-1TV FEM model geometry, load and boundary conditions.

beams underneath the roller supports are modelled as a rectangular beam. An equivalent modulus of elasticity is calculated to obtain the same bending stiffness for the modelled beam. The equivalent E-modulus is calculated here:

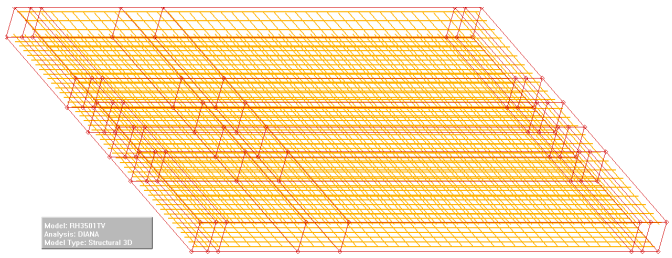

Figure 4.30: RH-350-1TV FEM model reinforcement layout.

$I_{yy} = 657000$ cm^4.

$$E_{\text{equivalent}} = \frac{EI_y}{I_{\text{box}}} = \frac{210000 \cdot 657000 \cdot 10^4}{\frac{1}{12} \cdot 100 \cdot 340^3} \approx 4200000 \text{ N/mm}^2$$

The roller supports and the layer of gypsum are modelled as an interface layer with a very low stiffness ($K_l = 0.3$ N/mm^3, $K_t = 0.03$ N/mm^3), enabling the modelled slab to rotate above the support just like in the experiment.

Material properties

A summary of the material properties used in the FEM model is given below:

Material Properties		
Parameter	**Value**	**Unit**
Concrete		
$f_{\mathrm{cm,cyl}}$	35.9	MPa
f_{ctm}	2.8	MPa
E	28200	MPa
ν	0.2	
G_f	0.14	N/m
G_c	35	N/m
Reinforcement $\phi = 15$ mm		
E	200000	MPa
f_y	885	MPa
Reinforcement $\phi = 12$ mm		
E	200000	MPa
f_y	573	MPa
Reinforcement $\phi = 10$ mm		
E	200000	MPa
f_y	573	MPa
Load plate		
E	200000	MPa
ν	0.3	
Supports		
$E_{\mathrm{equivalent}}$	4200000	MPa
ν	0.3	
Interface layer		
K_n	0.30	N/mm^3
K_t	0.03	N/mm^3

Element types, mesh and analysis method

The same element types as in the model for S8T1 are used: cubic elements CHX60 (figure 4.5), interface elements CQ48I (figure 4.6) and the bar reinforcement element type (figure 4.7). The mesh size is about 80 mm (figure 4.31). The analysis method used to perform the FEM analysis is also the same as for the S8T1 FEM analysis. The step size is increased from 0.1 mm displacement per load step to 0.15 mm per load step. Increasing the step size is done to save computational time. No significant effect was noticed on the number of iterations per load step in the analysis.

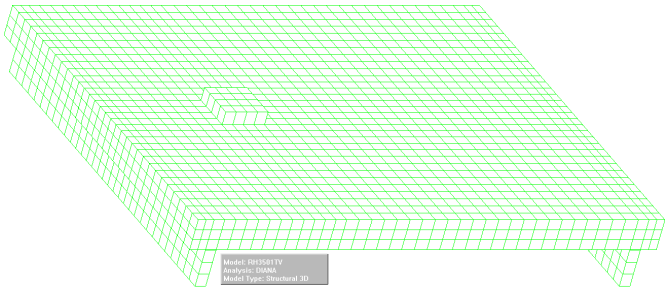

Figure 4.31: RH-350-1TV FEM model mesh.

4.2.3 Comparing FEM and experiment

Observations from RH-350-1TV

During the test, it was observed that the first bending cracks occurred around 10% of the predicted failure load on the bottom of the plate underneath the load plate. Crack widths did not exceed a width of 0.2 mm. As the load increased, more bending cracks occurred. The cracks extended on the side faces of the concrete in vertical direction. As the load increased a chequered crack pattern became visible on the bottom side underneath the load plate area. A radial crack pattern around the load can be seen in figure 4.32.

The deformations of the plate were measured during loading. The maximum deflection underneath the load plate just before failure of the plate was 19.8 mm at 990 kN.

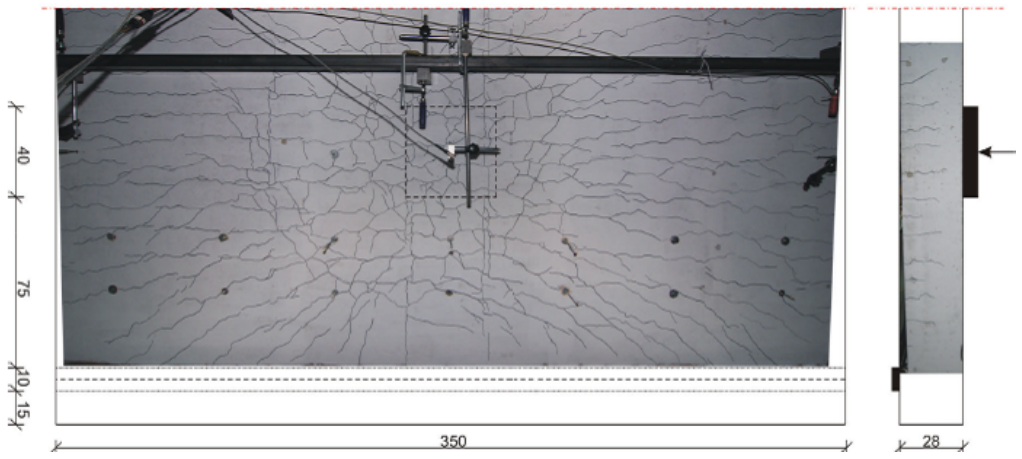

Figure 4.32: RH-350-1TV observed crack pattern.

Influence of the shear retention factor

The shear retention factor β had to be found since it is currently not possible to determine this factor beforehand. In figure 4.33 the influence of the factor β on the load-deflection diagram is shown. It can be seen that a shear retention factor of $\beta = 7.5$ % provides a reasonable failure load and ultimate deflection. The value is substantially lower than compared to the factor $\beta = 20$ % that was used in the modelling of S8T1. The difference is mainly caused by the different concrete mixtures and strengths that are used in the experiments. The shear retention factor mainly influences the maximum load capacity or deflection. For higher β values the cracking becomes more extensive, although a change in failure mechanism was not observed in the models.

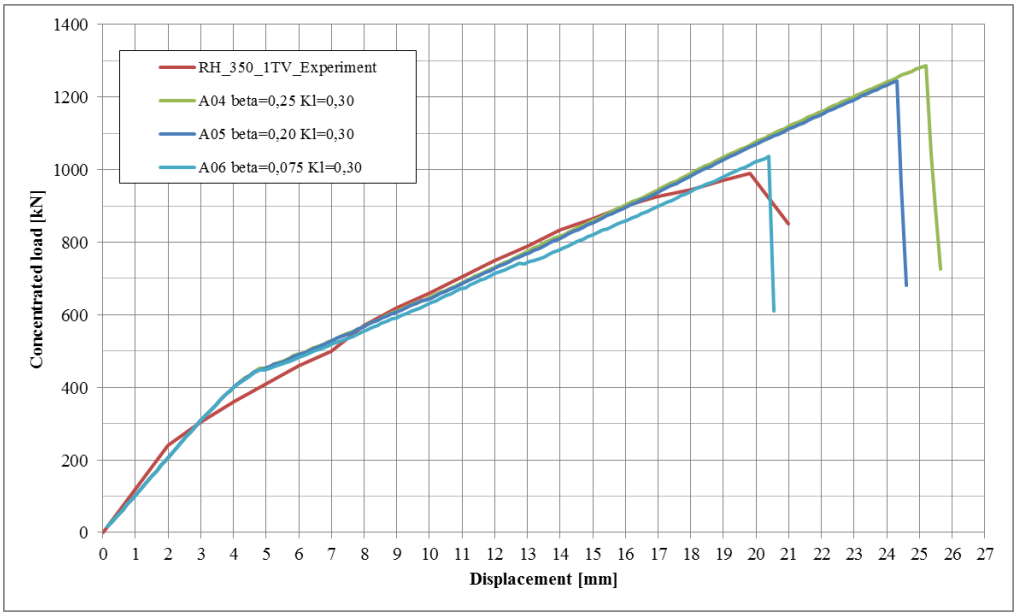

Figure 4.33: Shear retention factor β influence on the FEM model for RH-350-1TV load deflection curve.

Influence of the interface layer

The influence of the support on the behaviour of the slab can be seen in figure 4.34. Contrary to S8T1, RH-350-1TV has supports that can rotate freely. In experiment S8T1 the thick interface layer allowed for rotations. The layer of gypsum in RH-350-1TV between the support and the plate ensures a good contact between the plate and the support. The interface layer in the model

has a very low stiffness, which simulates the rotating support. In the graph shown in figure 4.34 The difference in behaviour of the plate is shown when the interface layer is removed. After a deformation of 30 mm the plate without an interface layer still had not failed.

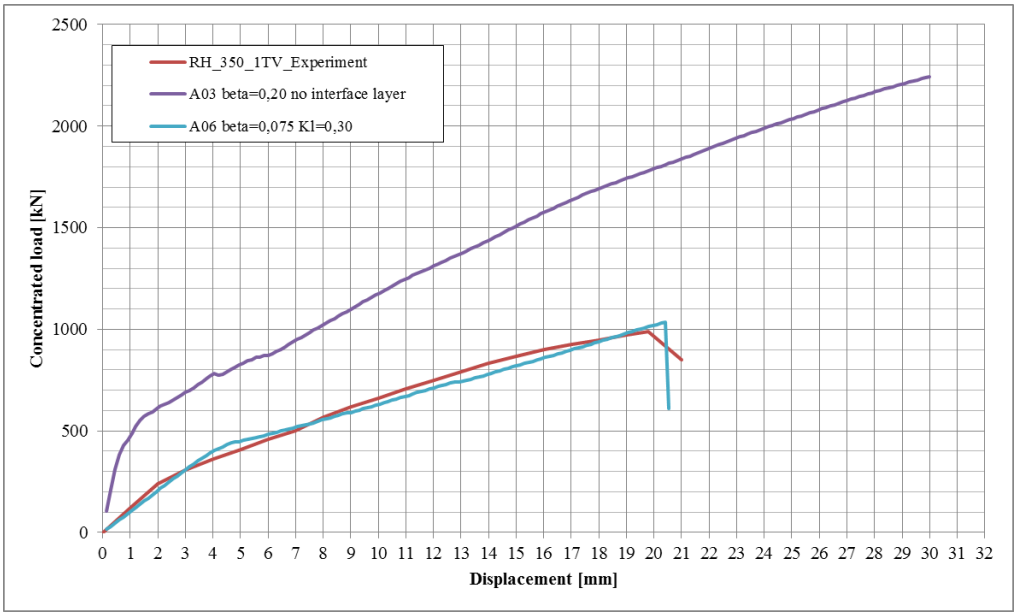

Figure 4.34: Influence of the support on the FEM model for RH-350-1TV load deflection curve.

Crack pattern

The crack pattern at the moment of failure (figures 4.36 and 4.35) is compared to the observed crack pattern in the experiment (figure 4.32). The crack pattern observed on the side face of the FEM model shows a great similarity to the experimental crack pattern. On the bottom side the crack pattern also has great similarities, but the chequered crack pattern underneath the area of the concentrated load can not be observed. When a cross section is made at two thirds from the top of the slab and the cracks at the bottom are shown again (figure 4.37) a more circular crack pattern around the load can be observed.

What happens inside the slab at the moment of failure is shown in figure 4.38. Multiple cross sections are made in both span and transverse direction to show the crack pattern in the area of the concentrated load. A contour plot of the principal tensile strains is also plotted for two cross sections (figure 4.38(f) and 4.38(g)). The strains are concentrated around the load in both

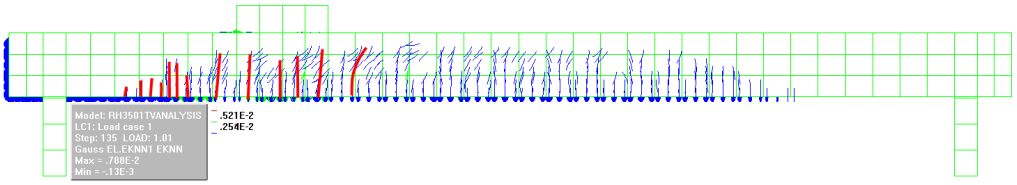

Figure 4.35: RH-350-1TV modelled crack pattern on the side face of the slab.

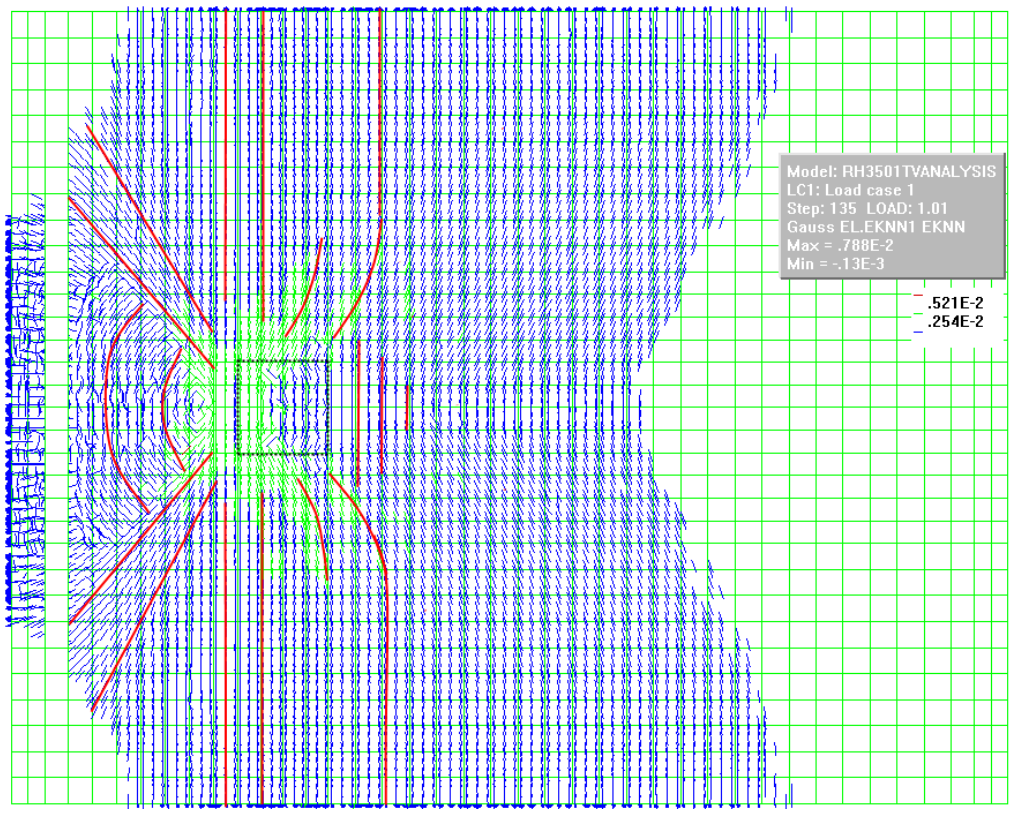

Figure 4.36: RH-350-1TV modelled crack pattern on the bottom face of the slab.

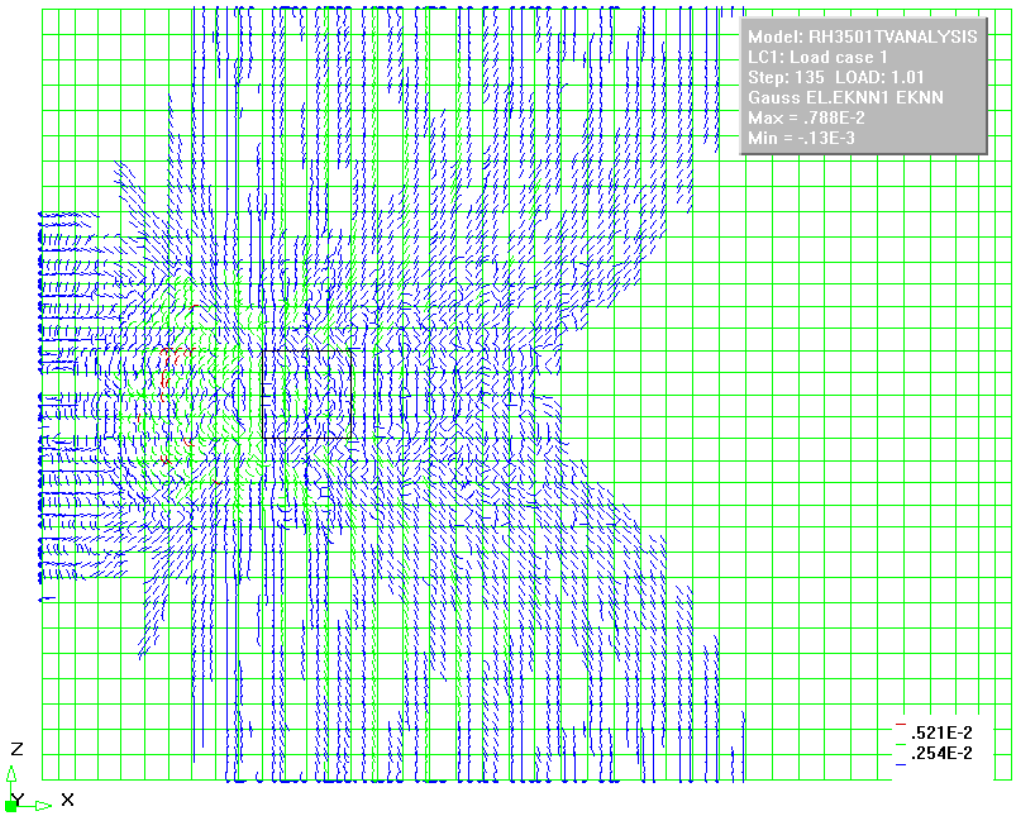

Figure 4.37: RH-350-1TV modelled crack pattern at two thirds of the height of the slab, shown from below.

directions, starting directly underneath the load plate and running towards the bottom while spreading to the sides. A larger concentration is observed between the load plate and the nearest support. The cracks run somewhat diagonally from the top towards the bottom (as indicated with the red lines in figures 4.38(d) and 4.38(e)). There are no shear cracks that run directly from the load plate towards the simple support, which would indicate one-way shear failure. Since cracking occurs around the whole load area, a truncated conical crack shape can be distinguished and there are no diagonal shear cracks that run from the load plate to the support. The failure mechanism that occurs in the FEM model is punching shear failure.

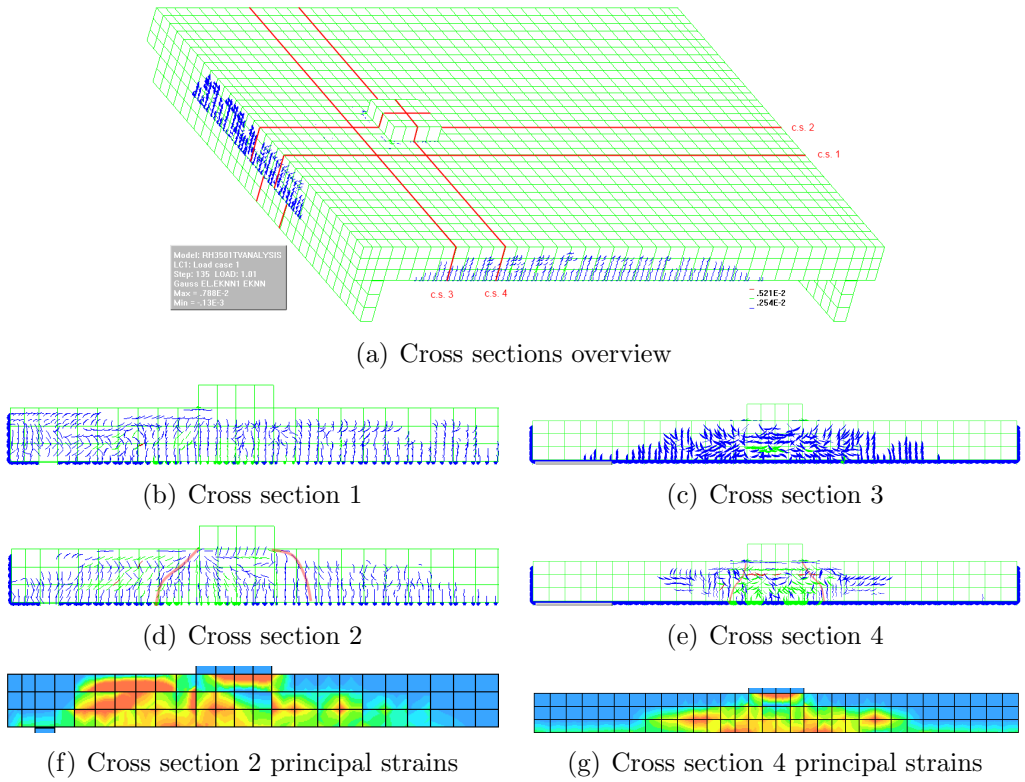

(a) Cross sections overview

(b) Cross section 1

(c) Cross section 3

(d) Cross section 2

(e) Cross section 4

(f) Cross section 2 principal strains

(g) Cross section 4 principal strains

Figure 4.38: RH-350-1TV modelled crack patterns and principal strains in the cross sections at failure load.

Reinforcement

The yielding of the reinforcement around the moment of failure is shown in figure 4.39. The yielded parts of the reinforcement are shown in red. At first only the bottom transverse reinforcement yields (at 573 MPa) directly

underneath the load plate (figure 4.39(a)). After that more yielding occurs in the bottom reinforcement around the load(figure 4.39(b)). Eventually the longitudinal reinforcement also starts to yield (at 855 MPa).

Effective width

In figure 4.2.3 the stress distribution on the interface layer, from the support closest to the concentrated load, just before the moment of failure is shown. It can be seen that the load is distributed over the whole width of the plate. The area enclosed by the rectangle is the same as the area underneath all the red arrows. The width of the rectangle is the effective width, which is 2630 mm. The calculated effective width is 3500 mm according the Model Code 2010 Final draft and 2700 mm according to the French method. The estimated effective width in the experiment is 2930 mm.

The Model Code 20210 Final draft overestimates the effective width (+20%) and the FEM model and French method slightly underestimate (-10%) the effective width.

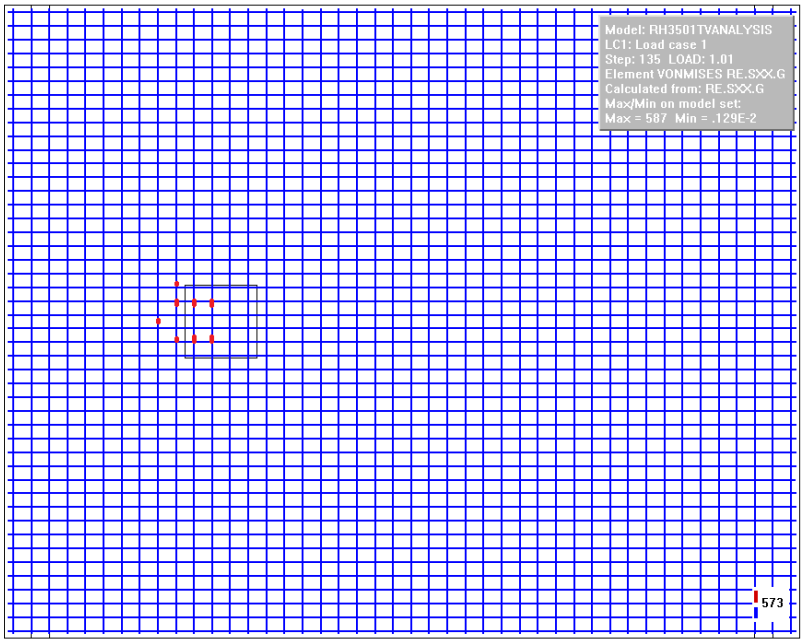

(a) Before failure

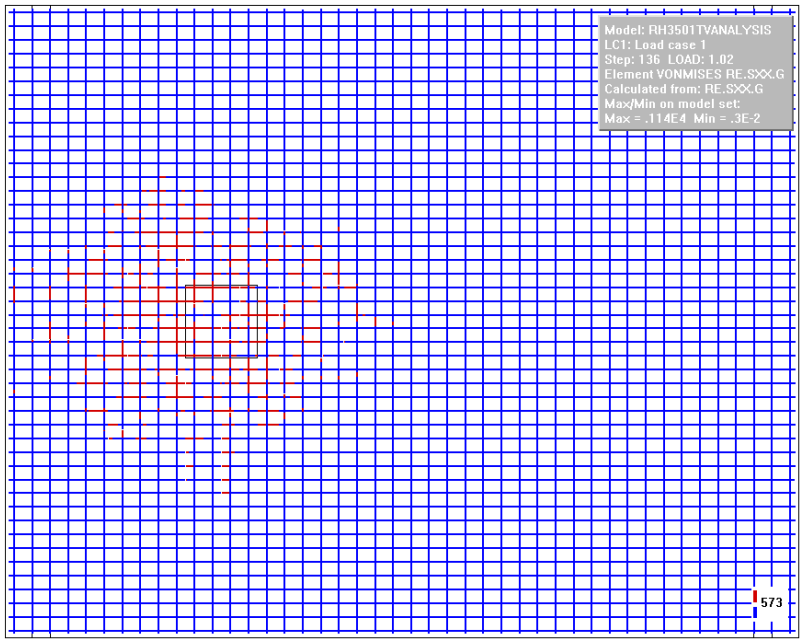

(b) After failure

Figure 4.39: RH-350-1TV FEM Model yielding of the bottom reinforcement.

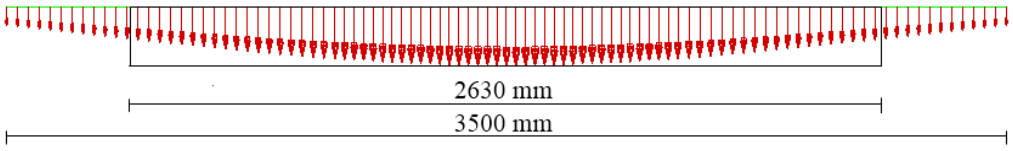

Figure 4.40: Stress distribution and effective width in the interface layer above the support closest to the concentrated load just before failure.

4.3 Conclusion and recommendations

In this chapter two FEM models have been made. One simulating one-way shear failure and one simulating punching shear failure. Both models behave like their experimental counterparts. Various parameters, like the interface layer stiffness, the continuous support rotation stiffness and the shear retention factor had to be determined for both models. The conclusions drawn is this chapter are given here:

- The FEM model for S8T1 that fails through one-way shear approaches the behaviour of the real experiment. The characteristic diagonal shear crack on the side face of the FEM model does not occur. Nevertheless it can be concluded that the failure mechanism is one-way shear. When cross-sections in span direction are made an inclined crack pattern is found between the support and the load plate, indicating that the characteristic diagonal shear crack is present inside the slab, but does not extend all the way to the side face.

- The FEM model for RH-350-1TV that fails through punching shear also approaches the behaviour of the real experiment. No direct diagonal shear crack between the load and the support can be found in the slab. Extensive cracks occur all the way around the load plate. The crack pattern that characterizes punching shear failure can be distinguished in the model.

- With the models and used method, two different failure mechanisms can be simulated. The area in between the two failure mechanisms can now be further investigated in the next chapter.

- It is still not possible to calculate or estimate the shear retention factor β beforehand. The factor depends on the amount of aggregate interlocking or crack friction. The concrete composition and strength are of significant influence. The shear retention factor influences the extensiveness of the crack pattern and the maximum load capacity. No

influence on the failure mechanism was observed in any of the performed FEM analyses. For S8T1 β was set at 25%, while for RH-350-1TV β was set at 7.5%. When $\beta = 0.25$ was also applied to RH-350-1TV, the predicted maximum load would be overestimated by 30%. The recommended value for β by the program is 1%, indicating that the FEM model, using the fixed smeared crack model, overestimates the degradation of the element. The capacity to transfer forces across cracks is underestimated.

- The shear retention factor β was only compared to two experiments. It might be useful to determine the shear retention factor for more experiments using the same model. In this way it would be possible to use an average shear retention factor which would enable the possibility to predict the maximum concentrated load with more certainty and accuracy.

- To limit the computational time, the minimum mesh size was limited. Using three elements over the height of the element most analysis could run within 24 hours. Due to the large width and length of the element, decreasing the mesh size would increase the computational time tremendously. Analysis with a finer mesh might be useful to get a more accurate view on the crack behaviour inside the slab. In that case using various mesh sizes in different areas of the model is advisable, this would require the application of interface layers inside the concrete part of the model.

- For both slabs the effective width was investigated. As can be seen in the table below, the measured, observed and calculated effective widths differ significantly. The difference between the experiment and the models is between -5% and -10% while the difference between the experiment and the code predictions is between -8% and +21%. The Model Code 2010 overestimates the effective width the most. In the previous chapter it was already concluded that the effective width calculated according to the Model Code 2010 is unsafe for larger shear spans.

Effective width				
	S8T1		RH-350-1TV	
Experiment	1680 mm	100 %	2930 mm	100%
FEM model	1590 mm	95 %	2630 mm	90%
French method	1700 mm	101 %	2700 mm	92%
MC2010FD	2032 mm	121 %	3500 mm	119%

Chapter 5

Transition between one-way shear and punching shear

In this chapter the area between one-way shear and punching shear will be investigated. In the previous chapter the two boundary situations were simulated by building a FEM model. The two FEM models were build using the same method and the same analysis procedure was applied. It was shown that both failure mechanisms can be modelled using the applied procedure.

Whether one-way shear failure or punching shear failure occurs depends on the concrete mixture, the concrete strength, the reinforcement layout, the reinforcement strength, the shear span, the plate dimensions, the load plate size, load location and the type of support. In this chapter the influence of the slab width and the shear span will be analysed through FEM analyses.

First the parameters used in the FEM model and analysis procedure that will be used to investigate the area between one-way shear and punching shear are described in section 5.1. In section 5.2 results of the analysis are presented. The conclusions drawn from the analysis can be found in section 5.3.

5.1 FEM model

The FEM model that will be used is based on the model used for the slab RH-350-1TV. The characteristics of the model and the analysis procedure are shortly described in paragraph 5.1.1. In paragraph 5.1.2 can be read how the shear span and the element width are varied.

5.1.1 Model properties

The dimensions and parameters used in the FEM model are the same as for the RH-350-1TV FEM model. The only parameters that are being varied are the plate width and the shear span. The element types, mesh size and analysis method is the same as before.

FEM Model Properties					
Parameter	**Value**	**Unit**	**Parameter**	**Value**	**Unit**
Concrete			Slab dimensions		
$f_{\mathrm{cm,cyl}}$	35.9	MPa	Plate length	4400	mm
f_{ctm}	2.8	MPa	Thickness	280	mm
E	28200	MPa	Width	-	mm
ν	0.2		Span	4000	mm
G_f	0.14	N/m	Shear span	-	mm
G_c	35	N/m	Cover depth	33	mm
Reinforcement $\phi = 15$ mm			Bottom reinforcement		
E	200000	MPa	Span dir.	ϕ15-75	mm
f_y	885	MPa	Transv. dir.	ϕ12-100	mm
Reinforcement $\phi = 12$ mm			Top reinforcement		
E	200000	MPa	Span dir.	ϕ10-75	mm
f_y	573	MPa	Transv. dir.	ϕ12-140	mm
Reinforcement $\phi = 10$ mm			Interface layer		
E	200000	MPa	K_n	0.30	N/mm^3
f_y	573	MPa	K_t	0.03	N/mm^3
Load plate			Supports		
E	200000	MPa	E_{eq}	4200000	MPa
ν	0.3		ν	0.3	
Load plate	400^2	mm^2	Support width	100	mm

5.1.2 Varied parameters

The next table shows how the parameters are varied in the analyses. A total of 12 analyses have been performed. The effective depth in span direction is $d_l = 240$ mm.

Varied parameters				
Slab width	Shear span [mm] and a/d_l ratios [-]			
1500	400 (1.67)	550 (2.29)	700 (2.92)	1000 (4.17)
2500	400 (1.67)	550 (2.29)	700 (2.92)	1000 (4.17)
3500	400 (1.67)	550 (2.29)	700 (2.92)	1000 (4.17)

5.2 Results

In this section the results of the FEM analysis, varying the element width and the shear span, will be discussed. This is done in three parts. The first part discusses the influence of the two parameters on the failure load, the second part is about the influence on the effective width and third part is about the influence on the failure mechanism.

5.2.1 Influence on the failure load

In figure 5.1 various graphs are plotted. They show the load deflection curves of the modelled slabs. In figures 5.1(a) to 5.1(d) the shear span differs. The graphs shows three lines, each representing a different slab width.

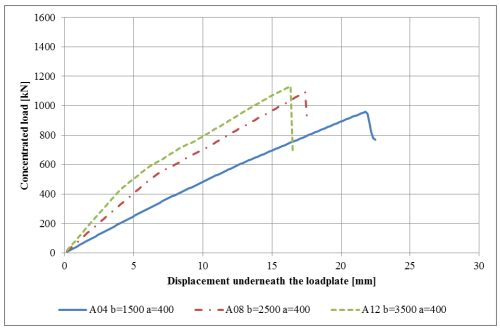

(a) $a = 400$ mm

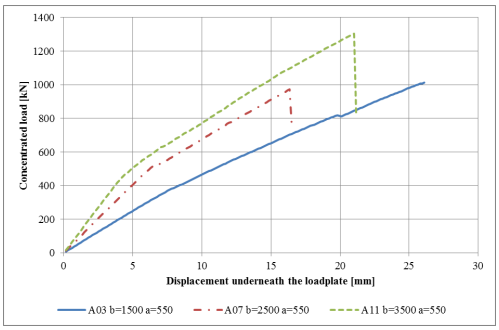

(b) $a = 550$ mm

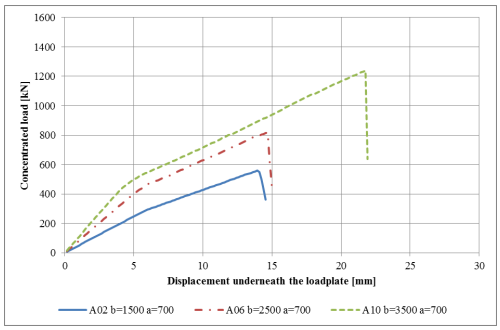

(c) $a = 700$ mm

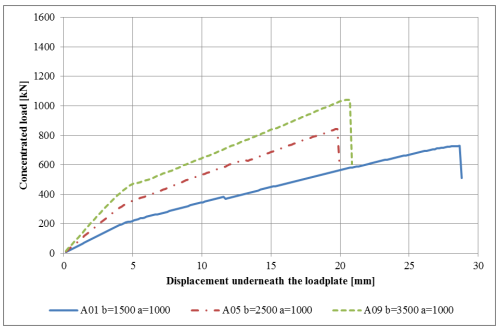

(d) $a = 1000$ mm

Figure 5.1: The influence of element width on the concentrated load and deformation of the slab for various shear spans.

For all four shear span variations the load deflection curve is steepest for the slab width of 3500 mm and the most gradual curve belongs to a slab width of 1500 mm. As the element width increases, there is more material

to provide resistance to the applied concentrated load. Deforming a larger slab requires more energy and therefore a higher load.

In figure 5.2 two graphs are plotted. The maximum shear force in the elements are provided for various shear span to effective depth (a/d_l) ratios in figure 5.2(a). Each curve represents a different slab width. In figure 5.2(b) the influence of the element width on the maximum shear force is plotted for various shear span to effective depth (a/d_l) ratios.

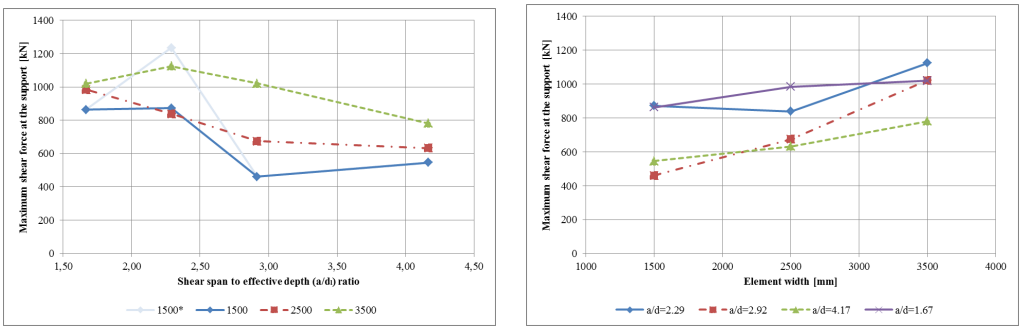

(a) Effect of the a/d_l ratio.

(b) Effect of the element width.

Figure 5.2: The influence of the a/d_l ratio and the element width on the maximum shear capacity.

The maximum shear force for each element width varies for each shear span. The concentrated load is redistributed trough the element and transferred to the supports. For wider elements, the forces can be redistributed over a larger width. The amount of redistribution depends on the shear span and the element width. In figure 5.2(a) the effects of these two factors on the maximum concentrated load can be observed.

In figure 5.2(a) the blue line represents an element width of 1500 mm. The FEM analysis for the element 1500 mm in width and a shear span of 550 mm provided inconsistent results. At first glance the element obtained a maximum shear force of 1235 kN (represented by the light blue line labelled as 1500*). This high capacity was very unexpected. Upon redoing the FEM analysis, analysing the FEM output, iterations per load step and crack pattern it was decided that the slab failed in an earlier stage (at a deformation of 19.80 mm caused by a concentrated load of 819 kN). After this step the model had difficulties converging and very unrealistic crack patterns were observed. More information on this decision can be found in appendixA.

Figure 5.2(a) also shows that the difference in maximum load capacity is small for low a/d ratios. The difference in capacity increases in between an a/d ratio of 1.67 and 4.17. For higher a/d ratios the difference in maximum load capacity decreases again.

When the a/d ratio is small the forces are transferred directly from the loading point to the support. Due to the small shear span the redistribution of forces is limited, so the width of the element has little influence on the load capacity.

When the a/d ratio is between 1.67 and 4.17 the concentrated load is transferred differently through the elements, activating a larger part of the element to transfer the forces. Larger differences in load capacity are the result.

In section 2.3.1 it was suggested that the valley of shear that is found in the shear capacity for beams may be found for slabs as well, but at lower a/d ratios. This effect is not seen in figure 5.2(a).

For a/d ratios of 4.17 the difference in load capacity is small. As will be shown in paragraph 5.2.3, the element width is not the limiting factor, but the failure mechanism is.

In figure 5.2(b) it is noticed that for the two low a/d_l ratio the curves tend to be horizontal, while for the two higher a/d ratios the curves are transcending. For the smallest a/d_l ratio (1.67) the shear capacity does not increase as the element width increases. When $a/d_l = 2.29$ a small increase in shear capacity is observed as the elements become wider. A strong increase in shear capacity is shown for $a/d_l = 2.92$. When the a/d_l ratio is increased to 4.17 the increase in shear capacity is smaller, suggesting that the effect of the element width on the shear capacity becomes smaller as the element width becomes larger.

5.2.2 Effective width

When structural elements are checked for one-way shear capacity, the shear stress over the width of the element is checked. This width is either the width of the element or the effective width. The effective width is determined by using the stress distribution in the interface layer of the support closest to the concentrated load. A vector plot of vertical stress distribution along the length of the support is plotted. The area covered by these vectors is calculated. The effective width is the width of a rectangular shaped stress distribution with the same area. The maximum vertical stress is used as the height of the rectangle. The vector plots and the effective widths of the modelled slabs are given in figure 5.3.

In figures 5.3(a) to 5.3(c) the forces are distributed almost equally over the full width of the plate for all three shear spans. The effective width is the same as the width of the element. For elements of 2500 mm in width (figures 5.3(d) to 5.3(f)) the forces are unequally distributed over the full width. The forces are concentrated in the middle of the plate. For elements

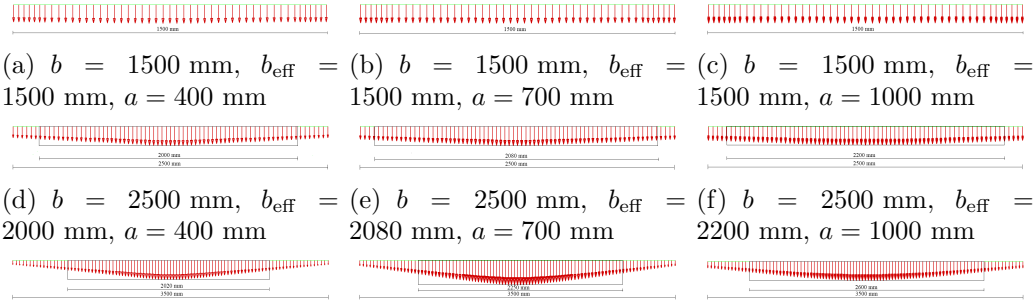

(a) b = 1500 mm, b_{eff} = 1500 mm, a = 400 mm
(b) b = 1500 mm, b_{eff} = 1500 mm, a = 700 mm
(c) b = 1500 mm, b_{eff} = 1500 mm, a = 1000 mm
(d) b = 2500 mm, b_{eff} = 2000 mm, a = 400 mm
(e) b = 2500 mm, b_{eff} = 2080 mm, a = 700 mm
(f) b = 2500 mm, b_{eff} = 2200 mm, a = 1000 mm
(g) b = 3500 mm, b_{eff} = 2020 mm, a = 400 mm
(h) b = 3500 mm, b_{eff} = 2250 mm, a = 700 mm
(i) b = 3500 mm, b_{eff} = 2600 mm, a = 1000 mm

Figure 5.3: The vertical stress distribution in the interface layer of the support closest to the concentrated load at the moment of failure.

with a width of 3500 mm (figures 5.3(g) to 5.3(i)) this force concentration is even more prominent.

In the table below the approximated modelled effective width is compared to the effective widths as determined by the Model Code 2010 final draft and the French method from the Eurocode.

Effective widths [mm]			
Shear span a	**400 mm**	**700 mm**	**1000 mm**
b = 1500 mm			
FEM Model	1500*	1500*	1500*
French method	1500*	1500*	1500*
Model Code 2010 f.d.	1500*	1500*	1500*
b = 2500 mm			
FEM Model	2000	2080	2200
French method	1500	2100	2500*
Model Code 2010 f.d.	2045	2500*	2500*
b = 3500 mm			
FEM Model	2020	2250	2600
French method	1500	2100	2700
Model Code 2010 f.d.	2045	2565	3500*
* limited by the element width.			

When one-way shear is considered, according to the codes, the effective widths are expected to increase as the shear span increases. The expected increase in effective width is observed in the modelled elements. The increase in effective width appears to be stronger for wider elements when the FEM models are considered. The Model Code 2010 final draft provides the largest

effective widths. In the previous chapters it was already pointed out that this may lead to unsafe predictions. It has to be kept in mind that the effective width is theoretical and that it is used to check the one-way shear capacity of the element, while the occurring failure mechanism can be punching shear as well.

5.2.3 Influence on the failure mechanism

To determine the failure mechanism the crack patterns and principal strains are analysed at the moment of failure. For each model the crack pattern on the bottom face and two cross sections are plotted. For the two cross sections a contour plot of the principal strains is also plotted. Cross section one is taken in span direction in the middle of the slab. Cross section two is in transverse direction taken in the middle of the load plate. In figure 5.4 the elements 1500 mm in width are compared. In figure 5.5 the comparing is done for elements 2500 mm in width. Figure 5.6 contains the images needed to compare the 3500 mm wide elements.

$b = 1500$ **mm**

From the images in figure 5.4 it is observed that on the bottom faces of all three elements the cracks run mainly from one edge to the other in transverse direction. For the two smaller shear spans (400 mm and 700 mm) there is some cracking in span direction from the support towards the load. When the cross sections are considered an inclined crack pattern (shear crack) can be distinguished between the load and the support. In transverse direction there are no cracks running from the load plate all the way to the bottom of the slab. The strains are concentrated mainly between the load area and the support. It can be concluded that for all three shear spans the failure mechanism is one-way shear.

$b = 2500$ **mm**

When the element width is increased from 1500 mm to 2500 mm (figure 5.5), the shear failure mechanism is subjected to change for large shear spans. For all three shear spans cracks occur on the bottom face in transverse direction and in span direction between the load and the support. Between the load area and the support there are also inclined cracks. The cracked area at the edge of the slab parallel to the support has about the same width for all three cases. In the cross sections the inclined crack pattern between the load and the support (characteristic for one-way shear failure) occurs. At a shear

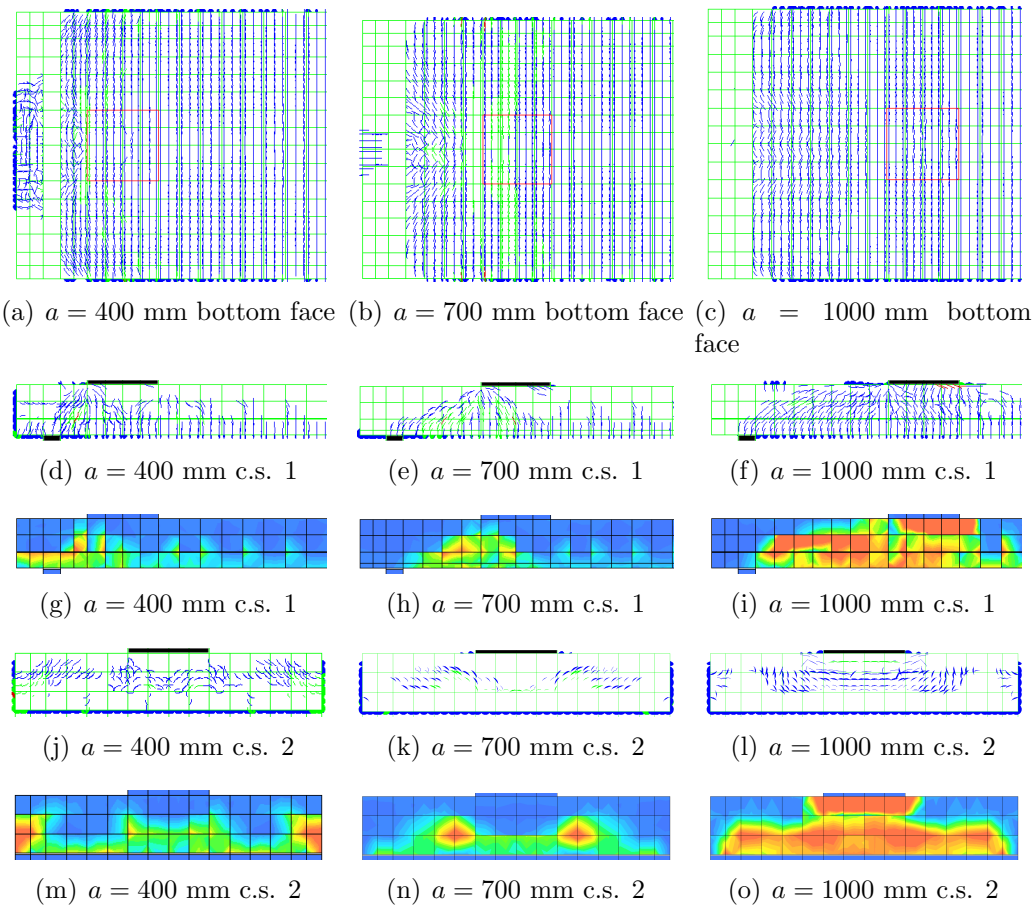

(a) $a = 400$ mm bottom face (b) $a = 700$ mm bottom face (c) $a = 1000$ mm bottom face

(d) $a = 400$ mm c.s. 1 (e) $a = 700$ mm c.s. 1 (f) $a = 1000$ mm c.s. 1

(g) $a = 400$ mm c.s. 1 (h) $a = 700$ mm c.s. 1 (i) $a = 1000$ mm c.s. 1

(j) $a = 400$ mm c.s. 2 (k) $a = 700$ mm c.s. 2 (l) $a = 1000$ mm c.s. 2

(m) $a = 400$ mm c.s. 2 (n) $a = 700$ mm c.s. 2 (o) $a = 1000$ mm c.s. 2

Figure 5.4: A comparison of the crack patterns and contour plots of the principal tensile strains at the moment of failure for elements $b = 1500$mm in width.

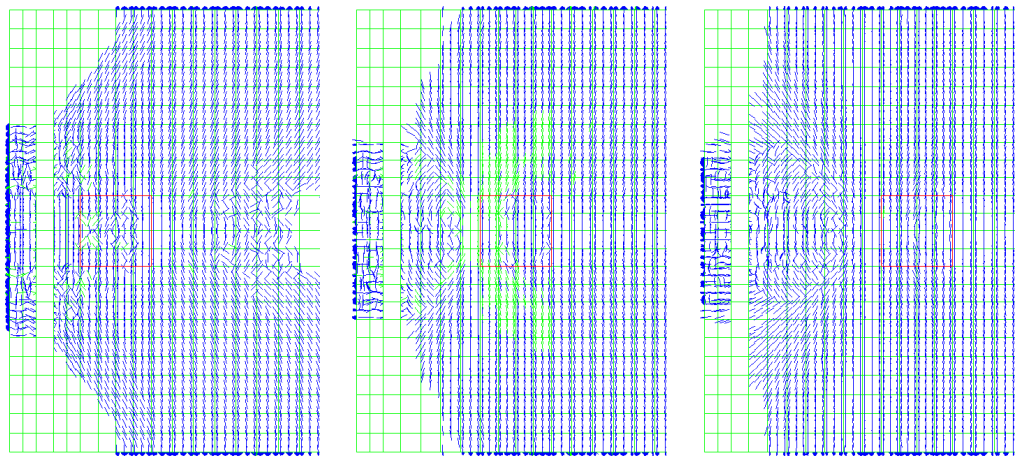

(a) $a = 400$ mm bottom face (b) $a = 700$ mm bottom face (c) $a = 1000$ mm bottom face

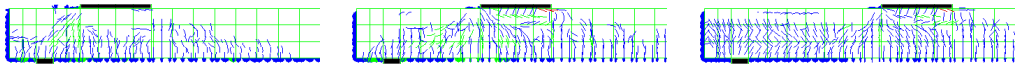

(d) $a = 400$ mm c.s. 1 (e) $a = 700$ mm c.s. 1 (f) $a = 1000$ mm c.s. 1

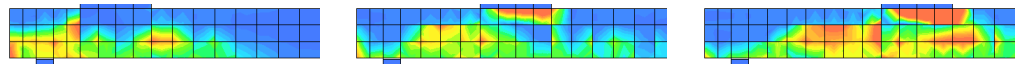

(g) $a = 400$ mm c.s. 1 (h) $a = 700$ mm c.s. 1 (i) $a = 1000$ mm c.s. 1

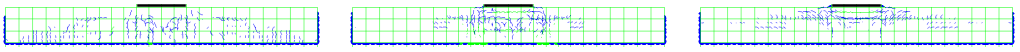

(j) $a = 400$ mm c.s. 2 (k) $a = 700$ mm c.s. 2 (l) $a = 1000$ mm c.s. 2

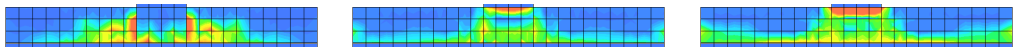

(m) $a = 400$ mm c.s. 2 (n) $a = 700$ mm c.s. 2 (o) $a = 1000$ mm c.s. 2

Figure 5.5: A comparison of the crack patterns and contour plots of the principal tensile strains at the moment of failure for elements $b = 2500$mm in width.

span of 700 mm the inclined crack pattern between the load and the support also appears. On the other side of the load plate, between the load plate and the far support, cracks on the bottom face of the slab run parallel to the support straight from one edge to the other. The failure mechanism is one-way shear failure. The third case ($a = 1000$ mm) the cross section in span direction shows diagonal cracks on both sides of the load plate running from the edges of the load outward to the bottom of the slab. A diagonal shear crack between the load and the support is not observed. In span direction cracking from top to bottom underneath the load plate can be seen. This indicates punching shear failure.

$b = 3500$ **mm**

For the largest modelled slab width (figure 5.6) the failure mechanisms are analysed here. All three crack patterns show inclined cracks on the bottom face running from the far side of the load area towards the edges of the slab. For the two larger shear spans there are also inclined cracks running from the corners of the loaded area towards the left support. For a shear span of 700 mm on both the left and right side of the loaded area the crack pattern seems to run around the load area in a circular manner. For a shear span of 400 mm this is only observed on the right hand side of the load plate. In the cross sections in span direction for $a = 400$ mm a steep inclined diagonal crack pattern occurs between the support and the load plate. This inclined crack pattern can also be seen in the cross section for the element with a shear span of 700 mm but not in the cross section for the largest shear span. The cross sections in transverse direction all show an inclined crack pattern with the cracks running from the edges of the load plate outward towards the bottom of the slab.

For $a = 400$ mm a diagonal shear crack occurs between the load and the support indicating one-way shear failure. On the other side of the slab a circular crack pattern around the load area appears which indicates punching shear. This combined behaviour of one-way shear and punching shear has been observed by Regan and it is discussed in chapter 2.1.2 as unbalanced punching failure due to non-axis-symmetrical conditions. Regan developed a calculation method based on this intermediate failure mechanism which is discussed in section 2.4.5. This combined failure mechanism is also seen when $a = 700$ mm. Punching failure occurs when $a = 1000$ mm.

The table below summarizes the observed failure mechanisms in the modelled elements.

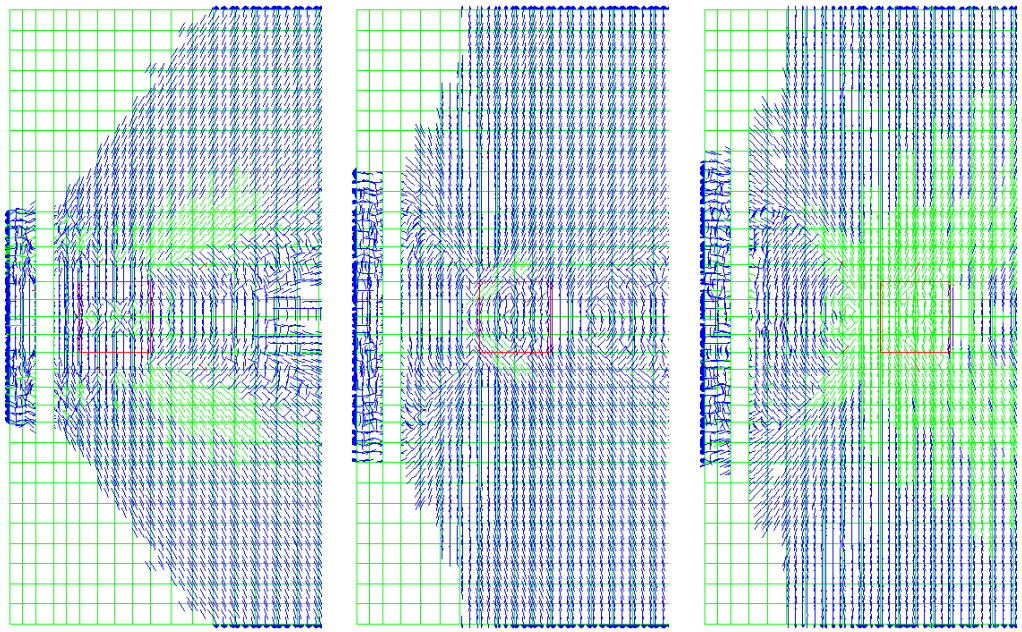

(a) $a = 400$ mm bottom face (b) $a = 700$ mm bottom face (c) $a = 1000$ mm bottom face

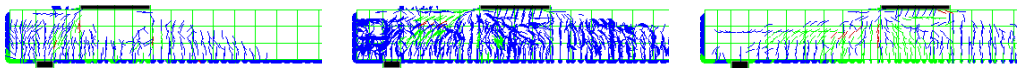

(d) $a = 400$ mm c.s. 1 (e) $a = 700$ mm c.s. 1 (f) $a = 1000$ mm c.s. 1

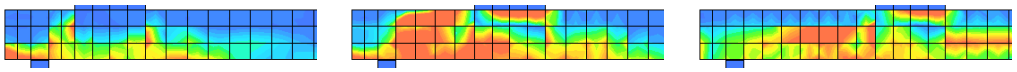

(g) $a = 400$ mm c.s. 1 (h) $a = 700$ mm c.s. 1 (i) $a = 1000$ mm c.s. 1

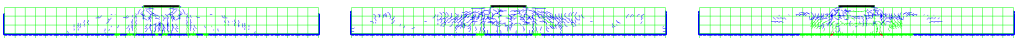

(j) $a = 400$ mm c.s. 2 (k) $a = 700$ mm c.s. 2 (l) $a = 1000$ mm c.s. 2

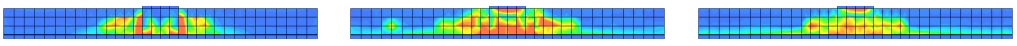

(m) $a = 400$ mm c.s. 2 (n) $a = 700$ mm c.s. 2 (o) $a = 1000$ mm c.s. 2

Figure 5.6: A comparison of the crack patterns and contour plots of the principal tensile strains at the moment of failure for elements $b = 3500$mm in width.

Observed failure mechanisms			
Shear span a	**400 mm**	**700 mm**	**1000 mm**
a/d_l **ratio**	**1.67**	**2.92**	**4.17**
$b = 1500$ mm	S	S	S
$b = 2500$ mm	S	S	P
$b = 3500$ mm	S+P	S+P	P
One-way shear (S), punching shear (P) or combined (S+P)			

According to Gardner (1990) [11] punching failure will occur only if the distance between the support and the load is at least three times the slab thickness. According to the table above this statement still holds.

5.3 Conclusion and recommendations

After investigating the behaviour of slabs, focusing on the transition between one-way shear failure and punching shear failure, various conclusions have been drawn. The conclusions are listed here:

- While performing FEM analyses on slabs, varying the element width and the shear span, three failure mechanisms are observed: one-way shear failure, punching shear failure and one-way shear failure with punching shear failure characteristics.

  The failure mechanism is considered as one way shear when a inclined shear crack appeared between the load plate and the support (figures 5.7(a), 5.7(d) and 5.7(g)). The failure mechanism was set to punching shear failure when the cross sections showed a truncated conical shaped crack pattern around the load area (figures 5.7(c), 5.7(f) and 5.7(i)). In two cases a combined failure mechanism was found in which the diagonal shear crack occurred between the load plate and the support and on the other side of the load plate a circular crack pattern running around the load area appeared (figures 5.7(b), 5.7(e) and 5.7(h)). The crack pattern indicating the failure mechanism is drawn with a semi transparent red line. Only a part of the total element, containing the relevant crack pattern, is plotted.

- Figure 5.8 shows a graph in which the two investigated parameters are combined. Three areas are marked representing the three failure mechanisms that have been observed in the FEM analyses.

  The element width is divided by the effective element thickness to factor out the thickness of the plate. The elements 1500 mm in width al failed through one-way shear. The plates 2500 mm in width failed either in one-way shear or punching shear. A clear transition was not observed. For elements 3500 mm in width there was no one-way shear failure. Only a combination of one-way shear failure and punching shear failure. As the shear span increased, the failure mechanism became punching shear

  It has to be kept in mind that the models all share the same concrete strength, reinforcement ratios and free span lengths. Also the support type was not changed. These factors are known to influence the failure mechanism and need to be investigated as well to be able to predict the failure mechanism in a more general way.

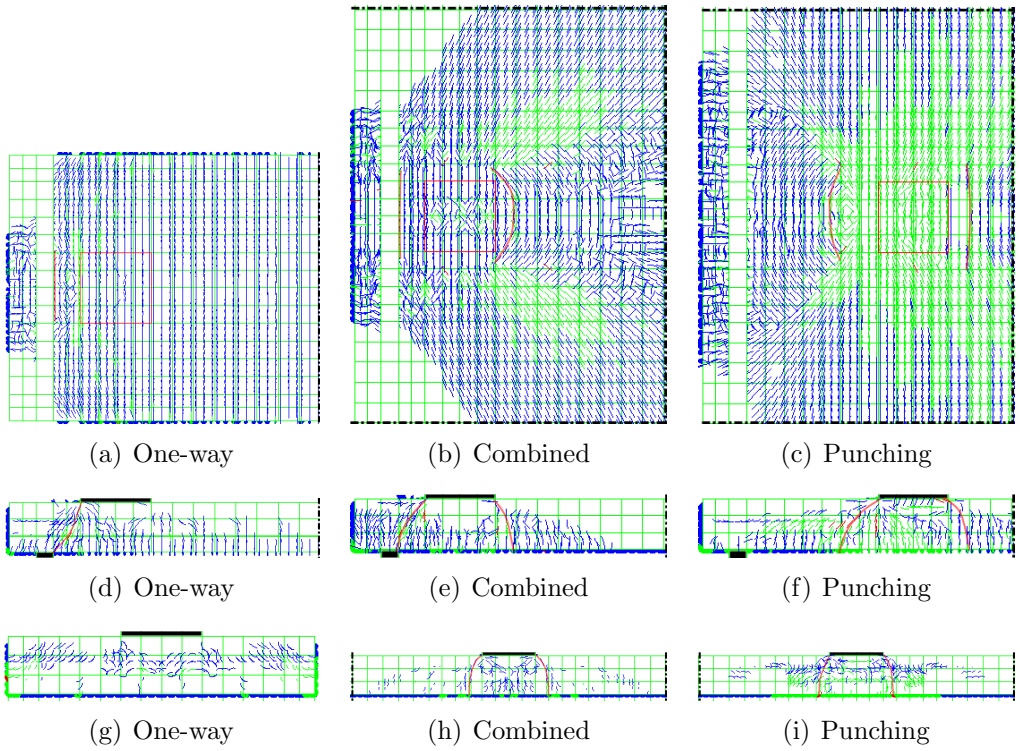

(a) One-way (b) Combined (c) Punching

(d) One-way (e) Combined (f) Punching

(g) One-way (h) Combined (i) Punching

Figure 5.7: The three observed failure mechanisms: one way-shear failure (left column), combined shear failure (middle column) and punching shear failure (right column).

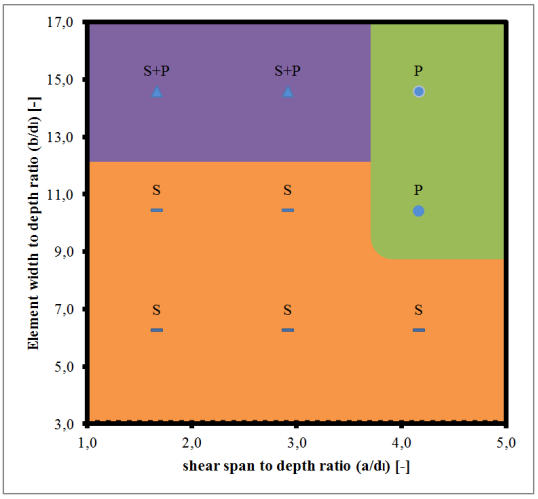

Figure 5.8: The occuring failure mechanism as a function of the shear span to depth ratio and the element width.

- Figure 5.8 can be used as a tool to determine when the structural element needs to be checked for one-way shear or on punching shear. When a combined failure mechanism is expected the method provided by Regan can be used to determine the load capacity of the slab. For very small shear spans ($a_v/d_l < 0.5$) Regan's method might over estimate the load capacity, as can be seen in chapter 3.5.5.

- In this chapter the modelled effective width was estimated and compared to the Model Code 2010 final draft and the French method recommendations. It was again concluded that the code predictions, especially for the Model Code, are unsafe for large shear spans ($a/d \geq 3$) on wide slabs .

Chapter 6

Conclusion and recommendations

In chapter one the following question was asked: Is there a way to predict the governing shear failure mechanism in wide beams and in one-way slabs loaded close to supports? Will there be one-way shear, will there be punching shear, or will there be a combination of these two? The study performed for this master thesis was done to answer the questions above. In the preceding chapters, conclusions were drawn. The most important conclusions and recommendations are listed here.

- Calculation methods to determine the effective width are not generally provided by the current building codes. The Eurocode French national annex and the new Model Code 2010 provide a recommendation. These recommendations, especially the one from the Model Code 2010, can provide unsafe results for large shear spans. It is recommended that the effective width is applied in the building codes. A limit should be applied as well: the effective width obtained for an a/d ratio of 3.5 when the French method is used and 3.0 when the Model Code 2010 method is used.

- As shown in chapter 4, it is possible to model both one-way shear failure and punching shear failure with the same procedure of building the model and performing the analysis. This creates the opportunity to investigate the behaviour of the slabs for situations in between one-way shear and punching shear.

- Currently one-way shear and punching shear both need to be checked in wide beams or one-way slabs subjected to concentrated loads. Analysis of the failure behaviour showed two different shear failure mechanisms

and a intermediate failure mechanism: one-way shear, punching shear and a combined failure mechanism (figure 5.7). In figure 5.8 it can be seen which of the three failure mechanisms will occur for various combinations of the shear span and element width. For each area the corresponding code provision should be applied. When a combined failure mechanism is likely to occur Regan's method is to be used. For one-way shear the predictions found when using the Eurocode turned out to be conservative for low a/d ratios, it is therefore recommended to apply the less conservative Model Code 2010 one-way shear provision. The model Code 2010 punching shear provisions are recommended when punching failure is checked.

- Because the classification system in figure 5.8 is based on elements with the same reinforcement ratios, concrete strength, length, thickness and load plate dimensions the classification system needs to be extended. Further investigation, varying other parameters, is required to provide a more general system.

- The shear retention factor β was determined for two experiments. The values found (7.5%, 25%) were substantially higher than the recommended values by the software (1% in TNO Diana). The smeared cracking model underestimates the transfer of shear forces across the cracks.

- The shear retention factor β used in the FEM models was found in an iterative manner. The shear retention factor influenced the ultimate failure load, but not the failure mechanism. Therefore it is currently not possible to accurately predict the maximum failure load with the used FEM model, only the shear failure mechanism can be determined. The shear retention factor β was found for two experiments. When β is determined for more experiments modelled in FEM, it might be possible to obtain an average value for β. The average value can be used to predict the maximum load capacity more accurate.

The answer to the research question: yes, it is possible to predict the occurring failure mechanism. However the prediction capabilities are limited for now. The important parameters known to influence this behaviour are the shear span, the element width, the reinforcement ratios, the load plate dimensions, the concrete strength and the support conditions. In this thesis the first two parameters were investigated and a classification system was developed to predict the failure mechanism. The influence of the other parameters on the failure mechanism still has to be investigated.

One parameter can have an effect on all other parameters, therefore investigating all the involved properties is very difficult, but it is necessary. Knowing the effect of all these parameters on each other is important because it is required to understand the shear behaviour in beams and plates subjected to a concentrated load close to the support.

In this thesis the influence of the shear span and the element width on the shear failure mechanism is investigated. Hopefully the data, results and conclusions can and will be used in future research on shear failure and predicting failure mechanisms.

Appendix A

FEM analysis results

The analysis of the FEM model 1500 mm in width and with a shear span of 550 mm (a/d_l ratio = 2.29) provided dubious results on the shear capacity. In this appendix the information is provided on which the decision to reduce the capacity has been made.

In figure A.2 a graph is provided showing the number of iterations required for each load step (0.15 mm) to obtain convergence. The maximum amount of iterations was set at 150. Steps 95, 133 - 135, 163, 173 - 175, 190, 220, 269, and ≥ 271 did not obtain convergence after 150 iterations. Between step 133 and 135 the applied load on the load plate decreased with 6 kN. A physically nonlinear analysis was performed using a modified Newton-Raphson iterative method. The convergence norm was Energy and Force based (both norms had to be fulfilled). The Energy convergence norm tolerance was set at 0.0001 and the force convergence norm tolerance at 0.01.

During the other FEM analysis convergence did not always occurred. The analysis kept on running. When the load-deflection behaviour of the element did not show strange results it was allowed that one or two consecutive load steps did not converge. As long as the steps afterwards did. The element was said to fail when no convergence was reached for any subsequent step and the applied load decreased quickly. Decreasing the step size or increasing the number of maximum iterations might result in convergence for more steps, however it also means a significant increase in computational time for each analysis. The computational time for one analysis often already exceeded 24 hours. In the figure it can be seen that convergence was not obtained for three succeeding steps (twice).

In figure A.1 the crack pattern on the side face and in a longitudinal cross section in the middle of the element is shown for load step 133 (first time three steps no convergence) and for load step 270 (after which no convergence is reached any more). In figures A.1(c) and A.1(d) the area between the load

and the support is severely cracked over the full height of the element. This is very unrealistic because it means that the plate is cracked over the full width between the load and the support. In figures A.1(a) and A.1(b) it can be seen that the element has already succumbed. Cracks are running over the full height of the slab.

Based on the lack convergence, the unrealistic crack pattern after step 133, and the decreasing concentrated load, it is decided to use this step as the moment of failure of the element, and not step 270.

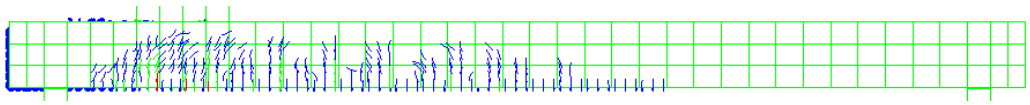

(a) Side face, load step 133

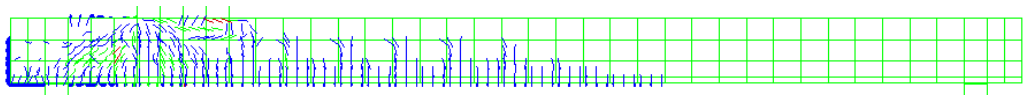

(b) Longitudinal cross section, load step 133

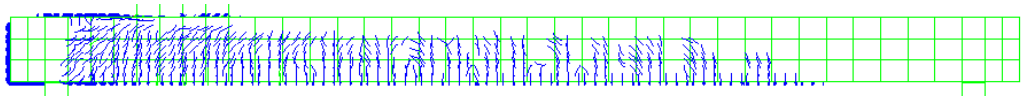

(c) Side face, load step 270

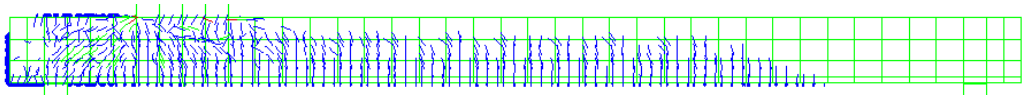

(d) Longitudinal cross section, load step 270

Figure A.1: The crack patterns on the side face and the longitudinal cross section in the middle of the width.

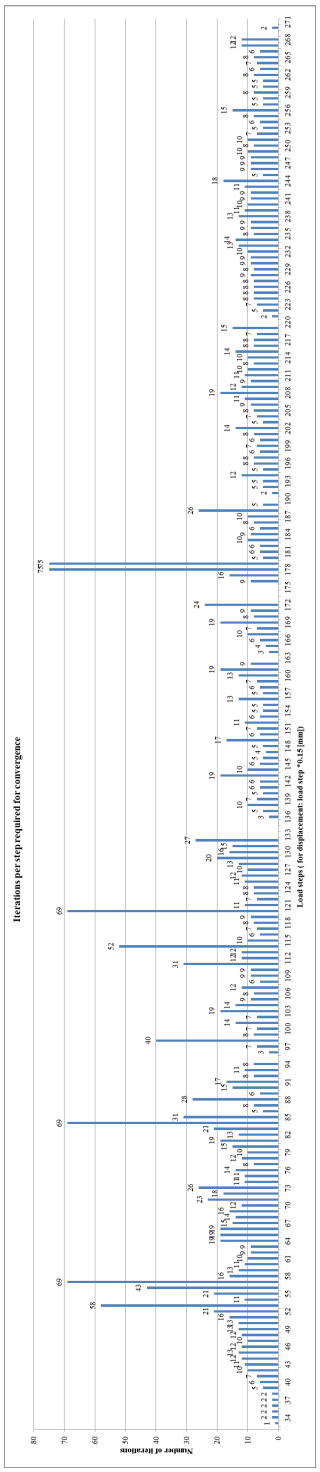

Figure A.2: FEM analysis b=1500 mm, a=550 mm number of iterations required per load step of 0.15 mm

References

[1] Shear strength of members without transverse reinforcement as function of critical shear crack width. *ACI Structural Journal*, 105(2):163–172, March 2008.

[2] Joint ACI-ASCE Committee 445. Recent approaches to shear design of structural concrete. *ACI445-99*, 1999.

[3] S. D. B. Alexander and S. H. Simmonds. Ultimate strength of slab-column connections. *ACI Structural Journal*, 84(3):255–261, May 1987.

[4] D. E. Allen. Limit states design – a probabilistic study. *Canadian Journal Of Civil Engineering*, 2(1):14, March 1975.

[5] American Concrete Institute Committee 318. *Building Code Requirements for Structural Concrete (ACI 318-08)*, 2008.

[6] E. C. Bentz, F. J. Veccio, and M. P. Collins. Simplified modified compression field theory for calculating shear strength of reinforced concrete elements. *ACI Structural Journal*, 103:614–624, July-August 2006.

[7] R de Borst, J.J.C. Remmers, A. Needleman, and M.-A. Abellan. Discrete vs smeared crack models for concrete fracture: bridging the gap. *International Journal for Numerical and Analytical Methods in Geomechanics*, (28):583–607, 2004.

[8] European Commission for Normalisation 351 001. *Eurocode 2: Design of concrete structures - Part 1-1: General rules and rules for buildings (NEN-EN 1992-1-1:2005)*, 2005.

[9] J. Falbr. Shear redistribution in solid concrete slabs. Master's thesis, Delft University of Technology, August 2011.

[10] H. Furuuchi, Y. Takahashi, T. Ueda, and Y. Kakuta. Effective width for shear failure of RC deep slabs. *Transactions of the Japan concrete institute*, 20:209–216, 1998.

[11] N. J. Gardner. Relationship of the punching shear capacity of reinforced concrete slabs with concrete strength. *ACI Structural Journal*, 87(1):66–71, January-February 1990.

[12] N. J. Gardner. Verification of punching shear provisions for reinforced concrete flat slabs. *ACI Structural Journal*, 108:572–580, Septeber-October 2011.

[13] Normcommissie 351 001 Technische grondslagen voor bouwvoorschriften. *NEN 6720: Voorschriften Beton TGB 1990 - Constructieve eisen en rekenmethoden (VBC 1995).* Nederlands Normalisatie-institut, 1995.

[14] P. A. Gutierrez and M. F. Canovas. The modulus of elasticity of high performance concrete. *Materials and Structures*, 28(10):559–568, December 1995.

[15] International Federation for Structural Concrete (fib). *Model Code 2010 - Final draft*, 2011.

[16] J. N. G. Kani. The riddle of shear failure and its solution. *ACI Journal Proceedings*, 61(4):441–467, April 1964.

[17] S. Kinnunen and H. Nylander. *Punching of Concrete Slabs Without Shear Reinforcement*, volume 158, page 112. Transactions of the Royal Institute of Technology, Stockholm, Sweden, 1960.

[18] J. S. Kuang and C. T. Morley. Punching shear behavior of restrained reinforced concrete slabs. *ACI Structural Journal*, 89(1):13–19, Januari 1992.

[19] E. O. L. Lantsoght. Shear tests of reinforced concrete slabs - experimental data of undamaged slabs. concept, April 2011.

[20] E. O. L. Lantsoght, C van der Veen, and J. C. Walraven. Experimental study of reinforced concrete bridge decks under concentrated loads near to supports. In *Proceedings of the 13th international conference and exhibition on structural faults and repair*, Edinburgh, Scotland, June 2010a.

[21] E. O. L. Lantsoght, C van der Veen, and J. C. Walraven. Shear tests of reinforced concrete slabs with concentrated loads near to supports. In *Proceedings of the 8th fib international PhD Symposium in Civil Engineering*, pages 81–86, Kgs. Lyngby, Denmark, June 2010b. Technical University of Denmark.

[22] E. O. L. Lantsoght, C van der Veen, and J. C. Walraven. Experimental study of shear capacity of reinforced concrete slabs. In *Proceedings of the 2011 Structures Congress*, volume 401. American Society of Civil Engineers ASCE, April 2011a.

[23] E. O. L. Lantsoght, C van der Veen, and J. C. Walraven. Experimental study of shear in reinforced concrete one-way slabs subjected to concentrated loads. In *Proceedings of the fib Symposium Prague 2011*, volume 1, Praha, Czech Republic, June 2011b. American Society of Civil Engineers.

[24] E. O. L. Lantsoght, C van der Veen, and J. C. Walraven. Shear capacity of slabs and slab strips loaded close to the support. In *Proceedings of the ACI Fall 2011 Convention*. ACI, 2011c.

[25] A. S. Lubell, E. C. Bentz, and M. P. Collins. One-way shear in wide concrete beams with narrow supports. In *Proceedings of the 2008 Structures Congress 2008: Crossing Borders*, Vancouver, BC, Canada, April 2008. American Society of Civil Engineers.

[26] D. M. Masterson and A. E. Long. The punching strength of slabs, a flexural approach using finite elements. In *Special Publication - Shear in Reinforced Concrete*, volume 42, pages 747–768. American Concrete Institute, Detroid, 1974.

[27] A. Muttoni. Punching shear strength of reinforced concrete slabs without transverse reinforcement. *ACI Structural Journal*, 105(4):440–450, July 2008.

[28] A. Muttoni and M. Fernández Ruiz. Shear strength in one- and two-way slabs according to the critical shear crack theory. In *Tailor Made Concrete Structures*, pages 559–563. Taylor and Francis Group, 2008.

[29] A. A. Olonisakin and Alexander S. D. B. Mechanism of shear transfer in a reinforced concrete beam. *Canadian Journal of Civil Engineering*, 26(6):810–817, 1999.

[30] Task Group on Utilisation of concrete tension in design. Punching of structural concrete slabs. bulletin 12, fib (CEB-fip), Lausanne, Switzerland, 2001.

[31] Z Prochazkova and E. O. L. Lantsoght. Material properties - felt and reinforcement for shear test of reinforced concrete slab. report 25.5-11-11,

Delft University of Technology, Factulty of Civil Engineering and Geosciences, Department of Design and Construction - Concrete Structures, September 2011.

[32] P. E. Regan. *Shear resistances of concrete slabs at concentrated loads close to supports*. Structures research group, Polytechnic of Central London, 1982.

[33] P. E. Regan. Research on shear: a benefit to humanity or a waste of time? *The Structural Engineer*, 71(19):337–347, October 1993.

[34] P. E. Regan and H. Rezai-Jorabi. Shear resistance of one-way slabs under concentrated loads. *ACI Structural Journal*, 85(2):150–157, March 1988.

[35] K Reissen and J Hegger. Zwischenbericht - anpassung des DIN-fachberichtes "betonbrücken" an endgültige einschiesslig vergleichsrechnungenspeziell: Querkrafttragfähigkeit von fahrbahnplatten. Technical report, RWTH Aachen University, February 2010.

[36] J. Sagaseta, A. Muttoni, M Fernández Ruiz, and L Tassinari. Non-axis-symmetrical punching shear around internal columns of RC slabs without transverse reinforcement. *Magazine of Concrete Research*, Paper 1000098, 2011.

[37] E. G. Sherwood, A. S. Lubell, E. C. Bentz, and M. P. Collins. One-way shear strength of thick slabs and wide beams. *ACI Structural Journal*, 103(6):794–802, November 2006.

[38] A. N. Talbot. Tests of reinforced concrete beams: Resistance to web stresses - series of 1907 and 1908. *University Of Illinois Bulletin No. 29*, V1(12), January 1909.

[39] A. Uzel, B. Podgorniak, E. C. Bentz, and M. P. Collins. Design of large footings for one-way shear. *ACI Structural Journal*, 108(2):131–138, March 2011.

[40] R. Vaz Rodrigues. Shear strength of reinforced concrete bridge deck slabs. thesis, École polytechnique fédérale de Lausanne, Lausanne, 2007.

[41] Muttoni A. Vaz Rodrigues R., Fernández Ruiz M. Punching shear strength of R/C bridge cantilever slabs. *Engineering structures*, 30:3024–3033, 2008.

[42] F. J. Vecchio, M. P. Collins, and ASCE Members. Compression response of cracked reinforced concrete. *Journal of Structural Engineering*, 119(12):3590–3610, July-August 1993.

[43] F. J. Veccio and M. P. Collins. The modified compression-field theory for reinforced concrete elements subjected to shear. *ACI Journal*, 83:219–231, March-April 1986.

[44] J. C. Walraven. *Aggregate Interlock: A theoretical and experimental analysis*. PhD thesis, Delft University of Technolody, 1980.